Aston University

Some pages of this thesis may have been removed for copyright restrictions.

If you have discovered material in Aston Research Explorer which is unlawful e.g. breaches copyright, (either yours or that of a third party) or any other law, including but not limited to those relating to patent, trademark, confidentiality, data protection, obscenity, defamation, libel, then please read our Takedown policy and contact the service immediately (openaccess@aston.ac.uk)

A STUDY OF THE WELD HEAT AFFECTED ZONE OF CARBON MANGANESE MICROALLOYED STEEL

BY

SERGIO DE CARVALHO PERDIGÃO MSc

A Thesis Submitted to
THE UNIVERSITY OF ASTON IN BIRMINGHAM
For The Award Of Doctor Of Philosophy

JUNE 1980

To Mema and Trish, and in

memory of Ivan and Marita

SUMMARY

A STUDY OF THE WELD HEAT AFFECTED ZONE OF CARBON MANGANESE MICROALLOYED STEEL

Sergio de Carvalho Perdigão PhD 1980

The toughness and the microstructure of the weld Heat Affected Zone (HAZ) of a Quenched and Tempered High Strength Low Alloy Steel containing microadditions of niobium and vanadium, have been investigated by Charpy Impact tests and Metallographic examination.

The real HAZs were obtained from bead-on-plate deposits made by Submerged Arc Welding at 3.6 and 6.3KJ/mm. These experiments provided toughness, microstructural and welding thermal cycle data. Welding Simulation, combined with Dilation techniques, were employed for the majority of the investigation. This involved toughness, microstructural and phase transformation data corresponding to heat inputs equivalent to cooling times from 800 to 500°C of 25, 90 and 220s respectively. Simulation thermal cycles were mainly obtained from finite element heat flow calculation. The nominal peak temperatures tested ranged from 700 to 1400°C, thus providing detailed information for all the regions of the HAZ.

A variation of the HAZ toughness relative to the base metal was confirmed. An improvement of the toughness with the increase in the peak temperature up to 1000°C was found, and it was attributed to a refinement of the prior austenite grain size. Deterioration in toughness was observed at peak temperatures $\geqslant$ 1150°C. This embrittlement increased with the increase in heat input and was associated with the presence of proeutectoid ferrite and upper bainite. No precipitation of microalloys was evident but the practice of Post Weld Heat Treatment provoked further embrittlement in the tested samples. The nature of the transformed microstructures was considered to be the major embrittling mechanism of the HAZ, and an experimental CCT diagram was produced for predicting the weld HAZ microstructures in the coarse grained region.

Key Words : WELD HEAT AFFECTED ZONE
TOUGHNESS
STEEL
SUBMERGED ARC WELDING
MICROSTRUCTURES

DECLARATION

No part of the work described in this thesis was performed in collaboration with anyone else, except where specifically stated. Although advice and help was sought and received from a number of people, all the work described herein is my own.

Acknowledgements have been given to the people whose advice and aid was sought.

This work has not been submitted before for any other award to this, or any other, University.

Sergio de Carvalho Perdigão
Department of Production Engineering

1980

CONTENTS

CHAPTER 1 - INTRODUCTION

CHAPTER 1 - INTRODUCTION

The design and development of high strength low alloy steels (HSLA) early in this century involved 0.3% carbon as the main alloying element, and technically was only based on tensile strength. In the thirties, Mn additions were increased up to 1.5% suiting the existing engineering requirements as little attention was paid to the production processes that are of major and economic importance today. The II World War demanded faster production rates and welding became more attractive than riveting. When the welded "Liberty" ships started to crack in the winter of the Northern Sea, requirements for toughness properties were raised to the same level of importance as the tensile ones. This boosted the development of materials and processes providing the basis for the modern technology of HSLA steels.

Significant production of Nb steels began about 15 years ago opening the market for the microalloyed steels. These steels are now in continuous development to meet the industrial requirements for new products with increasing strength/weight ratios, higher toughness and better weldability. When designing for welding, one has to consider and balance costs with performance of the final product. Automatic processes reduce costs as they speed up the production. For this reason they are welcome in modern plants. The ideal is a high heat input automated process which would reduce even more the production time. However, amongst the problems generated by increased heat input when welding HSLA microalloyed steels, one of importance is the loss of toughness

at the border region with the fusion line, and here the present research finds its foundations.

Microalloying elements are added to HSLA steels to induce, by suitable means, a small grain size in the final flat product. Grain size is the only parameter quoted to increase both the toughness and the tensile properties of the steels. The microalloying elements precipiate very finely in the later stages of production, acting as barriers which will prevent grain growth. The most commonly used microalloying elements are Nb and V. They are most frequently employed separately, but occasionally they are used together. One modern approach to the development of the HSLA microalloyed steels is the use of the Quenching and Tempering process route. Their production at the moment has some economic drawbacks. Although the steels exhibit yield strength up to 850 MPa, they have limited toughness. The only steel-maker currently producing this type of product in Europe is the British Steel Corporation (BSC) at the Clydebridge Works. The steels belong to the RQT series and contain both Nb and V microalloying additions.

When a high heat input welding is performed in the HSLA microalloyed steels, the microalloying elements go into solution in the austenite at the high temperatures of the process. Consequently their grain refining capability is lost and the Heat Affected Zone (HAZ) at the interface with the fusion line will exhibit a coarse austenitic grain size. The literature provides a wide range of controversy on the beneficial effect of Nb and V microadditions to HSLA steels that are to be welded. There is some evidence that when

these elements are used in combination, a higher degree of deterioration should be expected. The investigations involving these types of steel are scarce and hardly any information is given on the causes of the deterioration. Few papers compare the HSLA microalloyed steels in an increasing deterioration of toughness sequence. They mentioned that the combined use of Nb and V provokes always the most embrittling conditions than if these elements were employed separately. The degree of deterioration is reported to increase with the increase in the heat input supplied by the welding process.

The BSC RQT-500, a HSLA microalloyed quenched and tempered steel containing 0.15%C, 1.44%Mn, 0.06%Nb and 0.03%V was chosen as the material for the present investigation. The reasons for the choice are many: these steels are relatively new in development, they are seldom mentioned in the literature, whenever mentioned they are rated as a potential hazard to the HAZ toughness if high heat input welds are to be used. Besides, the causes for the deterioration have not been investigated systematically.

When determining the toughness of the HAZ of HSLA steels, two types of test are outstanding; the Charpy V Notch test and the Crack Opening Displacement (COD) test. The COD test provides data on the initiation of a crack long enough to propagate an unstable fracture at the current test temperature. Its increasing popularity suggests that the future specifications will be based on such fracture mechanics parameter. The classical Charpy V Notch test gives

information on both the initiation and the propagation of the fracture. It measures the absorbed energy to fracture a notched sample at a certain temperature. At the present time this test still remains the most practical engineering approach to toughness evaluation in welded joints. Consequently, Charpy V Notch test will be the test employed in the current work to evaluate the toughness of the HAZ.

When investigating the deterioration of the toughness of HSLA microalloyed steels caused by the use of high heat input welding processes, the various authors refer to different basis of comparison. The deterioration is mainly established relatively to the reference steel or to the parent metal. Reference steel is a steel containing the same amount of C and Mn as the microalloyed steel, but no microalloying elements. A typical investigation from the current literature would compare the toughness deterioration of specific regions of the HAZ for several materials and heat inputs. The region frequently tested is the coarse grained region because it is the one always exhibiting the highest embrittlement in the HAZ. The materials tested would contain different levels of microalloying, distinct microalloying elements, or both. The conclusions usually involve a rating of the materials according to the toughness deterioration and qualitative considerations about the causes for the deterioration. Two main theories explain the loss in the toughness: the Microstructural theory and the Precipiation theory. Precipitation of any microalloying elements in the HAZ has seldom been detected, but is always referred to in a speculative way. The intricate nature of the microstructures

produced, and the difficulty associated with their identification seems to discourage the authors from analysing the phenomena in depth. The microstructural analysis is frequently recommended as further work.

On the basis of the reasons given above, it was decided that one of the tasks of the present work was to clarify the inter-relation between microstructure and toughness of the weld HAZ of the RQT-500 steel. This would involve microstructural and property measurement of HAZ produced at three levels of heat input, namely 3.6, 6.3 and 14.4KJ/mm. In this way detailed information would be gained for one particular steel and, in addition, insight gained into the significant factors governing weld HAZ microstructure and properties. The terminology heat input supplied to a plate needs some clarification, since without the specification of the plate thickness, it would be meaningless. Currently, the range of heat inputs and plates thickness investigated is so vast that to avoid difficulty in the interpretation of the results, the international literature has introduced a new welding parameter: the cooling time between 800 and 500^{o}C. This parameter is a function not only of heat input supplied, but also of the thickness of the plate to be welded. That temperature range was chosen because it is considered the one where all the important structural transformations occur. In this work it will be further referred to as $\Delta t_{800-500}$ for convenience of impression. The original plate thickness of the RQT-500 steel was reduced from 38 to 25mm and the heat inputs supplied can be defined by the new parameter as equivalent to 25, 90 and 220 seconds respectively for the

heat inputs of 3.6, 6.3 and 14.4KJ/mm. The former two heat inputs correspond to the boundary between low and high heat inputs, and to a high heat input Submerged Arc Welding (SAW) processes respectively. The latter heat input corresponds to an extremely high weld energy three wire SAW process, or could be associated with an Electrogas or Electroslag Welding process. The figures relative to the two former SAW heat inputs were obtained practically and from theoretical calculations respectively. For the actual measurements, results were derived from thermal cycles obtained from the insertion of Pt/Pt-13%Rh under the welding bead of bead-on-plate weldments. The other cooling time was obtained by means of theoretical calculations based on a research performed at the University of Trondheim, Norway. The cooling times, representative of the highest heat input used, were estimated based on data of the current literature.

When welding HSLA microalloyed steels, special attention must be paid to the solution temperature of the microalloying elements in the matrix. The moment they go into solution they lose their grain pinning capability, and the austenitic grain at the border with the fusion line will coarsen. The latter occurrence usually results in an impairment of the toughness of this region of the HAZ. Vanadium is quoted to go into solution at 1100-1150^{o}C, and the niobium at approximately 1200-1250^{o}C. The precise solution temperature is dependent on the composition of the steel. In addition to the reported brittleness of the grain coarsened region of the HAZ, some authors found a secondary hardening or deterioration at the sub critical HAZ. This is the inter-

face of the parent metal with the starting of the transformed intercritical region. The intercritical region of the HAZ itself, as well as regions that experience temperatures just above A_3, are reported to possess very fine grain and extremely attractive toughness properties.

In the light of this knowledge, a range of Peak Temperatures were chosen to be investigated in the current research, as follows :

- 700°C - Sub critical HAZ, the steel is heated to a temperature just below the A_1.
- 800°C - Inside the intercritical region of the HAZ, the material has started the austenitisation, but that transformation is interrupted.
- 900°C - Upper limit of the intercritical region of the HAZ, the transformation of the matrix into austenite is nearly completed.
- 1000°C - The matrix is now fully austenitic and exhibits a considerable amount of nucleation.
- 1150°C - Temperature range where vanadium precipitates are expected to be in solution.
- 1250°C - Temperature range where niobium precipitates are expected to be in solution.
- 1400°C - Temperature representative of the structures formed very close to the fusion boundary.

Having stablished the material, test, heat inputs, and peak temperatures to be studied, it remains to be decided on how to produce the samples to be tested. From practice it is known that difficulties are met in locating accurately the Charpy Notch Tip in the region of the HAZ to be investigated. Furthermore, cases have been reported where the crack path

initiated at a certain region changed its direction running through a totally different structure than the one to be observed. The welding simulation technique provides a solution for that problem, duplicating regions of interest of the HAZ. These regions would be wide and homogeneous enough to provide an accuracy of notching and certainty of testing. Some investigators are concerned that one could be studying and correlating with actual weldment HAZs, simulated structures based only on the reproduction of the real weld thermal cycles. This doubt arises because of reports that simulators do not always reproduce the microstructure, even although experiencing the same thermal cycle. Based on the above comments, in the current research samples were extracted from bead-on-plate welds performed to match the two lower figures heat inputs to be studied. These were then compared to similar samples produced by the simulation techniques that constituted the bulk sample producing method of the work. For the highest welding energy employed in the investigation, the only samples used were those produced by simulation techniques.

A further benefit from the simulation method is that simultaneously to the duplication of a sample, its dilation history can be obtained. It gives information on the start and finishing of the transformation temperatures on cooling for any thermal cycle employed. This is an important tool that helps the analysis of the obtained microstructures. It also allows the building up of a CCT diagram for the given material. Frequently, information on the last two points are not found in the current literature.

Bead-on-plate welds were laid along the rolling direction of the plate sections to provide actual weldment specimens for the conventional Transverse Charpy V Notch Impact tests. Specimens to be duplicated by welding simulation were extracted from the plates in a similar way to the ones mentioned above. The impact tests were performed at a range of temperatures mainly varying from -80°C to 20°C. Tests at elevated temperatures were not performed because the RQT-500 is not specifically designed for use at such temperatures. For every condition of heat input and peak temperature tested, two sets of data were obtained: one based on the energy absorbed, and the other based on the fracture appearance at the test temperature.

The specimens were analysed systematically as follows :

- Optical Metallography, Fractrography and Quantitative Metallurgy methods were used for qualification and quantification of the produced structures. The austenitic grain sizes were determined by linear intercept method. The fracture path of the subsidiary cracks was observed and related to the produced microstructures.
- Scanning Electron Microscopy was used to perform microscopic observation on the nature of the fracture surface of the several specimens tested. The aim was to establish a qualitative ordered correlation on their behaviour.
- Transmission Electron Microscopy was employed with two objectives. One was to resolve to a finer detail the structures previously observed under the optical micro-

scope. This was accomplished by the use of double stage carbon shadowed replicas. The other goal was an attempt to detect and decide on the nature of the carbides present in some of the structures. For this purpose carbon extraction replica techniques were used.

- Hardness - Microhardness tests were employed in a trial to locate accurately the boundaries of the regions of the HAZ in real weldments. Macrohardness tests were performed to supply figures for a general metallurgical analysis. A correlation hardness-structure was also attempted.

The effect of Post Weld Heat Treatment (PWHT), which frequently is not recommended for that class of steels, is considered in the current work. The information sought was its influence on the most embrittled condition obtained, as well as its influence on the base metal. For a specific case it was employed as an extra support to clarify the nature of an observed microstructure.

Finally, all the data obtained were analysed on a global basis of classical metallurgical concepts. A correlation of the welding thermal cycles employed, the resulting microstructures and their influence on the HAZ toughness was attempted. The results were also expected to clarify the causes for the deterioration of the toughness of the coarse grained region of the HAZ, since that area has long been neglected.

CHAPTER 2 - LITERATURE SURVEY

CHAPTER 2 - LITERATURE SURVEY

2.1 Introduction

The demands from the modern structural engineering design for new materials are a combination of high strength and reduced weight, allied to an improvement in the toughness characteristics. These were met by the High Strength Low Alloy (HSLA) steels containing microalloying additions.

A high strength steel is regarded as one presenting a yield stress of at least $300N/mm^2$ (1). Elements such as Nb, Ti, V, Al, Ta and Zn, which are strong carbide, nitride or carbonitride formers, when added to the steels in compositions that very seldom exceeds 0.15%, are defined as Microalloying elements (2).

Amongst the many ways to strengthen a steel, the most effective can be considered to be the controlled precipitation of the microadditions. This is achieved by the sophisticated modern process routes. Particular attention must be given to the particle size and to particle distribution. The small particles ($10-20A^{o}$) inhibiting to a greater extent the dislocations movement, are much more potent strengtheners than the large particles ($100-200A^{o}$) (3).

The immediate consequence of the increase in the yield point of a steel is a decrease in the toughness of the material, and the mechanism used to counterbalance that deleterious effect is the control of the grain size of the alloy. This is achieved by both compositional and thermomechanical manipulations.

Process routes leading to tough, strong steels, i.e. steels containing basically C, Mn, Si and usually microalloyed with AL, Nb and V, are many. The materials are generally supplied in one of the following conditions :

- As Rolled
- Controlled Rolled
- Normalised
- Quenched and Tempered

Each one of these manufacturing processes has its advantages and its shortcomings, but all of them are based on the production of very fine precipitates of nitrides, carbides or carbonitrides. These precipitates retard the austenite recrystallisation or arrest its grain sizes. The latter mechanism is more usual than the former one, but both yield products with smaller grain sizes. When HSLA microalloyed steels undergo welding, the process routes that lead to a fine grained structure are absent. A good review of the HSLA microalloyed European steels, presenting also a welding point of view, was given in an American Society for Metals (ASM) conference in Rome, 1976 (1).

2.2 The Role of Some Constituents On The Toughness Of The Parent Plate

As the composition of the material will strongly affect the properties of the Heat Affected Zone (HAZ) of a weldment, some brief comments will be made on the main elements of a HSLA microalloyed steel.

2.2.1 Carbon

It was the first element to be employed to strengthen the steel at the turn of the century, in amounts of 0.30%C. However, with the growing importance of the welding process,

its level had to be reduced since its hardenability effect was deleterious to the toughness required from the welded product. For this reason the strength of the steel has been kept, or improved, by the use of other additions.

Nowadays in the HSLA microalloyed steels, the carbon composition seldom exceeds 0.20%C. Further reduction of the carbon level has proven to be an excellent technique, but economic and production difficulties in obtaining very low carbon, pearlite free steels, kept the carbon level above 0.03%C.

2.2.2 Manganese

It became an important alloying element in the thirties, when its amount was raised to about 1.50%Mn in the steels. The manganese effect on the structure is usually beneficial as it changes the morphology of the pearlite and other carbide regions, but its content must be limited to a figure of 1.70%Mn (4), or the depression that it will induce in the transformation temperature may favour the production of upper bainitic brittle structures (5).

2.2.3 Silicon

Silicon raises the $\gamma \rightarrow \alpha$ transformation temperature and promotes solid solution strengthening (3). For this reason, after welding a harder HAZ will develop in a high silicon steel, as opposed to a steel containing lower silicon, and a poorer resistance to cleavage is to be expected.

2.2.4 Aluminium

Strain induced precipitation of aluminium nitrides (AlN) will occur in the latter stages of rolling, and will retard the growth of the recrystallised austenite. To precipitate as a nitride, the aluminium will remove some nitrogen from solid solution, lowering the yield strength of the steel, but presenting a tougher material.

2.2.5 Niobium

Niobium can retard the austenite recrystallisation when in solid solution, or when precipitated as very fine particles ($<150A^{\circ}$) in the austenitic phase. Larger Nb precipitates (300 to $1000A^{\circ}$) will prevent austenite grain growth after its recrystallisation. In all cases, the steel produced will present a smaller grain size. At the low to medium Nb levels (up to 0.10%Nb), the precipitation occurs at the interface of the $\gamma \rightarrow \alpha$ transformation, thus if that reaction can be forced to occur at lower temperatures, finer grain size structures will be obtained by the retention of Nb in solution, or by the effect of the fine precipitated Nb particles, avoiding austenite recrystallisation. If higher levels of Nb are to be used (0.07 to 0.15%Nb), the grain refinement will be achieved by the larger formed Nb precipitates (300 to 1000 A°) obstructing the austenitic grain growth, after the recrystallisation (3).

2.2.6 Vanadium

Vanadium presents a higher solubility than niobium in the austenitic phase, therefore, it is much more effective as a precipitation strengthening element. Controlled Rolling

Process force an early precipitation of vanadium nitrides or carbonitrides within the austenite. On the other hand, normalising heat treatment nucleating new austenite grains will also result in a finer grain size structure. The latter structure in both cases is due to the fine vanadium precipitates preventing the austenitic grains growing.

2.3 Problems Encountered When Welding HSLA Microalloyed Steels

All the benefits brought about by the contribution of microadditions and thermomechanical processing to the parent plate, are affected to a great extent when the material is welded. The welded regions undergo high temperatures and specific cooling rates, which are dependent on the welding process and thickness of the plates. The absence of controlled deformation and/or thermal treatments will usually result in a final product with structures and properties in the HAZ, which are totally different from those of the parent plate.

The regions of the HAZ have been classified in order of increasing temperature (6) as :

i) Sub critical HAZ - Temp. below A_1.

ii) Inter critical HAZ - Temp. between A_1 and A_3.

iii) Fine grain HAZ - above A_3 but below grain coarsening temperature.

iv) Coarse grain HAZ - Up to the melting point of the alloy.

Or simply as (7) :

i) Sub critical HAZ.

ii) Transformed (visible) HAZ.

The main causes of lower toughness of the HAZ regions are recognised to be as follows :

i) Hydrogen embrittlement.

ii) Sub critical HAZ embrittlement.

iii) Coarse grained HAZ embrittlement.

Hydrogen embrittlement associated with martensitic formation, which is a problem concerning low heat input welds and sub critical HAZ embrittlement, are usually not as important in order of magnitude for the actual investigation, and will be mentioned briefly. Coarse grained HAZ embrittlement constituting the main body of the present work, will be considered per se, as one item.

2.3.1 Hydrogen Embrittlement

When the welding process allows rapid cooling rates, the chemical composition of the steel may favour low transformation temperature shear structures, which are susceptible to hydrogen embrittlement in the presence of stress raisers. Cracking will occur when all the following factors are simultaneously present :

- Sufficient hydrogen concentration.
- Susceptible microstructure.
- An applied tensile stress.

To estimate the tendency of a material to that kind of failure, an empirical formula was developed as a relative measure of the hardenability of steels, and it was named Carbon Equivalent Formula, or simply CE. Nowadays it has taken many forms.

The practical upper limit for a Carbon Equivalence is determined experimentally and experience in AP1 5L and AP1 5LX type steels has shown that they are weldable, provided that $CE = C + \frac{Mn}{6}$ [1] is less than 0.43 (8).

Gray reviewing a work by Benko and Hrivnakova (9) on micro-alloyed FAMA-type steels, pointed out the deficiency of the carbon equivalent formula adopted by Sub-Commission IX - G of the International Institute of Welding (IIW).

$C\ eq = C + \frac{Mn}{6} + \frac{Cr + Mo + V}{5} + \frac{Cu + Ni}{15}$ [2], since these steels were quite weldable despite their carbon equivalent equal to 0.78.

It has been constantly mentioned that CE formulas are not very effective when the steels have a low carbon content ($C < 0.10\%C$) and that the Ito-Bessio factor

$P.\ cm = C + \frac{Mn + Cu + Cr}{20} + \frac{Si}{20} + \frac{Ni}{60} + \frac{Mo}{15} + \frac{V}{10} + 5B + \frac{(H)}{60}$ [3]

gives a more realistic estimate (10, 11, 12).

Although V is commonly used in the CE calculations, some authors consider its influence negligible (13, 14). Niobium not increasing the amount of martensite (15), nor influencing the martensite hardenability (6), does not by itself affect the risk of hydrogen cracking, thus not appearing in the CE formulae.

The most popular test providing a quantitative rating of the susceptibility of steel to Cold Cracking is the Implant Test

(16). It allows the determination of the critical cracking stress above which cracking will be systematically observed at a given heat input. In this method a notched cylindrical test piece of the steel investigated - the implant - is closely inserted into a mild steel host plate. A weld bead is deposited across the assembly so that the notch is partially located in the HAZ. A constant load is then applied to the implant and maintained for a predetermined period of time. The testing criterion could be either fracture or crack initiation.

2.3.2 Sub Critical HAZ Embrittlement

Initially this type of embrittlement was noted for C and C/Mn steels in the thermally strained zone outside of the HAZ, and in the presence of stress raisers. It was commented that it can occur only rarely in welded structures (17).

However, Aronson (18) registered that type of embrittlement for a low carbon Nb bearing HSLA steel, and attributed the phenomena to NbC precipitation hardening. Wada (19) studying Mn-Mo-Nb steels, arrived at the same conclusion. This fact was also mentioned in the Doc. IIW-382-71 (2) for C/Mn/V steels, where it was observed that a possible reprecipitation of VC could occur in conjunction with plastic strain at temperatures over 650^{o}C. Canadian researchers (20) noticing the embrittlement in a C/Mn/Nb/V steel Sub critical HAZ, considered that the A_1 temperature must have been exceeded, and that the former pearlite bands transformed into Martensitic-Austenitic (M-A) brittle structures during the rapid cooling of the weld process employed.

2.4 Coarse Grained HAZ Embrittlement

When HSLA microalloyed steels are welded by means of high heat input processes, it has been widely reported in the literature, as it will be later specified, that embrittlement occurs in the coarse grained region of the HAZ.

During the welding heating cycle, high temperatures are attained and the microalloying elements go into solution in the austenitic phase, allowing the grain to coarsen. As no recrystallisation is forced to occur during the cooling cycle, the grain size will remain coarse. The registered embrittlement is mainly explained by two theories :

a) Structural change theory : Remaining in solution the microaddition elements, notably the Nb, lower the temperature of the $\gamma \rightarrow \alpha$ transformation, thus increasing the hardenability of the steel. As a result, coarse grained upper bainitic structure will normally be produced.

b) Precipitation theory : At the transformation interface $\gamma \rightarrow \alpha$, the microalloying elements that were in solution at higher temperatures will precipitate. This provokes second phase hardening in a structure already composed of large grains.

Before embarking into a deeper explanation and the outlining of illustrations of the theories, comments will be made, first, on the tests and methods currently employed in order to facilitate an evaluation of the results.

2.4.1 Test Procedures

The toughness test to be chosen when trying to quantify the HAZ toughness of the materials under a certain welding condition, will be primarily based on the specifications of the engineering design criteria, rather than on the testing philosophy of the laboratory team.

The existing toughness tests are many, and amongst them, two are of particular importance :

- Charpy V Notch Impact Test
- Crack Opening Displacement Test

2.4.1.1 Charpy V Notch Impact Testing

It is the classical resilience test and is relatively easy to perform. It is based on a crack initiation and propagation from a standard notch acting as a strain concentrator when a specific amount of kinetic energy is supplied to the specimen. The measured absorbed energy to fracture the specimen at several test temperatures, will permit the estimation of the impact transition temperature of the material. This is the temperature at which the material changes its mode of fracture from predominantly brittle to predominantly ductile. Another popular immediate interpretation is known as the Fracture Appearance Transition Temperature, meaning the temperature at which the fractured surface exhibits 50% brittle fracture and 50% ductile fracture. This type of test is described in the ASTM no. A 370 (21).

2.4.1.2 Crack Opening Displacement - COD - Tests

These tests represent a modern and more realistic approach to situations where the structures are under nominal static loading. They derive from the concepts of fracture toughness as they are an extension of the Linear Elastic Fracture Mechanics, into situations where a significant yielding occurs. The COD is represented by the symbol δ, i.e. the displacement at the ends of a defect normal to the crack faces when a stress is applied to the material in which the defect lies. The displacement leading to the propagation of the fracture is known as the critical COD, and represented by the symbol δ_c. This situation can be simulated in the laboratory using single-edge-notched specimen loaded either in tension or in three-point-bending, and plotting the load versus crack opening. The latter is not measured directly, but assessed by monitoring the displacement of two knife edges at the top of the notch using a clip gauge. δ_c is then obtained by conversion of the clip gauge displacement at fracture using a previously determined calibration. If δ_c and the relevant applied strain are known, the critical crack size $\bar{a}$ can be determined by calculation. Made simple, this test indicates the tendency of a crack to propagate at a certain test temperature under a certain load. Similarly to the Charpy V Notch Tests, the COD exhibits a transitional behaviour with temperature. That characteristic is in these tests, thickness dependent. Thick materials will show a higher transition range and lower COD values than thin materials (22). These tests are the concern of the British CODA P54 (23).

2.1.4.3 Charpy Vs COD

The main criteria designs specified for toughness, nowadays, are still governed by the initiation and propagation of the fracture. Consequently they favour the Charpy Impact tests as opposed to the COD tests. Structural steels behave in a brittle way when dynamically loaded, but in most engineering structures the loading conditions are essentially static. Thus, a design philosophy based on a non-initiation criteria could prove to be more economical (24, 25).

The Charpy test is very popular in pipeline engineering, due to its low cost and simplicity of interpretation (3, 26), though Preston (1) mentioned that, for High Strength Pipeline, it is common practice to design against fracture propagation, rather than initiation. The wide use of Charpy test has also been reported in the Pressure Vessel Industry (27). Bernard (28) defends that type of test as the most practical engineering approach for toughness evaluation in welded joints nowadays, but foresees that in the near future design requirements are likely to be expressed in terms of fracture mechanics parameters (29).

The British Welding Institute is one of the leaders in supporting the popularity of the COD tests (22), and outlines as a further advantage for the test data, the assessment of defect significance in the welded structures (30).

Bonomo and Rothwell (31) observed a considerable difference between the tendencies of the results of Charpy and COD tests, and though they have recommended the use of Fracture

Mechanics techniques, they have outlined that Charpy tests would be a useful way to compare different materials.

It will be of value to mention now that no direct correlation exists between COD results and weld failures (6). Also, there is no test unequivocally valid for defining the toughness of a welded joint completely, i.e. in the presence of services stresses and residual stresses (32).

2.4.2 Choice Of Test Specimens

After deciding on the testing techniques to be used, difficulties will be faced when trying to evaluate the toughness of the weld HAZ, i.e. where and how accurately to locate the stress concentration element within the narrow region of interest (3, 28). Another difficulty is concerned with the hetereogeneity of the zones that will be present along the crack path, due to the HAZ profile (32).

The problem can be approached by two ways, involving :

a) Actual weldment HAZ specimens, when the test pieces are extracted from a real weld.

b) Simulated HAZ specimens, when by special techniques the parts undergo a thermal cycle to represent in a reasonable band the narrow HAZ regions observed in practice.

2.4.2.1 Actual Welding Specimens

Some authors defend the use of COD type tests on real weld HAZ as the better approach to the practical conditions (17, 22, 30, 31, 32).

Sawhill and Wada (34) observed that when the notch tip was contained in 50% of the Weld Metal and 50% of the HAZ of a double side, one pass per side welded joint, the toughness of the coarse grained HAZ governed the energy absorption in the Charpy tests. They concluded that the 50/50 notch position adequately represented the lowest toughness in the HAZ of practical pipeline welds. This criteria has been adopted elsewhere (35, 36), whereas Bernard (28), in a similar type of joint, placed the notch in a 50/50 position as well, but only containing the second pass, non-refined HAZ.

The use of special shape edges such as square cut with backing strip (34), or K preparation (37), will provide a multipass weldment with an almost planar HAZ region. The use of a high heat input process would also exhibit a planar HAZ on a one side welding procedure (28). The advantage of a planar HAZ is to provide a homogeneous region for the fracture propagation.

Dolby (38) studying the influence of defect orientation by COD tests, concluded that the measured fracture toughness of HAZ regions was found to depend on the orientation of the specimen notch in relation to the fusion boundary, and on the direction of the initiation of the fracture. He recommended that the notch, where possible, should simulate the orientation of typical HAZ defects with respect to the fusion boundary.

2.4.2.2 Simulated Specimens

To overcome the problem of the location of the crack in a specific HAZ region, as well as to allow the fracture to propogate in a homogeneous zone, Savage and Nippes (39) designed the original model of the Welding Simulator, i.e. an equipment permitting a pre-stablished thermal cycle to be imposed on a specimen, thus duplicating a zone similar to the real one of interest, but with expanded dimensions.

Nowadays these equipment possess facilities to superimpose stresses on the test piece during the simulation cycle, and to provide recording of the duplicating specimens dilation behaviour. Thus, some authors have applied stresses to the samples, during simulation, but little or no influence of this effect on the subsequent toughness tests was noticed (14, 40, 41).

2.4.2.3 Actual Vs Simulated Specimens

The two types of specimens mentioned above are widely used, depending on the philosophy of the research centres.

The British Welding Institute at first took interest in Welding Simulation, even promoting a Seminar to discuss the subject (42). At the time, the only limitation presented was that the exact reproduction of an actual thermocycle would not always produce an identical austenitic grain size for the simulated and real HAZ. Due to the absence of steep temperature gradients, which would limit the size of the coarsened region of an actual HAZ, consequently limiting its grain size, the simulated HAZ would exhibit larger

austenitic grain size. Nevertheless, that would be easily overcome by lowering the peak temperature of the simulating thermal cycle (43). That practice found support elsewhere (44), but their approach changed and is summarised in a recent paper highlighting the importance of performing tests on real weldment specimens (30).

A certain number of authors (13, 14, 18, 25, 28, 35) have no restrictions to the use of simulated specimens, mentioning that a region similar to the weld HAZ can be duplicated with a small amount of material. It has been reported that due to severity of notch positioning, thermal simulated specimens produces poor toughness results if compared to real weld HAZ specimens (28, 45, 46).

2.4.3 Determination Of A Welding Thermal Cycle

In order to simulate a specimen, the real weld thermal cycle which is attempted to be duplicated must be known, and there are two ways of solving this problem :

a) Local thermal cycles measurement by means of thermocouples embedded in the plate to be welded.

b) Theoretical calculations based on heat flow equations.

2.4.3.1 Actual Thermal Cycle Measurement

This is accomplished by insertion of thermocouples inside holes drilled in the plate to be welded, whose weld bead profile is known beforehand. After the weld is performed, the actual thermal cycle will be registered on a X-t graph plotter where the cold junction of a specific thermocouple

was connected previously. The plate is then sectioned and the position of the hot junction to the fusion line is measured (18, 47).

2.4.3.2 Theoretical Calculations For The Welding Thermal Cycle

These are based on the Heat Flow theory and the pioneer work in the area belongs to Rosenthal (48). Simplifications and new approaches are known (49, 50), and the use of finite element methods associated with computer calculations has improved the results (51).

Recently the British Welding Institute has launched a research programme to study the Arc Energy and the Weld Thermal Cycles in the Submerged Arc Welding (SAW) process, and the resulting paper (47) reviews some nomograms to predict the parameters proposed to define a welding thermal cycle. Similar nomograms can be currently found in the literature (28).

Now an explanation of the nature of the above mentioned proposed parameters is necessary. When a weld is performed, the cooling cycle will be of vital importance in controlling the structural changes and reactions which will occur in the former parent metal. If one specifies the heat input supplied to a plate without mentioning the joint geometry, the existence or not of a preheating temperature and the plate thickness, that information will be incomplete. Furthermore, in practice the cooling cycle is used on a quantitative basis, thus a parameter becomes necessary to

express it and among the ones proposed, as reviewed by Kohno and Jones (47), the most acclaimed was the cooling time between 800 and 500°C. This is the range of temperatures where the most important structural changes are believed to occur. It is represented by $\Delta t_{800-500}$ and sometimes by Δt. In the present work the last notation will be adopted.

2.4.4 The Concept Of Deterioration

When discussing the effects of an element on the weld HAZ, a comparative basis must be established, and that leads to the exact definition of deterioration.

For a specific steel, the toughness deterioration of a region of the weld HAZ has been compared to :

i) The parent metal.

ii) Another region of the HAZ.

iii) Another steel presenting the same C/Mn content or not, plus different microalloying additions or levels.

iv) Another steel with the same C/Mn levels, but no microalloying, known as the reference or base steel.

v) An identical region of the HAZ, but welded at a different heat input.

At the moment, while quantifying heat input, the nomenclature is confusing. Care also must be taken when reviewing the subject since sometimes, what may appear to be a totally controversial result for similar steels, would probably represent differences in testing practice or

deterioration approach. Unfortunately the ways of obtaining and presenting the results are so many, that comparisons on unified ground become very difficult, if not speculative.

2.4.5 Elements Influencing The HAZ Toughness

Some of the elements present in a steel are more effective than others in influencing the transformation temperature of the $\gamma \rightarrow \alpha$ reaction, or in promoting solid solution or secondary precipitation hardening. They can be added to the steel during processing, or they are inherent in the production method employed. The elements to be discussed will be those known to play an important part on the weld HAZ toughness of the steels, and they are C, N, Al, Nb, V and Ti.

Nb and V are the main concern of the present work, and will be reviewed under a more conceptual point of view, i.e. on their capabilities to influence a structural change or to precipitate. A more quantitative point of view will be adopted when the current results are analysed.

Steels of the family C/Mn/Mo are not of primary interest in this research, but they will be mentioned whenever considered illustrative. In addition, steels microalloyed with Ti will be considered as the modern approach for the problem.

2.4.5.1 Carbon

The influence of carbon on the weldability at heat inputs that will produce martensitic products in the HAZ is well documented. It is unavoidably connected with the concepts

of Hydrogen Embrittlement, and the authors conclude that the lower the carbon content, the higher the chances of a HAZ of high toughness (11, 17, 52, 54).

At the BWI (22), 1.0KJ/mm heat input welding beads were deposited on two C/Mn steel plates, 3.8mm thick, and the HAZ was COD tested. The carbon content of the steels was 0.14 and 0.17%C, respectively, and when the toughness values of the HAZ were compared to the toughness values of the parent metal, it was seen that, whereas the steel of lower carbon content showed no deterioration, the other one was embrittled The author observed that the steel containing 0.14%C had an upper bainitic and finer pearlitic structure, whilst the 0.17%C steel consisted of a mixed lower bainitic and martensitic structure, which had much less resistance to cleavage than the former one.

For two C/Mn steels of similar composition and carbon level of 0.18%, Bernard (28) plotted a curve of the influence of the heat input on the Charpy Impact Transition Temperature. The specimens were weld simulated and the best toughness conditions were obtained for $\Delta t = 5s$. The worse results appeared at cooling times Δt in excess of 10s. The author remarked that the optimum microstructure corresponded to lower bainite, in spite of occasional martensite pools. The poor results corresponded to coarse upper bainite or grossly acicular ferritic-carbidic decomposition products. If one compares the micrography of the poor structure of the former work with the one from the best structure for the latter work, one will not notice much difference and, given

the similarity of the steels composition, their opposite conclusions may lead to some confusion.

In a review paper Hart (54) superimposed on a known C/Mn/V Swedish curve (55), points from another graph for a similar steel, simulated and Charpy tested under the same conditions but containing a lower carbon level (25). The carbon levels were 0.15 and 0.13%C respectively, and the curve can be seen from Fig. 1. Hart uses the best results of the second work to show the beneficial effect of lower carbon levels on the HAZ toughness of V microalloyed steels.

Signes and Baker (36) employed Charpy tests using the 50/50 criteria on real weldments of several C/Mn steels. They possessed 0.08, 0.013 and 0.018%C, 0.10, 0.05%V and no V additions. The heat input was equivalent to a Δt = 25s, and the authors concluded that for C, Mn, V steels, the lower the C content, the lower the toughness. Taking into account that one of the heat inputs seen from Hart's superimposition of results was Δt = 33s, one observes that his conclusions are opposing the ones from this last work.

Signes and Baker for the same reference levels of carbon, prepared a combination of C/Mn/Nb steels with two levels of Nb: 0.03 and 0.06%Nb and welded and tested then as they did for the V steels. Here they observed better toughness at lower C levels. Schoffield and Weiner (44) studied C/Mn steels microalloyed with Nb and/or V simulated to a heat input equivalent to Δt = 70s, and Charpy Impact tested. They observed that there appeared to be no correlation

between the HAZ coarse grained region toughness of the individual steels studied and their carbon contents. The range of the C composition for their steels was between 0.11 and 0.23%C.

Bernard (29) is of a different opinion; he studied C/Mn/Nb steels in both simulated and real welding conditions, varying heat inputs up to Δt = 100s and using Charpy Impact testing to measure a deterioration relative to the reference steel. He concluded that the carbon content plays a most important role on the toughness of the HAZ.

2.4.5.2 Nitrogen

This element is present in the parent metal or in the HAZ in two forms: the first is a mobile (interstitial or free) form and the second is a combined form, as nitrides or carbonitrides. The total amount of nitrogen will be the sum of these two forms. In its mobile form it has been reported as hazardous to the fracture toughness properties of the steel (5, 29).

Combined nitrogen originally from the parent plate would be liberated to its interstitial form as the result of the dissolution of nitrides or carbonitrides caused by the welding heating cycle. This was, in fact, observed by Dolby (56) for Electroslag welding process when working with C/Mn/Al and C/Mn/Al/Nb steels. The same conclusion was reached by Greday et al (53) for lower heat input processes (Δt = 5 and 12s), when simulating manual arc and semi-automatic arc welding for C/Mn/Nb/V steels. They have stated that the

decrease in impact strength and that the increase in hardness observed in higher nitrogen steels originate partly from the freeing of nitrogen by nitride dissolution.

Hannerz (14) observed an increase in the Charpy transition temperature of simulated HAZ of a 0.20%C, 0.82%Mn steel when the nitrogen level was increased from 0.005 to 0.015 and to 0.020%N. Two levels of weld energy were used and referred to as low and high (no figures have been associated with these energy levels. Presumably they would be equivalent to Δt = 30s and Δt = 100s, common heat inputs used by this author). The observed deterioration was more evident at the low heat input HAZ simulations. As it can be seen from the Fig. 1, when testing in a similar way the simulated HAZs of two C/Mn/V steels presenting respectively 0.05 and 0.013%N, cycled to identical heat inputs of the order of Δt = 33, 100 and 300s, the same author (55) would find no changes due to the difference in nitrogen content. It was explained that the influence of the remaining free nitrogen level or toughness is minor if compared to that of the VN precipitation.

For low carbon Mn/Mo/Nb steels simulated to correspond to a weld heat input of Δt = 29s and Charpy tested, the toughness of the HAZ was impaired when the nitrogen level was increased from 0.005 to 0.010%N (13); the authors mentioned also that the effect of nitrogen Mn/Mo/Nb/V steels parallels the effect for the Mn/Mo/Nb steels.

The BWI opinion on the subject is that if the problem occurs, it is most likely to be seen for steels with a higher nitrogen level, e.g. 0.015 - 0.020%N.

Finally, it will be mentioned that the interstitial nitrogen level is also given account as one of the possible factors responsible for the sub critical HAZ embrittlement by mechanisms of strain ageing (30, 57).

2.4.5.3 Aluminium

This element is incorporated into the parent plate during manufacture processes, and combines with the free nitrogen forming the aluminium nitride (AlN) which will hinder austenite grain growth. These two actions will improve the toughness.

During a welding process the AlN will dissolve easily: the HAZ grain size at the boundaries with the fusion zone will coarsen, and there will be a higher content of interstitial nitrogen (14, 56).

There is no evidence of aluminium embrittlement effect by precipitation of AlN in the HAZ and Dolby (56) recommended the use of Al treated steels for the following reasons :

i) Structures with a finer grain size at regions where the AlN dissolution temperature has not been attained.

ii) For some welding conditions not all the AlN will go into solution, then the free nitrogen will be less than if Al was not present.

2.4.6 Mechanisms of Nb, Ti and V and Their Influence On The HAZ

It has been mentioned previously that during a welding thermal cycle, the microalloying elements Nb and V will dissolve in the austenitic phase, allowing the grains to grow. The extent of that dissolution and growth will depend on the peak temperature reached, as well as on the temperature gradient present in the HAZ. An attempt to quantify heat inputs involved some controversy, since there are no precise figures associated with the nomenclature low and high heat input. Dolby (7) quotes as slow cooling rates those for $\Delta t > 30s$. Sawhill et al (13) considered welds of moderately high heat inputs the ones exhibiting $25s < \Delta t < 100s$, and Tichauer (3) called high heat inputs associated with SAW those of 2.4 to 4.0KJ/mm. In the actual review, the boundary between low and high weld energy was considered $\Delta t = 25s$.

When the welding heat input supplied to the plate is not very high, the residence time at high temperatures will not be a long one, and a steep temperature gradient will assist the cooling cycle, both factors limiting the austenitic grain size growth (43, 58). If a high energy process is employed, longer time at higher temperatures and smooth temperature gradients in the HAZ will allow the austenitic grain size to coarsen.

The structural changes that Nb and V can provoke in the coarse austenite on cooling, or their ability to precipitate in the newly formed ferritic phase, will be discussed later. It will be preceded by some information on the dissolution of these

elements due to the high temperatures of the welding heating cycle. Titanium microaddition, the new approach to the problem, will also be mentioned, separately.

2.4.6.1 Dissolution Of Nb And V In The Austenite

Dissolution is a function not only of the temperature attained during the welding heating cycle, but also of the composition of the steel. Several formulas, tables and nomograms exist in the current literature to predict the dissolution temperature of a carbide, nitride or carbonitride (5, 14, 59, 60).

Bernard (28) and Hannerz (14) comment that the dissolution process should be time dependent, but that it happens virtually instantaneously as soon as the dissolution temperature is attained, whereas other authors (6, 61) observed that dissolution rates are dependent on peak temperature and time.

Niobium precipitates are reported to be more stable than the vanadium ones (5, 14, 53), and dissolution ranges for NbC are quoted as 1150 to 1350^{o}C, depending on the Nb content (14). A CRM ("Centre de Recherches Metallurgique - Belgium) report established as 1100 to 1150^{o}C the dissolution range for the Nb (CN) of a 0.17%C, 0.02%Nb and 0.007%N, and for a 0.15%C, 0.084%V and 0.0152%N steel quoted the complete dissolution of the VN in the vicinity of 950^{o}C (53).

2.4.6.2 The Influence Of Nb And V On The Structural Changes

The structural theory states that the major cause for the toughness deterioration should be attributed to the formation of a structure of poor properties, as a result of the steel composition and the welding cooling cycle inherent in the process employed.

Microalloyed steels, particularly those containing niobium, when welded at high heat inputs will tend to exhibit a considerably amount of upper bainite (UB) within the coarse grained structure. This constituent is known to be particularly harmful to the toughness properties (24, 29, 30, 54).

Usually Nb is regarded as depressing the austenite transformation temperature, repressing the formation of proeutectoid ferrite (PEF) and favouring the appearance of upper bainitic structures (6, 33, 35, 40, 54, 56). A few authors, however, produced micrographs of Nb microalloyed steels where PEF is seen surrounding the UB colonies (29, 61). It will be of interest to point out that the welding simulation conditions used in these cases are very similar to the simulations or actual weldments performed by the authors that found little or no PEF delineating the prior austenite grain boundaries.

Schoffield and Weiner (44) referring to a V microalloyed steel where, by simulation techniques, a significant amount of PEF was observed, concluded that the V remaining in solution affects the transformation temperature of the austenite. The effect is to retard the transformation to

bainite. A similar trend was observed by a Canadian Research Centre (61).

For a constant carbon content Signes and Baker (36) found little influence on Nb and V levels on the microstructure of a weld HAZ, whilst Sawhill et al (13) investigating Mn/Mo/Nb steels did not find any significant change in the microstructure due to Nb additions. Swedish authors (14, 55) studying V alloyed steels stated that V additions up to 0.35% did not significantly affect the optical metallographic structures of the weld HAZ.

A good example of the complexity of influence of microalloying elements on the microstructure of the weld HAZ can be seen from the micrographs of a recent work performed at the CANMET (61) to simulate heat inputs of the order of Δt = 100s. A C/Mn and two C/Mn/Mo steels microalloyed with 0.034%Nb failed to show any PEF at the former austenite grain boundaries; two C/Mn steels with respective additions of 0.09 and 0.14%Nb, and a C/Mn steels containing 0.042%Nb and 0.09%V exhibited a thin layer of PEF delineating the grain boundaries, whereas a plain C/Mn steel and a C/Mn steel microalloyed with 0.09%V exhibited a higher amount of that constituent.

The CANMET researchers concluded their microstructural observations stating that, (i) Nb has little effect on the major transformation product, but tends to encourage the retention of martensite-austenite (M-A), (ii) V promotes the formation of a more randomly oriented bainitic ferrite at slow cooling rates and (iii) Mo eliminates the formation of grain boundary ferrite and promotes the retention of M-A.

It is of interest to point out that the steel containing the lowest amount of Nb does not exhibit PEF, whilst the other two with a higher Nb level exhibit some of that constituent.

Some authors parallel the effects of microalloying elements in the fusion metal with those in the coarse grained HAZ, thus Levine and Hill (62) reviewing the subject, commented that for weld metal at low Nb levels, the deteriorating influence of this element may not be observed, since it appears to at first reduce the amount of grain boundary ferrite before extension growth of UB and M-A occurs. This could explain why no PEF is seen in the lower Nb content steel of the former work, but what explanation would exist for the "re-appearance" of the constituent at higher Nb levels?

2.4.6.3 The Influence Of Nb And V On The Precipitation Hardening

As it has been mentioned previously, one of the theories attributes the loss of toughness on the weld HAZ to the re-precipitation of Nb and V causing second phase embrittlement. The chief supporters of the theory come from Sweden and so far they have failed to produce evidence of Nb (14) or V (55) precipitation in the as welded state. Nb and V precipitates were observed by thin foil - Transmission Electron Microscope techniques after heat treatments of 32 hours at 610^{o}C and 2 hours at 620^{o}C respectively. The authors explained that in the as welded condition, the precipitates were too small to be resolved by their TEM, so they were heat treatment coarsened until an adequate resolution size. Levine and Hill

(62) reviewing the Swedish papers observed that the little change in their simulated HAZ hardness data appears to contradict the precipitation argument proposed, unless compensating structural changes were masking the precipitation hardening increment. Some other authors could not detect Nb or V precipitates via thin foil techniques (33, 36, 54, 56) nor using carbon extraction replicas (36, 63).

Using secondary ion probe analysis, Bernard et al (29) observed experimentally the precipitation of Nb in the HAZ of a 20mm thick C/Mn/0.035%Nb plates welded at two energy levels, namely 3.0 and 7.0KJ/mm. They concluded that microstructural changes were the main parameters affecting the impact toughness of the HAZ, but remarked that precipitation effects need to be considered, together with microstructural features, for assessing the overall effect of Nb and V.

A recent paper received from Canada (61) presents evidence of Nb and V precipitation for several microalloyed steels by means of carbon extraction replica. They claim their success to the longer etching time of their samples as opposed to the normally recommended light etching technique (64). It was observed that the weld HAZ toughness is a complicated function of many microstructural variables, but that for cooling times in excess of $\Delta t = 40s$, precipitation hardening due to microalloying elements does contribute to a deterioration in toughness. However, the effect appears to be small in the as welded condition. In a way, that conclusion is somewhat similar to the one reached by Bernard et al (29).

One of the points the Swedes (14, 55) use to stress the precipitation theory is in the explanation of the known phenomena of toughness deterioration with the increase of the welding cooling time, since longer cooling times permit a more complete precipitation of carbonitrides. This seems to be in contradiction to the results of the CANMET report (61) since at least half of the steels studied exhibited a maximum deterioration for cooling times Δt = 80s, recovering slightly at cooling times Δt = 160s. Unfortunately, these authors did not comment on the fact.

Sawhill et al (13) studying Mn/Mo/Nb steels and using Start of Transformation Temperature concepts, stated that precipitation should not occur during continuous cooling if the Bainite Start Transformation Temperature is below 620^{o}C. They deduced that for a weld simulating cooling times of the order of Δt = 29 and 91s, which were employed in the work, Nb (CN) was unlikely to precipitate. On the CANMET report (61) it is commented that as the rate of Nb precipitation is very slow in the ferrite at temperatures below 600^{o}C, and since for one of the cooling times employed, Δt = 16s, the Start of Temperature Transformation was reduced to 580^{o}C, no precipitation should be expected for heat inputs of that value. Constant et al (65) suggest a critical cooling rate Δt = 50s for the precipitation of NbC in a C/Mn steel containing 0.05%Nb and simulated at a peak temperature of 1300^{o}C. The association of precipitation of microalloying elements with a critical cooling rate, consequently with the start of the Transformation Temperature, is explained on the basis of the most accepted model for precipitation proposed by Gray

and Yeo (66). They stated that precipitation takes place during the growth of α grains into the γ grains, thus depending on the $\gamma \rightarrow \alpha$ start of transformation temperature.

2.4.6.4 Ti, A Modern Approach

A recent trend amongst the microalloying steels is the use of small amounts of Ti and the fact has been acknowledged by a considerable number of authors that usually refer to Japanese sources of information (67, 68, 69, 70). It is accepted that Ti combines with N forming a very stable nitride, capable of remaining undissolved during almost all the range of the high temperatures of the welding heating cycle where Nb and V would have dissolved into solution. In this way the austenitic grain growth is limited and a finer grained HAZ of high toughness is obtained.

The leading work in the area belongs to Kanazawa et al (71) and consists of a comprehensive analytical study of the effect of TiN on the toughness of the fusion zone (which he denotes as the boundary zone between the weld metal and the coarse grained region), and its physico-metallurgical mechanism. In their work they have used both simulated and actual weldment samples, Charpy and COD tests. The main conclusions have been that a marked improvement in the toughness of the fusion zone of a weldment made by large heat input, one pass welding process, has been accomplished through a refinement of the fusion zone microstructure. This is caused by the fine TiN precipitates favouring fine pearlite structures formation instead of the coarse, brittle intermediate stage structures. At peak temperatures of the

order of 1400°C, the austenite grain diameter is a function of the precipitate fraction and size, i.e. the more TiN precipitates smaller than 0.05μ remained undissolved at 1400°C, the more refined become the austenite grains. Besides the austenite grain growth inhibition effect, fine TiN precipitates were found to stimulate polygonal ferrite nuclei on cooling, exhibiting as a final product a more refined, tougher structure than the intermediate transformation products. These tough ferrite pearlite structures resemble the ones other authors named interlocking acicular ferrite (72). It is not known here if there is the case of a duality in the nomenclature, or of a misinterpretation caused by comparative observations based on small micrographic reproductions.

Sawhill et al (13) also studied Ti microalloyed steels, but their reference steel contained 0.20 and 0.30%Mo. The results from his work are in agreement with the ones above mentioned. They have observed as well that Ti did not consistently improve the toughness of the specimens simulated at Δt = 29s, whereas at Δt = 91s that improvement was significant. It was mentioned that the Ti level should be kept below the stoichiometry of TiN. If it goes above that value, precipitate coarsening may occur with consequent loss in the grain boundary pinning. Also, it could provoke TiC precipitation embrittling the matrix. The use of Nb and Ti microalloyed steels is thus not recommended since Nb combining with N will increase the effective Ti/N ratio.

2.4.7 Influence Of The Parent Plate Fabrication Process

Authors have a divided opinion on the influence or not of the thermal processing history of the plate on the HAZ toughness. So, Bernard (28), Greday et al (53), Dolby and Saunders (17) and Meyer and Boer (73) tend to think that the processing parameters used in manufacturing the base metal have practically no effect on the local HAZ toughness. Gray (6) and Sawhill et al (13) stated that is is difficult to predict or generalise the role of Nb affecting the HAZ toughness for steels that were processed by different methods. Both authors did not indicate in which way the original condition of the base metal would influence the toughness of the HAZ. Italian authors (26) believe that a small initial ferritic grain size of the base metal will, to a certain extent, limit the austenitic grain resulting from a high rate heating. Japanese authors (74) observed that the process of formation of austenitic grains at high heating cycles is dependent on the initial microstructure of the base metal. They performed tests on ferrite-pearlite structures, martensite structures and tempered martensite structures. There was a variation of the final grain size with the original grain size and structure, but only for temperatures up to 1200^{o}C. For temperatures above the latter, the grain sizes tended to have similar values for the peak temperature considered, disregarding the original conditions. The exception was registered for martensitic structures, mainly those which had coarse (0.38mm) original grain size. The latter tended to provide larger grain sizes than the ones seen for the other structures studied, even at temperatures as high as 1350^{o}C.

2.4.8 Current Results On The HAZ Toughness Of The C/Mn Microalloyed Steels

Some of the existing data will be reviewed to show the overall influence of the welding thermal cycle and microalloying levels on the C/Mn steels in a comparative basis. The behaviour of plain C/Mn steels will be commented on because sometimes they are used as reference materials. The microalloyed steels will be rated in two groups :

i) Those with carbon content under 0.10%C.

ii) Those with carbon content in excess of 0.10%C.

Steels containing Mo will be mentioned whenever considered illustrative, and Ti as a microalloying element will deserve more than a comment. Finally, a general picture of the problem will be attempted.

2.4.8.1 C/Mn Steels

Dolby (30) studied two C/Mn steels with the following compositions: 0.16%C, 1.30%Mn and 0.17%C, 1.10%Mn. The welding was performed with heat inputs ranging from 1KJ/mm up to 25KJ/mm on plates 25mm thick, and the coarsened HAZ was COD tested. The toughness was considered good in the heat input range of 3.0KJ/mm to 7KJ/mm and was considered low outside these values, as seen from figure 2. The author seeking support for his findings mentioned the work by Ivens and Bergh (75) where no need for HAZ Charpy Impact testing is proposed if the cooling time Δt lays in the range of 5 to 40s. Thus, at these heat inputs the HAZ performance presents no problems. Furthermore, for the same reason, a HAZ of good toughness is also expected in the range of Δt from 40 to 125s. In this latter case, to be on the safe

side, Charpy testing should be advised (the authors were referring to C/Mn steels generally and no specific composition was given). Remarking that such a good performance is not always observed, the former author also presented in the graph of figure 2, the results for a 0.24%C, 0.7%Mn steel which exhibits a marked deterioration relatively to the other C/Mn steels.

Banks (76) COD testing 0.16%C, 0.80%Mn, 25mm thick plates at several heat inputs observed an increasing embrittlement in the order 3.6, 1.8, base metal, 5.4 and 40KJ/mm. When testing a steel with 0.17%C, 0.99%Mn, the embrittlement increased in the order: base metal, 2.7 and 7.4KJ/mm. The author concluded that for these steels the toughness was a function of the heat input supplied. Bonomo and Rothwell (25) simulated a 0.18%C, 1.18%Mn steel at several heat inputs, equivalent to Δt cooling times up to 100s. Their Charpy Transition Temperature curve shows that an initial deterioration occurs up to Δt = 5s, tending to remain stable as the heat input is increased in excess of this amount. Bernard (28) studying the Charpy Impact toughness of a 0.18%C, 1.40%Mn, simulated to correspond to a range of weld heat inputs observed a maximum toughness at Δt = 5s. The deterioration increased up to Δt = 10s. He also observed a stabilisation of the toughness showing signs of slight recovery as the heat input was increased to about Δt = 100s. These results are in a fairly good agreement with those from Bonomo and Rothwell, though the latter exhibited better toughness levels than the former. The work by Dolby appears to be in disagreement with these last two, and taking into account that these used simulation and Charpy, whilst the former used real weld-

ments and COD, one must ask how far can the laboratory processes employed influence the results.

2.4.8.2 C/Mn/Nb Steels - C $<$ 0.10%

Kaae and Bailey (37) studied two steels 0.04 and 0.07%C containing the same amount of Mn and Nb equivalent to 1.45% and 0.024%, respectively. Charpy Impact tests were obtained from planar HAZ at three weld energy levels : 0.08, 6.7 and 80.0KJ/mm performed on plates 25mm thick. A similar or better toughness than the one of the base metal was observed for the two lowest heat inputs, whilst the higher heat input exhibited a noticeable deterioration. Levine and Hill (77) tested a reference 0.09%C, 1.7%Mn steel and another one containing 0.10%Nb. The welds were performed on a double V edge preparation, one pass on each side and the notch of the 2/3 of the real size Charpy specimens was placed at the non-refined, coarse grained HAZ of the second pass. The heat input used was equivalent to a cooling time of Δt = 30s. Within the scatter band of the results presented, the authors noticed no difference in the behaviour of the two steels. A recent paper by Signes and Baker (36) deals with a steel containing basically 0.08%C, 1.40%Mn to which 0.03, 0.06, 0.12 and 0.15%Nb have been added. The plates were welded as in the previous paper at a heat input equivalent to Δt = 25s and Charpy tested at a 50/50 position. The results for the base metal were always better than for the HAZ. The steels containing 0.06 and 0.12%Nb exhibited the higher toughness, if compared to the other two, for both base metal and HAZ. Graville and Rothwell (78) studied a base 0.09%C, 1.30%Mn steel with three levels of Nb additions : 0.034, 0.09 and

0.14%, respectively. Instrumented Charpy Impact tests were performed in samples welded at heat inputs equivalent to cooling times Δt of 6.5, 16, 39 and 160s. The results have shown that at the longest cooling time there appears to be a detrimental effect of the Nb on the toughness; this effect was not observed in the Δt = 39s cooling time. At the two faster cooling times an improvement in toughness was observed, at least at Nb levels lower than 0.10%Nb. Cordea used a table of an unpublished work (79) to illustrate the deterioration of the HAZ toughness of 0.08%C; 1.5%Mn; 0.05%Nb steel plates, 32mm thick, with the increase in heat input. The toughness of the HAZ matched that from the base metal when the heat input was 1.6KJ/mm (Δt = 10s). At higher heat inputs of 4.8 and 25KJ/mm (roughly equivalent to Δt of 30 and 300s), strong embrittlement was observed. All the samples were Charpy tested.

Hannerz (14) tested a 0.03%C, 2.03%Mn basic steel containing additions of up to 0.30%Nb. The Charpy Impact results obtained for simulated HAZ at four different cooling times equivalent to Δt of 10, 33, 100 and 300s were compared not only to the reference steel, but also to the base metal of each of the combinations. From the graph in the Fig. 3, it is seen that the base metals always exhibited better toughness than their equivalent HAZ at any heat input level. If the comparison is based on the reference steel, it was observed that :

i) Δt = 10s: the transition temperature is practically independent of the Nb additions.

ii) Δt = 33 and 100s: both cooling times exhibited similar deterioration and the level of deterioration increases with the level of Nb.

iii) Δt = 300s: the most embrittled condition of all and the toughness also decreases with increasing Nb content.

From the experiences listed above, a tendency emerges in the sense that low heat inputs on low Nb levels will even be beneficial, whereas higher Nb levels allied to higher heat inputs seem to bring a detrimental effect.

2.4.8.3 C/Mn/Nb Steels - C $>$ 0.10%

Bonomo and Rothwell (25) compared a 0.17%C, 1.20%Mn, 0.05%Nb steel to a C/Mn steel of similar, but non identical composition. The specimens simulated at several heat inputs up to a cooling time equivalent to Δt = 100s were Charpy Impact tested. The authors found that for heat inputs lower than Δt = 8s, the Nb steel exhibited better results than the C/Mn steel, whereas for cooling times Δt in excess of 8 s a toughness deterioration was observed, increasing with the increase in heat input. Hannerz (14) compared a reference steel having 0.19%C, 1.33%Mn with other steels with increasing Nb content. The simulated specimens equivalent to cooling times Δt of 33 and 300s were Charpy Impact tested, similar deterioration was observed for both heat inputs, at Nb contents up to 0.02%Nb. From this value upwards, up to 0.11%Nb, the higher heat input deterioration increased with increasing Nb content, whereas for the low heat input, the deterioration became stable at Nb levels in excess of 0.05%Nb. Signes and Baker (36) studied some combinations

of C/Mn steels containing 0.13 or 0.18%C, 1.40%Mn and 0.03 or 0.06%Nb. The specimens were welded at a heat input equivalent to Δt = 25s and were Charpy Impact tested. At carbon levels of 0.13%C, the toughness passed a minimum at approximately 0.03%Nb, whilst for the higher carbon level the toughness decreased with increasing Nb additions. Bernard (28) has shown a curve which is reproduced in the Fig. 4, concerning the comparison of a reference steel with a Nb steel. The compositions were 0.18%C, 1.35%Mn and 0.035% Nb. There is a noticeable deterioration on the Charpy Impact Transition Temperature of the two steels, with increasing heat input, denoting that the effect of the Nb addition to the basic steel is very small even for simulated thermal cycles at heat inputs in excess of Δt = 100s. The same author in another paper (29) presented results for a 0.12%C, 1.53%Mn and 0.031%Nb, tested in a similar way as in the former paper, and detected the start of the embrittlement at cooling times above Δt = 10s, and its maximum around Δt = 28s when then an independence of the embrittlement with the heat input was noticed, tending to a certain recovery of toughness at longer cooling times. A COD approach to the problem was employed by Dolby (30) testing a range of heat inputs from 1 up to 25KJ/mm of welds performed on 25mm thick, 0.15 - 0.16%C, 1.20 - 1.40%Mn, 0.056%Nb steel plates. The results can be seen from Fig. 2 and it is noticed that the toughness passes a maximum at heat inputs just under 2KJ/mm, whereas in excess of that figure there is an accentuated increase in the embrittlement.

From the results listed above, there is some evidence of the detrimental effect of Nb at higher carbon levels, increasing with the increase in heat input, though Bernard's results oppose the first comment.

2.4.8.4 C/Mn/V Steels - C $<$ 0.10%

Signes and Baker (36) testing a reference steel containing 0.08%C, 1.40%Mn and two others of identical composition and microalloyed with 0.05 or 0.10%V, in the same way as previously described (Δt = 25, actual weld HAZ, Charpy), have shown that V had little or no influence on the toughness of the HAZ. A CANMET report (61) performed Instrumented Charpy tests on a 0.08%C, 1.26%Mn and 0.09%V steel actual weld HAZ for several heat input conditions. When the results were compared to those from a similar C/Mn steel, it was observed that if cooling times were not in excess of Δt = 40s, little or no deterioration was to be expected. Levine and Hill (77) also performed some tests for a 0.09%C, 1.7%Mn reference steel and for two others microalloyed with 0.06 and 0.21%V. The test procedures have been previously described (Δt = 30, actual weld HAZ, 2/3 Charpy real size) and the authors could not find any particular influence of V in the weld HAZ toughness. The same authors reviewing a report from the BWI (80) mentioned that for a 0.07%C, 1.8%Mn basic composition steels, increasing the plate V and/or N from a base of 0.10%V, 0.01%N, decreased the HAZ fracture toughness. So, the picture for the lower carbon, vanadium microalloyed steels seems to show that no increase in the Charpy Impact Temperature is to be expected if the cooling times Δt are under 40s. Although a loss in toughness was mentioned by

Levine and Hill reviewing a report from the BWI, no description of test techniques or heat input was made.

2.4.8.5 C/Mn/V Steels - C $>$ 0.10%

Swedish authors (55) varied the V content up to a level of 0.40%V in a reference steel with 0.15%C, 1.3%Mn. The Charpy Impact tests were simulated at cooling times equivalent to Δt equal to 33, 100 and 300s, and the authors concluded that for the lowest cooling time, the deterioration in the toughness appears at V levels in excess of 0.20%V, whereas at the other two cooling times, a V content higher than 0.08%V is sufficient to lower the HAZ toughness of the steel. Bonomo and Rothwell (25) have also simulated a 0.13%C, 1.20%Mn and 0.067%V steel to a range of cooling times and, via Charpy Impact tests, they only observed deterioration at cooling times Δt in excess of 40s, taking for reference a similar, non identical C/Mn steel. Hart (54) superimposed some results of the latter work on the graph of the first paper and this can be seen in Fig. 1. Soininen (81) deposited a single pass weld on each side of a plate, at a heat input of 2.4KJ/mm, which he considered "rather low". The steel was a 0.17%C, 1.39%Mn, 0.016%V and it was observed that the transverse Charpy results for the HAZ were similar to those of the parent plate. A table from an unpublished work performed by Smith (82) on real HAZ, produced by multipass weldings at a heat input of 1.7KJ/mm on a 19mm thick plate ($\Delta t \cong 10s$), showed that for a 0.21%C, 1.31%Mn and 0.08%V steel, the absorbed energy of longitudinal Charpy Impact specimens extracted from the HAZ matched the one from the base metal at temperatures as low as -45°C. Similar results were

obtained by Pollard and Aronson (83) when testing by means of half size Charpy specimens the HAZ of four steels welded at heat inputs ranging from 1 to 4KJ/mm. The steels compositions were 0.16 - 0.18%C, 1.10 - 1.35%Mn with V content varying from 0.08 to 0.13%V. The authors observed that the toughness of the HAZs were comparable to the ones of the base metal, and independent of the heat input used. Schoffield and Weiner (44) testing three V steels with the composition in the range 0.16 - 0.18%C, 1.10 - 1.45%Mn and 0.06 - 0.07%V, simulated to present a cooling time $\Delta t \cong 70s$ and Charpy Impact tested, found that these steels exhibited a tougher HAZ than the one of a C/Mn steel of similar composition. Finally, the report from Signes and Baker (36) whose tests conditions have already been described ($\Delta t = 25s$, actual HAZ, Charpy) deals with steels 0.13, 0.18%C and 1.30, 1.40%Mn containing no additions or additions of 0.05 and 0.10%V. It was observed that a slight increase in toughness occurred for the 0.13%C steel at V levels in excess of 0.05% and that a noticeable improvement in toughness was obtained when increasing the V content for the 0.18%C.

Bernard (28) presented a curve, which is reproduced in figure 5, where it is seen that for a reference 0.18%C and 1.35%Mn steel and two others microalloyed with 0.06 and 0.135%V, respectively, the simulation at heat inputs within the range $\Delta t \cong 20s$ up to $\Delta t \cong 100s$ failed to show different impact transition temperatures, leading to the observation that the toughness was independent not only from the V additions, but also from the heat input in the range studied.

From the results presented, it appears that V additions to C/Mn steels do not impair, to a considerable extent, the toughness of the HAZ of the steel. The work from Schoffield and Weiner, at a somewhat higher level of heat input, is fairly consistent with the results presented by the Swedes, and the interesting findings of Signes and Baker of toughness increasing with the carbon content has been previously commented on.

2.4.8.6 C/Mn/Nb/V Steels - C $<$ 0.10%

Signes and Baker (36) studied some steels: one basic composition presenting 0.08%C and 1.30 - 1.50%Mn, and the others containing the same level of C/Mn and combination of 0.03 - 0.06%Nb plus 0.05 - 0.10%V. For the mentioned test conditions (Δt = 25s, actual HAZ, Charpy), deterioration of the HAZ toughness was found relative to the reference steel and to the base metals. The CANMET report (61) performed Instrumented Charpy tests on the real HAZ of a 0.08%C, 1.26%Mn, 0.042%Nb and 0.09%V welded at several heat inputs. They conclude the work stating that at heat inputs equivalent to cooling times under Δt = 40s, the HAZ toughness levels are of the order of the one exhibited by the parent metal. The two papers, basically, observed the opposite results.

2.4.8.7 C/Mn/Nb/V Steels - C $>$ 0.10%

Signes and Baker (36) also combined 0.03 - 0.06%Nb and 0.05 - 0.10%V additions to basic reference C/Mn steels at two levels: 0.13 - 0.18%C, 1.25 - 1.50%Mn and for the test conditions (Δt = 25s, actual HAZ, Charpy) employed, it was

concluded that for any of the Nb/V combinations, mainly those presenting higher levels of these elements, the toughness was impaired. Soininen (81) performed what he called "a rather low" heat input weld (2.4KJ/mm, plate 20mm thick) on basic 0.17%C, 1.35%Mn, 0.031%Nb steels containing two different levels of V: 0.012 and 0.088%V. The Charpy Impact tests supplied toughness values for the HAZ equivalent to those for the parent plate. Bonomo and Rothwell (25) studying the HAZ of simulated specimens at several heat inputs, detected by Charpy testing deterioration of the HAZ of a 0.16%C, 1.32%Mn, 0.047%Nb and 0.10%V steel, relative to the parent plate, when cooling times exceeded $\Delta t = 5s$. Schoffield and Weiner (44) testing the Charpy absorbed energy for specimens simulated at a heat input equivalent to $\Delta t \cong 70s$, observed that for steel combinations in the range 0.11 - 0.21%C, 1.35 - 1.54%Mn, 0.035 - 0.04 - 0.06%Nb and 0.01 - 0.025 - 0.05%V, a strong deterioration in toughness of the HAZs were detected, if compared to that of the parent plate.

It seems that three of the papers which were consulted detected deterioration of the toughness properties in excess of 5, at 25 and at 70s Δt cooling times, whereas Soininen results, whose Δt could be roughly estimated as 20s, did not observe any HAZ deterioration. The general tendency of C/Mn/Nb/V steels indicates a strong deterioration of the HAZ toughness for reference steels containing both microelements than for C/Mn steels containing either one, or the other elements (25, 36, 44). However, Levine and Hill reviewed an Italian paper (84) where the advantage of adding 0.03%Nb

and 0.03%V to a C/Mn steel was mentioned as a prevention for excessive grain growth at welding energies of the order of 1.2KJ/mm.

2.4.8.8 Comments On The Current Results

For the sake of classification and understanding, the previous discussion has, on many occasions, considered select groups of the results from the papers which have been consulted. Now, if one wants to analyse and rate the influence of the microalloys on a reference C/Mn steel, these results must be considered in their original presentation.

So, generalising qualitatively the results of Bonomo and Rothwell (25), Signes and Baker (36), Schoffield and Weiner (44), and Kanazawa and Sato (85), one could group the steels in ascending order of toughness deterioration as :

i) Steels containing no additions or vanadium microalloyed steels.

ii) Steels containing niobium.

iii) Steels presenting niobium and vanadium additions.

To illustrate better the difficulties encountered when evaluating the influence of the microalloying elements on the toughness of the weld HAZ, reference can be made to the work from Kanazawa and Sato (85). The Table 1 shows the composition of the materials tested and the Fig. 6 presents the histograms for the impact energies at $-10^{o}C$ for the actual weldments performed at a heat input of 20KJ/mm. It will be interesting to notice that the com-

position of the steel V (H) is very similar, almost identical to the composition of the steel V (Y), but that their response to toughness is different, since the former steel presents better results than the latter. The carbon equivalent for the steel V (H) is just smaller than the one for the steel V (Y), but at that high level of heat input, such a small difference should not be important.

Bernard (29) simulated a 0.07%C, 1.35%Mn, 0.18%Mo and 0.035% Nb steel to correspond to a heat input of $\Delta t \cong 28s$, and determined the HAZ toughness via Charpy Impact tests. Sawhill et al (13) performed an actual weld on a 0.09%C, 1.40% Mn, 0.20%Mo and 0.05%Nb plate, determining the heat input as $\Delta t = 29s$. He also performed Charpy Impact tests, but on the 50/50 region of the HAZ. Results from the former work exhibit a high level of deterioration, whilst the ones from the latter exhibited good toughness. It seems that the major difference here is in the nature of the test pieces, one author using simulated specimens, known to produce poorer results than actual weld specimens, the ones used by the other authors.

Sawhill et al (13), now commenting on effects of Ti on reference steels, observed as Kanazawa et al (71) that Charpy Impact tests exhibited better results than COD tests, remarking that the degree of improvement caused by titanium additions depends upon the fracture design considerations.

Hart (54) and Levine and Hill (62) attempted to give a brief account on the influence of microalloying elements in the toughness of C/Mn steels, but due to the differences in

testing practices, and due to contradictions found in the literature, their summary lack significance. A simplification for generalisation will be considered a dangerous approach for immediate practical application, and this review shares the opinion of Bernard (28) that a search for hypothetical "maximum tolerable" amount of microalloys is bound to be misleading.

2.4.9 Post Weld Heat Treatments (PWHT)

The toughness recovery of an embrittled HAZ by methods of stress relieving treatments depends basically on the nature of the microstructure obtained, and on the possibility of microelements present in solid solution precipitating during the process.

If the HAZ product is martensitic, the reduction on dislocation density and the removal of interstitial carbon from the lattice will yield a tougher structure. On the other hand, low angle boundary upper bainitic structures are not that sensitive to heat treatment (62), and in the presence of microalloys in solution, precipitation may occur, bringing to an even lower figure the toughness of the HAZ. Made simple, the overall effect of the PWHT will be the net result of competitive mechanisms of stress relieving and second phase precipitation hardening. It must be kept in mind that sometimes a thermal treatment could annihilate the beneficial effects of the process fabrication of the parent metal.

Improvements in the HAZ toughness of C/Mn steels welded at low heat inputs are well known (22, 30, 86) and the same tendency has been observed for high heat inputs, as shown in figure 7 by Bernard (28). Also in figure 7 are shown the results from the same author for a C/Mn/0.035%Nb steel simulated at several heat inputs, and it was observed that at heat inputs equivalent to cooling times under $\Delta t \cong 80s$, tempering exhibited a slight improvement on the toughness of the weld HAZ, whereas at heat inputs in excess of 80s, toughness deterioration was observed. That tendency of deterioration of the high heat input weld HAZ with stress relieving treatments has been acknowledged elsewhere (2, 14, 30, 54, 61, 87).

British Steel Corporation (BSC) technical brochure for Quenched and Tempered microalloyed plates (88) specifies that in cases where stress relieving heat treatments are to be considered, the stress relieving temperature should never exceed the tempering temperature quoted in the test certificate, and recommends that both plates and the electrode manufacturers should be consulted in advance on any stress relieving operation.

2.4.10 The Crack Path In Weldments

Watkins (24) in his 1972 paper dedicated one whole item to the welding fracture path. Though special attention was drawn to mild and alloyed steels, he mentioned no personal knowledge of service failures following the HAZ, but that examples did exist for tests in model vessels. Quoting two distinct private communications (89, 90) examples are

provided for fast failures following the HAZ in pipework, and he concludes that crack propagation can occur along the HAZ of high heat input welds, when catastrophic failure will proceed. Rodgerson (91) reported that in semi-skilled pipeline steels, fracture has been observed to run in the HAZ. In artic grade pipe containing 1.0%Ni, Myioshi (92) mentions that during burst tests, fractures have been observed to initiate in the HAZ, although they invariably propagate through the parent plate.

Concerning laboratory tests and microstructures of Nb micro-alloyed steels, Cane and Dolby (33) observed that COD specimens crack propagate primarily through upper bainite colonies, but also through acicular ferrite where this constituent lay in the fracture path. It was also mentioned that the fracture facet size appeared greatest in the upper bainite and acicular ferrite regions. The facets associated with proeutectoid ferrite (PEF) were smaller and irregular. Gittos and Dolby(93) discussing 25mm thick microalloyed steel plates welded at a heat input equivalent to 2KJ/mm, said that lowest cleavage resistance may be expected from microstructures presenting high proeutectoid ferrite (PEF) and high upper bainite (UB) content. This was attributed to the fact that strain could be concentrated in the relatively soft but coarse microstructural regions, therefore nucleating cleavage cracks. Evidence for cleavage cracks following the PEF is provided for Weld Metals (29, 30) and the result is a lowering of the toughness.

Another factor that may influence the crack path is the geometry of the weld bond. Pellini (94) says that the HAZ geometry will exert a strong protective influence on the weldment, because brittle fracture tends to run normal to the main stress direction. On the other hand, Italian authors (26) state that to improve the toughness of the coarse grained HAZ, the geometry of the boundary line between the melted and the HAZ welded regions must deviate as far as possible from the plane perpendicular to the pipe surface. Pollard and Aronson (83) commented that in a weld, the zones of varying structure are very narrow and often tend to balance each other in properties. Thus, Aronson (18) observed a deterioration when testing the coarse grained region of the HAZ, but no loss in toughness was documented when the composite was tested. Authors have reported that a change in the welding process (95), or that an increase in the welding speed (30, 96) leading to a narrower HAZ reduces the tendency to brittle failures, without significant lowering in the welding heat input.

2.5 Summary

Niobium and/or vanadium are added to C/Mn HSLA steels to provide a tough, high yield strength fine grained product. This is accomplished by Nb and/or V precipitation grain pinning action. When these steels are welded, peak temperatures in the region of 1200^{o}C will dissolve these precipitates. If the cooling cycle is slow enough ($\Delta t > 25s$), the HAZ grains at the border with the fusion zone will coarsen, and the local toughness deteriorates. Two main theories attempt to explain the behaviour: the structural

theory and the precipitation theory. The structural theory supports that microelements in solution will depress the austenite transformation temperature and the resulting product will dictate the toughness values. The extension of this depression and the temperatures at which it starts to be effective are seldom quantified. Nb is considered to favour the formation of brittle upper bainite. V is mentioned either not influencing the microstructures, or retarding the formation of upper bainitic structures. In the latter hypothesis, proeutectoid ferrite should be present along the prior austenite grain boundaries. Nb + V are considered a potential hazard, especially at higher heat input levels of welding. Combined, they are reported to promote coarse upper bainitic structures. Quantitative investigation on the influence of Nb and/or V on the microstructures of the HAZ is rare, and frequently recommended as further work. Also, there is no unified opinion on the maximum recommended amounts for these materials. Nb has been reported to provoke embrittlement in amounts of 0.01 - 0.04%Nb. Contents of V up to 0.10%V have not been considered harmful. The levels of Nb + V must be kept below 0.05% for each element according to the ASTM 572 standards. The precipitation theory proposes that microelements in solution will precipitate during the cooling cycle. Precipitation hardening occurs and the toughness decreases. Up to date only two authors detected the microalloying precipitates in the HAZ. They have concluded that, although some toughness deterioration should be attributed to the precipitation hardening, it appears not to be the toughness controlling mechanism. Many authors

refer to the precipitation of the microalloying elements in a speculative way, because they themselves could not detect the phenomena. Also, there is controversy in the hardness figures as a support for that type of mechanism.

An attempt to rate C/Mn HSLA steels with or without Nb and/or V additions in sequence of increasing toughness deterioration would give: C/Mn and C/Mn + V steels, C/Mn + Nb steels and C/Mn + Nb + V steels. There is some comparative work performed on the first three categories of steel above mentioned, but very little is found in the current literature about Nb + V steels. Also, systematic information on the relation peak temperature attained /microstructure produced, and on the influence of the latter on the local HAZ toughness has been neglected.

Two main tests are employed when quantifying the toughness of the HAZ: the Charpy V Notch Impact test and the Crack Opening Displacement (COD) test. The region of the HAZ commonly tested is the coarse grained region, because due to its coarse grain size, this is where the deterioration of the toughness is expected to occur. The Charpy test represents the most popular approach in engineering nowadays, and it is of easy interpretation. The COD test is of increasing popularity and represents a more economic criterion on the design of statically loaded structures. These tests are performed either in samples extracted from actual weldments, or in specimens produced by welding simulation methods. The results obtained from simulated specimens exhibit poorer toughness than those extracted from real weldments. The reason for that behaviour is the

severity of notch positioning.

Another accepted concept is that the degree of toughness deterioration increases with increasing heat input. The quantification of that deterioration is relative and the common chosen basis for the comparison are: the reference steel (a steel with some C/Mn content and no Nb nor V), or the base metal. If the influence of the nature of the specimen is considered along with the different methods of testing and basis for comparison, perhaps one could explain the conflicting results in the current literature.

CHAPTER 3 - MATERIALS, METHODS AND RESULTS

ASTON

CHAPTER 3 - MATERIAL, METHODS AND RESULTS

Within the present chapter there will be, mainly, the listing of the results obtained from the present work. Also included is a description of the materials and methods leading to these results.

3.1 Material

The chosen material was the British Steel Corporation (BSC) RQT-500, i.e. a Quenched and Tempered HSLA steel plate containing Nb and V. This steel is produced by the basic open hearth process, austenitised at 900^{o}C for one and half hours for the 38mm thick plate, roller quenched* and tempered at 600^{o}C for one hour and fifteen minutes (88, 97). The material is not specifically designed for use at high temperatures and is employed in the construction of earth moving equipment, agricultural machinery, shipbuilding, offshore, liquidified gas storage tanks, etc. The chemical composition of the steel can be seen from table 2 and the mechanical properties from table 3.

The 38mm thick plates were received already cut in sections of 30 x 60mm. They were then stone ground to 25mm thick. Their rolling direction was later determined as being parallel to the longer dimension of the plate section. This was accomplished by optical microscopy observation of the inclusions, and by the Charpy Impact test performed in specimens extracted from the two main directions of the plate sections.

* The main feature of the roller quenching process is that rotating rolls hold the plate during quenching. The result is a product with improved flatness, greater uniformity of properties and low residual stresses.

3.2 Methods

Two main processes were employed to obtain the HAZ to be studied. One was the Submerged Arc Welding (SAW) process which generated the actual weldment HAZs. The other was the Welding Simulation technique which produced synthetic HAZs. The reason for the choices is the fact that SAW is an automatic process providing a broad range of welding energies and Simulation techniques constitute a time saving, economical approach to the problem of location of the stress concentrator on the specific region to be tested.

The toughness of the HAZs obtained by any of these two methods was determined by standard Charpy V Notch Impact testing. The latter has the advantages of simplicity and economy in execution, and the possibility of direct comparison with the bulk of previous experimental work in this field. It is realised that the technique has the disadvantage compared with COD method, of not being directly applicable to the practical evaluation of the fracture performance of components in service. Besides, Charpy testing is still the most widely employed toughness evaluation test specified on the design of welded structures.

Techniques for the subsequent analysis of the specimen, to be described later, are listed below :

- Optical Microscopy.
- Quantitative Metallography.
- Transmission Electron Microscopy
- Fractography - Scanning Electron Microscopy.

- Micro and Macro Hardness Testing

3.3 The Submerged Arc Welding (SAW) Experiments

An attempt to define the welding parameters leading to the planar HAZs, which are ideal for Charpy toughness measurements, was made by successive deposition of bead-on-plate weldments on mild steel trial plates of 20mm thick. The first welding conditions chosen for these trials were based on data collected from the specific literature on deep welding penetration techniques (98, 99, 100). The maximum welding heat input attained, namely 5.6KJ/mm, did not exactly provide a planar HAZ, though it would be possible to extract a quasi-planar HAZ Charpy specimens from these weldments. The use of higher heat inputs provoked through penetration, but one has to bear in mind that the trial plates were 5mm thinner than the RQT-500 ones.

In order to avoid damage to the welding tractor in the case of burning through, and also to allow a passage for the wires for future actual thermal cycle measurement, a simple jig was built up. This can be seen from figure 8, aside with the electrical device permitting the recording of current and voltage during the welding, on a X - t graph plotter. One should note that the earth lead is connected to one corner of the welding tractor.

Due to a particularity presented later in the experiments, and to be discussed during the measurement of welding thermal cycles (item 3.3.2), the welding energy which

provided the specimens for the high energy Charpy testing was changed from 5.6 to 6.3KJ/mm. Besides the high heat input condition, a more moderate energy input, namely 3.6KJ/mm was chosen to be examined during the present work.

The Submerged Arc Welding equipment used during these experiments was a BOC Universal Welding Head, and the source was a MCRA 1200 Welding Rectifier with a drooping characteristic, also from BOC. The welding consumables were :

i) Flux : Alumina Grade OP 170 - Oerlikon.

ii) Wire : Ø = 5mm, cast 7631 coil 23007 - Oerlikon.

Before the welding, the plate was degreased with a commercial solvent named Solvere, and the welding conditions and parameters can be seen from table 4; they are representative of bead-on-plates performed in the 25mm thick RQT-500 steels.

After the welding, the HAZs were examined visually and through an optical microscope, and as no defect was found, the weldments were considered sound for further impact testing.

3.3.1 Measurement Of The Welding Thermal Cycle

Earlier on it was decided that welding simulation techniques were to be used on the project, as well as real weldments, thus the thermal cycle to be duplicated needed to be known. The measurement technique to be used was that developed by the British Welding Institute (101) and is described below.

3.3.1.1 Description Of The Method Employed

The welding bead profile corresponding to the welding condition of interest must be determined in order to locate the thermocouples for thermal cycle measurement, and this is accomplished by a bead-on-plate deposition followed by sectioning, polishing, etching and visual observation. The maximum depth h of the fusion zone is measured from the upper surface of the plate for the steady state condition. Cylinders of the same material as the plate, named pegs, with the height equal, smaller or longer than the length h by amounts in multiples of 0.5mm, and with diameter equal to 4mm were precisely ground. Then a series of holes just in excess of 4mm diameter were finely drilled along a marked line on the plate to be tested. The idea of different heights for the pegs is to balance the effect of small changes in the welding condition affecting the depth of the welding bead; the location of thermocouples at several heights will bring a higher probability of success to the experiment, and provide data for a range of peak temperatures. Pt/Pt-13%Rh wires of 0.25mm diameter were micro-spot welded apart, 1mm from each other, to the centre of the base of the pegs. That technique has been mentioned as the one presenting hot junctions supplying the most accurate temperature measurement (102).

Twin bore ceramic sheaths were inserted on the wires for protection and separation, and it was ensured that the total length of the assembly, peg-plus-sheath, was marginally longer than the thickness of the plate to be welded. The assembly was carefully inserted within the holes drilled

in the plate and gently hammered to the level of the plate surface. The thermocouple free ends, now on the lower surface of the plate, were inserted into a small connecting block. The other end of the block was connected to the appropriate cup ro-nickel/copper compensating leads, and these were attached to the X - t recorder, where the millivoltage later to be translated into the thermal cycle for the specific thermcouple location point, was recorded. The connecting blocks were glued to the plate with Araldite to avoid tilting, and the handling of the plate from the thermocouples insertion site to the jig on the welding tractor was carefully managed. In this way the thin 0.25mm diameter wires were not broken, although inevitably some losses always occurred. Each thermocouple was numbered and that number was printed on the X - t recorder channel for ease of identification. The X - t recorders were calibrated with the help of a standard D.C. Voltage Calibrator. Figure 9 helps the explanation.

3.3.1.2 Results and Comments

The results obtained for the actual measurement of the welding thermal cycles for peak temperatures 790 to 1600^{o}C, can be seen from the graphs of figures 10 and 11, for the heat inputs equivalent to 3.6 and 5.6KJ/mm, respectively. In table 5 these thermal cycles are represented by the cooling time $\Delta t_{800-500}$ and it is observed that the figures are usually very much the same for each input condition, despite the different peak temperatures, which is in good agreement with the current literature. These results are representative of a total of five trials: two for the lower heat input

3.6KJ/mm and three for the higher heat input of 5.6KJ/mm. At the start of the test series, five thermocouples were being used, but since very few positive results were obtained, that number was increased to ten per plate. This type of experiment is of a trial and error nature, and the more they are performed, the more experienced becomes the operator.

Although these experiments supplied the indication of the welding thermal cycles for certain peak temperatures, no systematic information on the distribution of the peak temperatures with the distance away from the fusion line was available. An investigation on the possible causes for that lack of information, other than the operator's inexperience, is listed below :

i) Weld Bead Penetration Toe Instability.

ii) Variation in the Mains Voltage.

iii) Sensitivity of the Nominal Current Setting Dial.

iv) Influence of the Earth Lead Location.

3.3.1.2.1 Weld Bead Penetration Toe Instability

Some instability of the weld bead toe was noticed for the higher heat input welding, more pronounced in the surroundings of the thermocouples insertion. This can be seen from the pictures of figures 12 and 13. The tendency of the bead tip to curve always to the same side was easily noticed and this was associated, as it will be commented later, with the positioning of the earth lead. Although in the present work it seems that the drilled hole accentuates the deflect-

ion of the bead toe, researches from the British Welding Institute stated that the weld bead was unaffected by the presence of thermocouples hot junction and drill holes (47). They have worked with heat inputs up to 7.2KJ/mm, but the macrographs presented to illustrate the fact are for low heat input, where the phenomena are more unlikely to occur. The macrographs of the figure 14 are representative of two successful points of the present work. It was observed that the instability was reduced for the higher heat input by increasing the distance between the drill hole and the weld bead. In discussing the problem at GKN Wolverhampton, it was learned that above 70% of the weld bead penetration instability may occur due to a heat sink effect (103).

3.3.1.2.2 Mains Voltage Oscillation

To investigate the possible influence of the mains voltage oscillation on the weld bead depth, beads-on-plate were deposed on trial mild steel plates 20mm thick. The nominal current chosen was 700A and all through the experiments the current setting knob was not touched after the original positioning. The beads-on-plate were performed during different days and hours of the work to provide a good batch of samples. A digital voltmeter was installed in the equipment mains lead to allow the monitoring of the mains voltage; the voltage and current supplied to the plate were recorded on a X - t recorder. The resulting variations are listed in table 6 and the corresponding bead depths are listed in table 7, for the five sections observed from each weld run. From the results, it is seen that the maximum variation of the bead penetration with the mains

voltage oscillation is equal to 2mm for the welding conditions used. That variation could increase for the higher weld heat inputs and deeper bead penetration seen on the RQT-500 steel plates.

3.3.1.2.3 Sensitivity Of The Nominal Current Setting Dial

The rectifier that supplied the power to the welding head exhibited a dial for nominal current setting with sensitivity of 50A. Thus, it was not possible to accurately reset a nominal current value if, between experiments, the dial has been displaced to supply other nominal currents to other weldments. This fact, if combined with the mains voltage oscillation towards the same direction, could increase the discrepancy of the depth of the welding bead from one operation to the other.

3.3.1.2.4 Influence Of The Earth Lead Location

It was mentioned previously, and illustrated in Fig. 12, that at higher heat inputs, the weld bead toe tended to curve to a constant side of the plate. This was the side where the earth lead was connected to one of the corners of the welding tractor. Also, it was noticed that the centre of the weld bead was not coincident with the marked welding direction; this could be a further characterisation of an arc blow effect, enlarged by the positive electrode connection (DCEP) used. To investigate the occurrence, the earth lead was split in two parts and each of the new leads was connected directly to the plate at two opposite points in line with the start and stop welding positions.

The experiment supplied no results since all the thermocouples melted. Investigating the reason for this behaviour, it was observed that the nominal current value was more likely to be set as 910A, rather than the original intended value of 900A. The recorded current and voltage figures supplied to the plate were of 1200A and 35V respectively, and the welding heat input calculated was shifted from 5.6 to 6.3KJ/mm.

When the weldments were sectioned, polished, etched and observed, it was verified that they were rather straight and longer than the ones resulting from the former 5.6KJ/mm heat input welding conditions, and furthermore they exhibited a planar coarse grained HAZ.

Taking into account all the factors mentioned previously, it seems that the positioning of the earth lead was the major factor influencing the results of the actual thermal cycle measurement practice.

3.3.2 Consequences

In view of the above findings, the higher welding energy to be considered for the present work was changed from 5.6 to 6.3KJ/mm, and all the specimens needed for the actual weldment Charpy Impact testing, for the higher welding energy condition, were to be provided by the above welded plate.

Since the actual thermal cycle measurement is an expensive and time consuming technique, it was decided that these trials would not be continued. Instead, the determination

of the cooling time $\Delta t_{800-500}$ for the heat input equivalent to 6.3KJ/mm was to be evaluated by theoretical calculations, as it will be seen in item 3.4. It was also decided that structures associated with the various peak temperatures were to be obtained by methods of welding simulation. Figure 15 illustrates the macrographs of the actual weldments to be considered in the present work for the heat inputs equivalent to 3.6 and 6.3KJ/mm, respectively.

3.3.3 Specimen Preparation

The welded plates had the top 2mm removed by stone grinding, and then 10 sq. mm, square cross section transverse specimens were extracted with an axial length in excess of 55mm, the specified dimension for the standard Charpy test pieces. These specimens were numbered in order from their relative position to the starting point of the weld. Thus, two consecutive test pieces were prevented from being tested at two consecutive temperatures. This provided a better sampling of the results of the toughness curve to be plotted. Figure 16 shows the layout of the specimens extraction.

Each individual specimen was polished by the traditional method, i.e. from grinding paper no. 100 up to diamond paste 1μ, etched in Nital II and were marked after visual observation, as follows. The higher heat input sample seen in figure 17a presented no problem concerning the choice of the notch centre due to its planar coarse grained HAZ, and the marking was performed as illustrated in figure 17b. This choice was not as simple for the lower heat input

actual weldment specimen where it was possible to test only one region of the HAZ, and the whole composite was tested, as seen from the sample in figure 18a. The same approach that led to Sawhill et al (34) to determine that for a single pass on each side weldment, the 50/50 positioning of the notch tip was the location supplying the lowest toughness for the composite was used here, as illustrated by figure 18b. Three trial locations, three specimens each were to be Charpy tested at a constant low temperature and the one exhibiting the lowest absorbed energy values would be the notch centre position to be considered in the further testing, to build up the whole of the toughness curve for that heat input condition.

The standard Charpy dimensions were obtained by means of a jig, where the positioning of the centre for the future notch of the actual weldment specimens would allow an easy and precise cutting operation to eliminate the excess in length.

3.4 Computer Calculation

The determination of a new cooling time 800 to 500°C, Δt, was necessary for the heat input equivalent to 6.3KJ/mm, and to avoid more time consuming and expensive experiments, as well as to try a new approach to the problem, the use of theoretical calculations of the thermal cycle was considered. A numerical temperature calculation with temperature-dependent material properties computer program from a Norwegian doctorate thesis (51) was at hand, which only needed some adaptations to suit the available computing facilities. Besides, the differences between the curves contained in the

original mild steel program and those developed for the steel RQT-500, in the light of the approximations involved, have not been considered significant enough to impeach a first trial run, especially when experimental $\Delta t_{800-500}$ data were available for comparison.

The thermophysical parameters supplied for the steel RQT-500, the trial run history, the data fed to the program, the interpretation of the numerical output, the improvement in the program to supply a time saving graphical output and the curves obtained to calculate the welding thermal cycle, are all included in Appendix I. In this chapter are presented the results of the several $\Delta t_{800-500}$ times for the various welding conditions employed, the curve obtained from the regression analysis applied to these results, and the superimposition of actual measurement data to that curve, as a basis of comparison.

3.4.1 Theoretical Values for $\Delta t_{800-500}$

These values were calculated for an arc efficiency factor $\eta = 0.85$, which was reported by Ives and Bergh (75) as the average engineering value for Submerged Arc Welding process. The $\Delta t_{800-500}$ figures after the calculations were very similar to the actual measured ones for the nominal heat inputs equivalent to 3.6 and 5.6KJ/mm. Thus, the cooling time $\Delta t_{800-500}$ for the weld energy of 6.3KJ/mm was also calculated for $\eta = 0.85$. Because some practically measured Δt values were available from the literature for 25mm thick plates, three other cooling times Δt equivalent to arbit-

rarily chosen heat input values of 2.7, 4.5 and 7.0KJ/mm were calculated. This allowed the building up of a regression analysis curve based on theoretically obtained points, to be compared with the values observed from actual measurements. The calculated results for the present work can be seen from table 8.

3.4.2 Polynominal Regression Equation For Determination Of $\Delta t_{800-500}$

The results from table 8 were fed to the Application Program UA01 Version 1, of the University's Computer, and the best fit was obtained for the equation

$$Y = 0.15267 \times 10^{2} - 0.10902 \times X + 0.40176 \times 10 \times X^{2} + - 0.61366 \times 10^{-1} \times X^{3}$$

which is represented by the curve seen in figure 19. On that same curve, it can be observed the superimposition of points of different origins, all concerning 25mm thick plates, as follows :

i) The results from measurements in the current work for the heat inputs of 3.6 and 5.6KJ/mm.

ii) The results from calculated and practically measured Δt values obtained from the Welding Institute (56,104).

iii) One actual result extracted from a paper by Sawhill et al (13).

and these values can be seen from table 9 and table 10.

It is worthwhile noting the foregoing features of the data plotted :

i) The present work involved single wire Submerged Arc

Welding (SAW), whereas the Welding Institute (WI) high heat input data was obtained from single or tandem SAW.

ii) The low heat input Welding Institute data was obtained from mechanical CO_2 process and shielded metal arc welding was used in the experiment of Sawhill et al.

iii) Material composition were not identical.

iv) Data collection involved different personnel.

Clearly, the degree of match between the experimental data and the theoretical curve is very good. This must indicate on the reliability of the calculation of Δt values for 25mm plate over a wide range of heat inputs.

3.5 Weld Simulation Experiments

The process reproduces on a laboratory scale the heating and cooling cycles observed in an actual weldment. The advantages of this practice are the reproduction of a certain zone of interest, wide and homogeneous enough to allow an accurate location of a stress concentrator for the purpose of toughness testing. Thus, it annihilates the problems due to the weld bead geometry of the actual weldments, associated with the economical aspect of the use of a minimum amount of steel. A further advantage to be discussed later is the possibility of recording the dilatometric history of the specimen, and hence the details of the phase transformation.

3.5.1 The Equipment And The Method

The equipment used was the Mand Electro Hydraulic and Thermal Closed Loop Testing System, or simply the Mand Welding Simulator. Basically, the system consisted of a series of equipments, pumps and recorders assembled together with the aim of duplicating on a test piece, by electrical resistance heating, a pre-stablished thermal cycle. The heating and cooling cycle were attained via a temperature control system in association with a power supply. Thermocouples microspot welded to the specimen not only facilitated thermal control, but also allowed the recording of the simulation thermal cycle on a X - t recorder. Two strain transducers with silica probes resting on opposed sides of the surface of the specimen supplied in association with another thermocouple the recorded dilation temperature history of the sample on a X-Y recorder.

The specimen was made part of the system loop by connection to the copper jaws of the load frame. The upper jaw was fixed whereas the lower jaw was mobile and activated by the piston of a hydraulic power supply connected to a gear pump. These jaws, as well as the silica probe transducers, were water cooled. The specimen was contained inside a controlled atmosphere box where an overpressure of Argon gas followed the initial low vacuum established by a rotary pump, to avoid the oxidation of the sample. Before being set in the equipment, the test piece was degreased with Solvere and two thermocouples were microspot welded, using the same technique employed for the pegs, to the opposed sides of the central diameter of the specimen. The copper connections permitting the setting of the specimen, the collets, and the inner part

of the copper jaws were polished with Duraglit before the start of the day's work, or after five to seven runs were performed, to assure good electrical contact between the parts.

The temperature set in the Eurotherm was the Peak Temperature to be attained and was equivalent to the full scale deflection of the Data track chart, all the other temperatures of the thermal cycle being a percentage of that maximum temperature. One of the thermocouples connected to the test piece supplied continuous information on the sample's temperature to the Eurotherm, which then controlled the required heating power to reproduce in the specimen the thermal cycle printed on the Data track chart. This thermal cycle was also registered on a X - t recorder.

The printing of the thermal cycle on the Data track chart and the dilation system will be explained later in the present work. The listing of the main equipments of the system, as well as some set conditions used, are given in Appendix II.

A schematic drawing from the assembly, the thermomechanical diagram for the specimen set up, and a picture of the equipment and of the mounted specimen are seen from figures 20, 21, 22 and 23 respectively.

3.5.2 The Temperature Distribution In The Samples

It is good practice and it was observed in the present work, to verify the distribution of temperatures in the test piece to be used, before starting a wide range of welding simulation experiments.

So far the specimens used with the jaws associated with the controlled atmosphere box were of cylindrical shape, but since the specimens to be synthetized were to be employed in a subsequent Charpy testing, it was decided to simulate Charpy size test pieces, just with expanded axial length dimensions. This procedure represents an economy in time and money, because it eliminates the step "round cross section" in the machining sequence of the work shop operation.

To introduce the use of square section specimens, a square groove should be cut into the inner surface of the copper collets and the first simple approach used, illustrated in Fig. 24a, did not provide good contact between the collets and the sample with resulting heterogeneous heating of the specimen along its length axis. The grooving technique was then modified to a more difficult machining shape seen from Fig. 24b and that new design proved to be satisfactory with consequent homogeneous heating of the specimen. For one calibration mode, cylindrical specimens were also employed when the traditional round grooved collets seen from Fig. 24c were used, with no problem to the homogeneity of the heat distribution. The considerations made above concern normal visual observations.

A more precise temperature distribution verification was performed in three different modes, always related to the central-surface control temperature, as follows :

i) Centre/surface temperature distribution.

ii) Through thickness/surface temperature distribution.

iii) Gauge length/surface temperature distribution.

Two different kinds of thermocouple were employed :

a) A 50mm diameter sheathed Chromel/Alumel thermocouple.

b) A 25mm bare wire Pt/Pt-13%Rh thermocouple microspot welded to the sample as separate wires.

It will be referred to as Control thermocouple, the one of Pt/Pt-13%Rh which was attached to the central surface of the sample will supply the signals to the Eurotherm temperature controlling system. The other thermocouple whose nature and position could vary will be named Calibration thermocouple. The nominal temperature was the peak temperature set in the Eurotherm control dial.

The cooling time used during these experiments was the natural cooling time of the equipment, and two types of specimens, each with three different gauge lengths, were used as follows :

i) 10 sq. mm, square cross section specimen.

ii) 10mm diameter, round cross section specimen.

The cooling time of a sample is reported to be affected by its dimensions. The gauge length was the main factor affecting the cooling rate, and the diameter was of secondary importance (105). Since the larger number of specimens

for this work were intended for Charpy testing, the cross section should not be altered, thus if for flexibility of operation a cooling time lower than the natural cooling time of the sample was desired, the shortening of the gauge length would present a solution to the problem. On the other hand, longer specimens were expected to exhibit a more even distribution of central temperature due to a longer distance away from the water cooled jaws. This was the reason why three different gauge lengths were tested. Cylindrical specimens were also observed because due to their shape, one should expect a better radial temperature distribution; they were intended for dilation work and later it will be seen that for the determination of CCT curves, the cross section had to be altered, and that work shop operation is easier to perform in round test pieces.

For the two first calibration modes mentioned previously, the 20mm gauge length, cross square section specimen was used, whilst for the last mentioned calibration mode, all six possibilities of test pieces were employed. The test piece dimensions are seen from Fig. 25.

3.5.2.1 Centre/Surface Temperature Distribution

A Chromel/Alumel calibration thermocouple was inserted radially into a five millimetre long, close fitting, blind hole located at the specimen centre and the nominal temperature were varied from 400°C up to 1200°C, in steps of 100°C. The results obtained were compared to those of the control thermocouple as seen from the graph of Fig. 26, whose values are listed in the table 11.

3.5.2.2 Through Thickness/Surface Temperature Distribution

A Chromel/Alumel calibration thermocouple was inserted radially into a close fitting hole drilled through the thickness, at the specimen centre and withdrawn, step by step, at measured length intervals. For every interval, the calibration temperature was measured for two nominal levels of 800 and 1100^{o}C respectively, and compared with the temperature of the control thermocouple. Whenever a small length of the calibration thermocouple remained inside the specimen, a low temperature reading was registered; this phenomena has been called a thermocouple heat sink effect, and has been reported elsewhere (106). The results for that calibration are listed in table 12, and can also be seen from figure 27.

3.5.2.3 Gauge Length/Surface Temperature Distribution

Pt/Pt-13%Rh calibration thermocouples were microspot welded along the central region of the specimen gauge length at discrete intervals of 1mm to observe the existence and extension of a thermal stability plateau. The results for that experiment, which involved square and round cross section specimens in all their gauges, can be seen from the graph in figure 28, and the corresponding values are listed in table 13.

3.5.3 Specimen Preparation For Weld Simulation

Based on the results from the above mentioned temperature distribution tests, it was decided that the specimens with 20mm gauge length were to be used in the welding simulation techniques for the current research. The reasons for the choice were :

i) The existence of a suitable axial temperature plateau in the middle of the sample.

ii) More facility for manipulation of the sample than in the case of the 15mm gauge length.

iii) Higher natural cooling rate than in the case of the 25mm gauge length.

For the subsequent Charpy testing, the samples to be simulated were extracted from the RQT-500 steel plates in a similar way as those for the actual weldments. Side marking would allow the posterior V notching exactly in the same surface as for the actual weldment samples. Figure 16 helps the visualisation. The standard Charpy dimensions were attained in a similar way as for the actual weldment. In that case, the centre was the hot junction of the control thermocouple of the duplicated specimens. This can be seen from figure 29.

3.5.4 A Higher Heat Input - 14.4KJ/mm

In addition to the energies of 3.6 and 6.3KJ/mm, it was decided to include in the investigation a heat input corresponding to the higher levels currently used in welding practice. This would be achieved by the use of welding simulation techniques. In order to do this, it was necessary to obtain a representative thermal cycle for these conditions. Computing times to run a program for the calculation of the distribution of temperatures in a welding process involving large heat inputs would be extremely long. Moreover, the trial and error determination of the ideal inner and outer

zones would involve too much time. A solution to the problem was provided by an IIW document (71), where some actual heating cycles and cooling times Δt were available for heat inputs over 14.0KJ/mm. The condition chosen to be duplicated was equivalent to a one side, three wires Submerged Arc Welding (SAW) on a 25mm thick plate. The heat input was equivalent to 14.4KJ/mm and the cooling time Δt was equal to 244 seconds. Since the full thermal cycle was not provided, the thermal cycle employed for the simulation was estimated from the given heating cycle and cooling time Δt.

3.5.5 The Choice Of Peak Temperatures

Seven nominal peak temperatures were chosen for the simulation program. They were 700, 800, 900, 1000, 1150, 1250 and 1400^{o}C. The reason for the choice was the provision of structures over a wide range of the HAZ. This would include those structures present before, during and after the phase transformation, as well as those in the transformed coarse grained region. The peak temperature of 700^{o}C simulated the untransformed subcritical HAZ. The fine grained region was simulated at 800, 900 and 1000^{o}C, where austenitisation was interrupted, nearly and fully completed, respectively. At 1150^{o}C V would be in solution and the same would apply to Nb at 1250^{o}C. Finally, the border with the fusion line was duplicated at 1400^{o}C. These three last peak temperatures would represent the transformed coarse grained HAZ region.

The rapid heating cycle demanded from the equipment caused a certain scatter between the nominal peak temperature and the one to be duplicated. Trial and error runs were performed to

keep the scatter between certain limits, which are seen in the tables of the item 3.5.8.

3.5.6 Duplication Of Thermal Cycles

A thermal cycle to be duplicated was etched in the metalized surface of a coated conductive Mylar Chart Roll CMR 51 with a sharp stylus, which divided the surface of the chart into two eletrically isolated conductive planes. The chart was then mounted on the outer surface of the program drum, which was subsequently installed in the Data Track Programmer Model FGE 5110 (Research Inc.). As the drum rotated, a probe driven by a servo system continually sought the zero potential existing at the centre of the program curve. Signals were sent to the Eurotherm Temperature Control System, thus reproducing on the specimen, the desired thermal cycle.

To meet the cooling cycles requirements, one drum system was used for the 3.6KJ/mm heat input condition, and two drums - the strip chart adaptor - were used for the higher heat inputs. The conversion of the desired thermal cycle to the Data Track System was not reproduced accurately. Thus, trial and error modifications were performed on the first curve to minimise the cooling cycle scatter. Before the start of the day's work, all electrical connections were cleaned with the commercial product "Silvo". The thermal cycles which generated the duplicated specimens for the current work are seen from Figures 30, 31 and 32.

3.5.7 Dilation

The Welding Simulator is provided with a D-8 Creep Monitor apparatus, which allows dilatometric study of the test piece during the thermal cycle. Two silica probes resting on the sample vertical centre line and opposite to each other were connected to two LVDT linear displacement transducers, type D5/100A, which were subsequently zeroed in the monitor. The transducers were water cooled to prevent thermal drift, and the silica rods had spherical ends at the contact point to reduce thermal pick up. When the specimen was simulated, the transducer's signals were amplified by the monitor and continuously recorded on the horizontal channel of a X-Y recorder. The vertical channel was connected to a second auxiliary Pt/Pt-13%Rh thermocouple, which was microspot welded to the sample axially opposite to the control thermocouple. Thus, the dilatometric curves for the duplicated specimens were recorded. The displacement range adopted was usually 0.010", but sometimes for a more accurate determination of a specific transformation point, a displacement range of 0.003" was selected. The X-Y recorder was calibrated by means of a DC Voltage Calibrator 2003S. The dilation assembly can be seen from the picture in figure 23 where the probes are labelled A, the transducers B, and the control and calibration thermocouples C and D, respectively. A typical dilation curve involving a bainitic reaction is seen from figure 33 for a displacement range of 0.010". Figure 34 shows a similar curve for a bainitic and martensitic reaction at a set displacement of 0.003" and the hypothetical tangent method used to locate the change points is seen from figure 35.

3.5.8 Welding Simulation And Dilation Results

The results from the simulation tests can be seen from the set of tables 14, 15 and 16. The cooling times between the peak temperatures and 800°C were also included. They were used for the comparison of the reproduction of the curves of the same family, together with the cooling time Δt. Since the specimens to be heat treated and the specimens employed in the building up of the CCT curves were obtained by simulation, though both topics are to be commented on later, their simulation history is seen from tables 17 and 18, respectively. All the above mentioned tables include the dilation figures for better identification and facility of presentation.

3.5.9 CCT Curves

For the determination of the CCT curves, the nominal peak temperature considered was 1400°C. Since the cooling cycle of the apparatus is limited by the natural cooling of the tested specimen, two slight variations had to be introduced in the dilatometric experiments towards faster cooling rates. One was the reduction of the diameter of the test piece, as it can be seen from figure 36. The other was the lowering of the temperature of the cooling water. The latter was supplied from a container where water and crushed ice were mixed together, and forced to flow by two peristaltic pumps BYO 800 (Norris Industries), at a flow rate of approximately 0.8 litres per minute. The resulting CCT curves are seen from figure 37. The microstructures associated with the various cooling times will be exhibited in the Metallography section.

3.5.10 Other Representation Of The Transformation Points

Two other graph plottings of the transformation points were devised to help in the discussion of the phenomena. One is seen from Fig. 38 and shows the development of the start and finish of the transformation temperatures on their own cooling curves, with the increase in peak temperature. For that graph the average transformation temperature for each condition was considered. The other representation in Fig. 39 exhibits the scatter band for the start of transformation points for the conditions studied.

3.6 Charpy Impact Testing

The testing procedure chosen to be used in the investigation to evaluate the toughness of the actual weldments, and of the duplicated specimens was the transverse Charpy V Notch Impact test on samples of the standard size (21). It is a dynamic test, where the specimen is supported horizontally, as a single beam, with the axis of the notch vertical. The specimen is then struck in the middle of the face opposite the notch and fractured by a single blow of a pendulum released from a fixed height. The energy absorbed in fracturing the specimen is recorded and must be corrected for losses associated with the friction forces of the system. The energy values determined are qualitative, although frequently specified as an acceptance criterion. Testing temperatures other than the ambient temperature are commonly employed according to the specification required from the material.

The low toughness of the HSLA microalloyed steels is more commonly associated with sub zero temperatures. The RQT-500 steel is not specifically designed for use at high temperatures, thus the range of testing temperatures employed in this investigation was concentrated in temperatures below room temperature. They were obtained by a mixture of dry ice with commercial acetone, and kept inside a vacuum flask. Occasionally temperatures below - 80^{o}C were employed; these were obtained by a mixture of liquid nitrogen and commercial acetone. Water at a specific desired temperature was employed, when the testing temperatures were in the region of the room temperature. The specimens were kept inside the bath for five minutes before testing. Then they were handled with tongs, properly inserted in the machine by means of a centering jig and broken within five seconds, as specified in the ASTM standards. The equipment used was the Avery Testing Machine with a capacity of 300J and a striking velocity of 5m/s. The temperatures of the bath were monitored from an alcohol thermometer.

3.6.1 Results

The several purposes of the interpretation of the Charpy Impact tests in this investigation are listed below :

i) The determination of the rolling direction of the plate sections supplied by BSC.

ii) The choice of the notch positioning for the actual samples welded at 3.6KJ/mm.

iii) The variation of the absorbed energy with the testing temperature.

iv) The variation of the fracture appearance with the testing temperatures.

The first two sub items listed above are of auxiliary nature, whereas the remaining represent one of the main purposes of this work. Charpy tests were also performed in the post weld heat treated specimens to investigate the heat treatment effectiveness. These results will be shown and commented under a further specific topic, post weld heat treatment.

3.6.1.1 The Determination Of The Rolling Direction Of The Plate Sections

The plate sections supplied by BSC had no indication on the rolling directions. Since it should be known, this was derived from Charpy testing and supported by metallographic observation of the orientation of the inclusions. Two specimens were extracted from each of the two main directions of the plate sections supplied, care being taken to avoid sampling in the regions affected by the flame cutting. The test temperatures employed were between -30 and -50^{o}C. The results of the Charpy tests indicated that the rolling direction of the plate was parallel to the longest dimension of the plate sections. Individual results for each plate section will not be displayed; instead, the figures from the typical longitudinal and transverse Charpy results for the RQT-500 steel can be seen from the table 19. The graphical interpretation for the variation of the absorbed energy with the test temperatures, for both conditions, is seen from Fig. 40. The transverse specimens exhibited lower toughness values than the longitudinal ones, because the propagation of their fractures was favoured by the disposition of the inclusions.

3.6.1.2 The Choice Of The Notch Positioning For The 3.6KJ/mm Real Weldment Samples

The reasoning on this matter was given in item 3.3.3.. Here the results will be exhibited and their interpretation commented. The specimens were Charpy tested at -20°C. The values of the absorbed energies can be seen from table 20 and should be associated with the Fig. 18b. From the results, one should notice that the set of specimens II and III exhibited the lowest and somewhat similar results. The choice on the notch location fell on the position III because a larger extension of the HAZ would be tested, and the composite would involve only two zones, the HAZ and the base metal, the weld metal being excluded.

3.6.1.3 The Variation Of The Absorbed Energy With The Testing Temperatures

These results represent one of the main objectives of this investigation. The figures obtained for the many conditions tested can be seen from tables 21 to 24. The traditional manner of representing graphically the results of a Charpy Impact test is the freehand drawing of a curve through the plotted data. Some authors reported that whenever a large scatter exists in the results, other than the freehand curve drawing, the determination of the regression line for the points falling in the transition range ensures a more consistent representation of the phenomena (107). Thus, the graph plotting associated with the numerical values of the toughness were represented in more than one way, according to the different tendencies and allowing a better comparative observation of the results. For the base metal and for the two actual weldment conditions, graphs were drawn for the two

interpretations quoted above, and will be displayed before each set of graphs. The first set of graphs seen from figures 41 to 44 represent the freehand drawing criteria. Figure 41 exhibits the variation of the Charpy results for the parent metal, and for the two real weldments. The other graphs are representative of the tests performed on the simulated specimens. In each of these graphs, the peak temperature is varied and heat input is kept constant. The second set of graphs can be seen from figures 45 to 52 and represent the regression line criteria, displaying the transitional line variation for the heat inputs studied, the peak temperature being kept constant. The regression equations were calculated by means of the statistical package UA 01 from the University computer, and are displayed in the appendix III. A third type of interpretation, sought to give overall information on the tendencies of the toughness for all the conditions studied, is seen from figures 53 and 54. It displays the variation of the absorbed energy level at the testing temperatures of 0 and -20°C, respectively, with the heat input and peak temperatures used. These temperatures were selected because the absorbed energies associated with them were representative of the behaviour of the HAZ toughness throughout the range of testing temperatures.

3.6.1.4 The Variation Of The Fracture Appearance With The Testing Temperatures

Another interpretation commonly used for the Charpy tests is the appearance of the fracture, i.e. the percentage of crystallinity and shear exhibited in the fractured surface of the specimen, with the test temperature. These can be

estimated by the length and width of the cleavage portion of the fracture surface, and the percentage of shear is determined from a table given in the ASTM standards (21). In the present investigation, occasionally, that method would not supply the best estimation, when the presence of a certain number of inclusions surrounded by ductile zones occurred. This can be seen from the macrograph in figure 55. For these specific cases, the sample was mounted on a microscope at low magnification, and the percentage of the brittle fracture was estimated by the brittle areas counted on the screen of the microscope with the help of a super-imposed grid. The figures for the estimated percentage of shear and cleavage with the test temperatures can also be seen from the tables 21 to 24. The curves representing these values can be seen from the graphs in figures 56 to 59.

3.7 Optical Metallography

Classical optical metallography was employed to identify the phases, and to delineate the prior austenite grain boundaries of the microstructures exhibited in the specimens to be observed. This involved the cutting and the mounting of the samples, polishing to one micron standard and, finally, etching them. The area observed was always the cross section of the fractured samples.

The etching agent employed to reveal the phases in the current work was Nital II (2% of nitric acid in acoholic solution). The grain boundaries of the samples welded at 6.3KJ/mm and simulated at 6.3 and 14.4KJ/mm were also revealed by Nital II etching. Their identification was evident because of the

presence of proeutectoid ferrite along the grains. Because little or no such constituent existed in the samples welded or simulated at 3.6KJ/mm, some difficulties were faced on etching their grain boundaries. Recommended reagents such as SASPA or NANSA SS 60 (108) did not produce good results. Sophisticated etching techniques using Klemm's reagent (109) failed to reveal the grains. Thermal etching (the sample is heated just above A_1 for a few minutes, and then quenched; austenite which started to nucleate at the grain boundaries should transform to martensite; the latter is revealed by SASPA reagent, thus delineating the grain boundary), although controversial (110) was attempted, but no positive results were obtained. A paper dated from 1948 (111) provided the solution for the problem. The composition of the solution and the technique used for etching with 0.3% CTAB can be seen from table 25. The optical micrographs obtained during this investigation can be seen from figures 60 to 106. Figure 60 shows the microstructures of the base metal. Figures 61 to 67, 68 to 74, and 75 to 81 represent the peak temperatures from 700°C to 1400°C for the simulated samples at the heat inputs of 3.6, 6.3 and 14.4KJ/mm, respectively. The figures 82 to 86 exhibit subsidiary crack paths or fracture profiles, and will be commented on later, in the discussion on the fractography. The figures 87 to 89 and 90 to 92 show, comparatively, the structures for the peak temperatures of 1150, 1250 and 1400°C of the 6.3 and 14.4KJ/mm heat inputs, respectively. The figures 93 to 99 involve micrographs of the real weld HAZ and of the simulated ones. The latter will help comparisons and comments to be made on the reproducibility of real weld HAZ by simulation techniques. Finally, the figures 67, 89, 92 and 100 to 106 represent the structures

obtained from the cooling curves I to IX and of the cooling curve XI. The latter are the micrographs representative of the samples employed in the building up of the CCT curves. The structure equivalent to the cooling curve X is not shown, because it was very similar to the one of curve IX.

3.7.1 Classification Of The Microstructures To Be Observed

In order to quantify the various microstructures, they would have to be classified prior to examination. Some difficulties were met when first attempting that qualification. They were due to the intricate and similar nature of the phases to be differentiated. Similar structures sectioned in different angles would provide a totally different picture to the observer. A good example was outlined by Levine and Hill (72) concerning upper bainitic structures. Figure 107 illustrates the fact, which was previously mentioned by Pickering (112).

The structures to be observed were classified into two groups according to the peak temperature attained by the simulated sample. The first group consisted of these samples, whose maximum nominal peak temperature was equal to 1000^{o}C. Their grain size was fine and their microstructures were classified as follows :

i) Tempered martensite.

ii) Ferrite plus carbide aggregates.

iii) Intragranular carbides.

iv) Ferrite.

The second group consisted of those samples which were

simulated at nominal peak temperatures of 1150°C and above. Their grain size was coarse and their microstructures were classified as :

i) Proeutectoid ferrite.

ii) Pearlite.

iii) Intragranular ferrite.

iv) Interlocking acicular ferrite.

v) Upper bainite.

A brief comment will be made now on the nature of each of these structures :

Tempered martensite : As it was expected, that structure was observed in the base metal. The specimens simulated to 700°C, where no austenitisation occurred, also exhibited these tempered martensite needles. They can be seen from figures 60, 61, 68 and 75 where they are marked as "a".

Ferrite plus carbide aggregates : These structures were easily observed as groups or at "thickened" grain boundaries. At the latter position, their nature was revealed with the help of higher magnifications provided by the Transmission Electron Microscopy, as it will be seen later. They are considered to result from the austenitisation and subsequent cooling of the carbon rich areas. These structures are marked as "b" and can be seen from figures 62 to 64, 69 to 71, and 76 to 78.

Intragranular carbides : These are the carbides seen in the interior of the grains. They are considered to grow on sub-critical heating, thus they become easier to observe. As

the peak temperatures go above the A_1 temperature, the situation becomes difficult to be interpreted, since it is believed that some of the carbides continue to grow, whereas some of them start to dissolve. Because they can be easily identified from figures 60 to 64, 68 to 71, and 75 to 78, they are not indicated by a character .

Ferrite : Polygonal ferrite with tendency to some acicularity is the dominant constituent of this first group of structures. The aspect ratio of the acicular plates is higher in the base metal and in the two lower peak temperature samples. By ferrite, one means the ferrite formed on cooling, the untransformed ferrite, or a mixture of both, depending on the peak temperature attained. Since it is evident in the micrographs, it will not be indicated. It can be seen from figures 60 to 64, 68 to 71, and 75 to 78.

Proeutectoid ferrite : This is a common name given to the constituent which delineates the prior austenite grain boundaries of almost all the samples of the second group. It was not detected for the specimens heated to 1150 and 1250^{o}C for the 3.6KJ/mm heat input, although it was occasionally observed for the peak temperature of 1400^{o}C of the same condition. It is marked as "c" in the figures 72 to 74, 79 to 81, and 83.

Pearlite : This constituent was only observed at the peak temperature of 1150^{o}C of the 14.4KJ/mm heat input condition. It is marked "d" on the figure 79.

Intragranular ferrite : Very often an isolated ferrite plate or grain was observed inside the prior austenite grains.

These structures are called intragranular ferrite. Sometimes its recognition was doubtful, since they could be an unresolved small upper bainitic colony or a form of growth of the proeutectoid ferrite observed by a different sectioning plane. The samples simulated at 1150°C for the 6.3 and 14.4 KJ/mm heat inputs did not display these structures. They are marked "e" and can be seen from the figures 65 to 67, 73, 74, 80 and 81.

Interlocking acicular ferrite : It corresponds to the structure seen in figure 108, reproduced from a paper by Levine and Hill (72). In the current work, however, it did not appear so coarse and easy to detect as in that micrograph. This constituent is considered a good structure due to its fineness and high angle boundaries. These will oppose the propagation of the crack path on fracture. Sometimes it was difficult to differentiate this type of structure from the cross sectional intersection of small upper bainitic colonies. It was not observed for the peak temperature of 1150°C of the 6.3 and 14.4KJ/mm heat inputs. It is marked "f" in the figures 65 to 67, 73, 74, 80 and 81.

Upper bainite : A well known undesirable structure. Its low angle boundaries allow easy crack propagation. Its configuration can change according to the intercepting plane, as has already been mentioned, and shown in the micrograph of the figure 107. Parallel colonies of ferrite originating from the grain boundaries and propagating into the grains were also considered under this category. Some authors have called the latter structure Widmansttaten ferrite (113). The upper bainite was marked as "g" and can

be seen from the figures 65 to 67, 72 to 74 and 79 to 81.

During the metallographic observation, attention was drawn to a particular structure. It occurred at the peak temperature of 1150 and 1250^{o}C for the 3.6KJ/mm heat input condition, and has been described as "white areas". At the beginning they were thought to be a form of martensite-austenite (M-A). They can be seen from the micrographs 65 and 66 where they are marked "h". When the sample was more deeply etched, parallel arrays of carbides could be seen inside these structures, appearing to be of an upper bainitic nature. Later heat treatments and hardness measurements confirmed that these structures were to be classified as upper bainite.

3.8 Quantitative Metallography

This practice employed two different methods aiming at different objectives. One was the determination of the grain size of the specimens studied. The technique adopted was the mean linear intercept. The other objective was the quantification of the structures existing in the specimens studied. For the latter, the technique employed was the phase point counting.

3.8.1 Grain Size Measurement

The comparison of grain sizes is a common practice employed in assessing the reproducibility of real weldments by welding simulation methods. Grain size is also an important parameter to be considered when estimating the mechanical properties of the materials. The method employed in the current work to measure the grain size was the mean linear

intercept (m.l.i.). In this practice the image of the specimen is projected onto the screen of an optical microscope, where a grid has been superimposed. The m.l.i. is measured from a linear transverse by counting the number of grain boundaries that intercept a linear transverse of length L. Its equation is given by m.l.i. = $\bar{d} = \frac{L}{N}$ where N is the number of grain boundaries counted. The magnification is varied according to the grain size. This provides good sampling, allied with facility of identification of the intercepts. On average, more than 1000 intercepts were observed. This is equivalent to 95% confidence limits $\pm$ 4% of the value (114). The latter applies to the simulated samples due to its homogeneity. The grain size for these specimens can be seen from table 26. When evaluating the grain size of the real weldments, some limitations were faced. They were due to the variation in the grain size and variation of the width of the regions of the weld HAZ with the depth of the welding bead. The narrowness of each of the regions also contributed to aggravate the problem, since very few grains were available to be considered. The solution adopted was to take into account only the grains from the coarse grained region, i.e. those lying at the fusion boundary and their immediate neighbours. The results are seen from table 27. They represent the scatter band of grain size per range of weld bead depth. The precise accuracy of the measurement would be very low with relative errors above 5%, but if it is taken into account that the grains are rather coarse, one would agree that these estimates are representative of the observed grain size.

3.8.2 Phase Point Counting

In order to relate the microstructures produced with the toughness properties of the various samples studied, their quantification was needed. This was performed by means of the phase point counting using the Swift Point Counter. The instrument consisted of an electrically-triggered specimen carriage, which is attached to the stage of an optical microscope. This stage unit is connected to an electrical counting device which is hand operated by the observer during the entire analysis. Discrete movements of the carriage on the horizontal and vertical axis will describe an imaginary grid on the observed surface. The moving intercept point of the grid is seen by the observer as a faint cross. Whenever the operator records a phase on the counter, that cross is displaced automatically in the horizontal direction. The vertical displacement has to be hand operated at the end of each horizontal run. A total of ten counters were provided to be associated with the phases to be counted. An extra counter would record the total amount of points observed. The vertical displacement chosen was of 0.6 mm, to account for the large grain size of some of the specimens. The horizontal displacement was equivalent to 0.3mm. The magnification employed during the observation was of X400. The number of points counted for the specimens simulated at 1150^{o}C and above, was of a 1000 points. The specimens simulated at 1000^{o}C and below that peak temperature, as well as the parent metal, were counted up to 500 points.

The tests were performed only on the welding simulation specimens. The etching agent employed was Nital II. The

latter provided a good definition of the phases to be classified. An attempt was made to count the phases for the real weldment samples. The same problems mentioned before, when attempting to count their grain size, led to the abandonment of this practice. Other difficulties faced when counting the phases of the simulated specimens were based on their similarity. Some comments on this aspect were already made when mentioning the classification of these structures. The results are divided into two sets. Tables 28 and 29 show the results for the base metal and for the fine grained samples. The results for the samples simulated at 1150^{o}C and above are seen from table 30.

3.9 Fractography

The fractured surface of the specimens were observed by two different methods :

- Optical Microscopy.
- Scanning Electron Microscopy.

The optical microscopy was performed on the polished cross section of the fractured specimens. It aimed at the observation of the subsidiary cracks to attempt a correlation of their incidence with certain types of structures. The results obtained can be seen from the micrographs in figures 82 to 86.

The Scanning Electron Microscopy (SEM) is a commonly employed technique to assess the nature of the fracture by observation of the fracture profile. The instrument used was the Cambridge 150 S.E.M., 30KV Max. The fractographs obtained can be seen from figures 109 to 129.

3.10 Transmission Electron Microscopy (TEM)

This technique was used for two different purposes involving the observation of two distinct samples :

- Double stage replica.
- Carbon extraction replica.

The first sampling aimed at the observation of the micro-structural phases at higher magnifications. In this way, more support and further clarification would be given to the phases already examined under the optical microscope. A lightly etched, degreased sample surface was wet with a few drops of acetone and a BEX film (celulose triacetate) was deposed on it. After drying off the acetone, this film was detached, fixed on a thin glass and placed on the evaporator. A thin layer of carbon was deposed on the film, and then it was shadowed with gold paladium. Pieces of the film were carefully cut and mounted on copper support grids. These grids were placed on filter paper soaked with acetone and, after two days, the plastic would have dissolved and the samples were ready to be observed. The TEM used was the JEOL 100B, 100KV max. The results from the replicas observation can be seen from micrographs 130 to 144.

The second method aimed at the detection of microalloying element precipitates. The etched samples were degreased and placed on the evaporator, where a thin film of carbon was deposed on them. In sequence, they were electroetched for approximately 5 minutes at 4V, in an alcoholic solution of 10% HCl. They were then slowly immersed in water to force the detachment of the carbon film from the sample. The floating pieces of the carbon film were collected on

copper support grids, and dried. The sample was then observed under the TEM, switched to provide the diffraction pattern of the carbides which might have been trapped in the carbon film. No Nb or V precipitates could be detected by this method. The only carbides observed were cementite particles, as seen from the TEM micrograph, and from the diffraction pattern of figures 145 to 146, respectively. The interpretation is seen from figure 147.

3.11 Hardness Testing

Vickers hardness tests, both macro and micro, were performed on the samples studied. The indentation was always made in the cross section of the fractured specimen, after it was polished and etched. For macrohardness, it is currently recommended that the impression should be kept large enough to reduce errors in the measurement (115). Consequently, the load used in this investigation was 30Kg. The results for the simulated specimens, for the parent plate and for the coarse grained region of the real weldment specimens, are seen in table 31, and their graph plotting in figure 148. The hardness values for the specimens which were heat treated are seen from table 32. The hardness associated with the samples employed in the building up of the CCT curve for the RQT-500 steel, is seen at the end of each individual cooling curve from figure 37. Microhardness tests under a 25g load were used to investigate the hardness of individual micro-constituents. The observed samples were those simulated at 1150^{o}C and above. The figures for this measurement are seen from table 33. The phase noted previously as "white areas" exhibited a microhardness of 253 and 240Hv, respectively, for

the 1150 and 1250°C nominal peak temperatures of the 3.6KJ/mm heat input condition. Since the scatter exhibited in almost all the measuresments was considerable, besides the mean value of the readings, the figures for the minimum and maximum values are also provided in the tables. Unless otherwise stated, 10 readings were performed on each sample.

3.12 The Differentiation Of The Regions Of The Real Weld HAZ

The real weldment specimens were etched with Nital II and observed under the optical microscope. An attempt was made to determine the border lines for the different regions of the HAZ. It was observed that exact limits did not exist. Instead, a gradual change in the structures occurred. It was also observed that the width of certain marked areas decreased with the increase of the welding bead penetration depth.

Thus, the examination of the microhardness profile across the actual HAZs was performed at different depths of the welding beads. The practice intended to investigate the possibility of differentiation between the regions of the HAZ by definite changes in the microhardness. The measurements were performed under the load of 300g, at intervals of 2mm across the depth of the welding bead. The results provided a general tendency of the evolution of the microhardness across the HAZ. However, they were not definite enough to allow a precise determination of the boundaries of the different regions of the HAZ. These results are seen in figures 149 to 150, corresponding to the heat inputs of 3.6 and 6.3KJ/mm, respectively. Only a few scans were plotted, otherwise the

picture would be confusing. In these plots, the fusion lines were rectified, i.e. the origin for the measurements was considered the same for the different sets of data. Then a qualitative approach based on the size of the grains and/or on the appearance of the region was attempted. This was accomplished by observations made under the microscope of the Leitz Wetzlar microhardness tester. The X-Y stage micrometer would allow the measurement of the widths of the selected regions, discretely, throughout the entire HAZ. The chosen features for the 3.6KJ/mm heat input HAZ were :

i) The coarse grained HAZ.

ii) The region adjacent to the former, where the grain size would have approximately half of their grain size, or less.

iii) The fine grained region.

Four regions were distinguished for the 6.3KJ/mm heat input HAZ :

i) The coarse grained HAZ, where a thin layer of proeutectoid ferrite would delineate the prior austenite grain boundaries.

ii) The neighbouring region to the former, where the grain sizes were smaller and the proeutectoid ferrite coarser, delineating more evidently the other structures.

iii) A region consisting of coarse platelets of proeutectoid ferrite.

iv) The fine grained HAZ.

Two graphs were plotted to help the visualisation of the HAZ regions selected in that way. On these graphs there will be the superimposition of micrographs of the specific regions considered. They are seen from figures 151 and 152 for the 3.6 and 6.3KJ/mm heat inputs, respectively. A more general view of the variation of the width of the coarse grained HAZ region with the weld bead penetration depth can be seen from the micrographs in figures 93 and 96, respectively, for the 3.6 and 6.3KJ/mm welding conditions. For the latter, it would be interesting to point out that there is a continuity of the proeutectoid ferrite seen delineating the prior austenite grain boundaries of the coarse grained region of the HAZ, and that observed in the weld metal structure. This can also be seen from figure 96.

3.13 Post Weld Heat Treatment (PWHT)

This technique was used to evaluate the effect of tempering heat treatment on the toughness of a few chosen samples. These were specimens which exhibited a strong embrittlement after simulation at 1250^{o}C for a heat input equivalent to 14.4KJ/mm. The effect of PWHT on the toughness of the parent plate was also briefly investigated.

Tempering was further employed in the clarification of the nature of the phases defined as "white areas". These occurred at peak temperatures of 1150 and 1250^{o}C and at a heat input of 3.6KJ/mm. The experiment was based on a report from Biss and Cryderman (116). They observed that steels containing martensite-austenite constituent had poor impact properties which were recovered by tempering at 530

to 620°C. The tempering condition for all specimens, as well as their Charpy testing values at -20°C, can be seen from table 34.

CHAPTER 4 - DISCUSSION

CHAPTER 4 - DISCUSSION

4.1 Introduction

The toughness and microstructure of the whole of the weld HAZ of a Quenched and Tempered C-Mn, Nb and V microalloyed steel, has been systematically investigated. Simulation techniques were employed to reproduce the actual weld HAZs which had the advantage of offering a larger area for Charpy notch positioning, microstructural observation, and hardness testing. Handling of the samples was facilitated and dilation curves could be established for each set of conditions. Three heat inputs were examined: 3.6, 6.3 and 14.4KJ/mm at nominal peak temperatures ranging from 700 to 1400^{o}C. Some improvement of toughness occurred at peak temperatures up to 1000^{o}C, but serious embrittlement was observed when the samples were thermal cycled at peak temperatures which dissolved the microalloys into the austenitic phase. The present chapter will discuss the results found in the present investigation, and their significance, as well as making comparisons with published investigations. It will involve detailed treatment of the actual toughness changes observed and consideration of the mechanisms responsible, in particular the role of microstructures and precipitation hardening.

4.2 Assessment Of Experimental Technique

In this section, comments will be made on the techniques employed to produce the samples to be tested, as well as on their reproducibility. There will also be discussion about the decision which led to the use of simulated specimens,

together with comparison with investigations of the current literature.

4.2.1 Real Weld HAZ Thermal Cycles

Unlike the weld metal, the HAZ chemistry is only affected by the base plate composition. Consequently, the welding consumables used (wire and flux), were not chosen for their particular properties. They were consumables which were readily available, and provided the heat input and the protection needed for the reproduction of a sound weld HAZ at the desired energy levels.

The production of a planar HAZ was problematic at the beginning. A modification on the earth lead positioning provided a good solution to the difficulties encountered. The measurement of the welding thermal cycles was particularly successful in the determination of the cooling times from 800 to 500^{o}C, referred to as Δt in the current work. Further information required from the same set of experiments was the distribution of peak temperatures along the regions of the HAZ. The latter was not systematically obtained. This was due to the instability of the weld bead toe, and to the lack of experience of the data collector. Experience was being acquired with time, but because these experiments involved time and high costs for the preparation, that technique was substituted by theoretical computer calculations. However, the results obtained from these practical experiments provided an adequate basis of comparison to substantiate the results obtained by computer calculation.

4.2.2 Computed Thermal Cycles

These results could be summarised by the equation proposed in the item 3.4.2. That equation provided an extremely good fit, not only for the practical results of the current work, but also for the practical results of other authors (13, 56, 104). The theoretical calculations employed in the present investigation provided better match to the practical results than the calculations used by the authors of the Welding Institute (104), particularly at higher heat inputs.

4.2.3 Weld Thermal Simulation, Temperature Distribution, Weld Thermal Cycle Duplication And Reproducibility

i) Temperature Distribution

There have been some doubts in the literature concerning the homogeneity of the temperature distribution on thermally simulated samples. Swedish investigators (35) mentioned the occurrence of higher temperature in the centre of the sample. Other references on the same subject are given somewhere else (102). In the latter, it is proved that when the appropriate thermocouple attachment and calibration techniques are employed, measurements can be made that are easily reproduced and accurate for simulation work. The techniques involved were the ones used in the current work, and as it was seen from figure 26, there is an extremely good match between the centre/surface temperatures. The radial temperature distribution was verified and also proved to be acceptable, i.e. sensibly constant across the section thickness. The lower figures obtained towards the surface of the sample, seen from figure 27, are attributed to the thermocouple heat

sink effect (106). Finally, the longitudinal temperature distribution was determined, and the existence of a temperature plateau of approximately 4mm, at the centre of the specimen, was confirmed. The latter was sufficiently wide for a precise location of the Charpy V Notch and provided a good homogeneous region for microstructural work. This calibration can be seen from figure 28.

ii) Weld Thermal Cycle Duplication

In principle, the series of weld thermal cycles should not intersect, as Savage (117) shows in his idealised illustration reproduced in figure 153. In practice it was found difficult to achieve this experimentally. The limits for the sensitivity of the equipment do not allow the exact reproduction of the high heating rate of some welding processes. In fact, the cooling times have to be adjusted to approximate to the practical values on an adhoc basis. This is performed by trial and error runs, after the initial adaptation of the desired thermal cycle, to the temperature programmer of the equipment. Consequently, simulated thermal cycles are slightly different than the real ones. Often this difference is characterised by the intersection of the cooling cycle of a higher peak temperature, with the cooling cycle of a lower peak temperature. This is seen in figures 30, 31 and 32 of the current work. The same fact was noticeable in the simulation cycles produced by other authors (40, 44). It was observed that the samples simulated at 900^{o}C for the heat input of 6.3KJ/mm had their cooling cycles intercepting those for the peak temperatures of 700 and 800^{o}C. The cooling time Δt = 90s was maintained by a longer run time at lower temp-

eratures. This is believed to have caused an effect on the impact properties of the microstructures obtained, as it will be discussed later, in the section commenting on the Charpy testing.

iii) Reproducibility

Some authors stated that the steeper temperature gradients in the real weld HAZ will limit the grain size of the final coarse product. They mentioned that if the same region is to be synthetized by welding simulation, peak temperatures lower than the actual ones should be used (43, 44, 60). However, there are a number of uncertainties inherent in their approach, e.g. what do these authors consider as the real HAZ coarse region grain size. From the sketch in figures 151 and 152, from the micrographs in figures 93 and 96 and from table 27, it can be seen that the size of the coarse grains and the width of the coarse grained region of the HAZ are always changing with the depth of the welding bead. In the current work, the simulation practice produced specimens, whose grain sizes were comparable to those observed in the coarse grained region of the actual weld HAZ. This can be seen from the micrographs in figures 94, 95, 97 and 98, for the heat inputs of 3.6 and 6.3KJ/mm, respectively.

The following factors discussed above, and briefly listed below, constitute the reason why the current work was performed based on samples obtained by simulation techniques :

- Absence of a temperature gradient in the centre/surface of the simulated specimens, as well as the existence of a thermal plateau in their central region.

- Availability of a computer program to calculate the cooling time $\Delta t_{800-500}$ with a good fit to the practical situations.

- A reasonable reproduction of the actual thermal cycle by simulation techniques leading to a good match between actual and synthetized grain sizes and structures.

- The facility of handling simulated test pieces and their reduced cost relative to that of specimens extracted from actual weldments.

4.3 Austenite Decomposition Under Weld HAZ Cooling Conditions

The study of the transformation temperatures for the micro-alloyed HSLA steels is complex and very seldom approached in the literature. In the current work, the simulation equipment was also provided with dilation facilities. Thus, the dilation history of each synthetic sample was recorded. The exact location of the transformation points, sometimes, could not be accurately determined. Although the tangent method seen from figure 35 was employed, the dilation curves were not exactly smooth and many times their slopes departed from linearity near the transformation points. These factors contributed to the difficulties faced when determining the transformation points.

The values for A_1 and A_3 obtained on heating for the current work are seen from tables 14 to 18. One would observe that

they appear to be in excess of the values of approximately 720°C for A_1, and 900°C for A_3, which would be the figures expected for the transformation points of a steel containing 0.15%C. However, one must note that these points were obtained from specimens subjected to an extremely high heating rate. Therefore, it does not seem totally unreasonable that they have been distorted, displaced by the rapid heating rate, to higher temperatures. Rothwell et al (61) tested a total of seven Nb and/or V microalloyed steels and their reference steel containing 0.095%C and 1.27%Mn. They obtained results for A_1 and A_3 in the range of 700 and 900°C, respectively. Their conclusion was that A_1 appears to be relatively insensitive to microalloying additions. Regarding A_3, they observed that for the V steels it was somewhat higher than for the steels containing other microalloying elements. They also noticed that the end of the transformation on heating was not as well defined as the beginning. The fact was explained as a function of the vanadium carbonitrides immediate solubility above the ferrite-austenite transformation temperature, and it was mentioned that their progressive dissolution would be sufficient to distort the austenite dilation line in its initial stages and yield a high A_3 temperature.

The plotting of the scatter band for the variation of the transformation start temperature on cooling, with the heat input and with peak temperature variation is seen from figure 39. It gives a fairly good and consistent idea of the development of that parameter with the heat input and peak temperature. If a generalisation is attempted, one should

say that, for peak temperatures up to 1000°C, for the three heat inputs investigated, the start of the transformation temperature varied little and was kept above 720°C. At the peak temperatures of 1150°C and above, where the microalloys would go into solution, a noticeable variation occurred. At the two higher heat inputs, the start of the transformation temperature was lowered as the peak temperature was increased. The slope of the variation was very similar for these two heat inputs and the 14.4KJ/mm condition always exhibited higher values for the parameter than the 6.3KJ/mm condition. At the heat input equivalent to 3.6KJ/mm, the slope of variation was steeper than for the other conditions, but the peak temperatures of 1250 and 1400°C exhibited similar values for the start of the transformation temperature. Figure 38 shows the development of the start and finish of the transformation temperature with the heat input and peak temperature variation. The points were plotted on the cooling curve equivalent to the heat input and peak temperature considered. For a better picture, these cooling curves are not plotted. Generally, a continuous lowering of the transformation points with the increase in peak temperature, and with the decrease in heat input was noticed. In this concern, the start of the transformation temperature exhibited consistent behaviour. The picture for the finish points of transformation was not as clear. Sometimes "elbow" points were seen, as in the case for the 6.3KJ/mm heat input at 1000 and 1150°C. "Elbow" points similar to these have been previously observed for Ni, Cr and Mo, Quenched and Tempered steels, but no particular attention nor explanation was given to the fact (118). At a fixed heat input, as the peak temperature attains values

where the microalloys would go into solution, the austenitic grain size will coarsen and the amount of Nb in solution will increase with the increase in peak temperature. Both factors are reported to depress the transformation temperature on cooling, and that was observed in the current work. At a fixed peak temperature in the dissolution range of the microalloys, the grain size, the solubility of the microalloys in the austenite, the cooling time Δt and the start of the transformation temperature increase with the increase in the heat input. The cooling rate seems to be the major factor responsible for the depression of the transformation temperature, as it can be observed from figure 39. The structures formed on cooling are dependent on the temperature of the $\gamma \rightarrow \alpha$ reaction, consequently they are a function of the heat input and peak temperature involved. These structures will be considered later.

Few authors give an opinion on the effect of Nb and V on the transformation temperatures of their reference steel. Bonomo and Rothwell (25) observed that a rapid deterioration in the toughness properties occurred in coincidence with a sharp rise in the transformation temperature, as the cooling rate decreased. Bernard (28) stated that their influence was quite small, but that a slight effect was observed for slower cooling rates corresponding to a lowering of the transformation temperatures. Both authors shared a common opinion that the effect seems to take place in the same region where partial precipitation is thought to occur upon cooling. Rothwell et al (61) observed that V alone has little effect on the transformation temperatures, but in the presence of Nb it causes a

significant decrease in the transformation temperature at fast cooling rates of Δt = 3s. Although the observation was made, no explanation was given.

The continuous cooling diagrams (CCT) for the welding condition cannot be predicted on the basis of the existing continuous cooling transformation curves usually prepared with a view to the heat treating of the steels (118). Consequently, a continuous cooling diagram for the welding of the RQT-500 steel was built up, from simulation samples heated to a nominal peak temperature of 1400°C. It can be seen from figure 37. The interpretation of the transformation points, mainly the start of the martensitic transformation amidst the bainitic transformation, were clarified in the light of the work of Martin and Roques (119). It was noticed that the martensite start temperature was lowered as the cooling time was increased. This phenomena has been observed before and was attributed to a substantial carbon gradient present in the untransformed austenite in the course of the bainitic transformation (120).

4.4 Toughness Variations In The Weld HAZ

A considerable amount of information was obtained from the results of the Charpy Impact tests. The figures obtained were compared in more than one way, allowing a better understanding and rating of the toughness properties with the heat inputs and peak temperatures used. The following considerations were based on the absorbed energy criterion and the comparisons were performed based on the straight line graph representation seen from figures 45 to 52. In fact,

they differed very little from the free hand plot of the Charpy curves. Also, the general tendencies found for the Fracture Appearance criterion (when the percentage of crystallinity and shear appearance of the fracture, estimated from the broken surface of the specimen is plotted against test temperature) differed very little from those encountered for the absorbed impact energy criterion. Consequently, the comments which will be made for the latter would be generalised for the results found from the appearance of the fractured surface. The many comparisons performed involved :

i) Comparison of real HAZ to base metal.

ii) Comparison of real and simulated HAZs.

iii) Toughness variation with peak temperatures and heat input.

iv) Comparison of toughness of simulated HAZ to toughness of the base metal.

v) Comparison to previous works.

For a better, general quantification of the results obtained, a terminology was devised. Thus, by "slight" variation, one should understand a variation in the absorbed energy, not exceeding 5J. The "higher" or "lower" terminology would involve a variation in the range of 5J to 10J. Finally, a "considerable" variation would be one involving figures in excess of 10J.

i) Comparison Of Real HAZ To Base Metal

It was observed that, at the heat input of 3.6KJ/mm, the toughness of the real weld HAZ was very similar, just slightly

lower than for the base metal. When the heat input was raised to 6.3KJ/mm, a considerable fall in the absorbed impact energy occurred. This behaviour is not surprising. When the actual HAZ specimens were prepared, those representative of the lower heat input were notched in a region comprising the coarse and fine HAZ regions, plus the base metal. Consequently, it was not only the coarse grained HAZ which was being tested, but a composite with a large amount of fine grained structures. This fact is usually referred to as the protective influence of the HAZ profile. In contrast, the specimens extracted from the 6.3KJ/mm actual weldment exhibited a planar HAZ allowing the Charpy notch to be totally located in the homogeneous coarse grained region. The consequence of the fracture crack, propagating through a brittle region of homogeneous structure, was the considerable lowering of the HAZ toughness relative to the base metal one. Based on these results, one could observe that when the steel RQT-500 is welded, there is a deterioration of the toughness of the HAZ coarse grained region relative to the toughness of the base metal, and that this deterioration increases considerably as the heat input is raised from 3.6 to 6.3KJ/mm.

ii) Comparison Of Real And Simulated HAZs

The comparison will only be made for the specimens simulated at peak temperatures of 1150°C and above, for the 3.6 and 6.3KJ/mm heat input conditions. At the peak temperature of 1150°C, the lower heat input exhibited a very similar result for the actual and for the simulation HAZs observed. At the heat input of 6.3KJ/mm, for that same peak temperature, the simulation HAZ exhibited a higher impact energy than the

actual HAZ. At the peak temperature of 1250°C, the results for the 3.6 and 6.3KJ/mm simulation HAZs were almost identical and coincident with the results obtained for the 6.3KJ/mm actual weld HAZ. Consequently, due to the HAZ profile effect, the 3.6KJ/mm actual weld HAZ results were considerably higher than those for the simulation at 1250°C, whereas the 6.3KJ/mm heat input simulated condition provided an extremely good match for the actual weld 6.3KJ/mm condition. Finally, at the peak temperature of 1400°C, impact energies exhibited by the synthetized 6.3KJ/mm HAZs were higher than those exhibited by the actual weld HAZ. However, at the heat input of 3.6KJ/mm, the synthetized HAZs had a lower impact energy than the actual weld HAZ. It has already been mentioned that the latter represented a composite involving HAZ and base metal, whereas the former consisted of a homogeneous region exhibiting structures characteristic of those found only in the coarse grained HAZ region.

Bernard (28) and Dolby (30) have mentioned that Charpy testing in simulation specimens produced lower results than the tests performed in the actual HAZ samples. The latter explained that in the synthetized specimens, there is a constant yield strength and constant microstructure across the ligament below the notch, which is unlikely to occur in the actual weld HAZ specimen. The extraction of the sample and the notch positioning in the HAZ of the deep weld penetration specimen of Bernard's work were very similar to those practices adopted in the current research, i.e. there was a constant microstructure below the ligament across the notch. However, he observed better toughness for the real HAZ weldments. Due

to the similarity of the results obtained in the current work for the actual and simulation HAZ Charpy testing at the 6.3KJ/mm - 1250°C condition, it was definitely established that the study of the weld HAZs for the steel RQT-500 could be performed by means of simulation techniques.

iii) Toughness Variation With Peak Temperature And Heat Input

The picture was quite clear and could be generalised for the three heat inputs simulated. The toughness of the samples tested increased with the peak temperature in the following order: 1250, 1400, 1150, 700, 800, 1000 and 900°C. The coarse grained HAZ regions (peak temperatures of 1150°C and above) exhibited an extremely low level of absorbed energies, if compared to the fine grained HAZ regions (peak temperatures up to 1000°C). The exception occurred for the 3.6KJ/mm heat input simulated at 1150°C, which exhibited a level of absorbed energy similar to the ones obtained for the 700°C peak temperature. The absorbed energies were similar at the peak temperatures of 900 and 1000°C for the heat inputs of 3.6 and 14.4KJ/mm. The highest toughness observed in the current work was for the heat input of 6.3KJ/mm at the peak temperature of 900°C. This seems to be related to the shape of the simulation cooling curves for these specimens. Attempting a generalisation, one would observe that there was a lowering of the toughness of the HAZ when the peak temperature exceeded 1150°C. The higher the heat input of the process, the higher the deterioration of the toughness properties in the following order of peak temperatures: 1150°C, 1400°C, 1250°C. In the fine grained region of the HAZ (peak temp-

eratures of 1000°C and below), the toughness could be said to be independent of the heat input, and to increase in the following order of peak temperatures: 700, 800, 1000 and 900°C.

iv) Comparison Of Toughness Of Simulated HAZ To Toughness Of The Base Metal

To provide a better picture of the overall effect of the heat input and peak temperature on the toughness of the simulated HAZ, as well as their comparison with the base metal toughness, a graphical representation was devised. It consisted of the plotting of the variation of the absorbed impact energies of specimen representative of the conditions tested at a fixed temperature. Two graphs were built up for testing temperatures of zero (0°C) and of minus twenty (-20°C) degrees centigrade, and are shown in figures 53 and 54, respectively. Also represented are the points equivalent to the base metal and to the two actual weld HAZ conditions for a better comparison. It was observed that at the peak temperature of 700°C, the three heat inputs exhibited less toughness than the one observed for the base metal, and generally the toughness was lower, the higher the heat input. At the peak temperature of 800°C, for the three heat inputs, the toughness of the simulated specimens was slightly higher than that for the base metal. At the peak temperature of 900 and 1000°C, the synthetized specimens at the three heat inputs investigated exhibited considerably higher energy levels than that for the base metal. The highest toughness observed for the 6.3KJ/mm - 900°C, condition was already mentioned to be related with the shape of the cooling curves obtained for that

particular set of specimens. Generalising, one could say that the simulated specimens investigated at the heat inputs of 3.6, 6.3 and 14.4KJ/mm, at peak temperatures up to 1000°C exhibited similar and better toughness than the one observed for the base metal, the best results occurring at the peak temperatures of 1000 and 900°C, respectively. When analysing the coarse grained HAZ regions, a different picture emerged. At the peak temperatures of 1150, 1250 and 1400°C, for the three heat inputs investigated, the toughness of the HAZ simulated specimens was considerably lower than that for the base metal. The only exception was seen for the condition 3.6KJ/mm - 1150°C, where the toughness of the synthetized HAZ was only slightly lower than the toughness of the base metal. That lowering in the toughness properties seems to be associated with the depression of the start of the transformation temperature not observed at peak temperatures up to 1000°C. It deteriorates with the increase in the peak temperature and heat input, although the lowest toughness was usually observed at 1250°C.

v) Comparison To Previous Works

The reason why a Quenched and Tempered steel microalloyed with Nb and V was chosen as the material for the current research, was that data on that steel, the RQT-500, was not reported hitherto. Also, that particular combination of Nb plus V, although seldom studied, is reported as the most dangerous one, regarding the toughness of the coarse grained region of the HAZ. Whenever the steels of that group Nb + V are studied, an attempt to compare their toughness level relative to a reference steel, base metal or steels contain-

ing different microalloys or levels of microalloying is more often found than an attempt to explain systematically why the deterioration occurs. Relationships between the transformation temperatures on cooling with the resulting structures are scarce, and a certain amount of speculation can be observed, since discussing the deterioration mechanisms many authors refer to microalloying precipitation without being able to prove it. The task undertaken involved a systematic investigation of the heat input covering the range for submerged arc welding from 3.6 to 14.4KJ/mm, and observing not only the most embrittled region, as it is usually found in the literature, but all the regions of the HAZ to observe the behaviour of the deterioration with heat input and peak temperature. It was observed that the higher embrittlement occurs in the coarse grained HAZ region, i.e. the region where the peak temperature allowed the dissolution of microalloys, thus, the austenitic grain coarsening. Namely, these were the peak temperatures of 1150, 1250 and 1400^{o}C. Amidst these, the highest embrittlement usually occurred at the peak temperature of 1250^{o}C. Concerning the peak temperatures in the range of the fine grains, the toughness of the regions involved was better than the toughness of the base metal. The maximum toughness occurred at the peak temperatures of 1000 and 900^{o}C, in that order. Generalising, one could say that the deterioration of the toughness properties of the steel RQT-500 increased with the heat input and peak temperature. The latter statements, as well as that mentioning the coarse grained HAZ as the most embrittled region of the HAZ, are in very good agreement with the data quoted in the literature. Comparisons on the behaviour of the RQT-500 steel relative to

a reference steel or steel of similar composition and different microalloys or levels of microalloying, will have to await further work, because these steels were not available to be tested at the time of the current investigation. What could be said is that in the absence of the protective influence of the weld HAZ profile, the toughness of the coarse grained HAZ regions of the RQT-500 steel was found to be extremely low. Comments concerning the rating of steels containing different microalloying were already made in the literature survey. It will be repeated that the consensus of current literature rates the steels in order of increasing deterioration of toughness as: C/Mn + V, C/Mn, C/Mn + Nb and C/Mn + Nb + V. Many times, the various authors displayed their toughness results as the variation of the test temperature where the Charpy absorbed impact energy equal to 28J (T_{28J}) was plotted against the variation of the cooling times Δt. Therefore, a graph using these parameters was built up for the results of the current work. The peak temperature considered was that which exhibited the lower toughness values, i.e. 1250°C. That graph can be seen from figure 154 and it will be noticed that data from other authors were superimposed on it. They involved results obtained from simulation work performed in Italian (25), French (29) and Swedish (35) research centres. Inserted on the graph there is a table giving the C/Mn/Nb/V composition of the steels involved in the experiments, for a better comparison. One would note that the results for the current work, represented by the curve V, are in a fairly good agreement with the other results, mainly with that from the Italian curve II, whose steel composition is the most similar to the RQT-500. The Italian curve I exhibits the

more critical conditions, this is thought to be due to the higher V level of the steel, over three times more than for the RQT-500. The two steels containing only Nb and represented by the curves III (French) and IV (Swedish) exhibited better toughness, as expected, than that of the other curves representative of steels containing Nb plus V, although the curve III (French) passing a maximum at Δt = 28s, had a peculiar behaviour, exhibiting only for that condition, higher deterioration than that observed for the steels of approximately similar composition, but containing Nb plus V. So, based on the data of the curves in figure 154, if a generalisation is attempted, one would say that as the cooling time Δt was increased from 5 to 25s, a strong increase in the transition temperature was observed. When the cooling time was raised to 100s, a moderate deterioration of the previously documented toughness occurred. When the cooling time was increased to 300s, an abrupt increase in the transition temperature was observed again. Finally, when the cooling times reached the 700s, a recovery in toughness was observed, although the impact transition temperature was higher than the one observed at Δt = 100s. It could also be said that the steels containing only Nb had a better toughness than the steels containing Nb plus V.

4.5 Analysis Of Factors Influencing The Weld HAZ Toughness

The present section will deal with the many factors which are considered as influencing the toughness of the weld HAZ, mainly oriented to the changes observed in the toughness of the weld HAZ regions for the steel RQT-500. So, an insight will be given on aspects such as the microstructures formed,

the fracture facets appearance, precipitation hardening, grain size, hardness, post weld heat treatment, and on their influence on the toughness of the weld HAZ of the steel RQT-500. The results observed in the current work, after analysis, will be compared to those found in the current literature and the elucidation of the deterioration mechanism will be attempted.

4.5.1 Microstructures

The observations for the microstructural work were performed on the simulated specimens. Basically, the microstructures could be classified into three main groups :

i) Structures where the peak temperature did not exceed the A_1 temperature.

ii) Structures where the A_1 temperature was exceeded, but the austenitic grain remained fine.

iii) Transformed structures where grain coarsening occurred.

4.5.1.1 Structures Where The Peak Temperature Did Not Exceed A_1

These structures corresponded to those found in the sub-critical HAZ and were obtained by simulation at peak temperature of 700°C. Observation on the dilation behaviour of the specimens confirmed that no austenitisation occurred. The toughness of the 3.6 and 6.3KJ/mm heat inputs were very similar and slightly lower than for the base metal. The 14.4KJ/mm specimens exhibited the lowest toughness of the group. The causes which have been suggested for the lower

toughness of the subcritical HAZ, relative to the base metal are :

i) Secondary precipitation hardening caused by NbC re-precipitation (18).

ii) Strain ageing and, as such, associated with the nitrogen content of the steel (30).

Neither of these two mechanisms were considered in the current work, since microalloy precipitation was not found, and the basic open hearth process employed in the production of the RQT-500 steel yields low nitrogen contents. When samples of the base metal and of the simulated specimens were studied in the transmission electron microscope (TEM), a higher amount of cementite particles precipitated at the boundaries of the tempered martensite needles was noticed for the simulated specimens than for the base metal. This can be seen from figures 130 to 132. Longer cooling times should increase the amount of precipitation. This would explain the lower toughness figures for the 14.4KJ/mm specimen. Table 38 shows the results of the point counting for the structures obtained at the three heat inputs tested and heated at a peak temperature of 700°C. The point counting for the structures observed in the base metal are also seen from table 28.

4.5.1.2 Structures Where The A_1 Temperature Was Exceeded, But The Austenitic Grain Remained Fine

These structures corresponded to those observed in the specimens simulated at 800, 900 and 1000°C. Their toughness results were the best observed in the current work. Within that region, the carbon rich areas were the first to transform

and on cooling they gave origin to the ferrite, plus carbide aggregates. The latter are thought to be a form of distorted pearlite, where the cooling time did not allow an ordered diffusional arrangement. From the electron microscopy investigation, it was observed that as the heat input and peak temperature increased, the disordered structure tended to a pearlitic configuration. The transmission microscopy pictures can be seen from figures 133 to 135. Generally, a higher amount of cementite was observed inside the grains of these samples, than was observed for the base metal. It was more likely that they resulted from carbide coarsening than from fresh precipitation. Depending on the degree of transformation attained, the ferrite, which was the main constituent of these samples, would represent a mixture of proeutectoid ferrite and untransformed ferrite. If the rating of the samples per order of increasing toughness was attempted, one would obtain : 3.6KJ/mm - 800°C, 6.3KJ/mm - 800°C, 14.4KJ/mm - 800°C, 3.6KJ/mm - 1000°C, 6.3KJ/mm - 1000°C, 3.6KJ/mm - 900°C, 14.4KJ/mm - 900°C, 14.4KJ/mm - 1000°C, and finally, 6.3KJ/mm - 900°C. An analysis to clarify this behaviour, based on the fraction of the microstructural constituents, grain size and hardness, failed to produce a clear picture, althought it is thought that the finer grain size was largely responsible for the good level of the toughness properties. It would be of particular interest to point out that the 6.3KJ/mm - 900°C specimens had the best toughness observed in the current work. These were the specimens whose thermal cycle differed slightly from the rest of its group. Its cooling was faster in the range near to the peak temperature, and slower at lowest temperatures to make up for the cooling time Δt = 90s, equivalent to the 6.3KJ/mm heat

input. Apparently, no particular reason could be documented for its best behaviour. Table 29 shows the results of the point counting for the structures obtained at the three heat inputs tested at the peak tempetures of 800, 900 and 1000°C, respectively.

4.5.1.3 Transformed Structures Where Grain Coarsening Occurred

These structures developed when the samples were heated to 1150°C and above. Microalloys went into solution to a greater or lesser extent, and the thermal cycles employed determined the coarseness of the grain size. Also, the starting of the transformation temperature was depressed originating shear-like structures. Sometimes their similarity was such that a differentiation was made difficult. This problem has been reported by others (32, 104). At the peak temperature of 1150°C, the 3.6KJ/mm condition exhibited an approximately equal amount of interlocking acicular ferrite and colonies of fine upper bainite. Light etching areas named "white areas" were classified under the latter. Isolated plates of ferrite or polygonal ferrite inside the grain were classified under "ferrite", and only a small amount was observed. Proeutectoid ferrite dominated the structures of the 6.3 and 14.4KJ/mm heat inputs at the 1150°C peak temperature. The cooling times used favoured the transformation of that higher temperature product and the size of the austenitic grain played an important role, because the natural site for the nucleation of that constituent is at the prior austenite grain boundaries (121). At the heat input of 6.3KJ/mm, the other structure observed was upper bainite. The latter was surrounded by proeutectoid ferrite. The longest cooling time corresponding to 14.4KJ/mm allowed the formation of pearlite, although some upper bainite was

also observed. The optical micrographs for the structures of that peak temperature can be seen from figures 65, 72, 79, 85, 87 and 90 and the smaller details resolved by the TEM are seen from figures 136, 139 and 142. The peak temperature of 1250°C corresponded to a maximum in the upper bainitic constituent for all the samples observed during this investigation. Proeutectoid ferrite delineated the prior austenite grain size of the 6.3 and 14.4KJ/mm conditions, but none was detected at 3.6KJ/mm. Polygonal ferrite and acicular ferrite were observed in the interior of the grains and so was interlocking acicular ferrite. At the heat input of 3.6KJ/mm, similarly to the fact observed at 1150°C,"white areas" were observed, as seen from figures 65 and 66. At the beginning they were thought to be of Martensite-Austenite (M-A) nature. Practices such as deeper etching, heat treatment and microhardness were employed to investigate the nature of these constituents. Deeper etching revealed parallel arrays of carbides, similar to those exhibited by upper bainite. Heat treatments which are reported to improve the toughness of structures containing Martensite-Austenite (116), provoked further deterioration in toughness. Finally, the microhardness measurements revealed figures in the same range as those obtained for upper bainite, as it can be seen from table 33. Consequently, these structures were classified in the upper bainitic category. This is in agreement with observations of authors from the Welding Institute (33, 56), which reported small amounts (1 to 3%) of retained austenite within these areas. During the discussion of his ASM paper in Rome, Dolby (122) stated that retained austenite was beneficial to HAZ toughness, assuming that it remains stable at all test temperatures. The

structures representative of the 1250°C peak temperatures are seen from figures 66, 73, 80, 82, 86, 88, 91 and their TEM details from figures 137, 140 and 143. At the highest peak temperature investigated, 1400°C, a small amount of proeutectoid ferrite was occasionally detected at the prior austenitic grain boundaries. This is seen from figure 83. Compared to the peak temperature of 1250°C, the proportion of ferrite and of interlocking acicular ferrite increase and the proportion of upper bainite was nearly halved. At the two higher heat inputs, the proportions of proeutectoid ferrite and upper bainite were lowed, whilst amounts of ferrite and interlocking acicular ferrite were raised. The associated micrographs are seen from figures 67, 74, 81, 83, 89, 92 and the TEM details are shown from figures 138 and 141. Table 30 shows the results of the point counting for the structures obtained at the three heat inputs tested at the peak temperatures of 1150, 1250 and 1400°C, respectively. The main observation regarding the structures formed in the coarse grained region of the HAZ were as follows :

i) At the fastest cooling rate, a small amount of proeutectoid ferrite was formed and only observed at the highest peak temperature. At the heat inputs of 6.3 and 14.4KJ/mm, the content of proeutectoid ferrite decreased with the increase in the peak temperature. This would be explained by the increase in grain size, the natural site for the nucleation of that constituent. With increasing heat input from 6.3 to 14.4KJ/m, the proeutectoid ferrite cell thickened, thus at the higher heat inputs, a high proportion of the constituent was observed. This can be comparatively seen from figures 87 to 89 and 90 to 92, respectively. However, at a fixed

heat input, the thickness of the cells was constant with varying peak temperatures. This remark is supported by the findings of the Swedish Delegation to the IIW (35).

ii) The constituents classified as ferrite were only observed at the peak temperature of 1150°C, for the 3.6KJ/mm heat input condition. At 1250°C it was detected for the three heat inputs in a similar proportion, which did not differ much from that observed at 1150°C for the fast cooling rate. At 1400°C the amount of that constituent was twice that found at the other peak temperatures for the 3.6KJ/mm heat input. It was only slightly increased for the other heat inputs.

iii) Interlocking acicular ferrite was only observed at 1150°C at the 3.6KJ/mm condition. As the peak temperature was raised to 1250°C, this constituent was observed at the three heat inputs, although its proportion at 3.6KJ/mm was considerably reduced. The peak temperature of 1400°C produced an increase in the proportion of that structure for the three heat inputs considered, the larger increase occurring at the highest heat input. The observation of the interlocking acicular ferrite was experimentally easier at the peak temperature of 1400°C, when the structure was coarser.

iv) At the peak temperature of 1150°C the dominant structure of the 3.6KJ/mm condition was the upper bainite. It was observed in a certain amount at the heat input of 6.3KJ/mm and at the highest heat input it was just detected. At the peak temperature of 1250°C, for all heat inputs, the upper bainite was a maximum relative to the other peak temperatures

considered. Thus, at 1400°C its amount was lowered. At the low peak temperatures and fast cooling rates, the bainitic ferrite laths were narrow and they thickened as the peak temperatures and cooling times were increased. This was reported previously and was associated with the depression of the transformation temperature (61, 112). It was explained that, with the decrease in the peak temperature, the rate at which carbon diffuses at the front of the austenite-ferrite interface is decreased, and so the sideways growth of the ferrite laths is slowed down, resulting in narrow ferrite laths. Also, in a bainitic structure, there will always be a variable bainitic ferrite "grain size", because the bainitic ferrite nucleated later in the progress of the transformation will invariably show a smaller "grain size". It is widely accepted that the bainitic ferrite lath width is one of the factors controlling the strength, but that it has no influence on the impact transition temperature (ITT) of the steel (61, 112, 123). In the current work, the bainitic packet size, or bainitic colony, which consists of bundles of ferrite laths of similar orientation separated from the adjacent bundles by high angle boundaries, was observed to decrease with the increase in cooling rate, and with the decrease in peak temperature. This is in good agreement with the current literature, which mentions the dependence of that parameter with the grain size (56, 61). Also, it is accepted that the bainitic packet size is one of the main factors influencing the impact transition temperature (1, 35).

4.5.1.4 Considerations On Proeutectoid Ferrite

In the current work, proeutectoid ferrite was observed

delineating the prior austenite grain boundary of the coarse grained HAZ of the 6.3KJ/mm actual weld and simulation specimens. Schofield and Weiner (44), investigating Nb and Nb + V microalloyed steels simulated at a heat input equivalent to $\Delta t_{800-500}$ = 70s, observed structures with very little, or no proeutectoid ferrite. The chemical compostion of their steels was not very different from the composition of the RQT-500. Dolby (56), investigating the toughness of actual weld HAZs of C-Mn-Nb steels, also reported a structure containing very little or no proeutectoid ferrite. Bernard et al (29), also studying C-Mn-Nb steel of a similar composition and similar heat input ($\Delta t \cong$ 100s) as those used by Dolby, reported proeutectoid ferrite at the grain boundaries. Schofield and Weiner used a HF simulator for their work and mentioned a short "hold" period at the peak temperature, to allow the homogeneization of the grain size throughout the specimen. Dolby used a tandem arc submerged arc welding process in his experiments, and that could have introduced also a short hold time at higher temperatures. To investigate if that "hold" time at the peak temperature would be the factor responsible for the reduction or elimination of the proeutectoid ferrite at the grain boundary, a simple experiment was performed in the current research. Two samples were simulated at an energy level equivalent to $\Delta t_{800-500}$ = 70s. One of the samples was synthetized in the usual way, whilst the other was held at 1400^{o}C for 20s before it was allowed to cool. The microscopic observation of the two samples exhibited proeutectoid ferrite at the grain boundaries. The difference between them was that the sample which was held at the peak temperature exhibited a grain size considerably

larger than that for the other normally simulated sample. Garland (124) mentioned that at a high weld metal oxygen content (e.g. 0.04%), the associated high inclusion content nucleated higher temperature transformation products such as proeutectoid ferrite, which are detrimental to the low temperature toughness. Bernard et al (29) giving a paper in the same conference where Garland made his previously mentioned remarks, concluded: "the effect of oxygen content, quite noticeable on the upper shelf energy level (and in a remarkably coherent manner with data collected from the literature), was found to have no significant effect on impact transition behaviour.". Indeed, inclusions are known to affect the upper shelf energy by microvoid coalescence and have no effect at all in the lower temperature toughness, when the fracture occurs mainly by cleavage. The concept which Garland was launching was slightly different. Depending on the welding conditions and the composition of the weld metal, inclusions could favour the nucleation of a structure such as proeutectoid ferrite, which is detrimental to the low temperature toughness. The oxygen content of the HAZs in the current research was 0.015%. It might have been possible that the level of inclusions of the steel used in the current research and that of the steel used by Bernard, was higher than the level of inclusions of the two other investigations. In the presence of slight changes in the composition and in the welding parameters, it could have had an effect, favouring the formation of the proeutectoid ferrite. Unfortunately, the level of inclusions was not provided in any of the reports, to allow a comparison to be made. In the current work, it was not uncommon to observe proeutectoid ferrite

nucleating at inclusion sites. This can be seen from figures 87, 88, 91, 92, 97 and 100. Sometimes, in the course of the discussion, analogies were established between the weld metal proeutectoid ferrite and the HAZ proeutectoid ferrite. It would be interesting to observe that for the actual 6.3KJ/mm weld, a perfect link existed between the weld metal proeutectoid ferrite veins and the proeutectoid ferrite delineating the grain boundaries near the fusion line, in the coarse grained HAZ. This can be seen from figure 96. Another interesting feature derived from the microscopical observation was the one seen in figure 99. It appears that the inclusions in that case are acting to provide barriers against the grain growth in the coarse grained HAZ. The significance of this observation is difficult to assess. An improvement resulting from the smaller grain sizes would probably be offset by the damaging influence on toughness, of the inclusions themselves.

4.5.2 Fracture Appearance

That study was performed by the observation of the subsidiary cracks and of the fracture facet appearance of Charpy specimens under the optical microscope, as well as by the observation of the fracture profile under the scanning electron microscope (SEM). The samples which were observed were those fractured at test temperatures below $-10^{o}C$. From the former technique, it was observed that subsidiary cracks are frequently associated with proeutectoid ferrite, being arrested, or tending to change slightly their direction of propagation at the proeutectoid ferrite cells' boundaries, as it can be seen from figures 85 and 86. That observation is confirmed by the HAZ work of Swedish authors (35) and by

the weld metal investigation of Levine and Hill (72). When the subsidiary cracks were running across the upper bainitic structures, it was observed that they were not arrested by the low angle cells of the bainitic ferrite, but that they would be arrested or exhibited a change in their direction of propagation at the bainite colony boundary, or if other structures such as interlocking acicular ferrite or isolated ferrite plates lay on their propagation path. This can be seen from figures 82 and 83. Figure 84 represents a nickel plates (for better contrast) fracture facet profile. It is clearly seen there that the straight fracture profile is cutting across a bainite colony, whereas some terraced fracture is observed associated with the interlocking acicular ferrite. This is confirmed by the work of Levine and Hill for weld metal (72). Cane and Dolby (33) have observed that the fractured facet size associated with the proeutectoid ferrite was smaller and more irregular than those observed in the upper bainite and acicular ferrite regions. Their findings on the crack propagation across the proeutectoid ferrite and the upper bainitic regions are in good agreement with those from the current work, although their observation concerning the interlocking acicular ferrite is in disagreement, not only with this investigation, but also with the results of Levine and Hill (72).

The fractrographs obtained from the scanning electron microscope (SEM) observations are seen from figures 109 to 129. For the heat input of 14.4KJ/mm, which was the one exhibiting the poorest toughness, fractrographs of all the peak temperatures are provided for a comparison. For the other two

heat inputs, only the fractrographs of the peak temperatures of the coarse HAZ, namely 1150°C, 1250°C and 1400°C are shown. It was observed that the fracture facet size increased with the increase in peak temperature and with the increase in heat input. This finding is in good agreement with the current literature, since the fracture facet size is a function of the "effective" grain size, i.e. the bainitic colony size, which is a function of the grain size. In other words, the higher the heat input and the peak temperature, the higher the grain size and the higher the bainitic packet size. At the two higher heat inputs, at the peak temperature of 1400°C, some ductile fractures were observed, as can be seen in figures 109 and 118. This is in good agreement with the phase point count results, since at these two conditions a higher amount of products of higher transformation temperature than the upper bainite one were formed. These ductile areas were not observed for the 3.6KJ/mm - 1400°C condition, where the amount of bainite was still higher than for the other two heat inputs at the same peak temperature and more, some proeutectoid ferrite was nucleated, contributing more to the deterioration of the HAZ toughness. Figures 110, 119 and 122 are representative of the fractrographs of the heat inputs of 14.4, 6.3 and 3.6KJ/mm, respectively, simulated at the peak temperature of 1250°C. It can be seen that the cleavage facets almost devoid of profile, only exhibiting a few river patterns are characteristic of the cleavage type of fracture across the bainite colonies. In these fractrographs, the small regions with more profile are representative of the fracture path around the interlocking acicular ferrite. Figure 126 exhibits a crack in a fractrograph

obtained from an actual weld HAZ at the heat input of 6.3KJ/mm. It can be observed that the crack running straight across the bainite colony is deviated when it reaches a different microstructure, presumably an interlocking acicular ferrite. The figure 116 represents the 6.3KJ/mm - 900°C condition. These set of samples were those produced with a slightly different thermal cycle and yielded the best toughness documented in the current investigation. It seems that its fracture facet size is slightly smaller than those exhibited for the 14.4KJ/mm - 900°C and 14.4KJ/mm - 1000°C conditions, which can be seen in figures 113 and 112, respectively. That would imply that the grain size of the former should be slightly smaller than the grain sizes of the latter. Table 26 shows the results for the mean linear intercept determination of the grain sizes. One can observe that the figures for the conditions mentioned above are very similar, moreover, due to the small numbers that these figures represent, any discussion on that ground would involve some speculation.

4.5.3 Precipitation Hardening

One of the main theories to explain the deterioration of the weld HAZ toughness proposes that the microalloys dissolved at the higher peak temperatures near the fusion line, according to the thermal cycle employed, will have a potential to precipitate, embrittling the transformed microstructure by secondary phase hardening. The size of these precipitated particles is suggested to be very small, consequently, one would have to employ Transmission Electron Microscopy (TEM) if they are to be detected. In the current work, carbon

extraction replicas were prepared from those samples which were expected to exhibit more precipitation, i.e. the samples which had higher embrittlement and those which had been heat treated. Namely, they were the samples 3.6KJ/mm - 1400°C, 6.3KJ/mm - 1250°C, 14.4KJ/mm - 1250°C and all the synthetized post weld heat treated specimens. The condition 14.4KJ/mm - 1400°C was also studied. It exhibited a higher hardness than the other peak temperatures in the coarse grained region at the same heat input, and due to its longer cooling time relative to the other two heat inputs, it should have more potential for precipitation. When preparing the samples, formerly and due to lack of practice, deeper etching was used. The replicas prepared that way contained few trapped carbides and were of difficult observation. With time, practice was acquired and the use of light etching of the samples yielded good replicas with a certain amount of trapped carbides observed. One of these can be seen from the micrograph in figure 145. A diffraction pattern obtained from one of these carbides can be seen from figure 146 and the associated interpretation from figure 147. The latter indicated their cementitic nature. During the course of the observations, no carbides disposition similar to that proposed for Nb or V precipitates (usually ver fine and in parallel rows) was seen, nor a diffraction pattern observed for the isolated carbides detected proved them to be of Nb or V nature. Other authors also failed to document microalloy precipitation by carbon extraction replica techniques (36, 63). No attempt of documentation of microalloy precipitation was made by thin foil transmission electroscopy. The reason lies in the fact that, as more than one author has

stated, the high dislocation densities exhibited by the coarse grained HAZ products would make imaging difficult, even if it was present (61, 62).

The main supporters of the precipitation theory are from Sweden (14, 55), but they failed to produce evidence of HAZ precipitation. After heat treating the samples (2 hours at 620°C for V steels and 32 hours at 610°C for Nb steels), precipitation was observed and their explanation was that before tempering, the precipitates were too fine to be resolved by the transmission electron microscope (TEM). Levine and Hill (62) were sceptical about the Swedish results. They observed that the slight change in hardness with the decrease in cooling rate was contradicting the precipitation argument, unless compensating structural changes have masked the precipitation hardening increment. In 1976, French authors (29) observed experimentally the precipitation of microalloys in the coarse grained HAZ. They applied secondary ion analysis on two welds performed at 3.0 and 7.0KJ/mm on 20mm thick plates. The consumables used were the same and the steel contained 0.035%Nb. It was concluded that :

i) In the base metal, the precipitation was incomplete.

ii) Going across the HAZ, immediately above the A_1 temperature, the precipitation was completed due to tempering effect.

iii) In the coarse grained zone near the fusion line at the 3.0KJ/mm welding, no precipitation was observed. This demonstrates clearly that all Nb is taken into solution in the coarse grained zone.

iv) In the 7.0KJ/mm weld where Nb will be a fortiori taken into solution in the coarse grained zone during the heating period of the welding cycle, it was noted, however, that substantial precipitation has occurred upon cooling.

v) In the weld metal it was found that precipitation was more important in the higher energy weld. Because precipitation was mainly noticed in the proeutectoid ferrite regions, it justifies the findings because this constituent was more abundant in the higher energy weld.

The two curves shown by Bernard et al to illustrate the behaviour of the precipitation across the HAZ and weld metal pointed out that for a certain heat input, the precipitate fraction decreased with increasing peak temperature. This seems reasonable considering the behaviour of the transformation temperature. It is accepted that Nb in solution depresses that parameter towards lower temperatures (28). Also, with increasing peak temperature, the austenitic grain grows, its hardenability is increased and that contributes to the depression of the start of the transformation temperature. Accepting Gray and Yeo's (66) model for microalloy precipitation at the interface of the $\gamma \rightarrow \alpha$ transformation, the lower the transformation temperature, the lower the precipitate fraction. Unfortunately, Bernard et al did not provide comments on the variation of the hardness associated with the change in precipitation fraction. However, they concluded their paper by confirming that the microstructure was the main parameter affecting the impact toughness of the HAZ of the weld

metal. Canadian authors (61) analysing carbon extraction replicas by transmission microscopy (TEM) reported Nb precipitation in microalloyed steels. They observed that deeper etching of the samples, as opposed to the generally recommended light etching practice (64), was the key to their success where others failed. They observed that :

i) At cooling times Δt = 160s, NbC precipitates were detected for steels containing 0.14, 0.09 and 0.034%Nb. Vanadium precipitation was observed for a steel containing 0.09%Nb, but the diffraction pattern could not be obtained because the precipitates were too fine.

ii) At the cooling times of Δt = 80s, the samples studied contained a minimum of 0.09%Nb and precipitation of NbC was detected.

iii) Actual weld HAZ of steels containing 0.09%Nb did not exhibit fine precipitation when the cooling time Δt was equivalent to 39s. The coarse precipitates observed were considered undissolved precipitates originating from the base metal. A simulated sample heated to 1320^{o}C in 10s, a slightly higher heating time than that for the actual weld heating cycle, exhibited fine reprecipitated NbC particles. It was considered that the difference in heating time to peak temperature was sufficient to dissolve all the precipitated NbC.

iv) Closing the discussion, the authors commented on the difficulties of evaluating the influence of the micro-

alloys precipitation on the hardening increment, because unequivocal information on the volume fraction of precipitates cannot be obtained from extraction replica precipitation techniques. They also mentioned that even at the highest heat input tested, it was unlikely that all the available Nb would have precipitated, as the 50% transformation temperatures were all 600^{o}C or lower.

It could be of interest to make a remark on some observations made by the Canadians concerning the vanadium precipitation. Because V precipitates in a wider band of temperatures than Nb does, it would be expected to be easier to observe the former, than the latter. Furthermore, it would be expected that vanadium precipitates would coarsen more easily than Nb ones. The last observation is based on the fact that Hannerz (14) had to temper HAZ of Nb steels for 32 hours before precipitates were observed, whilst it only took 2 hours to observe vanadium precipitation (55). Presenting the results, the Canadians mentioned that they could not obtain a diffraction pattern for the precipitates observed in the 0.09%V steels, consequently, they presumed that these precipitates should be V (CN). Discussing the results, they quoted the fact as evidence.

4.5.4 Grain Size

The prior austenitic grain sizes obtained for the coarse grained region of the real weld HAZ are listed in table 27. It was mentioned previously that they vary, decreasing in size with the increase of the weld bead penetration depth.

Table 26 lists the values for the peak temperature equivalent to 1400°C of the simulated sample at the three heat input conditions investigated. If these values are compared to those obtained from table 27, one would observe that the actual coarser grain sizes could be satisfactorily reproduced by simulation techniques. This can also be seen from figures 94, 95, 97 and 98.

From the simulated HAZs grain size figures listed in table 26, it is readily noticed that for peak temperatures up to 1000°C, little change occurred between the grain size of the cycled specimens and that of the base metal, the lower values being found for the peak temperatures of 900 and 1000°C. When the peak temperatures were raised to 1150°C and above, microalloys would dissolve into the austenitic phase allowing the grains to grow. This is evident if the figures for the peak temperatures above 1150°C are compared to those for the peak temperatures below 1000°C. There is a tendency for the grain size to increase with the increase in peak temperature, and with heat input in the grain coarsening region of the HAZ. The fact is more noticeable if the 3.6KJ/mm heat input is compared to the other two, than if the 6.3KJ/mm is compared to the 14.4KJ/mm. Grain size alone was found not be a sufficient criterion to evaluate a weld HAZ toughness. If the grain sizes obtained for the peak temperature of 1150°C are compared between themselves and to the associated toughness of the transformation product, it will be noticed that the grain sizes exhibited very similar values, but that the toughness of the 3.6KJ/mm condition was considerably higher

than those of the other two heat inputs, which exhibited a very similar value. At the peak temperature of 1250°C, the value for the grain size of the 3.6KJ/mm condition does not differ much from that observed for the peak temperature of 1150°C of the same heat input, but the toughness associated with the latter is higher than that observed for the former. At the same peak temperature of 1250°C, there is a difference between the values for the grain sizes of the three heat inputs investigated. That difference is more noticeable between the 3.6KJ/mm condition and the other two, than between the other two themselves. The toughness figures associated with the 3.6KJ/mm heat input are very similar to those associated with the 6.3KJ/mm condition. However, the highest heat input condition exhibited the highest embrittlement of all. Although not being a sufficient criterion to assess the toughness of the weld HAZ, the grain size must be taken into account when evaluating the toughness of the weld HAZs. This happens because it can influence the transformed structure in the following way :

i) The grain size is the natural site for the nucleation of the proeutectoid ferrite. The smaller the grain size, the higher the percentage of this constituent.

ii) To nucleate, the proeutectoid ferrite will reject carbon inside the grain it is delineating. Depending on the grain size and on the cooling rate, a local increase in the austenite carbon content would favour the transformation of a higher amount of upper bainite.

iii) The higher the grain size, depending on the cooling rate employed, the larger the colony size of the upper bainite that may form.

As it was listed above, the grain size can be of influence in three factors that would contribute to the deterioration of the toughness of the HAZ. Depending on the grain size (a function of the peak temperature and of the heat input employed), and depending on the cooling rate (a function of the heat input employed), a combination of those three factors could occur, where the deterioration in toughness would be maximised.

The figures found for the grain size in the current work are confirmed by those produced by Cane and Dolby (33), equivalent to grain sizes of 0.1 to 0.12mm when welding at 7KJ/mm, two Nb containing steels at the levels of 0.03 and 0.056%Nb, respectively. Canadian authors (61) produced results for the grain size of a C/Mn steel welded at heat inputs equivalent to Δt of 160 and 80s. The values obtained are higher than those for the steel of the current work, and that of the work by Dolby and Cane, but similar figures (0.15-0.16 and 0.16-0.17mm) were observed, despite the difference in heat inputs. That tendency is confirmed in the present work, since at the peak temperature of 1400^{o}C, when the heat input was raised from a Δt cooling time equivalent to 90s to another one equivalent to 200s. The findings of the current work stating that the grain size affects the amount of transformed proeutectoid ferrite is confirmed by the work of Aaronson (121).

4.5.5 Hardness

Vickers hardness tests under the load of 30Kg were performed in the current work, for all the tested conditions plus the base metal. The results can be seen from table 31 and from their graphical representation in figure 148. The results for the hardness of the post weld heat treated structures will be considered later in discussion of that specific item. A considerable scatter was found in the results from these experiments and this appeared to be related to the different nature of the microstructures which are present in the weld HAZs. That scatter has been reported previously in other investigation (33). At the heat input of 3.6KJ/mm, the hardness values increased continuously with the increase in peak temperature and were maximum at 1250°C. For the other two heat inputs, the picture was not that clear. At the peak temperatures within the range of fine grained products (up to 1000°C , the hardness values oscillated around a mean value of $215HV_{30}$. For the 6.3KJ/mm heat input condition, the hardness values increased at the peak temperature of 1150°C relative to the values observed for the fine grained regions. At 1250°C, the figures were slightly higher, but similar to the latter. Finally, at the peak temperature of 1400°C, the hardness results decreased a little. For the 14.4KJ/mm heat input condition, at 1150°C, the hardness values were still in the same range as the one observed for the fine grained regions. This seems to be in good agreement with the structures produced, where the dominant constituent was proeutectoid ferrite, although pearlite and a minimum amount of upper bainite was detected. At the peak temperature of

1250°C, the hardness values were raised and they were maximum at the peak temperature of 1400°C. If a generalisation is attempted, one would say that in the coarse grained HAZ region of the HAZ, the hardness values increased with the increase in peak temperature and with the increase in the cooling rate. However, it was found that hardness was not a sufficient criterion to assess the weld HAZ toughness. Only one example will be given to illustrate that statement, although other comparisons could be made. At the peak temperature of 1150°C, the toughness values for the samples representative of the heat input conditions of 14.4 and 6.3KJ/mm were very similar. At the heat input of 3.6KJ/mm, the toughness was considerably better than those observed for the higher heat inputs. However, the results for the hardness increased in that order: 14.4, 6.3 and 3.6KJ/mm. This statement is widely supported from findings of the current literature (28, 30, 76, 125), although Signes and Baker (36) have reported a correlation between the toughness of C-Mn, Nb and/or V steels, welded at Δt = 25s, and their associated hardness.

The hardness values obtained for the coarse grained region of the 3.6 and 6.3KJ/mm actual welds were higher than those exhibited by the equivalent simulated samples. The fact has been previously reported (61) and it was explained that the difference in regions sampled in the actual HAZ are responsible for the mismatch.

The microhardness tests were also performed in the individual phases of the coarse grained region of the HAZ. The problems

faced were the wide range in the size of the phases. These were a consequence of the differences in heat inputs and peak temperatures employed. The 25g load used would make an indentation which was sometimes too small, sometimes too large in the phases to be compared. The figures seen from table 33 give an idea of the behaviour of the microhardness for some of the phases found in the coarse grained HAZ. Detailed interpretation of the data would be too speculative, but some points of interest can be mentioned. The microhardness values exhibited by the "white areas" were similar to those of the upper bainite, at the same thermal cycle conditions. This could serve as another fact to stress that these areas are of a bainitic nature. The small size and the rare occurrence of the proeutectoid ferrite at the 3.6KJ/mm - 1400^{o}C condition could be the reason why their figures were so high. The latter results could have been influenced by the surrounding or backing microstructures. In general, it seems that these results are in good correlation with the ones exhibited by the macrohardness testing. The higher figures associated with the lighter indentation loads have been noted elsewhere (115).

4.5.6 Post Weld Heat Treatment (PWHT)

The effect of PWHT on the coarse grained HAZ of microalloyed steels has been described in the literature survey. It seems that an adequate summary for the phenomena was put forward by Bernard et al (29). They mentioned that the embrittling effect of secondary hardening precipitation should be balanced against the beneficial effect of tempering,

when PWHT is considered. From the same paper, it was seen that even for long cooling times $\Delta t \cong 110s$, there will be, still, a certain amount of Nb in solution. The Canadian authors who detected microalloy precipitates in the HAZ (61) observed that even at cooling rates $\Delta t = 160s$, it was unlikely that all the available Nb had precipitated. Thus, it seems that there is a fraction of microalloys available for precipitation. Now, the accepted deleterious structure towards toughness is the upper bainite. Tempering has little or no effect on these structures unless very high tempering temperatures are used. This is because the low energy bainitic ferrite boundaries, which are very slow to migrate, unless high tempering temperatures are used. According to Pickering (112), the tempering effect which occurs at high temperature is a fairly rapid ferrite grain growth, and this is detrimental to the impact properties. Thus, if the reasoning from Bernard et al (29) is applied to the RQT-500, the PWHT of these steels should not be beneficial. Precipitation or further precipitation will occur, the upper bainite would not be tempered and the toughness would be expected to fall. Tempering was performed in the most embrittled samples of the current work, those simulated at 14.4KJ/mm at a peak temperature of 1250^{o}C. Also, following a recommendation from the steel's manufacturer (88), the same heat treatment was applied to the base metal. The results are seen from table 34 and it was observed that in both cases the impact transition temperature was increased relatively to the non-heat treated samples. The TEM picture for the 14.4KJ/mm - 1250^{o}C condition can be seen from figure 144. One would observe that the ferrite bainite laths are still visible.

Precipitation was not observed in the carbon extraction replicas under the Transmission Electron Microscope (TEM), but the hardness of the samples, as it can be seen from table 32, were increased relatively to the untempered equivalent. When the fracture facet of these samples was studied under the Scanning Electron Microscope (SEM), occasionally, evidence was found for triple point fracture facets characteristic of temper embrittlement. That can be seen from figure 126. The figure 132 shows the TEM micrography for a tempered base metal. A considerable amount of precipitates are seen at the boundaries of the tempered martensite needles. The latter are very similar to the ones observed when the specimens were simulated at a peak temperature of 700^{o}C. The tempered base metal also exhibited a slightly higher hardness than the untempered one.

Tempering was also performed on samples simulated at 3.6KJ/mm at the peak temperature of 1250^{o}C, to investigate if the "white areas" contained Martensite-Austenite (M-A) structures. It has been reported that in cases where that constituent is present in the microstructure, tempering is beneficial to restore the toughness properties (116). As it can be seen from table 34, the impact transition temperature of the tempered samples was increased, relative to that of the untempered samples. That led to the conclusion that if M-A structures were present, they did not contribute much to the low impact results observed.

4.5.7 Summary

The results from the current research investigating the toughness of the whole HAZ of welds performed at 3.6, 6.3 and 14.4KJ/mm, indicated that an improvement of properties is to be expected in the fine grained region of the HAZ, and a strong deterioration occurs in the coarse grained HAZ region, both relative to the base metal toughness. The fine grained regions are those where the peak temperature attained was not sufficiently high to allow the dissolution of the microalloys into the austenitic phase. In the current investigation, these peak temperatures were represented by temperatures up to 1000^{o}C. The fine grains observed appear to be a good reason for the improvement observed in the toughness. However, when the peak temperatures at and above 1150^{o}C were tested, dissolution of the microalloys occurred, the prior austenite grain coarsened and the start of the transformation temperature was depressed towards lower temperatures. These factors influenced the nature of the transformation product and the toughness deteriorated. It is possible that some microalloy precipitation occurred at the higher heat inputs, namely 6.3 and 14.4KJ/mm, but the phenomena was not confirmed by carbon extraction replica techniques nor by hardness comparative analysis. The higher embrittlement was always associated with a combination of proeutectoid ferrite and upper bainite. From the fractrographic analysis it was evident that proeutectoid ferrite was the natural site for the nucleation of the cleavage cracks, which would propagate fairly easily through the large upper bainite colonies favoured by the dimensions of the coarse grains. Consequently, based on the experiments and analysis

performed in the current investigation, the microstructure of the transformed products was considered to be major embrittling factor responsible for the deterioration of the toughness of the coarse grained region of the HAZ. Proeutectoid ferrite and upper bainite were harmful structures and the toughness was minimum in the presence of proeutectoid ferrite and a maximum amount of upper bainite.

At the heat input of 3.6KJ/mm, the maximum deterioration occurred at the peak temperature of 1400°C, when a small amount of proeutectoid ferrite was detected in the microstructure. However, that deterioration was just slightly greater than the one observed at 1250°C, when no such constituent was present, but the proportion of upper bainite was maximum, amounting to 75%. At the heat inputs of 6.3 and 14.4KJ/mm, the maximum embrittlement occurred at the peak temperature of 1250°C. Since at the peak temperature of 1150°C, the deterioration of the toughness for the 6.3 and 14.4KJ/mm heat inputs was similar, at 1250°C the embrittlement exhibited by the 3.6 and 6.3KJ/mm conditions was nearly the same, and at the heat input of 3.6KJ/mm little difference was noticed between the toughness of the samples cycled at 1250 and 1400°C, all these conditions exhibiting different amounts of microconstituents, it appears that the loss in toughness was controlled by an interplay of factors such as the proportion of proeutectoid ferrite, the proportion of upper bainite and the colony size of the latter.

The formation of proeutectoid ferrite appears to be controlled by the start of the transformation temperature, although the

grain size could also be an influencing factor. The proeutectoid ferrite tends to form at the prior austenite grain boundaries, and when this occurs, it rejects carbon into the surrounding untransformed austenite. When the grain size is small and the cooling rate high, there should be no time for carbon diffusion and the whole austenite would transform in the upper bainitic range of transformation temperatures. At higher peak temperatures, the grain size is coarser and the austenite more homogeneous. On cooling it appears that some austenite would tolerate a higher carbon content, allowing the nucleation of some proeutectoid ferrite. That mechanism would explain why no proeutectoid ferrite was formed at the peak temperature of 1250^{o}C of the 3.6KJ/mm heat input, whereas it was found in a small amount, at the peak temperature of 1400^{o}C. Now considering the cooling times equivalent to 6.3 and 14.4KJ/mm where proeutectoid ferrite could nucleate, some mechanisms could be outlined. At a fixed heat input, the grain size increases with increasing peak temperature. The proeutectoid ferrite nucleation would reject carbon into the untransformed austenite. Then a carbon gradient is built up from the boundaries towards the centre of the grain and the austenite inside a smaller grain will have a higher carbon content than the austenite inside a larger grain. The former should yield a higher proportion of lower transformation products than the latter, on cooling. The influence of the grain size must be taken into account. At a "small" grain size, the dominant constituent would be proeutectoid ferrite due to the abundance of nucleation sites. The above explanation should clarify why the upper bainite content was maximum at 1250^{o}C.

Microalloy precipitation was not found in the current work, although it might have occurred. Observing the model exhibited by Bernard et al (29), it was noticeable that at the 7.0KJ/mm heat input condition, there was more precipitation away from the fusion line than in its vicinity. The reason for such behaviour would be the lower values for the start of the transformation temperature in the latter, than in the former region. Consequently, at the peak temperature of 1250^{o}C, if this is the case, there should exist more precipitation than at the peak temperature of 1400^{o}C. At the cooling time associated with the heat input of 3.0KJ/mm, the same authors found very little precipitation in the HAZ, whereas Canadian researchers (61) found none at cooling times lower than Δt = 39s. Consequently, at the heat input of 3.6KJ/mm investigated in the current work, little or no precipitation of microalloys was expected to occur. Although microalloy precipitation has been documented by the French and the Canadians, these authors did not commit themselves to stating that this should be the main cause for the deterioration of the coarse grained HAZ toughness.

4.6 Practical Implications And Future Work

The results observed from the Charpy testing performed on the weld HAZ of the steel RQT-500 indicated an improvement in the toughness of the fine grained region of the HAZ, and a strong deterioration of the coarse grained HAZ region relative to the toughness of the base metal. The cause for the embrittlement was considered to be the nature of the microstructures formed, mainly constituents such as proeutectoid ferrite and

upper bainitic structures forming larger colonies favoured by the coarse grain size. The deterioration increased with the increase in the heat input and the most brittle region at the higher heat inputs was not exactly adjacent to the fusion line, but the one next to that. The maximum deterioration was associated with the occurrence of proeutectoid ferrite delineating the prior austenite grain boundaries and a maximum content of upper bainite. The cleavage cracks are believed to nucleate in the proeutectoid ferrite and propagate easily across the larger colonies of upper bainite. Simulation techniques employed in the current investigation reproduced reasonably well the HAZ regions encountered in the actual weld HAZs. The latter technique provided an economical and practical solution to the study of the weld HAZ. It was economical because the material consumption and the work shop machining time were minimised. It is practical because of the facility in handling the samples, and because it provided a wide, homogeneous region for the location of the crack propagator. However, since the current work involved the investigation of the toughness of a Quenched and Tempered C-Mn steel microalloyed with Nb and V welded at higher levels of heat input, and then the determination of the causes of the deterioration of the toughness, the conditions used were very severe and a critical notch positioning was sought. This was performed to try to isolate the factors influencing the HAZ deterioration, eliminating other beneficial factors such as the protective effect of the HAZ geometry, which would have tended to mask the deterioration effects, making the analysis of the phenomena difficult. It is widely reported from the

literature that the reason why simulation specimens produce the poorest toughness results, is due to the severity of notch positioning, i.e. in a normal, actual weld HAZ, the crack would propagate through regions of different yield strength, whereas in a synthetized specimen, the crack would propagate through a region of constant yield strength. It was mentioned previously that the HAZ geometry will exert a strong, protective influence, since brittle failures tend to run normal to the main stress direction (94). It was also reported that little information exists in service failures following the HAZ (24). Changes in the welding process such as the use of higher welding speeds were considered beneficial (30). It was explained that the travel speed has a marked effect on the thermal cycle retention time above the A_3 temperature and on the width of the HAZ. The latter, in particular, is considered to govern the maximum prior austenite grain size at the fusion boundary. Consequently, an increase in the welding speed should give a higher HAZ toughness, despite the higher welding current needed to maintain the heat input at the fixed level. From the facts mentioned above, it is seen that a process providing a different weld HAZ profile than the ones tested in the current work or a process employing higher welding speeds and higher welding currents should yield a better tough final composite.

Concerning the microstructural work, one would observe that a decrease in the amount of proeutectoid ferrite, a decrease in the amount of upper bainite and a decrease in the grain size should yield a considerable increase in the toughness

of the weld HAZ. The proeutectoid ferrite was considered a very interesting microstructure. An intriguing fact was the question why that constituent was found in some HAZs, and was not observed in others of steels with similar compositions and welded at similar heat inputs. A possible explanation is that the inclusions content played an important role. Upper bainitic constituents, also, are a harmful microstructure to the toughness of the steel. The presence of Nb and the cooling times employed depressed the start of the transformation temperature and appeared to favour the production of that constituent. The size of their colonies is considered the "effective" grain size influencing the toughness, because the low angle between the bainite ferrite cell boundaries would allow easy crack propagation. Because the grain size of the upper bainitic colonies is related to the grain size of the prior austenite, the smaller the latter, the tougher the structure. Smaller prior austenite grain sizes are obtained by lower heat input welds, or as mentioned previously, by a higher travel speed of the electrode. Beneficial constituents were found to be the interlocking acicular ferrite and the isolated ferrite cells documented in the microstructures. They provided barriers to the crack propagation, increasing the absorbed impact energy. Molybdenum seems to be a desirable alloying element, since it is reported not only to depress the formation of the proeutectoid ferrite, but also to promote the formation of interlocking acicular ferrite.

In considering the significance of the present work, it is necessary to emphasise that it was aimed at discovering the most embrittling conditions occurring in the weld HAZ of the

steel RQT-500, attempting to isolate the brittle regions, to determine the causes for their loss in toughness. Consequently, some of the processes and techniques which have been employed were far from those recommended in the technical brochure issued by the steels' manufacturer (88).

In the light of the factors presented above, and taking into account the description of the current work, the following further research is proposed :

i) The investigation of the weld HAZs of steels with similar composition to that for the RQT-500, but with different levels of inclusion content, to observe the effect of the latter on the formation of proeutectoid ferrite, and the toughness of the steels.

ii) The investigation of the weld HAZs of steels of similar composition as the RQT-500, but also containing Mo as a further alloying element. The latter is expected to reduce the amount of proeutectoid ferrite, and to promote the formation of a higher amount of interlocking acicular ferrite, thus yielding a better tough structure.

iii) The investigation of the HAZs of the RQT-500 steel welded at the same heat inputs as those from the current work, but at different welding conditions, i.e. at a higher welding speed and at a higher welding current. Also, to test samples extracted from weldments performed by a single pass on each side and notched at the 50/50 position. These tests would give an information on the influence of the HAZ profile on the toughness of the composite.

iv) The investigation of the toughness of the weld metal of RQT-500 steels, welded at the same heat inputs as those for the current work. It might be verified that the deterioration in toughness is at the same level or even more important than the one observed for the HAZ.

v) The investigation of the toughness of similar HAZs as those produced in the current work, but tested by COD testing methods. A comparison could be attempted between the new set of data and those derived from Charpy testing. Also, a maximum defect size could be assessed.

vi) The establishment of sets of curves to predict the cooling times $\Delta t_{800-500}$ for plates with varying thickness. Based on these, a final equation could be attempted, taking into consideration the plate thickness factor.

CHAPTER 5 - CONCLUSIONS

CHAPTER 5 - CONCLUSIONS

1. It was observed that simulation techniques reproduce satisfactorily in the laboratory, the actual weld conditions.

2. It is shown that the toughness of the weld HAZ of the steel RQT-500 differs from that of the parent metal. The nature and the magnitude of the change are dependent on the heat input and peak temperature experienced during the welding thermal cycle.

3. Over the peak temperature range of 700 - 1000^{o}C (fine grained region), there is a progressive increase in toughness relative to that of the base metal, as indicated by the Charpy absorbed impact energy curves. Under some conditions, the toughness is at a maximum at 900^{o}C and under others at 1000^{o}C.

4. Over the peak temperature range of 1150 - 1400^{o}C (coarse grained HAZ region), a strong deterioration in toughness was observed relative to that of the base metal, the maximum embrittlement occurring at about 1250^{o}C.

5. The increase in toughness over the range 700 - 1000^{o}C is attributed to the finer grain size exhibited by the microstructure.

6. The decrease in toughness over the range 1150 - 1400^{o}C is

attributed to the nature of the microstructure formed, and its magnitude increased with the increase in heat input.

7. At any heat input investigated, the maximum embrittlement was associated with a structure containing proeutectoid ferrite and a maximum of upper bainite. It appears that the cleavage cracks nucleating in the proeutectoid ferrite propagated easily across the upper bainite colonies.

8. At the peak temperatures of 1150^{o}C and above, microalloys would dissolve into the austenite, allowing its grain coarsening. Also, the transformation temperature was depressed favouring the formation of upper bainitic microstructures exhibiting large colony sizes.

9. No precipitation of microalloys was found by transmission electron microscopy observations performed on carbon extraction replica of the most embrittled samples, and of the post weld heat treated samples.

10. A CCT diagram has been produced, involving heating to peak temperatures of 1400^{o}C and cooling times $\Delta t_{800-500}$ over the range of 4 to 954 seconds. The extent of the bainitic zone obtained gives a fairly good idea of the problems to be expected if welds above 3.6KJ/mm ($\Delta t_{800-500}$ = 25s) are to be used.

11. Post weld heat treatment over the temperature range of 550 to 650^{o}C causes further embrittlement in the weld HAZ and in the parent metal.

12. The results from the actual investigation confirm the data from the current literature which state that a strong embrittlement is to be expected from the HAZ of C-Mn steels microalloyed with Nb and V welded at heat inputs equivalent to $\Delta t_{800-500} > 25s$.

BIBLIOGRAPHY

on Welding of Pipe Girth Joints
Rome, Nov. 1971, No. 4

2. Guide to the Welding and Weldability of C-Mn Steels
C-Mn Microalloyed Steels. Doc. IIS/IIW-382-[illegible]
18-646-69) Commission IX.

3. DICKINSON, J.A., "The Submerged Arc Welding of [illegible]
Pipe - A Semi-Automatic Method", [illegible]
1972

4. British Standard BS3601.

5. DICKENSON, J.B., "High Strength, Low Alloy Steels - A
Decade of Progress", Microalloy 75 Symposium, Oct. 1975,
Washington, D.C.

6. GRAY, J.M., "Weldability of Niobium Containing HSLA
Steel", Paper presented to the "First Latin American
Congress on [illegible] Technology", Rio de Janeiro, Dec.
1975

7. SOLEK, K.A., "Factors Controlling Weld Thickness
Pendant Position. Part 1, Heat Affected Zone
Welding Institute Report 11/1976/M, Cambridge

8. HOWE, D.G., "Welding of Pipelines and Evolution of
New Techniques", Proceedings, IIW, 1972, [illegible]
Guide to Welding [illegible]

12. [illegible] Structure and [illegible] Steel Low Carbon Bainitic
Steels", Welding Research International, Vol. 8, No. 5,
1978, p. 349.

BIBLIOGRAPHY

1. PRESTON, R.R., "A Review of High Strength, Low Alloy Steel Metallurgy in Europe", Proceedings of Conference on Welding of HSLA (Microalloyed) Structural Steels, Rome, Nov. 1976, ASM.

2. Guide to the Welding and Weldability of C-Mn Steels and C-Mn Microalloyed Steels. Doc. IIS/IIW-382-71 (ex doc. 1X-646-69) Commission IX.

3. TICHAUER, P.A., "The Submerged Arc Weld in HSLA Line Pipe - A State-of-the-Art Review", WRC Bulletin 201, 1979.

4. British Standard BS4360.

5. PICKERING, F.B., "High Strength, Low Alloy Steels - A Decade of Progress", Microalloy 75 Symposium, Oct. 1975, Washington, D.C.

6. GRAY, J.M., "Weldability of Niobium Containing HSLA Steel", Paper presented at the "First Latin American Congress on Welding Technology", Rio de Janeiro, Sept. 1975.

7. DOLBY, R.E., "Factors Controlling Weld Toughness - The Present Position. Part 1. Heat Affected Zones", The Welding Institute report 11/1976/M, Cambridge, May 1976.

8. BOVE, O., "Welding of Pipelines and Evolution of the New Techniques", Svetsaren, no. 1-2, 1972, p. 13., as quoted in reference 3.

9. BENKO, B., HRIVANAKOVA, D., "Assessment of the Weldability of Microalloyed FAMA-type Steels by Noren Test". V.E. Rieconsky Translation VR/177/73 published in Welding Research Abroad Vol. XX1, no. 1, January 1975, as quoted in reference 6.

10. SUBBA RAO, K.F., RAMASWAMY, V., RAMACHANDRAN, S., "Heat Affected Zone Toughness of HSLA Steels Developed at Rourkela Steel Plant", Proceedings of Conference on Welding of HSLA (Microalloyed) Structural Steels, Rome, Nov. 1976, ASM.

11. PRESTON, R.R., "Low Carbon Structural Steels - Future Trends and Developments", Sprint Residential Conference on Low Carbon Structural Steels for the Eightees, Plymouth, March 1977, The Institution of Metallurgists".

12. QUINN, T.A., ROGERSON, M.A., "A Comparison of HAZ Microstructure and Properties of Some Low Carbon Pipeline Steels", Welding Research International, vol. 8, no. 5, 1978, p. 349.

13. SAWHILL JR, J.M., BOUSSEL, P., MORROW, J.W., "Heat Affected Zone Toughness of High Heat Input HSLA Welds", Proceedings of Conference on Welding of HSLA (Micro-alloyed) Structural Steels, Rome, Nov. 1976, ASM.

14. HANNERZ, N.E., "Weld Metal and HAZ toughness and Hydrogen Cracking Susceptibility of HSLA Steels as Influenced by Nb, Al, V, Ti and N", Ibid.

15. HANNERZ, N.E., FERENC, K., "Influence of Vanadium on the Weldability of Constructional Steels", IIW doc. no. IX-988-76 (1976), as quoted in reference 14.

16. GRANJON, H., "The 'Implants' Method for Studying the Weldability of High Strength Steels", Metal Construction and British Weld. Journal, vol. 1, no. 11, Nov. 1969, p. 509.

17. DOLBY, R.E., SAUNDERS, G.G., "Metallurgical Factors Controlling the HAZ Fracture Toughness of Carbon, Manganese and Low Alloy Steels", National Seminar on The Toughness of the Weld Heat Affected Zones, London, March 1974, The Welding Institute.

18. ARONSON, A.H., "The Weldability of Columbium Bearing High Strength Low Alloy Steel", Welding Research Supplement, June 1966, p. 266-s.

19. WADA, T., "Toughness of Planar Heat Affected Zones in Submerged Arc Welds of Mn-Mo-Cb Steels", Climax Molybdenum Company of Michigan report L-176-108, March 1974.

20. McGRATH, J.T., GODDEN, M.J., GORDINE, J., BOYD, J.D., "Fracture Resistance of Pipeline Weldments", CANMET report ERP/MRP/PMRL-79-48 (OP-J), June 1979, Ottawa.

21. ASTM A 370 - Book 10, 1978.

22. SAUNDERS, G.G., "Influence of Welding and Post Welding Heat Treatment on the Heat Affected Zone Fracture Toughness of Carbon, Manganese and Low Alloy Steels", National Seminar on the Toughness of Weld Heat Affected Zones, London, March 1974, The Welding Institute.

23. BRITISH CODA P 54 - Commission for Standardisation of Test Conditions.

24. WATKINS, B., "The Significance of the Heat Affected Zone in Fracture Initiation", Welding in the World, vol. 10, no. 9/10, 1972, p. 270.

25. BONOMO, F., ROTHWELL, A.B., "The Weldability of Steels and its Implications for Products Development Criteria", 1st Welding Congress, Bratislava, 1971.

26. CIVALLERO, M., PAPRINI, C., SALMONI, G., "Experience in the Development and Welding of Large Diameter Pipes", Welding Research Council bulletin no. 201, 1974.

27. CORDEA, J.N., "Niobium and Vanadium Containing Steels for Pressure Vessel Service", Welding Research Council bulletin no. 203, Feb. 1975.

28. BERNARD, G., "A View Point on the Weldability of Carbon-Manganese and Microalloyed Structural Steels", Micro-alloy 75 Symposium, Oct. 1975, Washington, D.C.

29. BERNARD, G., FAURE, F., MAITREPIERRE, Ph., "Properties of Welds in Submerged Arc Welding", Proceedings of Conference on Welding of HSLA (Microalloyed) Structural Steels, Rome, Nov. 1976, ASM.

30. DOLBY, R.E., "HAZ Toughness of Structural and Pressure Vessel Steels - Improvement and Prediction", Welding Research Supplement, August 1979, p. 225-s.

31. BONOMO, F., ROTHWELL, B., "Tenacite de la Zone Thermi-quement Affectee des Aciers Microallies", EEC Coal and Steel Commission Conference, Luxemburg, June 1971, p. 199.

32. Centro Sperimentale Metallurgico (Rome), Commission of the European Communities agreement no. 6210-41/4/041, Final Report on the "Study of Toughness Properties of the Heat Affected Zone of Steels", EUR5264i, 1975.

33. CANE, M.W.F., DOLBY, R.E., "Metallurgical Factors Controlling the HAZ Fracture Toughness of Submerged Arc Welded C-Mn Steels", National Seminar on the Toughness of Weld Heat Affected Zones, London, March 1974, The Welding Institute.

34. SAWHILL, JR, J.M., WADA, T., "Properties of Welds in Low Carbon Mn-Mo-Cb Line Pipe Steels", Welding Journal Research Supplement, Jan. 1975.

35. OTTERBERG, R., SANDSTROM, R., SANDBERG, A., "Influence of Widmanstatten Ferrite on Mechanical Properties of Microalloyed Steels", IIW doc. IX 1127-79.

36. SIGNES, E.G., BAKER, J.C., "Effect of Columbium and Vanadium on the Weldability of HSLA Steels", Welding Research Supplement, June 1979, p. 179-s.

37. KAAE, J.L., BAILEY, N., "The HAZ Fracture Toughness of Controlled Rolled, Nb Treated, Low C-Mn Steels", Metal Construction and British Welding Journal, Aug. 1979, p. 371.

38. DOLBY, R.E., "The Influence of Defect Orientation on HAZ Fracture Toughness Measurements", National Seminar on the Toughness of Weld Heat Affected Zones, London, March 1974, The Welding Institute.

39. NIPPES, E.F., SAVAGE, W.F., "Development of Specimen Simulating Weld Heat Affected Zones", Welding Journal, vol. 28, no. 11, 1949, p. 534-s.

40. WATKINS, B., VAUGHAN, H.G., LEES, G.M., "Embrittlement of Simulated HAZ in Low Alloy Steels", British Weld Journal, June 1966, p. 350.

41. SMITH, E., COWARD, M.D., APPS, R.L., Cranfield College of Technology Report Mat. no. 2, 1968.

42. "Weld Thermal Simulators for Research and Problem Solving", The Welding Institute, London, April 1972.

43. DOLBY, R.E., "Fracture Toughness Comparison of Weld HAZ and Thermally Simulated Microstructures, Ibid.

44. SCHOFFIELD, R., WEINER, R.T., "Simulating HAZ Toughness In pipeline Steels", Metal Construction and British Welding Journal, Feb. 1974, p. 45.

45. BACKSTROM, B. ET AL., "Effect of Grain Refining Elements on the Toughness of High Heat Input Welded High Tensile Shipbuilding Steels", Advanced Welding Technology: Proceedings 2nd International Symposium of Japan Welding Society, Osaka, Aug. 1975, JWS 1975, vol. 11, Paper 2-3-(8), as quoted in reference 28.

46. Commission for the European Communities "Study of the Mechanical Properties of the HAZ in Welded High Strength Steels", Technical Research "Steel", Report 5192 f, vol. 2, Dec. 1974, as quoted in reference 28.

47. KOHNO, R., JONES, S.B., "An Initial Study of Arc Energy and Thermal Cycles in the Submerged Arc Welding of Steel", The Welding Institute report 81/1978/PE, Cambridge, Dec. 1978.

48. ROSENTHAL, D., "Mathematical Theory of Heat Distribution During Welding and Cutting", Welding Journal Research Supplement, vol. 20, no. 5, 1941, p. 220-s.

49. ADRICHEM, Th. J. V., KAS, J., "Einfluss der Schoweiss-porwmeter auf den Abkuhlverlauf in der Schweissverbi-dung", Schweissen und Schneiden, vol. 21, no. 5, 1969, p. 199, as quoted in reference 69.

50. CHRISTENSEN, N., DAVIES, V. DE. L., GJERMUNDSEN, K., "Distribution of Temperatures in Arc Welding", British Welding Journal, vol.12, no. 2, Feb. 1965, p. 54.

51. WESTBY, O., Institute for Mekanisk Teknologies Norges Tekniske Høgskole, Trondheim, 1968.

52. PICKERING, F.B., "Low Carbon High Strength Structural Steels - A Status Report", Spring Residential Conference on Low Carbon Structural Steels for the Eighties, Plymouth, March 1977, The Institution of Metallurgists.

53. GREDAY, T., LAMBERIGTS, M., "The Combined Effect of Microalloying Steels with Columbium and Vanadium", Microalloy 75 Symposium, Oct. 1975, Washington, D.C.

54. HART, P.H.M., DOLBY, R.E., BAILEY, N., WIDGERY, D.J., "The Weldability of Microalloyed Steels", Ibid.

55. HANNERZ, N.E., JONSSON-HOLMQUIST, B.M., "Influence of Vanadium on the Heat Affected Zone Properties of Mild Steel", Metal Science, vol. 8, 1974, p. 228.

56. DOLBY, R.E., "The Effect of Niobium on the HAZ Toughness of High Heat Input Welds in C-Mn Steels", Proceedings of Conference on Welding of HSLA (Microalloyed) Structural Steels, Rome, Nov. 1976, ASM.

57. De KONING, A.C., "Loss of Ductility in Material Next to a Weld", IIW, doc. IX-471-65, as quoted in reference 22.

58. BERKHOUT, C.F., "A Comparison of the Microstructures in the Simulated and Weld HAZ", Seminar on Weld Thermal Simulators for Research and Problem Solving, The Welding Institute, London, April 1972.

59. LAMBERIGTS, M., GREDAY, T., "Aciers de Construction Metallique a Dispersoides", Centre de Recherches Metallurgiques, Liege, Jan. 1975.

60. HOOGENDOORN, T.M., "Quantifying the Effect of Microalloying Elements on Structures During Processing", Microalloy 75 symposium, Oct. 1975, Washington, D.C.

61. ROTHWELL, A.B., McGRATH, J.T., GLOVER, A.G., GRAVILLE, B.A., WEATHERLY, G.C. "Heat Affected Zone Toughness of Welded Joints in Microalloy Steels", CANMET report 79-6, Jan. 1979, Ottawa.

62. LEVINE, E., HILL, D.C., "A Review of the Structure and Properties of Welds in Columbium or Vanadium Containing High Strength Low Alloy Steels", Welding Research Council bulletin no. 213, Jan. 1976.

63. MORRISON, W.B. "The Influence of small Nb additions on the Properties of C-Mn Steels", Journal of the Iron and Steel Inst., vol. 201, 1963, p. 317.

64. GRAY, J.M., WEBSTER, D., WOODHEAD, J.H., "Precipitation in Mild Steels Containing Small Additions of Niobium", Journal of the Iron and Steel Inst., vol. 203, August 1975, p. 812.

65. CONSTANT, A., GRUMBACH, M., SANZ, G., "Etude des Transformations de L'Austenite et de L'Evolution des Precipites dans des Aciers a Dispersoides - Consequences Partiques", Revue de Metallurgie, vol. 67, Nov. 1970, p. 913.

66. GRAY, M., YEO, R.B.G., "Columbium Carbonitride Precipitation in Low Alloy Steels with Particular Emphasis on 'Precipitate Row Formation'", Trans. Quort. Amer. Soc. Metals, vol. 61, 1968, p. 255.

67. TAKAHASHI ET AL., "On High Strength Steel for High Heat Input Welding", Parts I-IV, Tetsu to Hagane, vol. 59, no. 173, p. S148, as quoted in reference 6.

68. SUZUKI, H., Public Session IIW Annual Assembly 1976, Sydney, Australia.

69. KANAZAWA, S., ET AL., Trans. ISI Japan, vol. 16, no. 9, 1976, p. 486.

70. MATSUDA, S., ET AL., Tetsu to Hagane, vol. 60, no. 4, 1974, p. 174s, as quoted in reference 27.

71. KANAZAWA, S., ET AL., "Development of New Steels for High Heat Input Welding", IIW doc. IX-952-76.

72. LEVINE, E., HILL, D.C., "Structure and Properties of HSLA Weld Metals containing Cb or V", Proceedings of Conference on Welding of HSLA (Microalloyed) Steels, Rome, Nov. 1976, ASM.

73. MEYER, L., De BOER, H., "Review of HSLA Plant Metallurgy - Alloying Normalising, Controlled Rolling", Proceedings of Conference on Welding of HSLA (Microalloyed) Structural Steels, Rome, Nov. 1976, ASM.

74. IKAWA, H., ET AL., "Austenite Grain Growth of Steels During Thermal Cycles", Transactions of the Japan Welding Society, vol. 8, no. 2, Sept. 1977.

75. IVENS, P.F., VAN Den BERGH, A.A., "Impact Testing of the HAZ", Metal Construction and British Welding Journal, vol. 6, no. 7, 1974, p. 234.

76. BANKS, E.E., "A Fracture Mechanics Assessment of the HAZ Properties of Australia Structural Steels", Australian Welding Journal, Sept./Oct. 1974, p. 59.

77. LEVINE, E., HILL, D.C., "Toughness in HSLA Steel Weldments", Metal Construction, Aug. 1977, p. 346.

78. GRAVILLE, B.A., ROTHWELL, A.B., "Effect of Nb on HAZ toughness Using the Instrumented Charpy Test", Metal Construction, Oct. 1977, p. 455.

79. KEAY, L.K., "Unpublished Data from Lukens Steel Company", 1974, as quoted in reference 25.

80. HART, P.H.M., DOLBY, R.E., "The Effects of Varying Nitrogen and Vanadium Levels on the Notch Toughness of Submerged Arc Welds in Experimental C-Mn-V Steels", Welding Institute Report no. LD 21481/2, July 1974.

81. SOININEN, R., "Brittle Fracture Initiation and Propagation in Killed Low-Carbon Structural Steels", Scandinavian Journal of Metallurgy, vol. 6, 1977, p. 97.

82. SMITH, R.C., TURNIPSEED, S.C., "Unpublished Data from Armco Steel", Houston Works, 1973, as quoted in reference 25.

83. POLLARD, B., ARONSON, A.H., "Weldability of VAN-80 Steel", Welding Research Supplement, Dec. 1970, p. 559-s.

84. SALMONI, G., "High Strength Nb-V Steel for the Construction of Two 127,000 Cubic Metres Storage Tanks", Symposium on HSLA, Metallurg Co, Pub. 1970, p. 115, as quoted in reference 58.

85. KANAZAWA, S., SATO, M., "Vanadium for the Improvement of Properties such as Weldability of High Strength Steels", Vanitec Meeting, 1976, Japan.

86. ARCHER, G.L., "Fracture Toughness in the HAZs of a C-Mn Steel (to BS4360, Grade 50) and a Low Alloy Steel", National Seminar on the Toughness of Weld Heat Affected Zones, London, March 1974, The Welding Institute.

87. KAAE, J.L., "Mechanical Properties, Microstructure and Susceptibility to Cracking in the HAZ of Controlled-Rolled, Nb-Treated, Low Carbon, Manganese Steels", British Welding Journal, Aug. 1968, p. 395.

88. "Quenched and Tempered Steel Plates", Technical Brochure published by British Steel Corporation March 1978.

89. WINTERLIN, K., Private Communication, CANMET, Ottawa, as quoted in reference 22.

90. FEARNEOUGH, G.D.S., Private Communicatio, as quoted in reference 22.

91. RODGERSON, P., Discussion of the Morning Session - "Methods of Testing", National Seminar on the Toughness of the Weld Heat Affected Zones, London, March 1974, The Welding Institute.

92. MIYOSHI, E., ET AL., "New Development and Welding Technique for Artic-Grade Line Pipe", Welding Research Council Bulletin no. 201, 1974, p. 31.

93. GITTOS, M.F., DOLBY, R.E., "Predicting the HAZ Toughness of C and C-Mn Steels - Welding at 2KJ/mm", report 15/1976/M, May 1976, The Welding Institute.

94. PELLINI, W.S., "Principle of Fracture Safe Design - Part II", Welding Journal, vol. 50, no. 26, 1971, p. 147s.

95. ONOE, H., ET AL., "Japanese LPG Tanker Constructed Using a New Welding Process and Improved Al Killed Steels", Metal Construction, vol. 11, no. 1, 1979.

96. CONINCK VAN NOYEN, P., Discussion of the Afternoon Session - "Metallurgical and Welding Procedure Factors", National Seminar on the Toughness of the Weld Heat Affected Zones, London, March 1974, The Welding Institute.

97. CHRISTIE, K.D., Private Communication, British Steel Corporation, Clydebridge Works, Dec. 1979.

98. RENWICK, B.G., PATCHETT, B.M., "Operating Characteristics of the Submerged Arc Process", Welding Journal Res. Supplement, vol. 55, March 1976, p. 69s.

99. APPS, R.L., GOURD, L.M., NELSON, K.A., "Effect of Welding Variables upon Bead Shape and Size in Submerged Arc Welding", Welding and Metal Fabrication, vol. 31, Nov. 1963, p. 453.

100. "Code of Good Practice for Deep Penetration Welding", Welding in the World, vol. 2, no. 1, 1964, p. 56.

101. DOLBY, R.E. Private Communication, The Welding Institute, Cambridge, March 1977.

102. PHILLIPS, R.H., JORDAN, M.F., "The Temperature Measurement and Distribution in Weld Thermal Simulation", Welding Research International, vol. 3, no. 3, 1973, p. 59.

103. FREEMAN, R., Private Communication, GKN Wolverhampton, June 1978.

104. GITTOS, M.F., DOLBY, R.E., "Predicting the HAZ Toughness of C and C-Mn Steels - Welding 25mm Plate at 1-7KJ/mm", The Welding Institute Publication 65/1978/M, June 1978.

105. PHILLIPS, R.H., "High Temperature Cracking in the Weld HAZ of High Strength Ferritic Steels", PhD Thesis, The University of Aston in Birmingham, 1973.

106. PHILLIPS, R.H., Weld Thermal Simulators for Esearch and Problem Solving, discussion of Session II - Applications, The Welding Institute Seminar, London, April 1972.

107. STRUNCK, S.S., STOUT, R.D., "Heat Treatment effects in multipass weldments of a High Strength Steel", The Welding Journal, vol. 51, Oct. 1972, p. 508-s.

108. GINN, B.J., HALL, G.T., "The Welding Institute Research Bulletin", vol. 13, no. 5, May 1972.

109. ANDERSON, B., UTTERBERG, B., "Colour Etching with Klemm's Reagent", Svetsaren, vol. 6, no. 3, 1970.

110. PAXTON, H.W., "The formation of Austenite", discussion, Symposium on "Transformation and Hardenability in Steels", Climax Molybdenum Co. of Michigan, Feb. 1967, p. 14.

111. McLEAN, D., NORTHCOTT, L., "Microexamination and Electrode - Potential Measurements of Temper-Brittle Steels", Journal of the Iron and Steel Inst., vol. 158, Feb. 1948, p. 170.

112. PICKERING, F.B., "The Structure and Properties of Bainite in Steels", Symposium on "Transformation and Hardenability in Steels", Climax Molybdenum Co. of Michigan, Feb. 1967, Feb. 1967, p. 109.

113. OBLAK, J.M., HEHEMANN, R.F., "Structure and growth of Widmanstaten Ferrite and Bainite", Ibid, p. 15.

114. PICKERING, F.B., "The Basis of Quantitative Metallography", Institute of Metallurgical Technicians, monograph no. 1, 1976.

115. BROOKS, T.L., HART, P.H.M., "Do Hardness Measurements impress you?", The Welding Institute Research Bulletin, March 1977, p. 69.

116. BISS, V., CRYDERMAN, R.L., "Martensite and Retained Austenite in Hot-Rolled Low Carbon Bainitic Steels", Metallurgical Transactions, vol. 2, Aug. 1971, p. 2267.

117. SAVAGE, W.F., "Evolution of the Gleeble", Seminar on "Weld Thermal Simulators for Research and Problem Solving", The Welding Institute, April 1972, p. 1.

118. Joint BWRA Report to IIW, Commission IX, Sub-Commission B. "Comparison of Continuous Cooling Transformation Behaviour and Weld HAZ Austenitising Conditions", June 1963.

119. MARTIN, P.F., ROQUES C., "Dilatometric Measurements with the Aid of the RPI Gleeble Machine", AWS Spring Meeting in Philadelphia in "Methods of Weldability Evolution", April 1969.

120. CIAS, W.W., "Austenite Transformation Kinetics of Ferrous Alloys", Climax Molybdenum Co. Publication.

121. AARONSON, H.I. "On the Problems of Definition and the Mechanisms of the Bainite Reaction", The Mechanism of Phase Transformation in Crystalline Solids, Institute of Metals, monograph no. 33, 1969.

122. DOLBY, R.E., "The Effect of Nb on the HAZ Toughness of High Heat Input Welds in C-Mn Steels", discussion of Session II, Proceedings of Conference on Welding of HSLA (Microalloyed) Structural Steels, Rome, Nov. 1976, ASM, p. 324.

123. PRESTON, R.R., "A Review of High Strength, Low Alloy Steel Metallurgy in Europe", discussion of Session I, Ibid, p. 127.

124. GARLAND, J.G., discussion of Session II, Ibid, p. 329.

125. BERSH, B., "Influence of Heat Input on the HAZ - Properties of Line Pipe Steels", Ibid, p. 271.

126. ANDREWS, K.W., DYSON, D.J., KEOWN, S.R., "Interpretation of Electron Diffraction Patterns", Adam Hilger Limited, 1071, p. 180.

TABLES

TABLE 1 - CHEMICAL COMPOSITION OF STEELS TESTED FOR THE DEVELOPMENT OF Y.S. $\geqslant$ 36kg/mm^2 HULL PLATE

Steel	Thickness (mm)	CHEMICAL COMPOSITION (%)										Ceq (%)
		C	Si	Mn	P	S	Nb	V	Ti	Nt	Al Sol	
Si-Mn	30	0.17	0.25	1.30	0.014	0.010	-	-	-	0.005	0.019	0.397
V(H)	30	0.16	0.40	1.32	0.015	0.007	-	0.054	-	0.006	0.040	0.397
Nb-V(K)	30	0.16	0.24	1.34	0.012	0.007	0.02	0.02	-	0.006	0.022	0.394
V(Y)	30	0.16	0.46	1.39	0.021	0.018	-	0.06	-	0.005	0.033	0.411
Nb(H)	30	0.15	0.37	1.36	0.020	0.012	0.037	-	-	0.006	0.040	0.392
Nb-V(N)	30	0.16	0.33	1.33	0.014	0.006	0.033	0.03	-	0.01	0.034	0.396
V-Ti(H)	30	0.15	0.36	1.45	0.014	0.004	-	0.051	0.018	0.0079	0.025	0.406
Nb-V-TI(N)	32	0.12	0.28	1.40	0.015	0.007	0.018	0.017	0.014	0.007	0.011	0.365
Ti(N)	32	0.12	0.28	1.46	0.018	0.005	-	-	0.013	0.0085	0.018	0.375

Remarks : Ceq = C + 1/24Si + 1/6Mn

All steels are produced in LD furnace

TABLE 2 - CHEMICAL ANALYSIS OF THE STEEL RQT-500

C	Si	Mn	P	S	Ni	Cr	Mo	Al	Cu	Nb	V	Co	Sn	N	O
0.15	0.34	1.44	0.011	0.025	0.06	0.08	0.02	0.004	0.08	0.06	0.03	0.02	0.008	0.005	0.015

TABLE 3 - MECHANICAL PROPERTIES OF THE STEEL RQT-500

Yield N/mm^2	UTS N/mm^2	El (200mm)	Charpy Impact (J)	
			Temp. (^oC)	Longitudinal
535	625	29%	-40	41

TABLE 4 - WELDING PARAMETERS FOR THE PRESENT WORK

Heat Input (HI) KJ/mm	Electrode Polarity	Stick Out mm	Weld Speed(v) mm/min.	Actual Current(A)	Volt (V)
3.6 5.6 6.3	DCRP (electrode positive)	25	400	750 1073 1200	32 35 35
$HI = \frac{VI \times 60}{v}$					

TABLE 5 - COOLING TIMES $\Delta t_{800-500}$ MEASURED FROM THE PRACTICE

HEAT INPUT (KJ/mm)			
3.6		5.6	
Peak Temp. ^{o}C	Δt S	Peak Temp. ^{o}C	Δt S
790	26	882	68
943	27	890	66
1210	26	903	69
1390	20	929	66
1510	27	937	70
1581	28	951	71
1625	27	1225	64
1675	21	1225	74
1700	26	1600	61

TABLE 6 - VARIATION OF THE WELDING CURRENT AND VOLTAGE WITH THE MAIN VOLTAGE OSCILLATION

NOMINAL CURRENT = 700 A						
Weld No.	Day	Time	Mains Voltage (V)		Recorded Weld Parameters	
			Before Welding	During Welding	Volts (V)	Current (A)
1	Tue	12.00	423	418	32	830
2	Wed	11.00 am	425	420	32	850
3	Thu	3.00 pm	444	438	33	900
4	Thu	5.15 pm	426	421	32	850
5	Fri	10.40 am	422	417	32	840
6	Fri	13.30 pm	425	419	30	850

TABLE 7 - VARIATION OF THE DEPTH OF THE WELD BEAD WITH THE MAINS VOLTAGE OSCILLATION

Section Number	Depth of the Weld for Different Trials (mm)					
	1	2	3	4	5	6
1	10.5	10.0	10.5	10.0	10.5	10.0
2	11.0	11.0	12.0	10.5	11.0	10.5
3	10.0	11.0	11.0	11.0	11.5	11.0
4	10.0	11.0	11.5	11.0	11.5	11.5
5	10.5	11.0	12.5	11.0	11.0	11.5

TABLE 8 - ESTIMATED VALUE FOR Δt, PRESENT WORK

Heat Input KJ/mm	Δt S
2.7	14
3.6	25
4.5	42
5.6	70
6.3	90
7.0	115

TABLE 9 - ACTUAL RECORDED VALUE FOR Δt, PRESENT WORK

Heat Input KJ/mm			
3.6		5.6	
Peak Temp. ^{o}C	$\Delta t_{800-500}$ S	Peak Temp. ^{o}C	$\Delta t_{800-500}$ S
790	26	880	68
940	27	890	66
1210	26	900	69
1390	20	930	66
1510	27	940	70
1581	28	950	71
1625	27	1230	64
1675	21	1230	74
1700	26	1600	61

TABLE 10 - ESTIMATED VALUE FOR $\triangle t$, OTHER AUTHORS

B W I (56,104)			Sawhill et al (13)	
Heat Input KJ/mm	Measured $\triangle t$ S	Estimated $\triangle t$ S	Heat Input KJ/mm	Measured $\triangle t$ S
3.5	26	25	3.9	29
5.0	60	-		
7.0	111	60		

TABLE 11 - CENTRE/SURFACE TEMPERATURE DISTRIBUTION

Nominal Temp. ^{o}C	Temperature Measured	
	Control Temp. Pt/Pt 13%Rh ^{o}C	Calibration Temp. Cr/Al ^{o}C
400	394	391
500	500	495
600	598	596
700	700	698
800	800	799
900	898	897
1000	1001	1000
1100	1101	1102
1200	1196	1201

TABLE 12 - DIAMETRAL TEMPERATURE GRADIENT ACROSS THE SPECIMEN

Depth of Couple Immersion mm	NOMINAL TEMPERATURE = 800°C		NOMINAL TEMPERATURE = 1100°C	
	Control Temp. (Pt/Pt 13%Rh) °C	Calibration Temp. (Chromel/ Alumel) °C	Control Temp. (Pt/Pt 13%Rh) °C	Calibration Temp. (Chromel/ Alumel) °C
10.0	791	802	1087	1094
8.5	791	801	1088	1099
7.0	795	793	1098	1092
6.0	795	811	1094	1104
5.0	796	816	1094	1114
4.0	799	805	1101	1114
3.0	801	808	1101	1107
1.5	799	737	1100	1010

TABLE 13 - TEMPERATURE DISTRIBUTION ALONG THE GAUGE LENGTH

	Sample Gauge Length mm	TEMPERATURE DISTRIBUTION ALONG THE SAMPLES - °C DISTANCE FROM THE CENTER - mm 4.0	3.0	2.0	1.0	0	1.0	2.0	3.0	4.0	Control Temp. °C
Square Cross Section	15.0	-	1150	1186	1197	1193	1171	1146	1095	-	1195
	20.0	1047	1110	1157	1175	1189	1183	1160	1128	1110	1199
	25.0	1117	1146	1168	1186	1197	1184	1168	1159	1122	1199
Round Cross Section	15.0	-	1073	1157	1175	1182	1150	1073	991	-	1202
	20.0	1099	1161	1178	1208	1201	1197	1176	1117	1066	1199
	25.0	1154	1176	1194	1187	1197	1190	1154	1132	1095	1200
	Upper Jaw ⟵ ∘ ⟶ Lower Jaw										
	Nominal Temperature = 1200°C										

TABLE 14 - SIMULATION AND DILATION FIGURES FOR THE HEAT INPUT EQUIVALENT TO 3.6KJ/mm

HEAT INPUT = 3.6KJ/mm								
Sample	Peak Temperature Nominal °C	Peak Temperature Attained °C	Δt_{p-800} s	$\Delta t_{800-500}$ s	A_s °C	A_f °C	T_s °C	T_f °C
INTENDED PEAK TEMPERATURE = 700°C								
V1	710	720	-	23*	-	-	-	-
V2	710	720	-	23*	-	-	-	-
V3	710	720	-	23*	-	-	-	-
V4	710	720	-	23*	-	-	-	-
V5	710	720	-	23*	-	-	-	-
INTENDED PEAK TEMPERATURE = 800°C								
U1	800	818	-	30	745	-	745	636
U2	800	818	-	27	753	-	753	636
U3	800	818	-	28	761	-	757	644
U4	800	818	-	28	757	-	757	644
U5	800	818	-	28	753	-	753	636
INTENDED PEAK TEMPERATURE = 900°C								
T1	870	897	7	28	-	-	-	-
T2	870	904	8	28	753	873	720	619
T3	870	902	8	28	761	877	737	619
T4	870	902	8	28	753	881	737	627
T5	870	902	8	28	757	877	737	619

* $\Delta t_{700-500}$

TABLE 14 - CONT'D

Sample	Peak Temperature Nominal °C	Peak Temperature Attained °C	Δt_{p-800} S	$\Delta t_{800-500}$ S	A_s °C	A_f °C	T_s °C	T_f °C
HEAT INPUT = 3.6KJ/mm								
INTENDED PEAK TEMPERATURE = 1000°C								
I1	980	1046	9	23	753	921	729	578
I2	980	1042	8	23	749	925	733	596
I3	980	1016	8	23	757	893	724	578
I4	980	1035	8	23	-	913	729	583
I5	980	1016	8	23	757	909	733	592
I6	980	1035	8	23	766	917	724	578
INTENDED PEAK TEMPERATURE = 1150°C								
F 1	1150	1157	12	24	752	962	643	472
F 2	1150	1169	12	25	744	958	612	463
F 3	1150	1180	12	25	752	966	638	463
F 4	1150	1180	12	25	-	-	-	-
F 5	1150	1173	12	25	756	970	638	458
F 6	1150	1171	12	25	764	-	643	-
F 7	1150	1173	12	-	752	977	660	463
F 8	1150	1180	12	-	748	966	643	465
F 9	1150	1173	12	-	740	970	643	465
F10	1150	1173	12	25	748	962	643	465
F11	1150	1180	12	25	752	954	612	458
F12	1150	1173	12	-	-	962	638	458
F13	1150	1191	12	25	748	962	643	465
F14	1145	1155	12	24	715	970	638	449

TABLE 14 - CONT'D

HEAT INPUT = 3.6KJ/mm								
Sample	Peak Temperature Nominal °C	Peak Temperature Attained °C	Δt_{p-800} S	$\Delta t_{800-500}$ S	A_s °C	A_f °C	T_s °C	T_f °C
INTENDED PEAK TEMPERATURE = 1250°C								
E 1	1280	1273	15	26	698	977	568	392
E 2	1270	1230	13	24	748	977	614	-
E 3	1285	1259	14	25	756	970	608	411
E 4	1285	1246	14	25	752	962	595	411
E 5	1285	1259	14	25	-	-	616	406
E 6	1285	1250	14	24	-	-	-	-
E 7	1285	1266	14	25	723	977	614	440
E 8	1285	1280	15	25	756	962	608	423
E 9	1280	1255	15	25	-	-	614	-
E10	1280	1241	14	25	723	958	614	-
E11	1285	1272	15	24	740	954	595	416
E12	1285	1259	14	25	756	962	605	420
E13	1285	1266	15	25	-	-	-	-
E14	1285	1280	15	25	756	970	599	-
INTENDED PEAK TEMPERATURE = 1400°C								
J1	1425	1422	18	27	757	948	596	422
J2	1425	1416	18	26	749	956	601	422
J3	1425	1422	18	26	-	-	-	-
J4	1425	1422	18	27	766	956	605	432
J5	1425	1413	18	26	766	960	605	-
J6	1425	1387	18	26	770	956	605	413
J7	1425	1394	18	27	-	956	605	422

TABLE 15 - SIMULATION AND DILATION FIGURES FOR THE HEAT INPUT EQUIVALENT TO 6.3KJ/mm

HEAT INPUT = 6.3KJ/mm								
Sample	Peak Temperature Nominal °C	Peak Temperature Attained °C	Δt_{p-800} S	$\Delta t_{800-500}$ S	A_s °C	A_f °C	T_s °C	T_f °C
INTENDED PEAK TEMPERATURE = 700°C								
S1	700	704	-	79*	-	-	-	-
S2	710	720	-	80*	-	-	-	-
S3	710	720	-	81*	-	-	-	-
S4	710	720	-	78*	-	-	-	-
S5	710	712	-	79*	-	-	-	-
INTENDED PEAK TEMPERATURE = 800°C								
R1	800	802	-	91	737	-	724	636
R2	800	802	-	92	745	-	728	636
R3	800	802	-	91	745	-	728	644
R4	800	802	-	91	745	-	720	644
R5	800	802	-	91	745	-	728	644
INTENDED PEAK TEMPERATURE = 900°C								
Z1	870	966	6	93	745	912	737	627
Z2	850	950	6	85	745	-	716	627
Z3	840	890	3	85	761	865	737	610
Z4	840	920	3	88	761	889	753	619
Z5	840	897	3	89	757	869	745	-
Z6	840	845	2	86	757	-	745	627
Z7	840	899	3	85	745	865	737	-
Z8	840	904	3	86	745	865	728	-

* $\Delta t_{700-500}$

TABLE 15 - CONT'D

HEAT INPUT = 6.3KJ/mm								
Sample	Peak Temperature		Δt_{p-800}	$\Delta t_{800-500}$	A_s	A_f	T_s	T_f
	Nominal °C	Attained °C	S	S	°C	°C	°C	°C
INTENDED PEAK TEMPERATURE = 1000°C								
H1	980	1050	11	82	745	909	737	631
H2	970	1012	11	84	766	902	741	640
H3	970	1012	11	84	749	894	733	636
H4	970	1042	10	83	-	898	-	-
H5	970	1016	10	83	749	902	729	636
H6	970	1020	11	82	766	902	741	640
H7	970	1005	10	80	766	905	745	640
INTENDED PEAK TEMPERATURE = 1150°C								
D 1	1130	1179	15	86	751	946	693	451
D 2	1130	1168	15	86	747	949	701	452
D 3	1130	1147	15	84	759	957	718	443
D 4	1130	1165	15	85	-	-	-	-
D 5	1130	1162	15	-	-	-	-	-
D 6	1130	1168	15	84	742	934	676	433
D 7	1130	1168	15	84	751	949	697	433
D 8	1130	1175	15	85	747	949	676	433
D 9	1130	1168	15	85	747	965	697	452
D10	1130	1168	15	84	751	942	701	451
D11	1130	1157	15	85	-	946	701	451
D12	1130	1162	15	84	767	934	701	433
D13	1130	1157	15	85	-	934	718	433

TABLE 15 - CONT'D

Sample	Peak Temperature Nominal °C	Peak Temperature Attained °C	Δt_{p-800} S	$\Delta t_{800-500}$ S	A_s °C	A_f °C	T_s °C	T_f °C
HEAT INPUT = 6.3KJ/mm								
INTENDED PEAK TEMPERATURE = 1250°C								
C 1	1240	1269	26	86	751	950	659	462
C 2	1240	1248	26	87	751	942	672	458
C 3	1240	1248	26	87	-	-	-	-
C 4	1240	1240	26	89	-	-	-	-
C 5	1240	1257	26	86	751	950	668	462
C 6	1240	1255	26	90	751	950	659	458
C 7	1240	1233	26	89	751	942	668	458
C 8	1240	1248	26	90	-	-	-	-
C 9	1240	1262	26	90	751	935	659	462
C10	1240	1262	26	88	751	935	663	458
C11	1240	1255	26	-	-	-	-	-
C12	1240	1240	26	-	-	-	-	-
INTENDED PEAK TEMPERATURE = 1400°C								
G 1	1400	1440	38	87	759	957	615	462
G 2	1400	1423	39	88	734	934	624	471
G 3	1400	1426	40	88	767	942	620	-
G 4	1400	1423	39	85	-	949	624	466
G 5	1400	1445	40	86	767	949	628	-
G 6	1400	1431	41	86	-	942	620	462
G 7	1400	1437	40	85	767	949	624	462
G 8	1400	1430	40	86	767	942	611	462
G 9	1400	1430	39	86	763	949	615	-
G10	1400	1432	40	86	-	949	-	462

TABLE 16 - SIMULATION AND DILATION FIGURES FOR THE HEAT INPUT EQUIVALENT TO 14.4KJ/mm

HEAT INPUT = 14.4KJ/mm								
Sample	Peak Temperature		Δt_{p-800}	$\Delta t_{800-500}$	A_s	A_f	T_s	T_f
	Nominal °C	Attained °C	S	S	°C	°C	°C	°C
INTENDED PEAK TEMPERATURE = 700°C								
Q1	700	712	-	160*	-	-	-	-
Q2	700	720	-	160*	-	-	-	-
Q3	700	720	-	160*	-	-	-	-
Q4	700	724	-	160*	-	-	-	-
Q5	700	720	-	160*	-	-	-	-
INTENDED PEAK TEMPERATURE = 800°C								
P1	800	810	-	235	753	-	753	627
P2	810	825	-	195	753	-	753	627
P3	810	818	-	195	753	-	753	644
P4	810	825	-	200	745	-	753	636
P5	810	818	-	195	745	-	741	636
INTENDED PEAK TEMPERATURE = 900°C								
O1	860	893	20	225	737	877	-	-
O2	860	898	24	235	745	873	761	584
O3	860	885	20	230	753	869	745	584
O4	860	881	21	230	737	869	753	584
O5	860	889	21	230	753	881	761	592
INTENDED PEAK TEMPERATURE = 1000°C								
N1	960	999	10	204	768	911	751	-
N2	960	992	9	202	751	911	743	581
N3	960	992	9	204	751	911	747	598
N4	960	999	10	212	768	896	743	590
N5	960	1033	10	225	-	-	-	-
N6	960	999	10	225	768	896	743	625
N7	960	992	9	205	751	903	743	581

* $\Delta t_{700-500}$

TABLE 16 - CONT'D

Sample	Peak Temperature Nominal °C	Peak Temperature Attained °C	Δt_{p-800} s	$\Delta t_{800-500}$ s	A_s °C	A_f °C	T_s °C	T_f °C
HEAT INPUT = 14.4KJ/mm								
INTENDED PEAK TEMPERATURE = 1150°C								
M1	1130	1183	21	220	768	942	697	581
M2	1130	1143	20	217	768	927	685	-
M3	1130	1197	23	223	772	927	693	563
M4	1130	1147	21	221	768	896	710	590
M5	1130	1147	20	221	751	903	701	585
M6	1130	1118	18	221	743	896	710	545
M7	1130	1121	18	219	755	919	718	581
INTENDED PEAK TEMPERATURE = 1250°C								
L1	1240	1290	29	222	751	942	685	490
L2	1240	1290	29	215	-	942	-	-
L3	1240	1304	28	223	763	934	689	490
L4	1240	1315	28	223	755	934	685	499
L5	1240	1304	-	-	747	934	680	499
L6	1240	1297	28	220	743	934	685	490
L7	1240	1283	28	218	751	934	685	499
INTENDED PEAK TEMPERATURE = 1400°C								
K1	1400	1444	60	213	759	942	633	499
K2	1400	1441	62	210	759	942	633	499
K3	1400	1448	58	211	768	942	642	-
K4	1400	1437	58	210	751	942	633	499
K5	1400	1437	60	210	751	934	633	490
K6	1400	1423	60	210	751	958	642	508
K7	1400	1409	58	214	759	950	633	499

TABLE 17 - SIMULATION AND DILATION FIGURES FOR THE CCT CURVE SPECIMENS

	Sample	Peak Temperature Nominal °C	Peak Temperature Attained °C	Δt_{p-800} s	$\Delta t_{800-500}$ s	A_s °C	A_f °C	B_s °C	B_f °C	M_s °C	M_f °C
	CCT1	1400	1453	4	4	-	-	-	-	483	262
	CCT2	1400	1460	4	5	-	-	-	-	488	273
	CCT3	1400	1448	4	4	-	-	-	-	492	262
	CCT4	1400	1440	5	6	-	-	-	-	484	301
*	CCT5	1400	1434	6	6	-	-	-	-	482	301
*	CCT6	1400	1435	7	8	-	-	529	-	422	334
	CCT7	1400	1429	7	8	746	937	534	-	422	324
	CCT8	1400	1429	-	-	746	-	531	-	417	339
	CCT9	1400	1422	8	10	746	926	529	-	413	329
	CCT10	1400	1418	8	9	762	914	529	-	413	324
*	CCT11	1400	1419	9	10	749	904	534	-	419	320
	CCT12	1400	1427	12	14	753	935	561	-	400	341
	CCT13	1400	1431	10	13	749	920	557	-	404	346
	CCT14	1425	1422	18	27	757	958	599	424	-	-
	CCT15	1400	1426	39	86	765	942	615	462	-	-
	CCT16	1400	1441	60	210	759	958	638	502	-	-
	CCT17	1400	1413	86	526	-	-	604	496	-	-
	CCT18	1400	1420	114	664	-	-	595	514	-	-
	CCT19	1400	1406	156	954	730	882	612	532	-	-

* - Displacement scale = 0.003"

TABLE 18 - SIMULATION AND DILATION FIGURES FOR THE SPECIMEN TO BE HEAT TREATED

Sample	Peak Temperature		Δt_{p-800}	$\Delta t_{800-500}$	A_s	A_f	T_s	T_f
	Nominal °C	Attained °C	s	s	°C	°C	°C	°C
HEAT INPUT = 3.6KJ/mm INTENDED PEAK TEMPERATURE = 1250°C								
HT1	1280	1237	16	23	-	-	-	-
HT2	1285	1294	15	24	752	933	592	418
HT3	1285	1266	15	24	752	942	592	409
HEAT INPUT = 14.4KJ/mm INTENDED PEAK TEMPERATURE = 1250°C								
HT4	1240	1295	27	255	753	923	683	511
HT5	1230	1274	26	240	753	923	679	-
HT6	1230	1288	25	240	-	-	670	503
HT7	1230	1274	26	245	762	930	683	503
HT8	1230	1281	26	240	758	930	679	503
HT9	1230	1288	26	240	745	925	670	494

TABLE 19 - RESULTS OF THE LONGITUDINAL AND TRANSVERSAL CHARPY TESTS FOR THE RQT-500 STEEL PLATES

LONGITUDINAL		TRANSVERSE	
Test Temp. °C	Absorbed Energy J	Test Temp. °C	Absorbed Energy J
-80	20	-80	22
-70	34	-70	24
-56	36	-56	26
-35	68	-35	32
-22	98	-22	42
- 5	112	- 5	52
5	118	5	70
18	118	18	66

TABLE 20 - RESULTS OF THE CHARPY TESTS FOR THE DECISION ON THE LOCATION OF THE NOTCH FOR THE 3.6KJ/mm ACTUAL SAMPLES

Group	Test Temp. °C	Absorbed Energy J
I	-20	38 36 50
II	-20	54 58 58
III	-20	40 38 40

TABLE 21 - RESULTS OF THE CHARPY TESTS FOR THE BASE METAL AND FOR THE 3.6 AND 6.3KJ/mm ACTUAL WELD CONDITIONS

Sample	Test Temp. °C	Absorbed Energy J	% Shear	% Cleavage
BASE METAL				
BM-1	- 80	22	0	100
BM-2	- 70	24	5	95
BM-3	- 56	26	5	95
BM-4	- 35	32	11	81
BM-5	- 22	42	45	55
BM-6	- 5	52	-	-
BM-7	5	70	80	20
BM-8	22	66	88	12
3.6KJ/mm ACTUAL WELDMENT				
A-11	- 75	5	-	-
A- 2	- 60	21	2	98
A- 7	- 50	29	6	94
A-17	- 40	30	6	94
A- 5	- 30	31	17	83
A-20	- 20	38	77	23
A-12	- 20	40	65	35
A- 6	- 20	40	70	30
A-16	- 10	57	75	25
A- 9	0	59	80	20
A- 1	20	64	98	2
6.3KJ/mm ACTUAL WELDMENT				
B-10	- 75	4	-	-
B- 2	- 60	9	2	98
B-11	- 50	5	0	100
B- 4	- 40	6	-	-
B-14	- 35	18	16	84
B-16	- 30	17	13	87
B- 9	- 30	10	15	85
B- 7	- 20	12	11	89
B-13	- 10	13	10	90
B-12	- 5	23	22	78
B- 6	0	14	11	89
B-15	0	28	-	-
B- 8	5	18	-	-
B- 3	10	31	23	77
B-19	15	32	17	83
B-17	20	50	27	73

TABLE 22 - RESULTS OF THE CHARPY TESTS FOR THE SAMPLE SIMULATED AT A HEAT INPUT OF 3.6KJ/mm

HEAT INPUT = 3.6KJ/mm - SIMULATED				
Sample	Test Temp. °C	Absorbed Energy J	% Shear	% Cleavage
INTENDED PEAK TEMPERATURE = 700°C				
V1	- 80	18	5	95
V2	- 55	24	2	98
V3	- 25	32	43	57
V4	0	52	85	15
V5	20	70	100	0
INTENDED PEAK TEMPERATURE = 800°C				
U2	- 80	24	2	98
U4	- 55	33	5	95
U5	- 25	51	60	40
U1	0	62	98	2
U3	20	70	100	0
INTENDED PEAK TEMPERATURE = 900°C				
T2	- 80	32	5	95
T4	- 55	42	38	62
T3	- 25	66	88	12
T1	0	70	96	4
T5	20	76	100	0
INTENDED PEAK TEMPERATURE = 1000°C				
I2	- 80	29	21	79
I6	- 60	35	26	74
I5	- 40	53	70	30
I4	- 20	64	96	4
I1	0	66	98	2
I3	20	65	95	5
INTENDED PEAK TEMPERATURE = 1150°C				
F 3	- 85	15	0	100
F 5	- 78	16	0	100
F11	- 60	13	0	100
F 2	- 46	28	5	95
F10	- 26	34	40	60
F 1	- 11	45	75	25
F12	0	46	77	23
F 4	9	54	77	23
F 7	15	65	95	5
F 8	29	66	100	0

TABLE 22 - CONT'D

HEAT INPUT = 3.6KJ/mm - SIMULATED				
Sample	Test Temp. ^{o}C	Absorbed Energy J	% Shear	% Cleavage
INTENDED PEAK TEMPERATURE = 1250^{o}C				
E11	- 78	4	0	100
E10	- 60	5	0	100
E12	- 46	8	0	100
E 3	- 26	12	0	100
E 6	- 11	22	2	98
E 7	0	20	2	98
E 1	9	24	12	88
E 9	15	34	52	48
E13	29	38	80	20
E 4	37	36	67	33
INTENDED PEAK TEMPERATURE = 1400^{o}C				
J3	- 80	6	0	100
J5	- 60	6	0	100
J1	- 40	8	0	100
J6	- 20	10	6	94
J2	- 10	21	11	89
J4	0	32	43	57
J7	20	31	45	55

TABLE 23 - RESULT OF THE CHARPY TESTS FOR THE SAMPLE SIMULATED AT A HEAT INPUT OF 6.3KJ/mm

HEAT INPUT = 6.3KJ/mm - SIMULATED				
Sample	Test Temp. °C	Absorbed Energy J	% Shear	% Cleavage
INTENDED PEAK TEMPERATURE = 700°C				
S3	- 80	18	0	100
S4	- 55	24	11	89
S1	- 25	32	21	79
S5	0	52	63	37
S2	20	70	100	0
INTENDED PEAK TEMPERATURE = 800°C				
R2	- 80	23	17	83
R4	- 55	32	38	62
R5	- 25	41	55	45
R3	0	62	96	4
R1	20	66	100	0
INTENDED PEAK TEMPERATURE = 900°C				
Z3	- 80	44	31	69
Z7	- 55	74	85	15
Z4	- 25	78	100	0
Z8	0	72	100	0
INTENDED PEAK TEMPERATURE = 1000°C				
H2	- 95	30	11	89
H4	- 75	28	17	83
H7	- 55	46	70	30
H1	- 40	46	75	25
H6	- 20	64	95	5
H5	0	68	100	0
H3	20	56	100	0
INTENDED PEAK TEMPERATURE = 1150°C				
D 3	- 75	14	0	100
D10	- 60	15	0	100
D 2	- 50	10	-	-
D 4	- 41	17	2	98
D 7	- 30	17	2	98
D 9	- 25	24	6	94
D 5	- 20	25	6	94
D13	- 10	25	6	94
D11	- 5	30	11	89
D12	0	30	-	-
D 1	5	37	17	83
D 8	10	35	21	79
D 6	25	43	68	32

TABLE 23 - CONT'D

HEAT INPUT = 6.3KJ/mm - SIMULATED				
Sample	Test Temp. °C	Absorbed Energy J	% Shear	% Cleavage
INTENDED PEAK TEMPERATURE = 1250°C				
C 8	- 75	4	0	100
C10	- 60	6	0	100
C 2	- 50	7	0	100
C 9	- 41	9	0	100
C11	- 30	8	0	100
C 7	- 20	19	0	100
C 4	- 10	19	0	100
C 1	- 5	18	6	94
C 6	0	22	6	94
C 3	5	25	17	83
C12	10	26	-	-
C 5	25	35	33	67
INTENDED PEAK TEMPERATURE = 1400°C				
G1	- 55	8	0	100
G3	- 35	9	-	-
G4	- 20	18	11	89
G2	- 15	16	11	89
G7	- 5	30	21	79
G9	0	34	27	73
G6	10	33	27	73
G8	24	46	35	65

TABLE 24 - RESULT OF THE CHARPY TESTS FOR THE SAMPLES SIMULATED AT A HEAT INPUT OF 14.4KJ/mm

HEAT INPUT = 14.4KJ/mm - SIMULATED				
Sample	Test Temp. °C	Absorbed Energy J	% Shear	% Cleavage
INTENDED PEAK TEMPERATURE = 700°C				
Q3	- 80	8	0	100
Q5	- 55	24	5	95
Q4	- 25	34	27	73
Q1	0	45	67	33
Q2	20	52	91	9
INTENDED PEAK TEMPERATURE = 800°C				
P2	- 80	27	0	100
P4	- 55	28	17	83
P1	- 25	45	44	56
P3	0	69	100	0
P5	20	66	100	0
INTENDED PEAK TEMPERATURE = 900°C				
O2	- 80	34	17	83
O3	- 55	48	42	58
O4	- 25	66	100	0
O1	0	72	100	0
O5	20	66	100	0
INTENDED PEAK TEMPERATURE = 1000°C				
N1	- 80	36	45	55
N6	- 70	44	58	42
N2	- 60	56	80	20
N4	- 40	62	-	-
N7	- 20	68	100	0
N5	0	68	100	0
INTENDED PEAK TEMPERATURE = 1150°C				
M5	- 80	6	0	100
M7	- 60	19	5	95
M4	- 40	26	5	95
M3	- 20	17	5	95
M1	0	28	17	83
M2	20	20	17	83
M6	40	76	100	0

TABLE 24 - CONT'D

HEAT INPUT = 14.4KJ/mm - SIMULATED				
Sample	Test Temp. °C	Absorbed Energy J	% Shear	% Cleavage
INTENDED PEAK TEMPERATURE = 1250°C				
L4	- 80	3	0	100
L2	- 60	4	0	100
L6	- 40	8	0	100
L1	- 20	6	0	100
L3	0	8	0	100
L5	20	14	5	95
L7	40	23	23	77
INTENDED PEAK TEMPERATURE = 1400°C				
K6	- 80	4	0	100
K4	- 60	5	0	100
K5	- 40	6	0	100
K3	- 20	10	5	95
K2	0	23	11	89
K1	20	32	17	83
K7	40	36	33	67

TABLE 25 - TECHNIQUE FOR ETCHING WITH 0.3% CTAB[111]

Etchant Composition	
20g	Picric Acid
100ml	Distilled Water
100ml	Ether
0.3g	Cetyl trimethyl ammonium bromide

Etching Conditions

15 to 30 minutes in a stirred solution at room temperature.

NOTES

1. The procedure produces a brown film on the surface of the sample. It can be removed at intervals of 5 minutes by wiping with NH_4OH solution.

2. Successive etching - polishing with Nital II (3 or 4 times) will help to attenuate the residual stresses at the samples surface, and will produce better results.

3. It was also observed that the grains were more evident after the sample was kept for about one week inside a desiccator. This was probably due to grain boundary corrosion provoked by residual etchant.

TABLE 26 - VALUES FOR THE GRAIN SIZE OF THE SYNTHETIC SPECIMENS AND BASE METAL

Nominal Peak Temp. ^{o}C	HEAT INPUT - KJ/mm		
	3.6	6.3	14.4
	GRAIN SIZE - mm		
700	8.2×10^{-3}	8.3×10^{-3}	8.2×10^{-3}
800	7.3×10^{-3}	8.2×10^{-3}	8.1×10^{-3}
900	6.0×10^{-3}	6.6×10^{-3}	6.3×10^{-3}
1000	5.0×10^{-3}	5.4×10^{-3}	5.5×10^{-3}
1150	0.022	0.024	0.024
1250	0.029	0.052	0.062
1400	0.080	0.102	0.103
BASE METAL GRAIN SIZE = 8.2×10^{-3} mm			

TABLE 27 - VARIATION OF THE GRAIN SIZE AT THE FUSION LINE FOR THE REAL WELDMENTS WITH THE DEPTH OF THE WELDING BEAD

Heat Input KJ/mm	Depth of The Welding Bead mm	Grain Size mm
3.6	0 - 2.0	0.07 - 0.09
	2.0 - 4.0	0.05 - 0.07
	4.0 - 8.0	0.04 - 0.05
6.3	0 - 4.0	0.10 - 0.12
	4.0 - 12.0	0.08 - 0.10
	12.0 - 16.0	0.05 - 0.08
	17.0 - 19.0	0.04 - 0.05

TABLE 28 - PHASE POINT COUNT OF THE STRUCTURES OF THE BASE METAL AND FOR THE SIMULATED PEAK TEMPERATURE OF 700°C

		PEAK TEMP. = 700°C		
		HEAT INPUT , KJ/mm		
Structures	Base Metal	3.6	6.3	14.4
Ferrite	75	68	74	70
Tempered Martensite	21	29	20	20
Intragranular Carbides	4	3	6	10

TABLE 29 - PHASE POINT COUNT OF THE STRUCTURES FOR THE SIMULATED PEAK TEMPERATURES OF 800, 900 AND 1000°C

	PEAK TEMPERATURE , °C								
	800			900			1000		
	HEAT INPUT KJ/mm			HEAT INPUT KJ/mm			HEAT INPUT KJ/mm		
Structures	3.6	6.3	14.4	3.6	6.3	14.4	3.6	6.3	14.4
Ferrite	52	49	53	48	56	51	48	57	55
Ferrite + Carbide Aggregates	43	48	40	42	35	44	46	36	38
Intra-granular Carbides	5	3	7	10	9	5	6	7	7

TABLE 30 - PHASE POINT COUNT OF THE STRUCTURES FOR THE SIMULATED PEAK TEMPERATURES OF 1150, 1250 AND 1400°C

	PEAK TEMPERATURE, °C								
	1150			1250			1400		
	HEAT INPUT KJ/mm			HEAT INPUT KJ/mm			HEAT INPUT KJ/mm		
Structures	3.6	6.3	14.4	3.6	6.3	14.4	3.6	6.3	14.4
Pearlite	—	—	17	—	—	—	—	—	—
Proeutectoid Ferrite	—	70	81	—	25	45	4	20	23
Intragranular Ferrite	16	—	—	13	16	12	34	18	19
Interlocking Acicular Ferrite	40	—	—	12	14	7	24	35	44
Upper Bainite	44	30	2	75	45	36	38	27	14

TABLE 31 - MACROHARDNESS VALUES HV_{30} FOR THE SIMULATED AND REAL WELDMENT SAMPLES AND FOR THE PARENT METAL

Heat Input KJ/mm	Nominal Peak Temp. °C	Sample	HARDNESS HV_{30} Minimum	Maximum	Average
3.6	700	V 3	210	214	212
	800	U 5	216	224	219
	900	T 3	225	235	230
	1000	I 5	235	249	243
	1150	F 4	254	266	258
	1250	E11	245	279	262
	1400	J 3	242	262	248
6.3	700	S 1	201	224	211
	800	R 5	209	216	213
	900	Z 4	210	224	219
	1000	H 4	212	218	215
	1150	D 2	235	238	237
	1250	C 1	230	249	239
	1400	G 3	228	238	232
14.4	700	Q 4	216	224	220
	800	P 3	206	228	215
	900	O 5	206	210	208
	1000	N 4	197	222	210
	1150	M 5	194	203	199
	1250	L 4	212	225	220
	1400	K 6	221	230	225
3.6KJ/mm REAL WELDMENT COARSE GRAINED REGION			266	287	276
6.3KJ/mm REAL WELDMENT COARSE GRAINED REGION			230	254	241
PARENT METAL			195	197	196

TABLE 32 - MACROHARDNESS VALUES FOR THE POST WELD HEAT TREATED SAMPLES

Simulation		Tempering Temp., °C	Sample	HARDNESS HV_{30}		
Heat Input KJ/mm	Peak Temp. °C			Minimum	Maximum	Average
14.4	1250	550 600 650	HT4 HT6 HT8	224 222 228	228 226 238	227 224 232
Parent Metal		550	BM1	226	229	227
Parent Metal		600	BM2	211	214	212

TABLE 33 - MICROHARDNESS OF SOME PHASES OF SIMULATION SPECIMENS

Heat Input KJ/mm	Nominal Peak Temp. °C	PHASES								
		PROEUTECTOID FERRITE			UPPER BAINITE			INTERLOCKING ACICULAR FERRITE		
		HV HARDNESS FIGURES - LOAD = 25g								
		Minimum	Maximum	Mean	Minimum	Maximum	Mean	Minimum	Maximum	Mean
3.6	1150	—	—	—	233	279	256	—	—	—
	1250	—	—	—	212	247	228	287	322	306
	1400	297	302	300*	237	274	250	266	327	292
6.3	1150	215	237	221	240	279	261	—	—	—
	1250	227	274	247	251	283	268	230	292	255
	1400	206	230	215	240	266	252	220	283	259
14.4	1150	212	254	233	254	270	266*	—	—	—
	1250	209	254	221	224	274	248	237	262	248
	1400	198	240	222	201	237	220	237	274	256

* Mean of four measurements

TABLE 34 - HEAT TREATING CONDITIONS AND RESULTS FOR THE CHARPY TESTING OF THE TEMPERED SAMPLES

Simulation		Sample	Tempering Temp. C	Absorbed Energy J	% Shear	% Cleavage
Heat Input KJ/mm	Peak Temp.					
3.6	1250	HT1	600	4	1	99
		HT2	600	4	1	99
		HT3	600	4	1	99
14.4	1250	HT4	550	3	1	99
		HT5	550	5	1	99
		HT6	600	2	1	99
		HT7	600	3	1	99
		HT8	650	3	1	99
		HT9	650	3	1	99
Parent Metal		BM1	550	36	17	83
Parent Metal		BM2	600	36	21	79

Notes :

1) All the samples were held at the tempering temperatures for one hour and were air cooled.

2) All the Charpy tests were performed at the temperature of $-20^{o}C$.

FIGURES

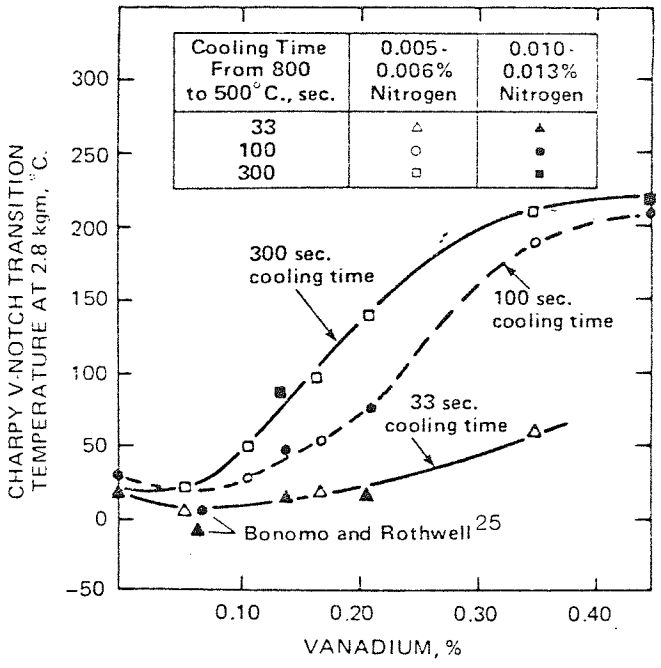

Figure 1 - Influence of vanadium on the simulated heat affected zone transition temperature after Hannerz and Jonsson-Holmquist[55] (after Hart et al [54]).

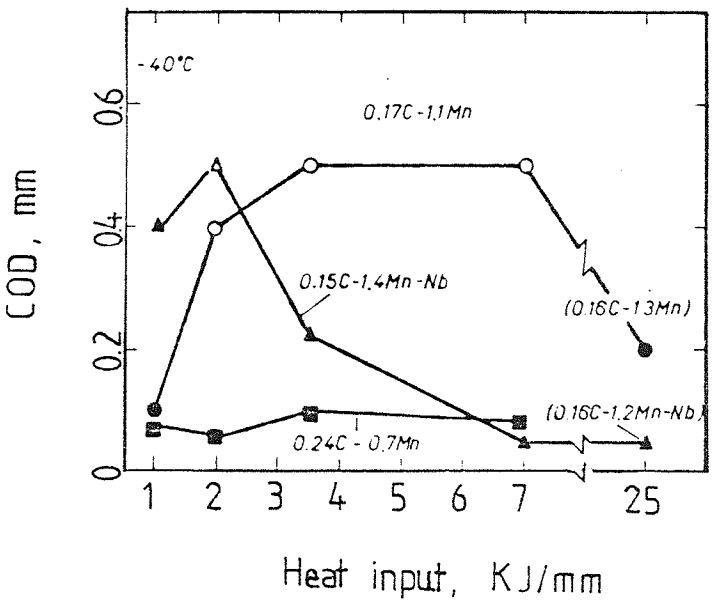

Figure 2 - COD data for grain coarsened HAZ regions of several C and C-Mn steels as a function of the heat input, at -40°C. Diagram appropriate to 25mm thick plate, sharpcracked specimens. Open symbols indicate no cleavage fracture in tests, with COD usually 0.5mm (after Dolby [30]).

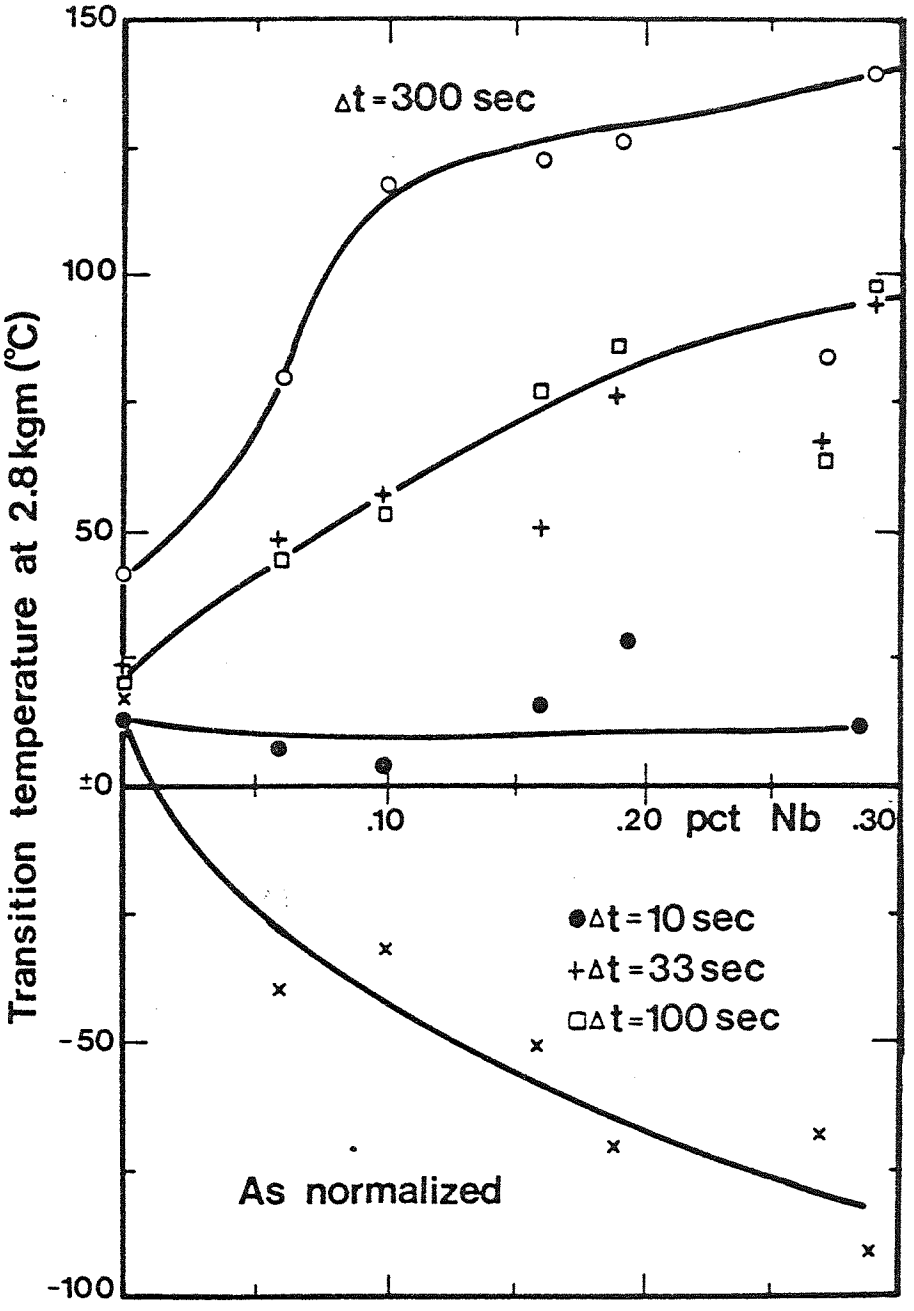

Figure 3 - The influence of niobium on the transition temperature of simulated HAZ. T_{max} = 1350°C, C = .03, Mn = 2.03 pct. (after Hannerz [14]).

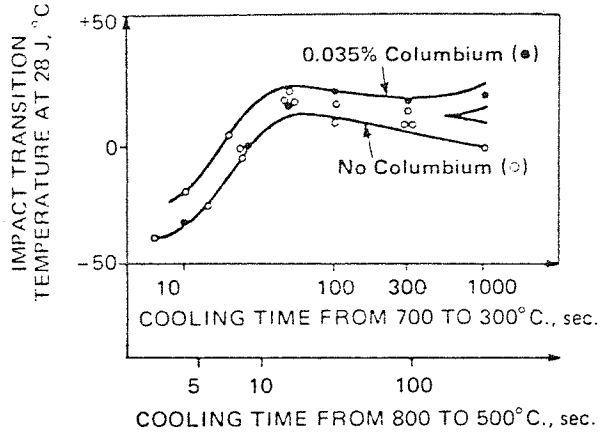

Figure 4 - Observed effect of columbium on simulated HAZ transition temperature. The base analysis was 0.18% carbon, 1.35% manganese, 0.35% silicon, and 0.015% aluminium (after Bernard [28]).

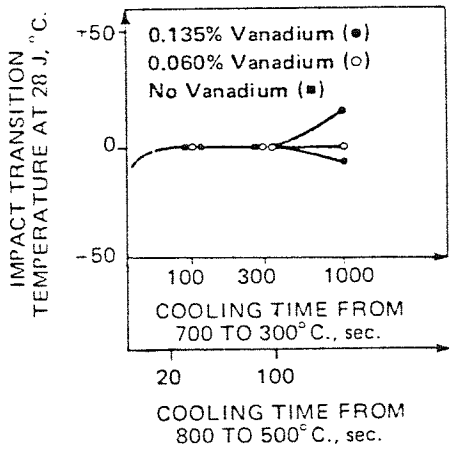

Figure 5 - Observed effect of vanadium on simulated HAZ transition temperature. The base analysis was 0.18% carbon, 1.35% manganese, 0.35% silicon, and 0.015% aluminium (after Bernard [28]).

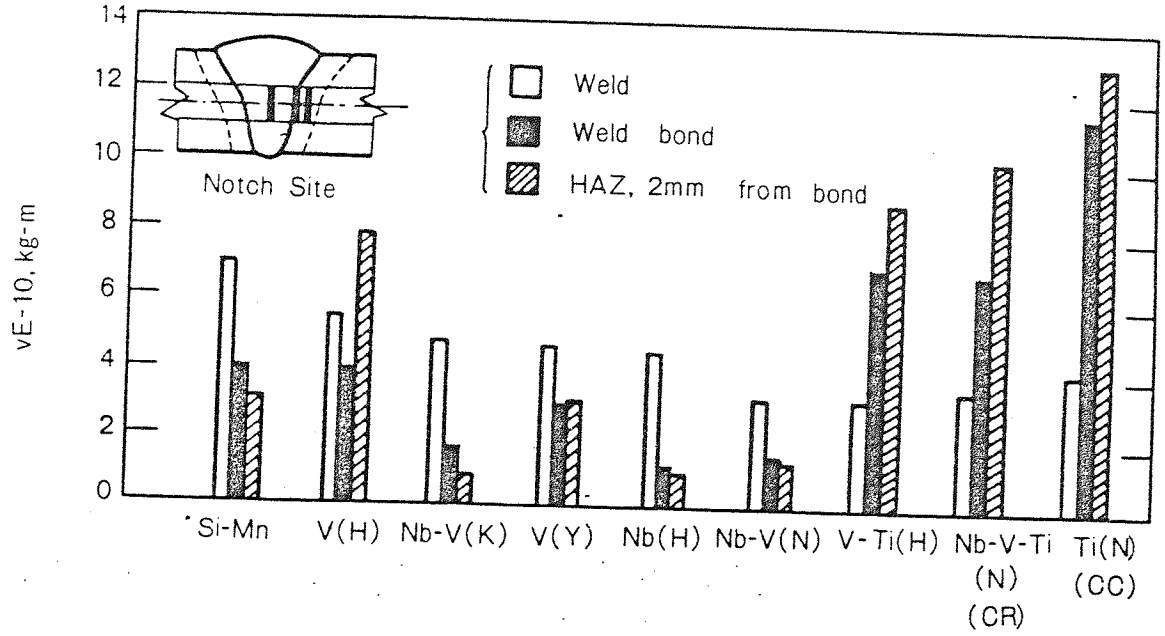

Figure 6 - Effect of microalloying elements on the notch toughness of welded joint. The composition of the steels is given in table 1 (after Kanazawa and Sato [85]).

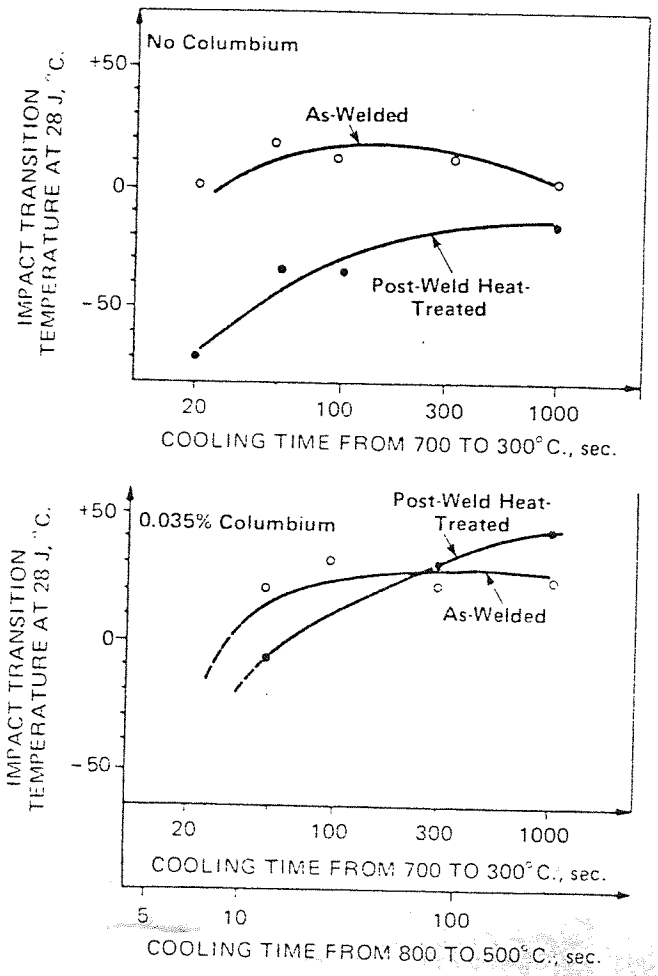

Figure 7 - Effect of a post-weld heat treatment (1 hour at 600°C) on the simulated HAZ transition temperature of a columbium-free and a columbium-treated steel, having a base analysis of 0,18% carbon, 1.35% manganese, 0.35% silicon, and 0.020% aluminum (after Pargeter [88]).

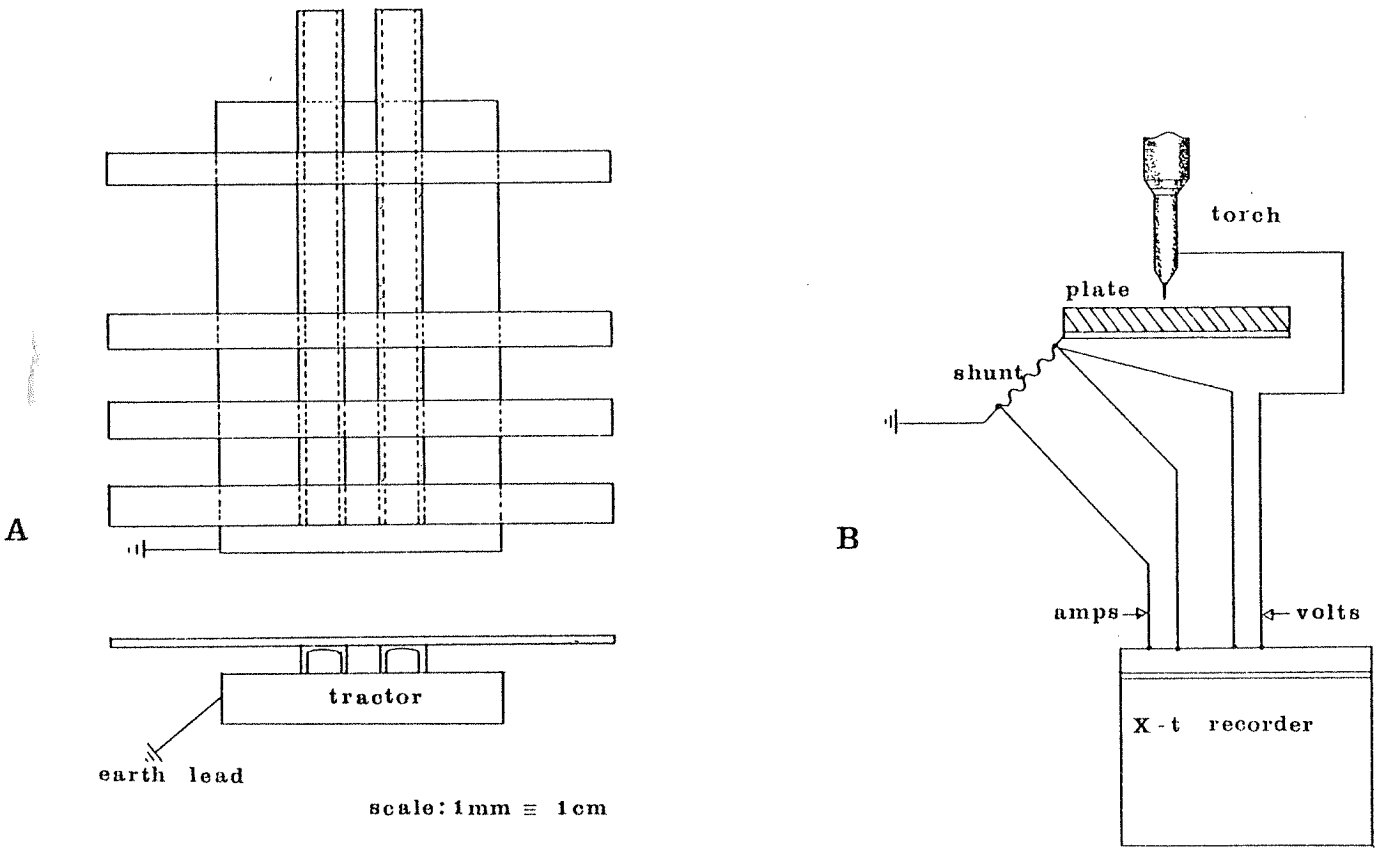

Figure 8

A) Welding jig.

B) Electrical set up to record the welding voltage and the welding current.

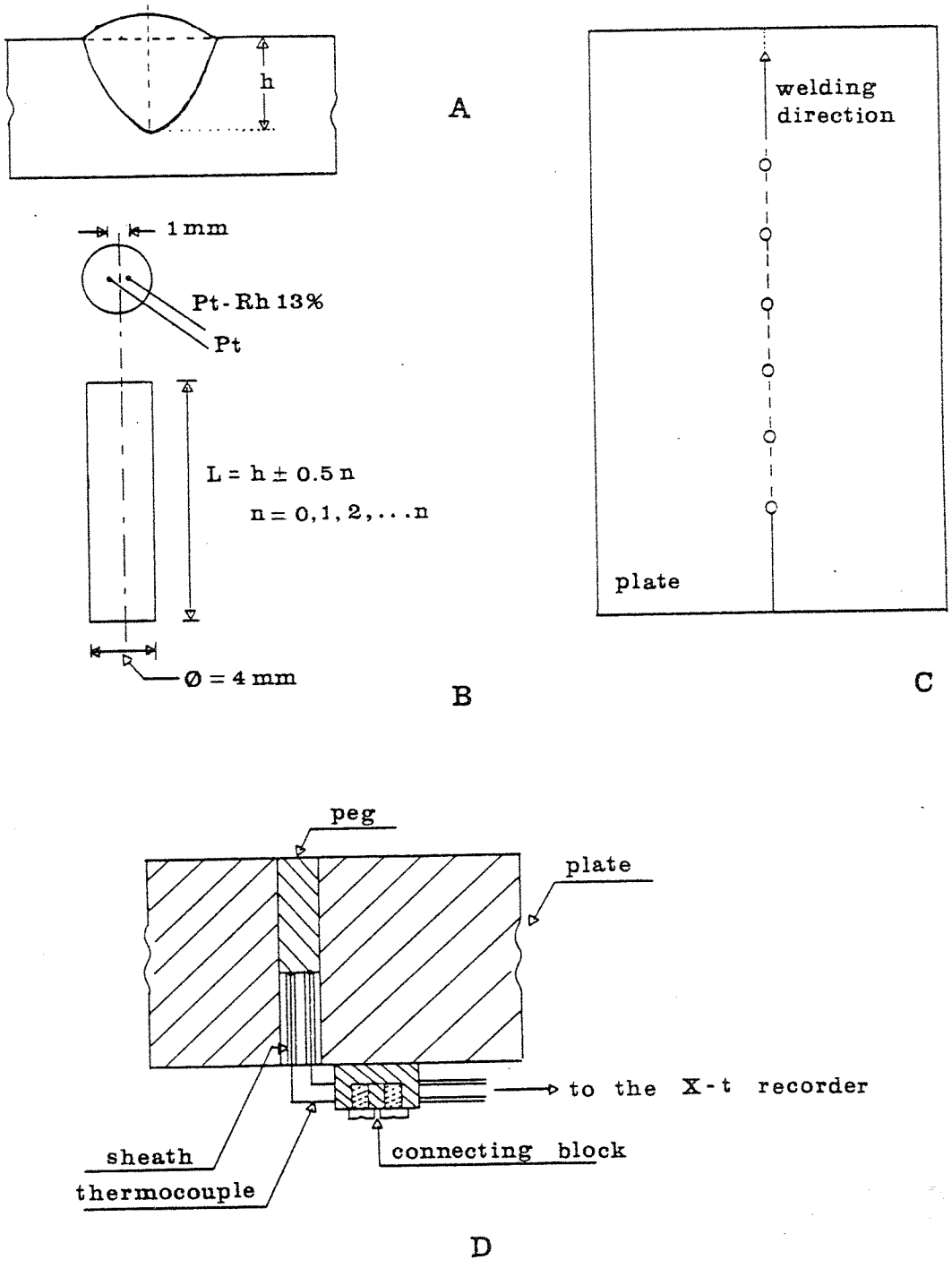

Figure 9 - Explanatory sketches for the thermocouple assembly.

A) Welding bead depth

B) Peg and attachment of the thermocouple to the peg

C) Hole drilling on the plate

D) Cross section of the assembly

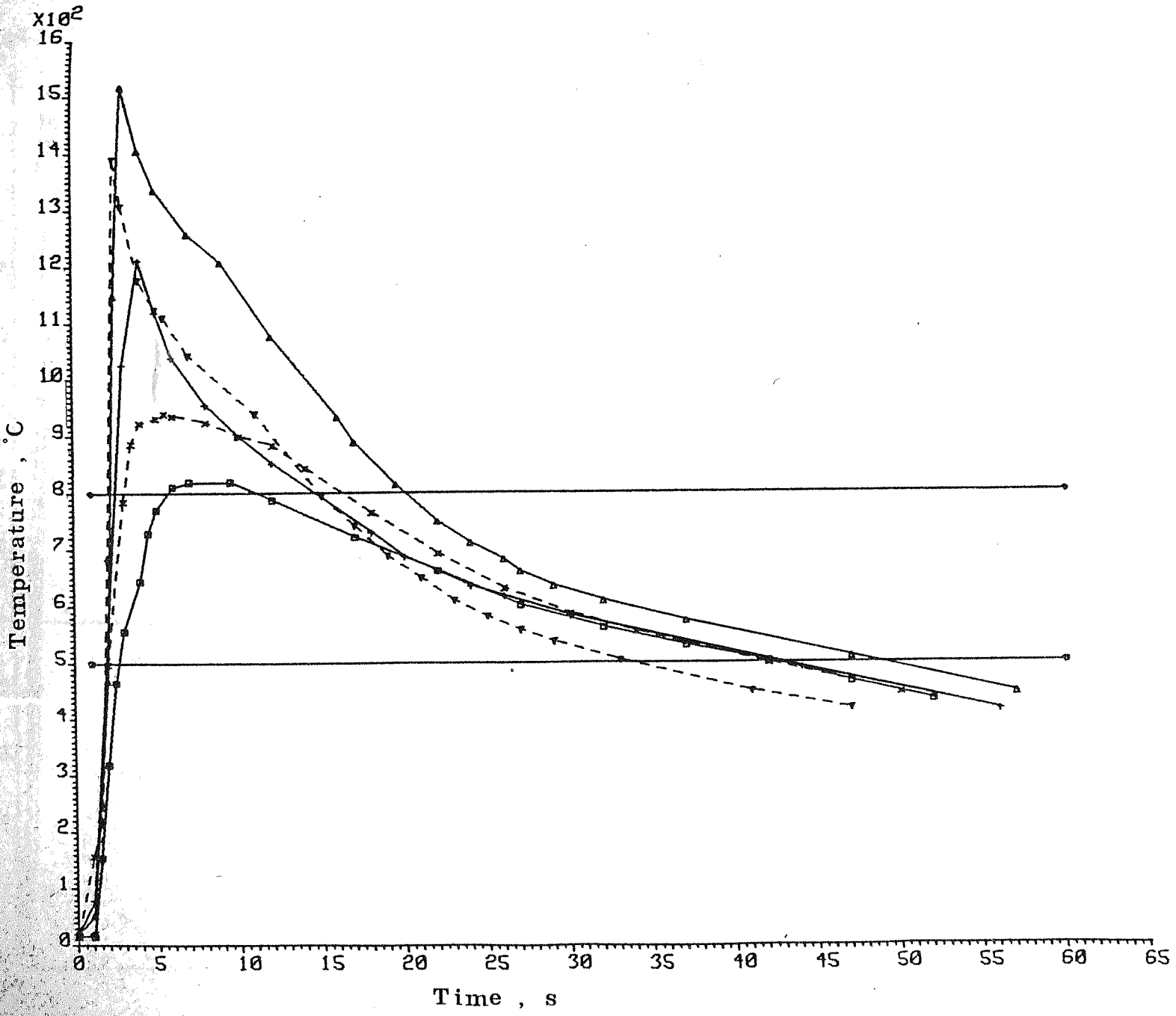

Figure 10

Actual welding thermal cycle - Heat input of 3.6KJ/mm, equivalent to Δt = 25s.

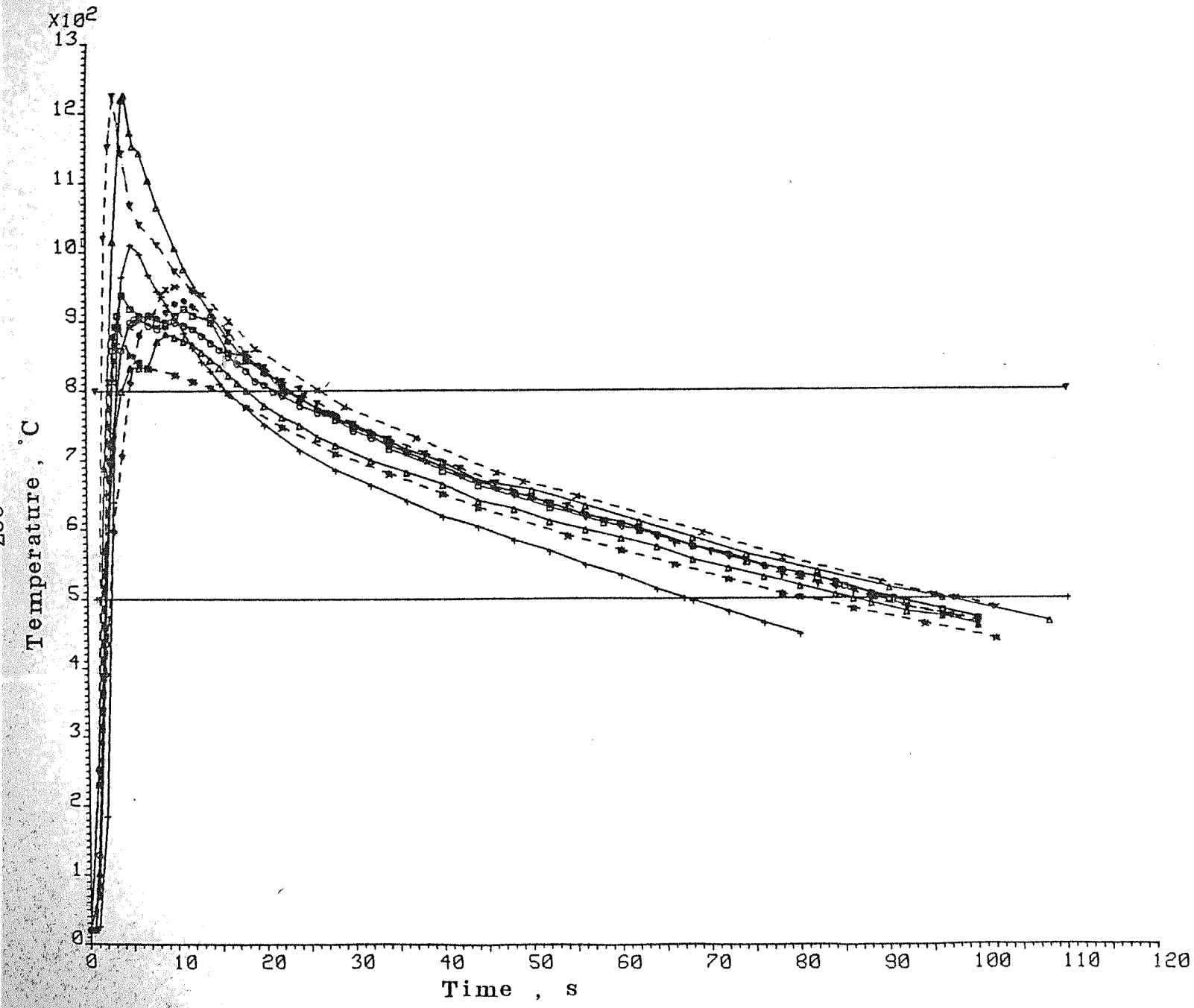

Figure 11

Actual welding thermal cycles - Heat input 5.6KJ/mm, equivalent to Δt = 70s.

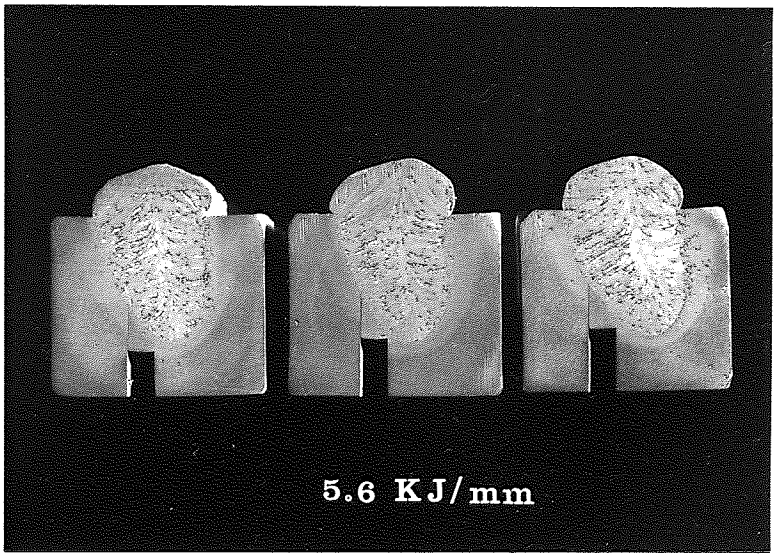

Figure 12 : Instability of the weld bead toe accentuated by the thermocouple insertion.

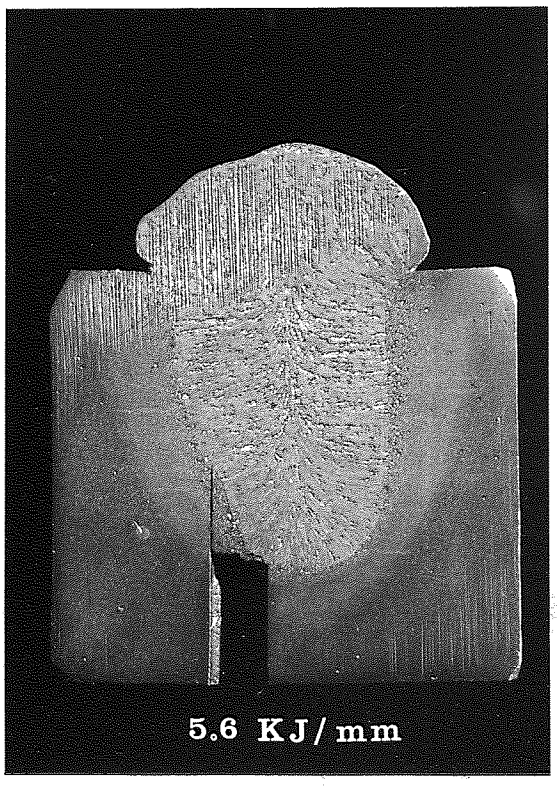

Figure 13 : Detail of the figure 12. Note : deviation of the weld bead profile at the assembly/plate gap.

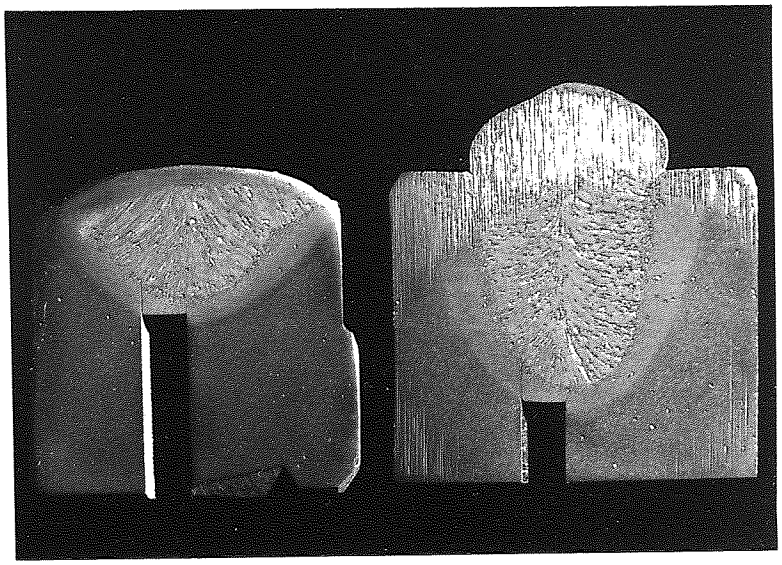

Figure 14 : Test pieces welded at 3.6 and 5.6KJ/MM which provided adequate measurement for the weld thermal cycles.

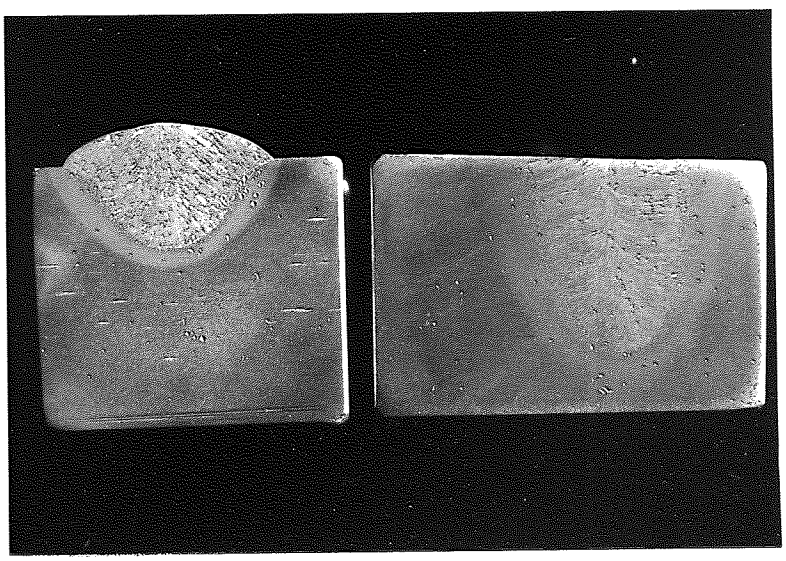

Figure 15 : Weld HAZs representative of heat inputs of 3.6 and 6.3KJ/mm, to be considered in the current work.

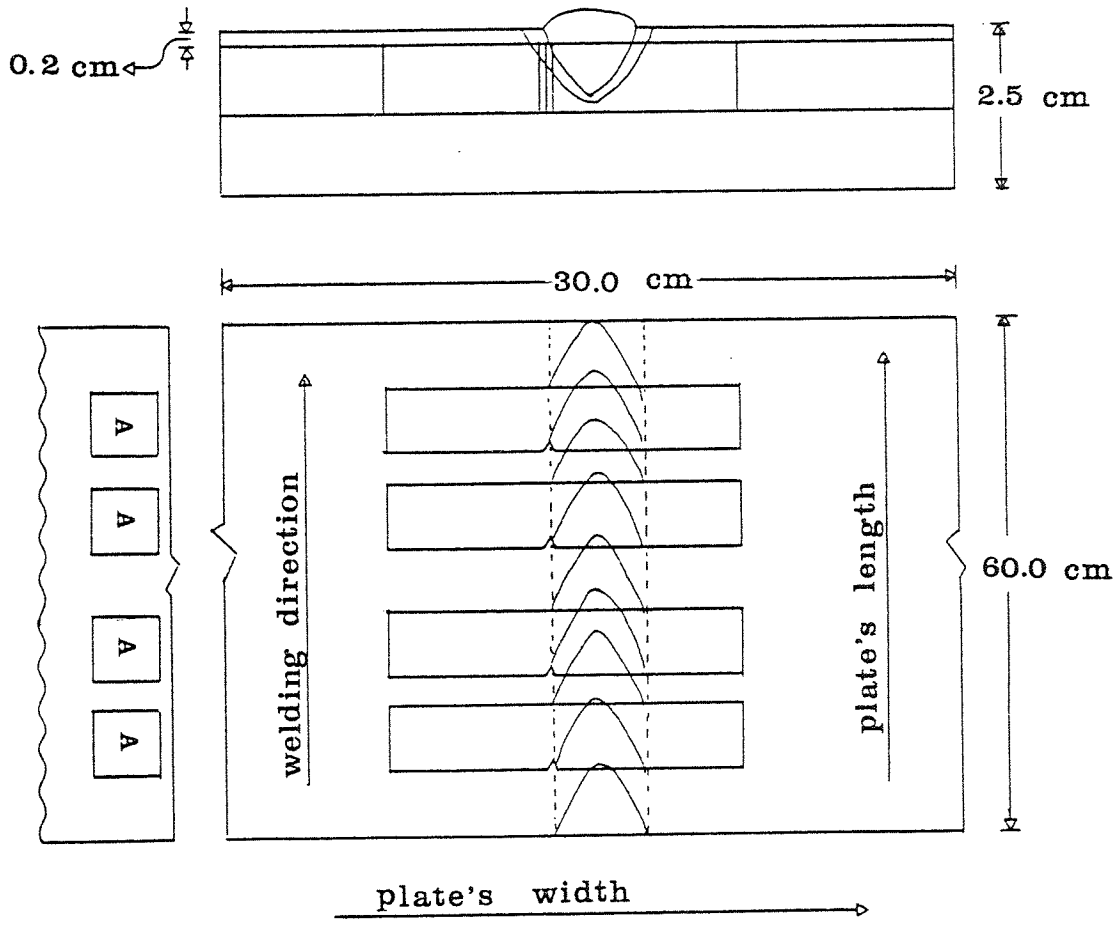

Figure 16

Layout of the extraction of the Charpy test pieces from the welded plates.

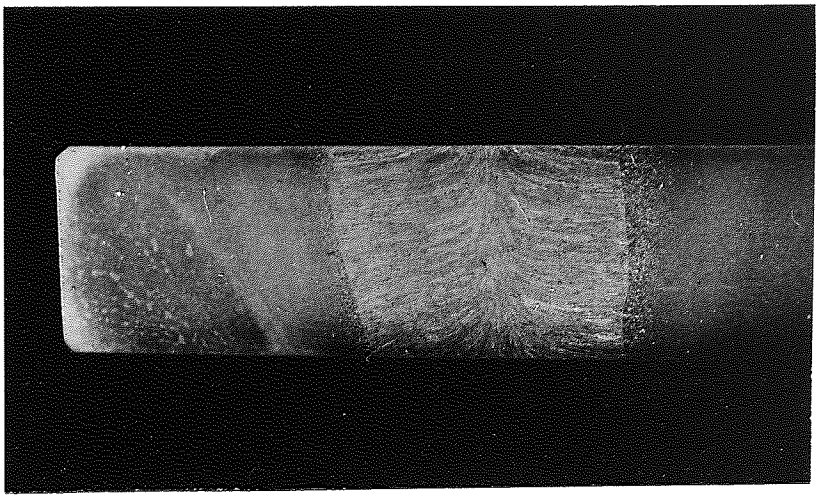

a

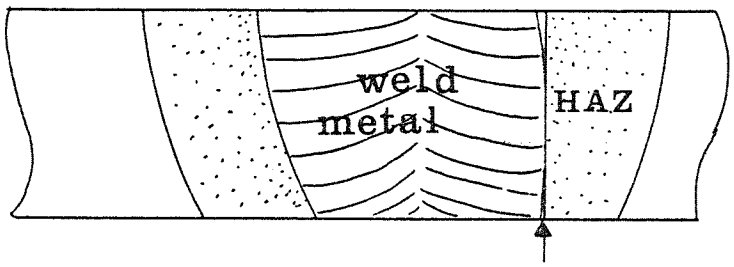

b

Figure 17

(a) Actual weld, planar HAZ Charpy test piece welded at 6.3KJ/mm.

(b) Notch tip location for the test piece displayed in (a) above.

a

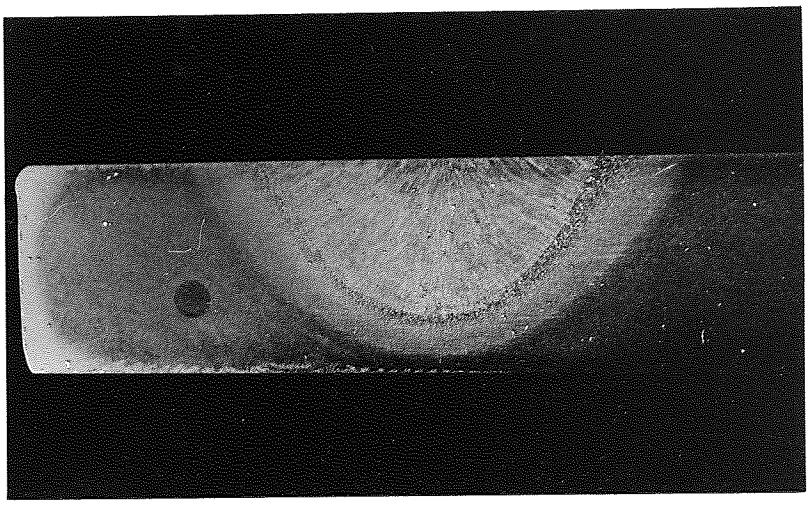

b

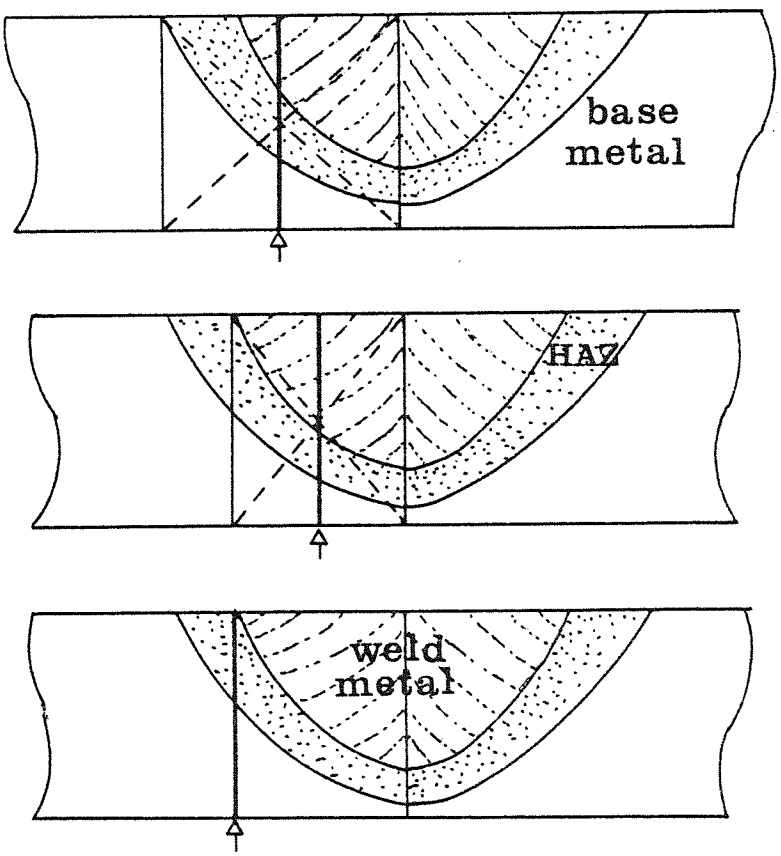

Figure 18

(a) Actual weld HAZ Charpy test piece welded at 3.6KJ/mm.

(b) Notch tip trial locations for the test piece displayed in (a) above. The position III was used in the current work.

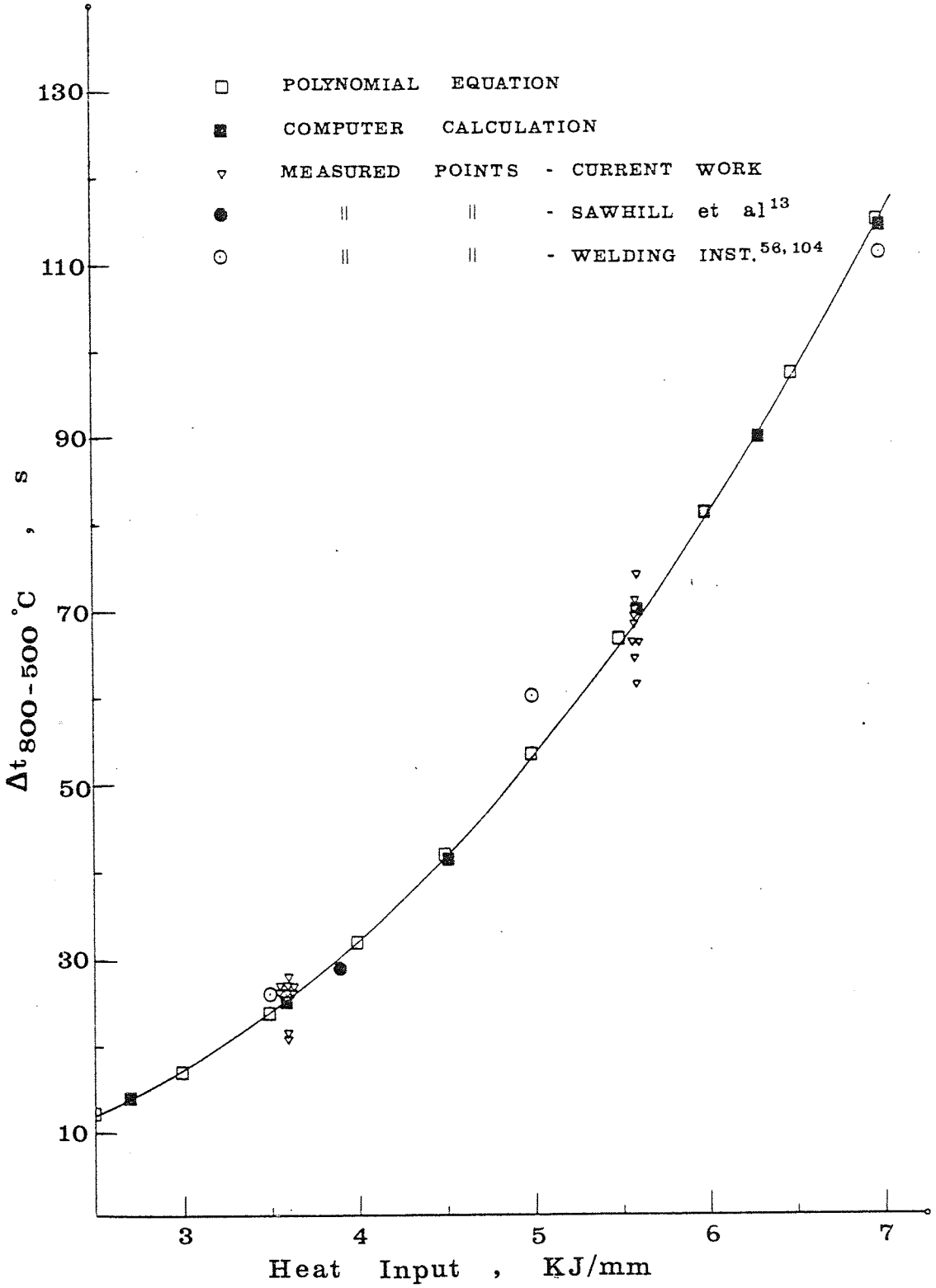

Figure 19

Variation of the cooling time $\Delta t_{800-500}$ with the heat input supplied to a 25mm thick plate. Actual data from several sources.

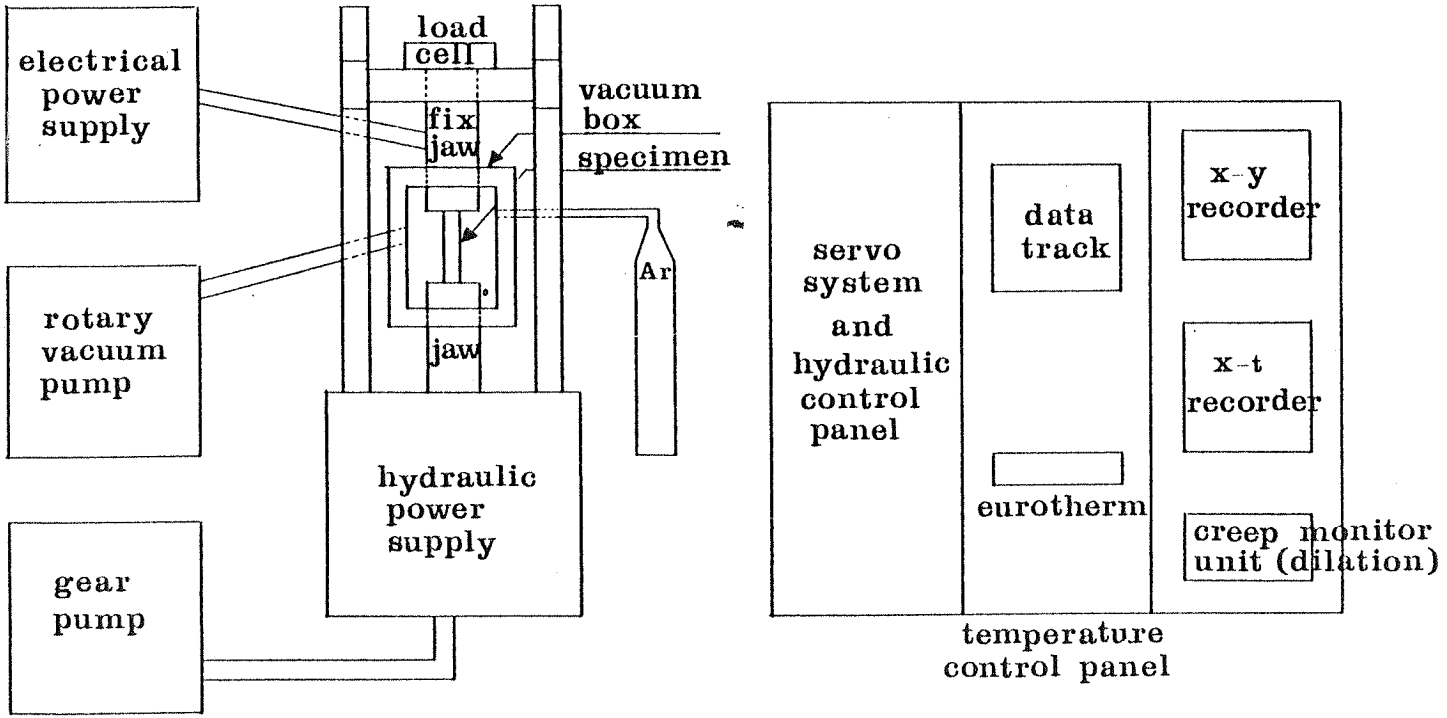

Figure 20

Schematic diagram for the Mand Thermomechanical weld simulation assembly

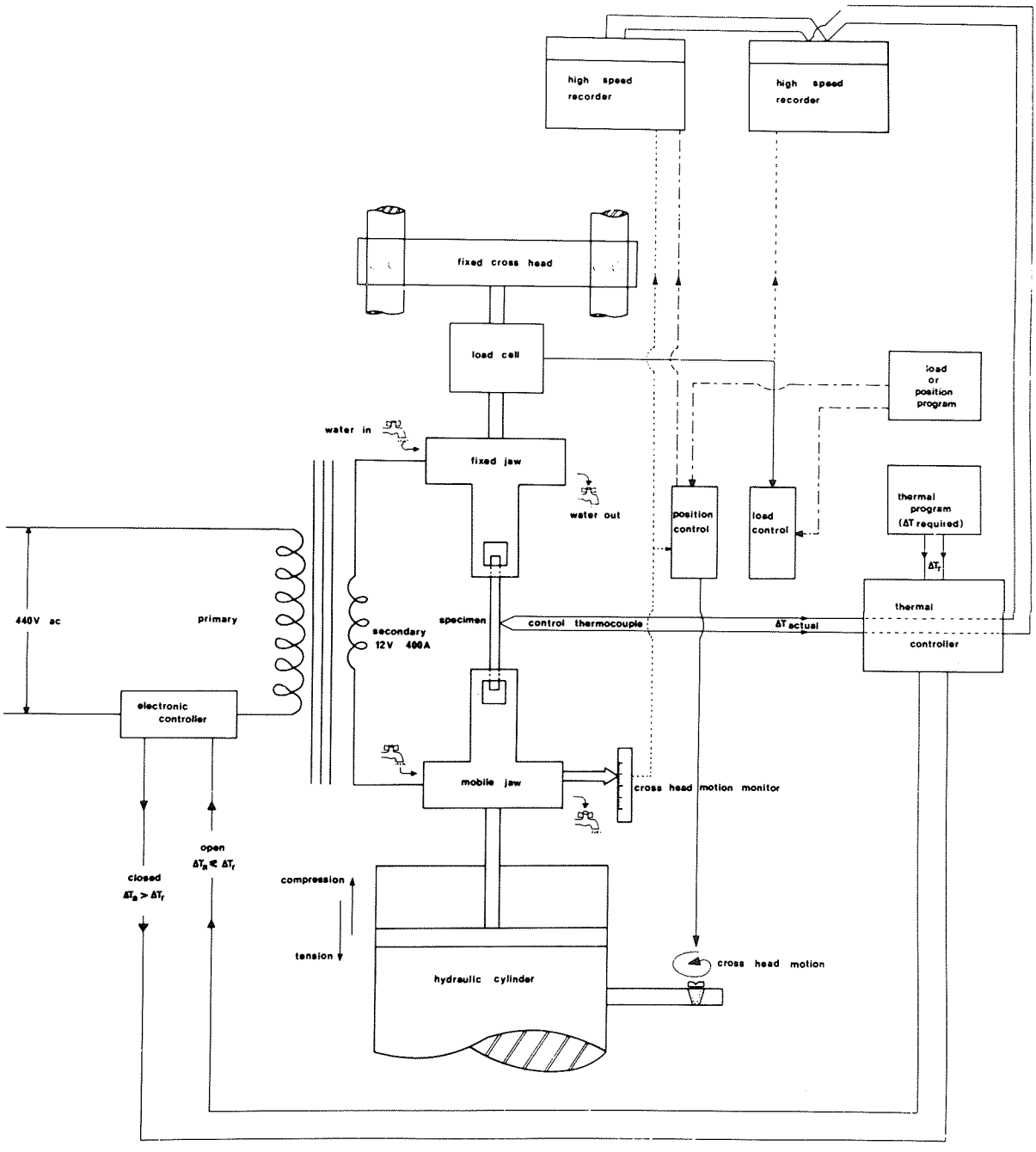

Figure 21

Thermomechanical diagram for the specimen set up in the Mand Weld Simulator.

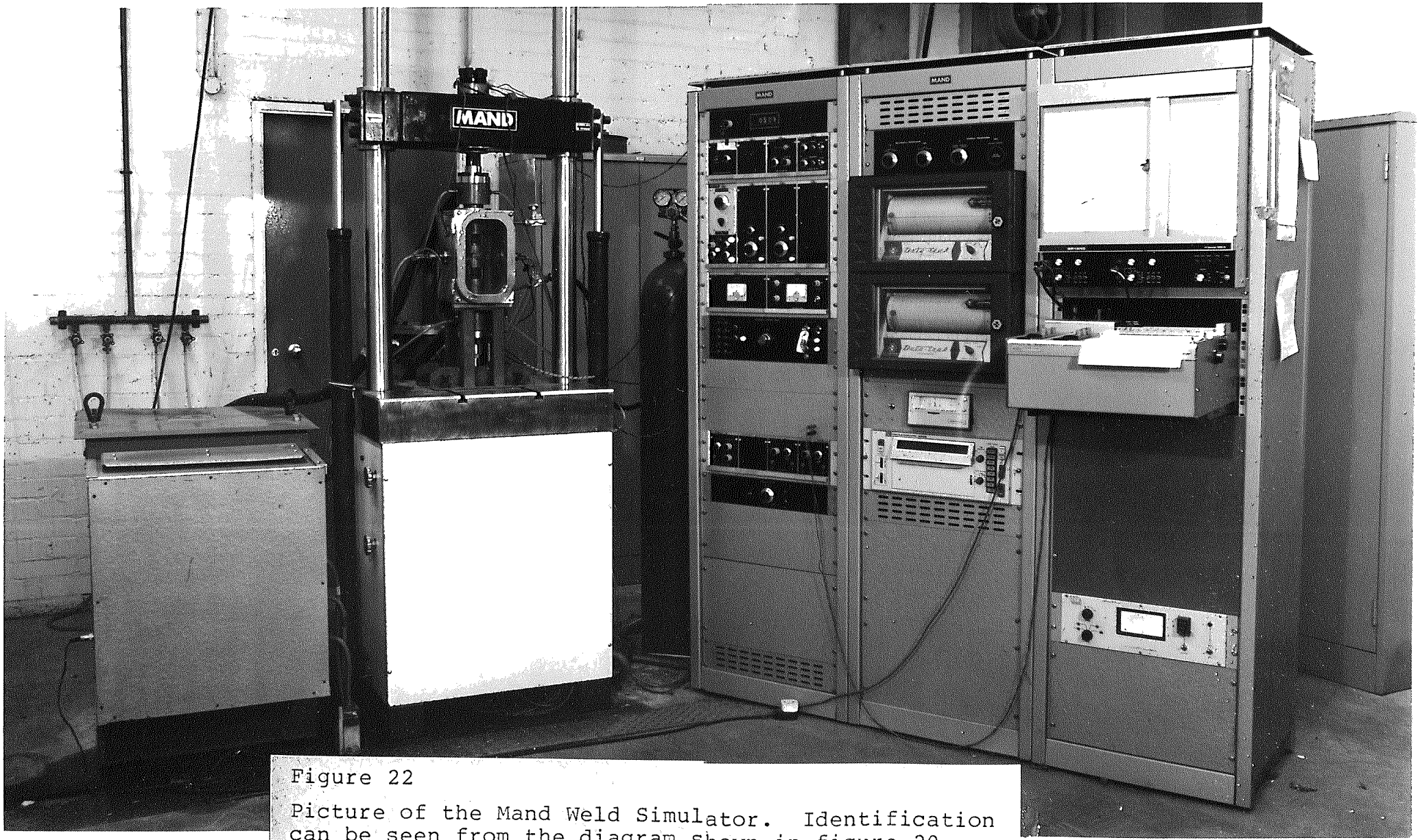

Figure 22

Picture of the Mand Weld Simulator. Identification can be seen from the diagram shown in figure 20.

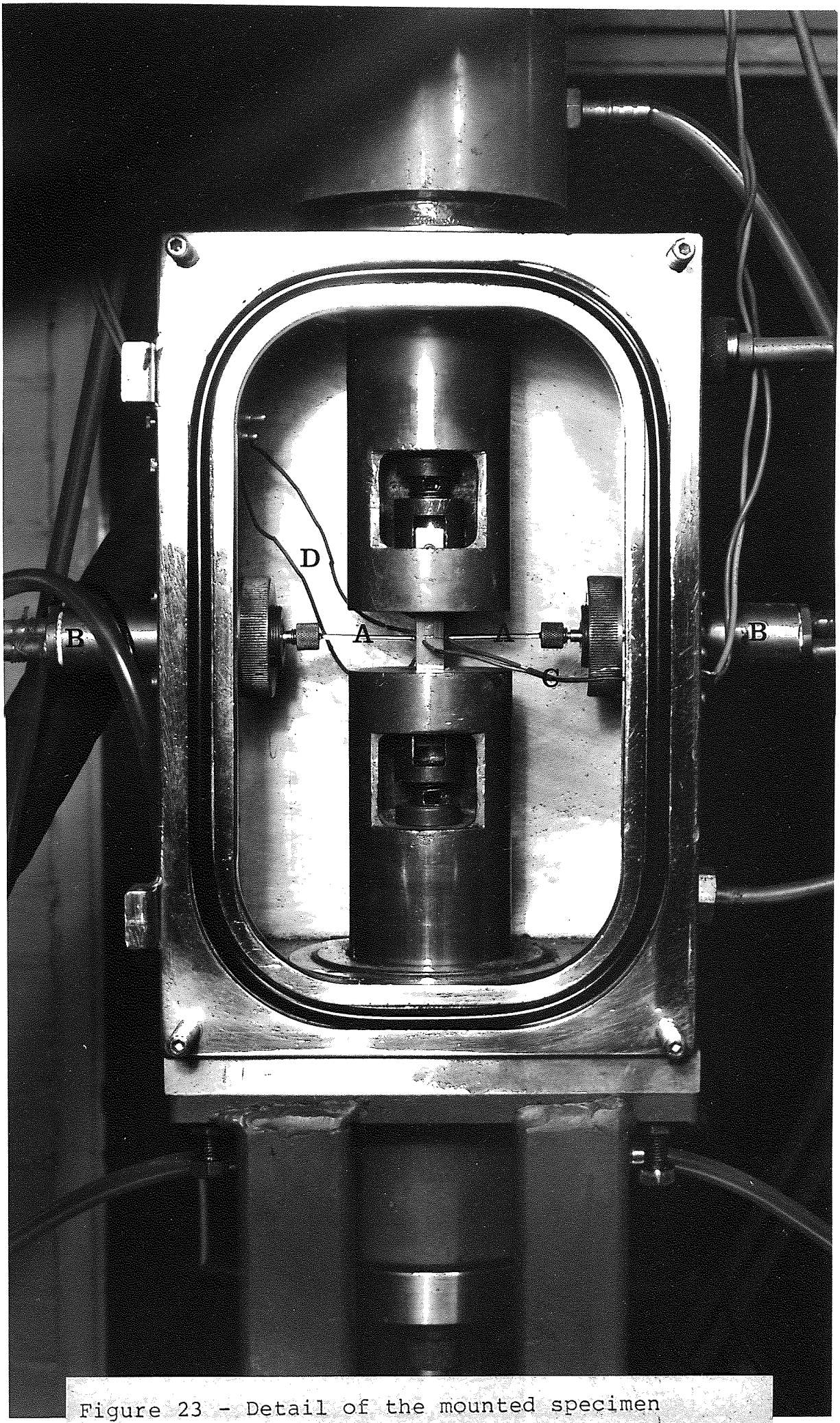

Figure 23 - Detail of the mounted specimen

A) Silica Probes
B) Transducer
C) Control thermocouple
D) Calibration thermocouple

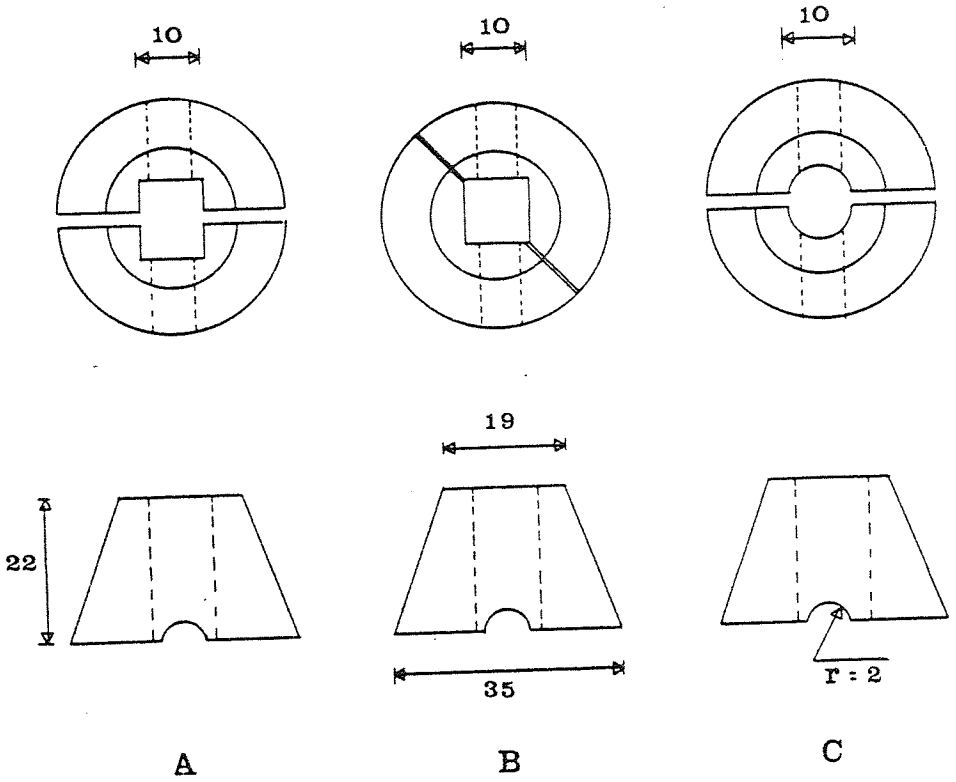

scale in mm

Figure 24

Design for the grooving of the copper collets

A) Square grooving, bad design.

B) Square grooving, good design.

C) Round grooving.

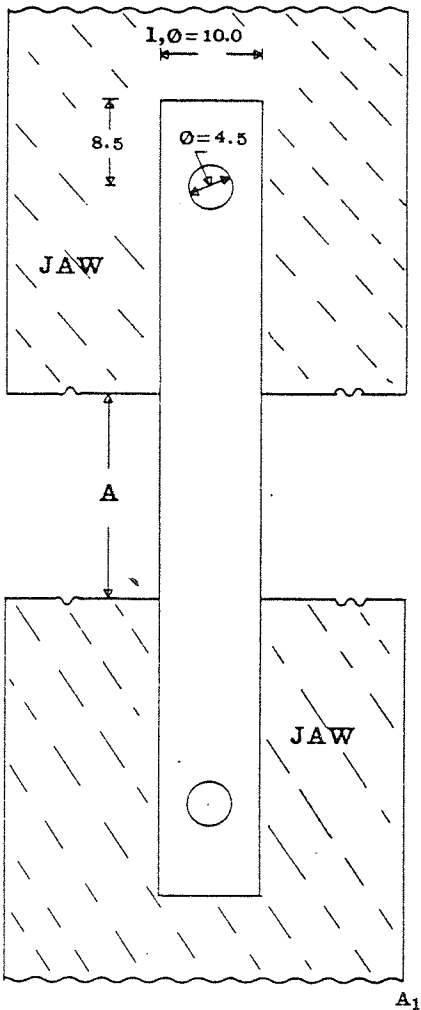

scale in mm

$A_1 = 15 \rightarrow L_1 = 74.5$
$A_2 = 20 \rightarrow L_2 = 79.5$
$A_3 = 25 \rightarrow L_3 = 84.5$

Figure 25

Dimensions for the simulation test pieces

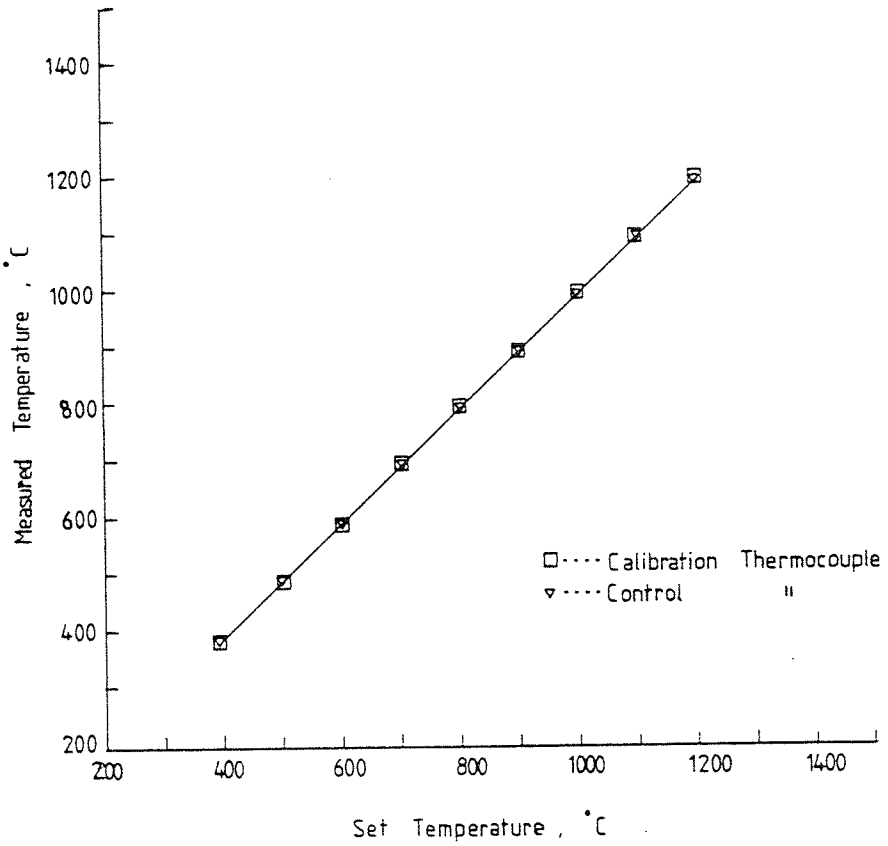

Figure 26

Weld simulation specimen temperature calibration. Centre/surface temperature distribution.

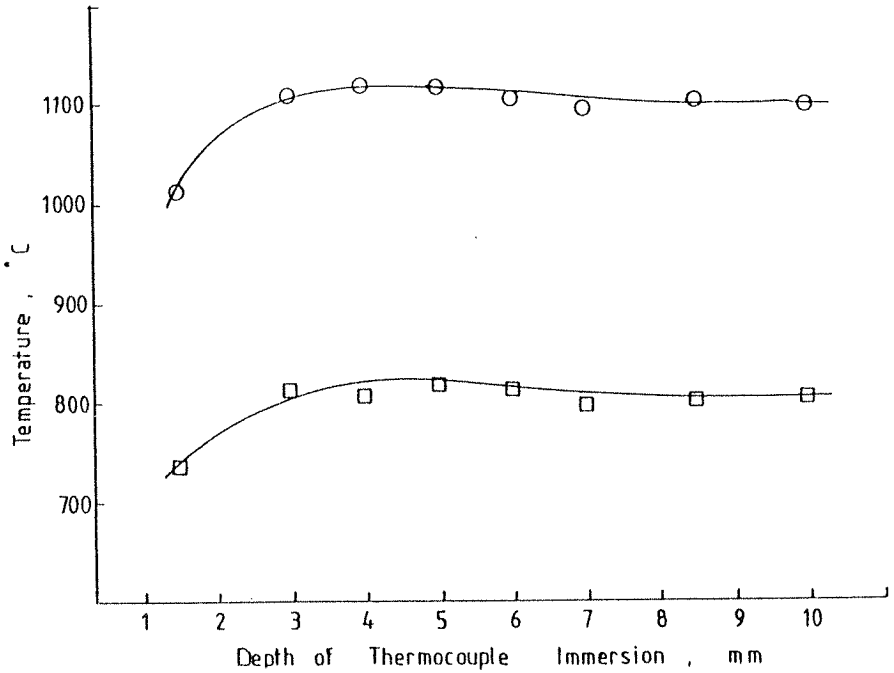

Figure 27

Weld simulation specimen temperature calibration. Through thickness/surface temperature distribution.

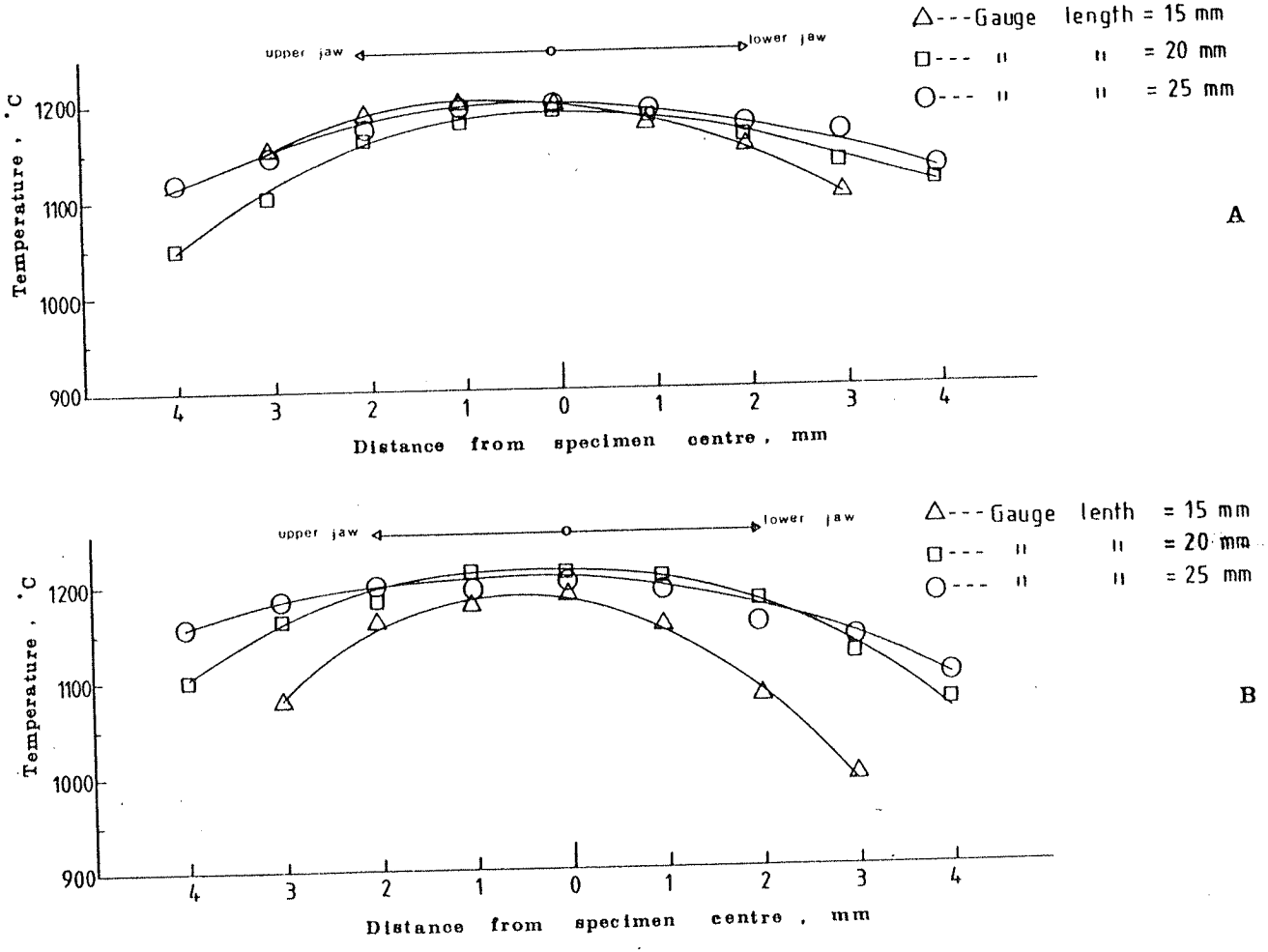

Figure 28

Weld simulation specimen temperature calibration. Distribution of the temperature along the gauge length of the specimen.

A) Square cross section

B) Round cross section

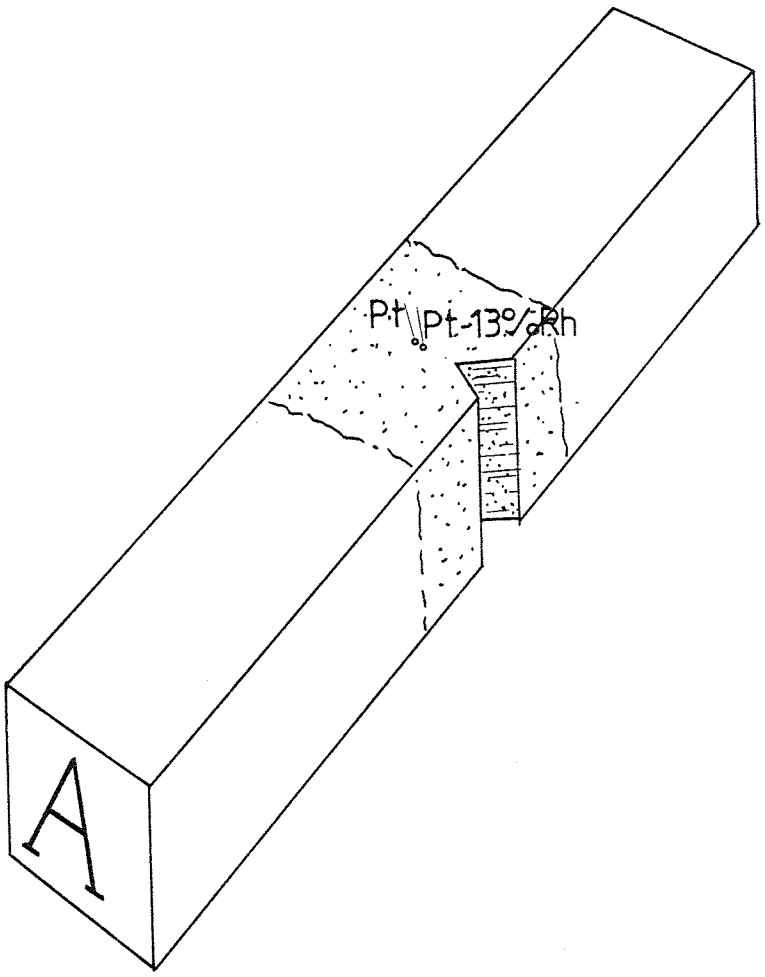

Figure 29

Notching of the simulated specimen using as centre reference the hot junction of the control thermocouple.

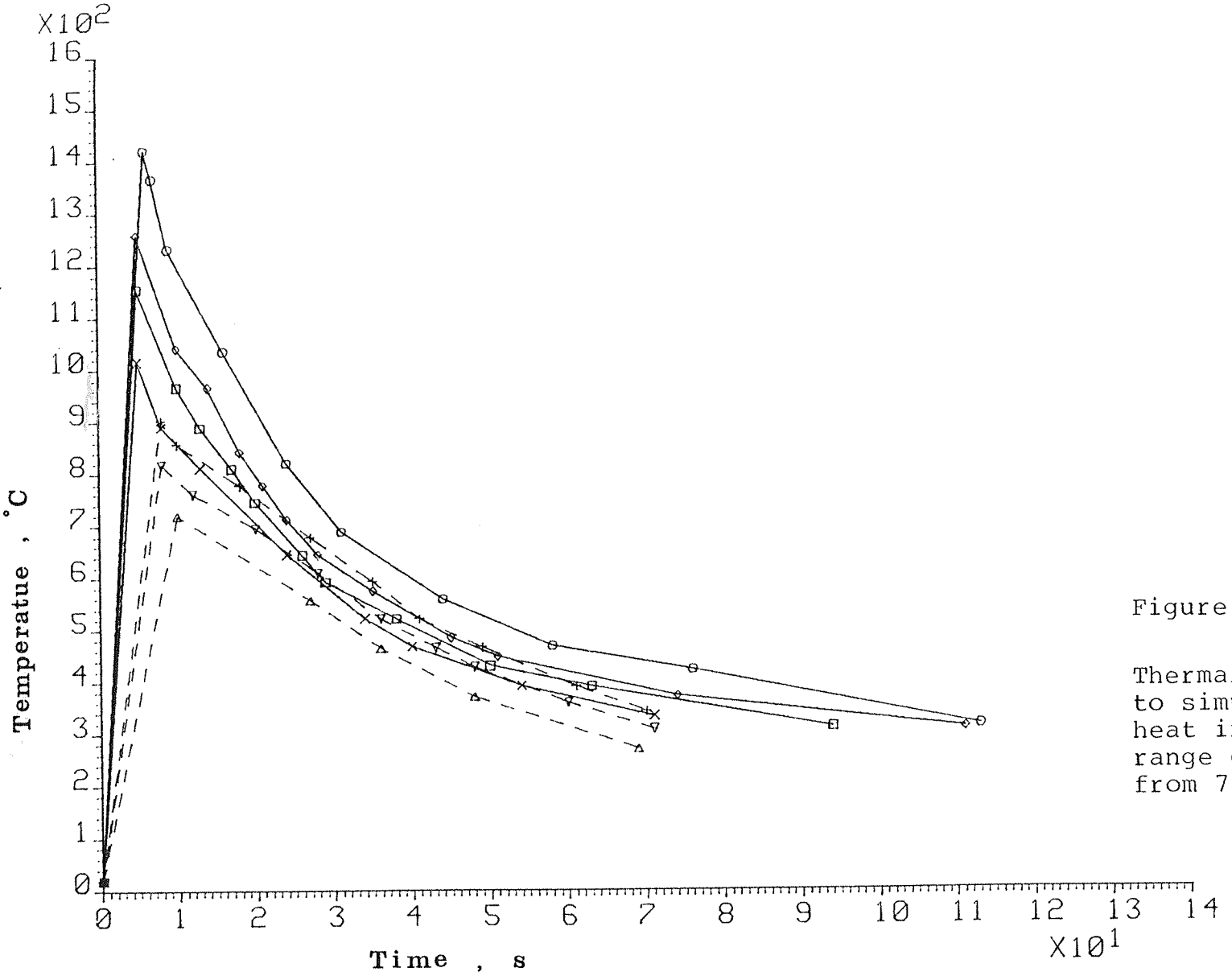

Figure 30

Thermal cycles corresponding to simulation of the 3.6KJ/mm heat input condition over the range of peak temperatures from 700 to 1400°C.

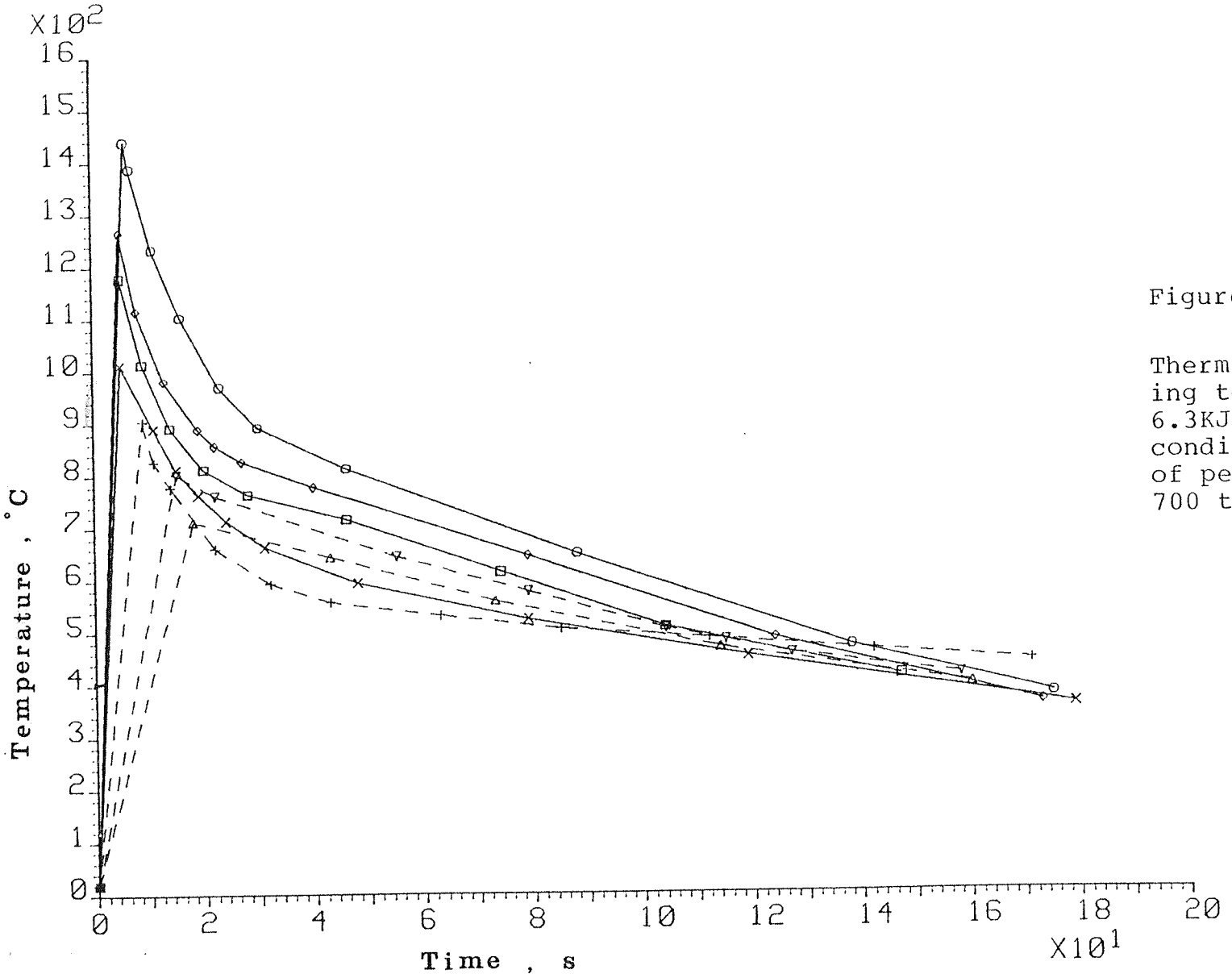

Figure 31

Thermal cycles corresponding to simulation of the 6.3KJ/mm heat input condition over the range of peak temperatures from 700 to 1400°C.

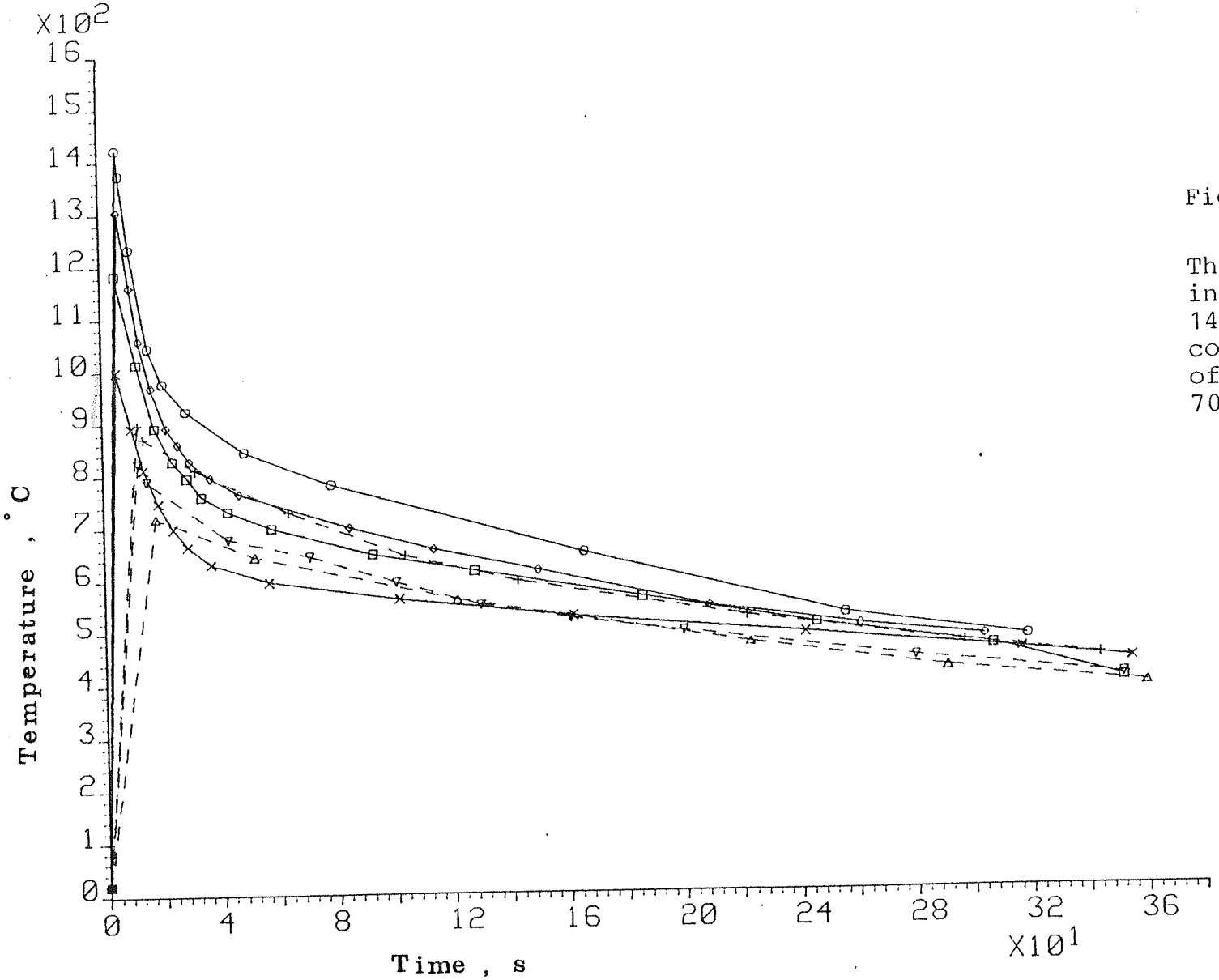

Figure 32

Thermal cycles corresponding to simulation of the 14.4KJ/mm heat input condition over the range of peak temperatures from 700 to 1400°C.

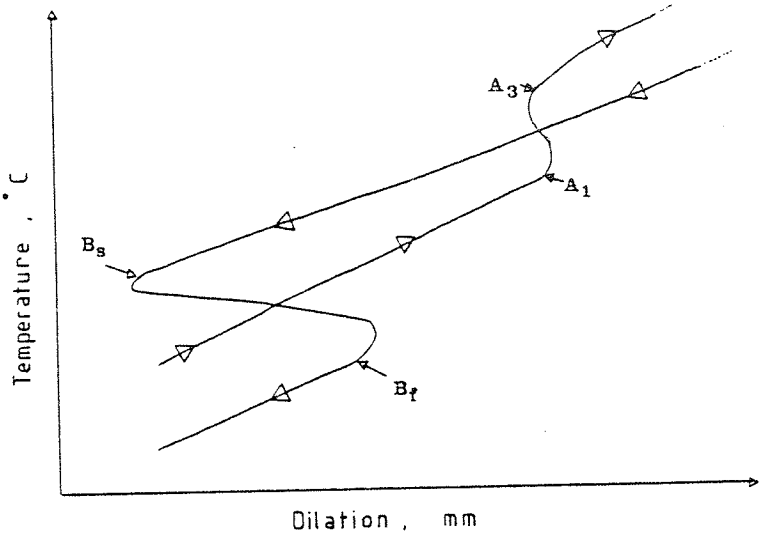

Figure 33 - Illustration of a dilation curve involving a bainitic reaction

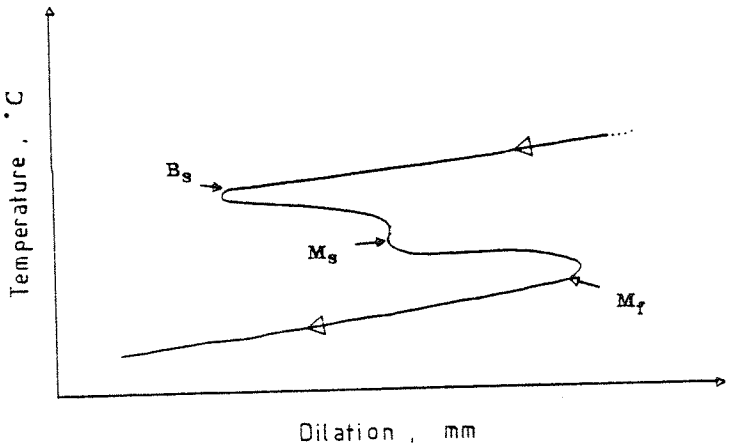

Figure 34 - Illustration of a dilation curve involving bainitic and martensitic transformations

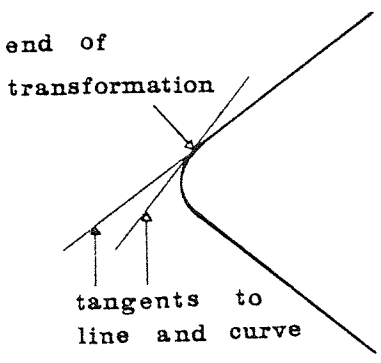

Figure 35

Determination of the transformation points by the tangent method.

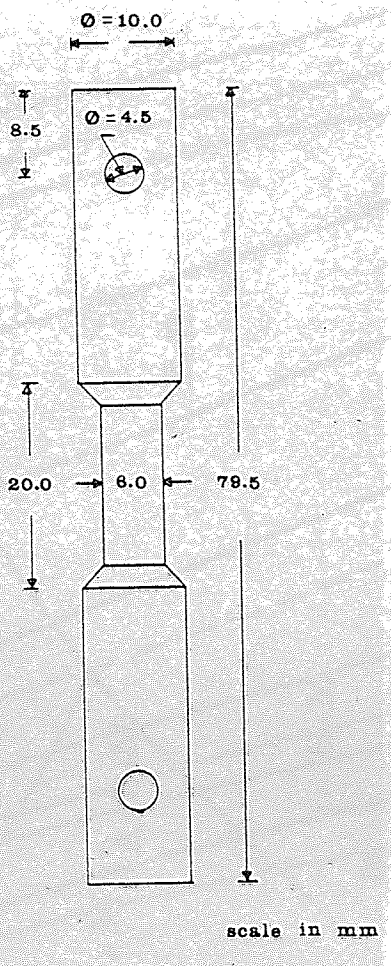

Figure 36

Specimen with reduced diameter for the simulation of faster cooling rates

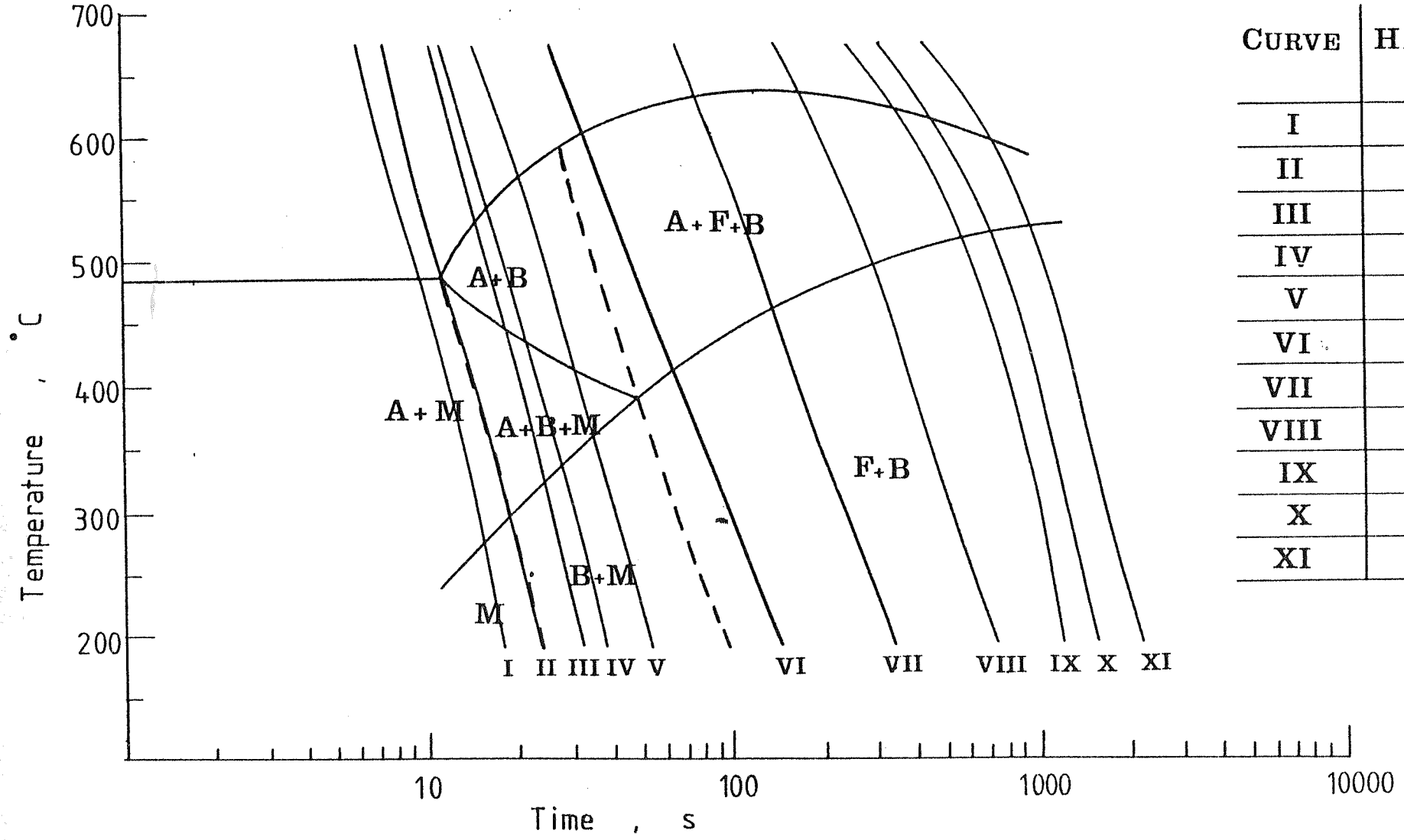

CURVE	HARDNESS HV_{30}
I	388
II	381
III	338
IV	317
V	287
VI	248
VII	232
VIII	226
IX	225
X	223
XI	220

Figure 37 - CCT curves for the steel RQT-500. Cooling from a nominal peak temperature of 1400°C.

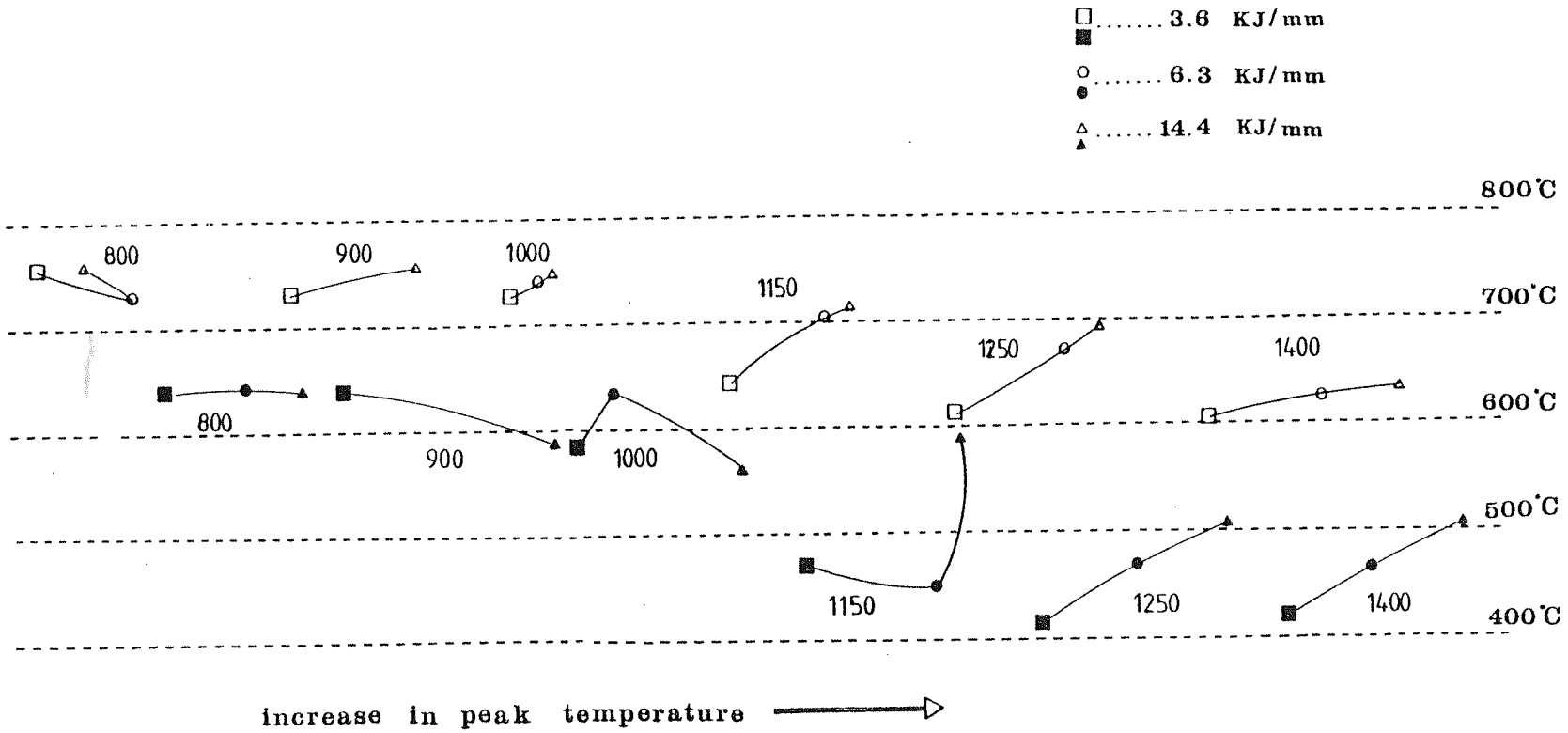

Figure 38

Behaviour of the start and finish transformation temperatures with the heat input and with the peak temperature. Open symbols represent the start of the transformation and shaded symbols the finish of the transformation.

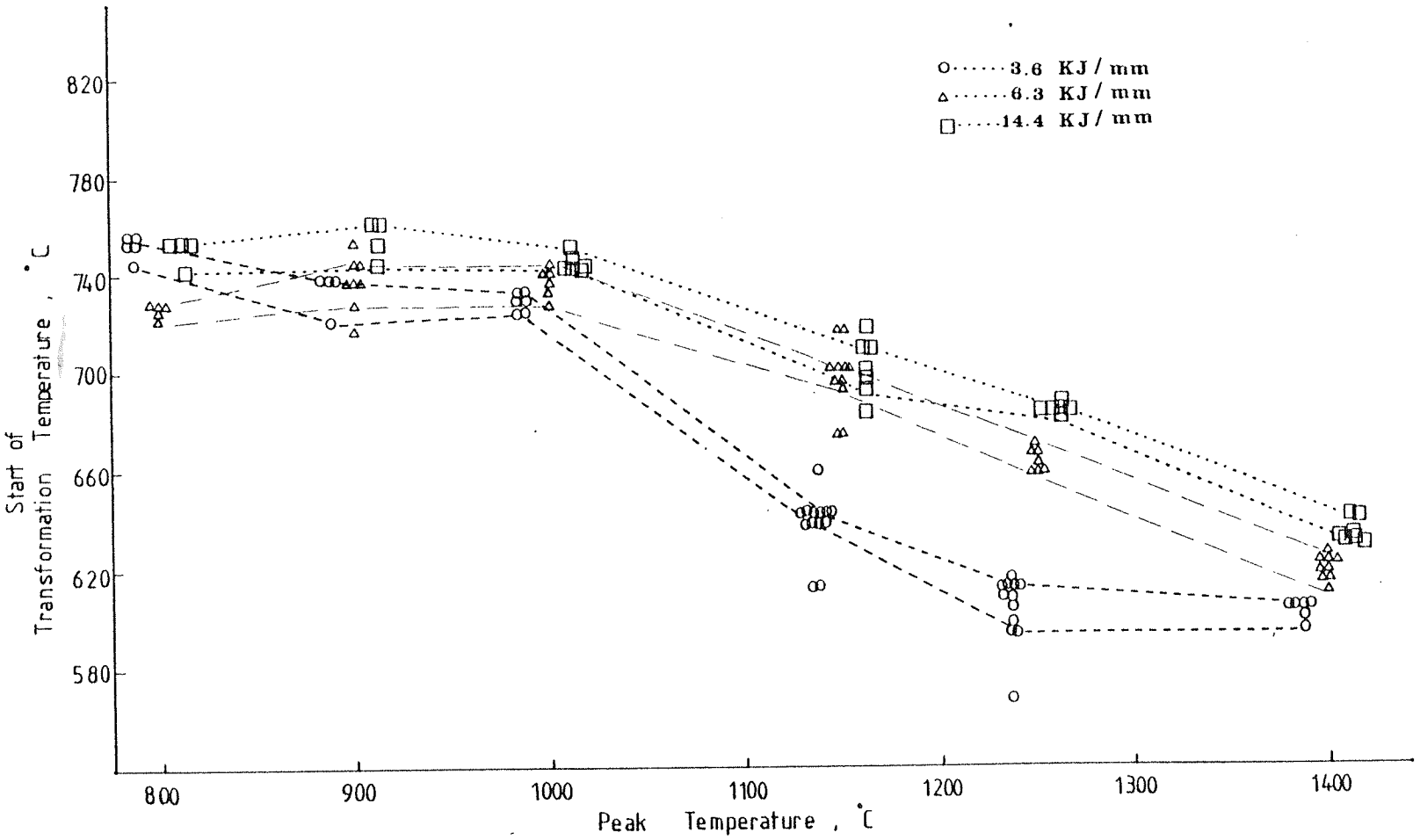

Figure 39

Behaviour of the scatter band of the start of the transformation temperatures with the heat input and with the peak temperature.

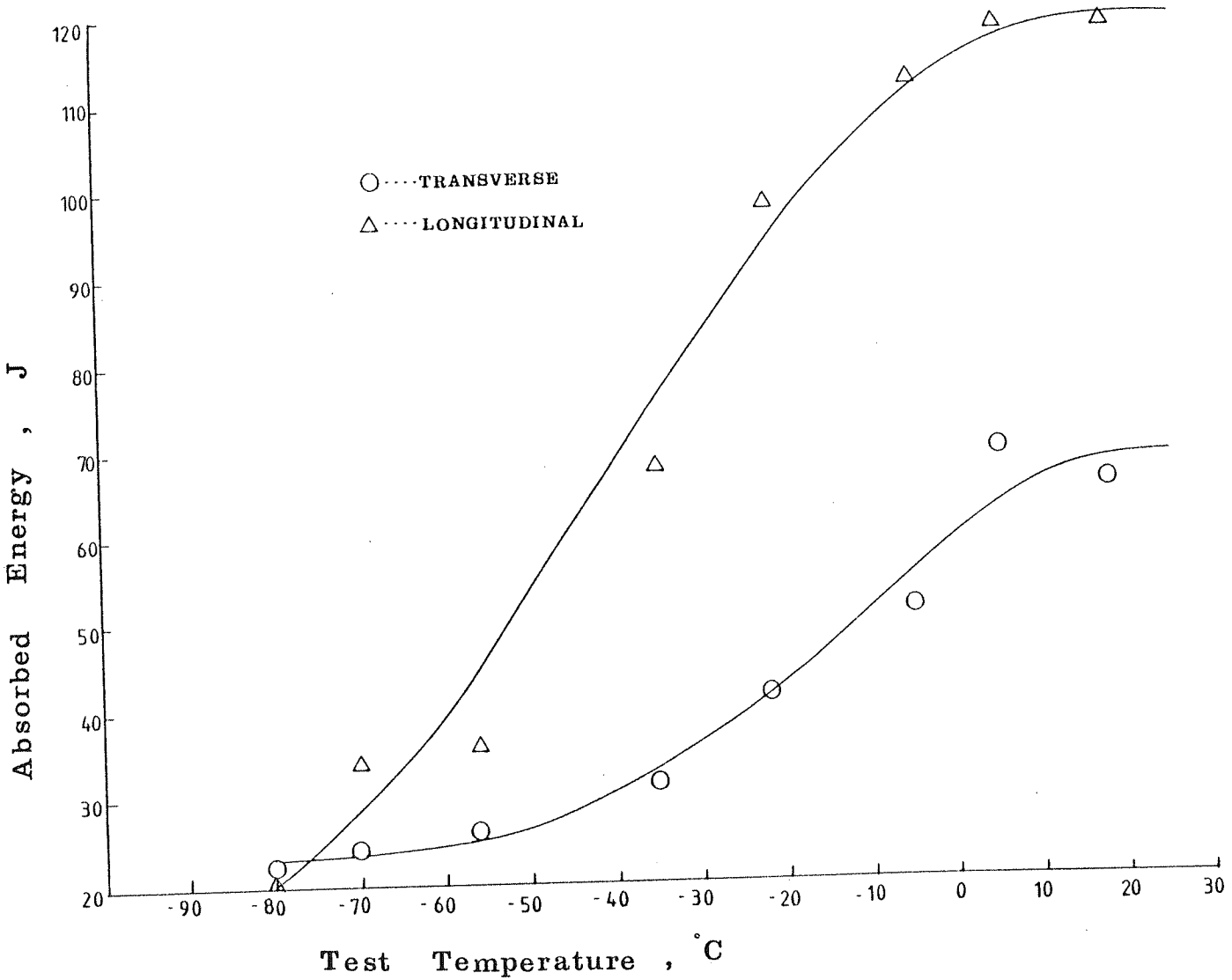

Figure 40 - Curves representative of the transverse and of the longitudinal Charpy absorbed impact energy for the steel RQT-500.

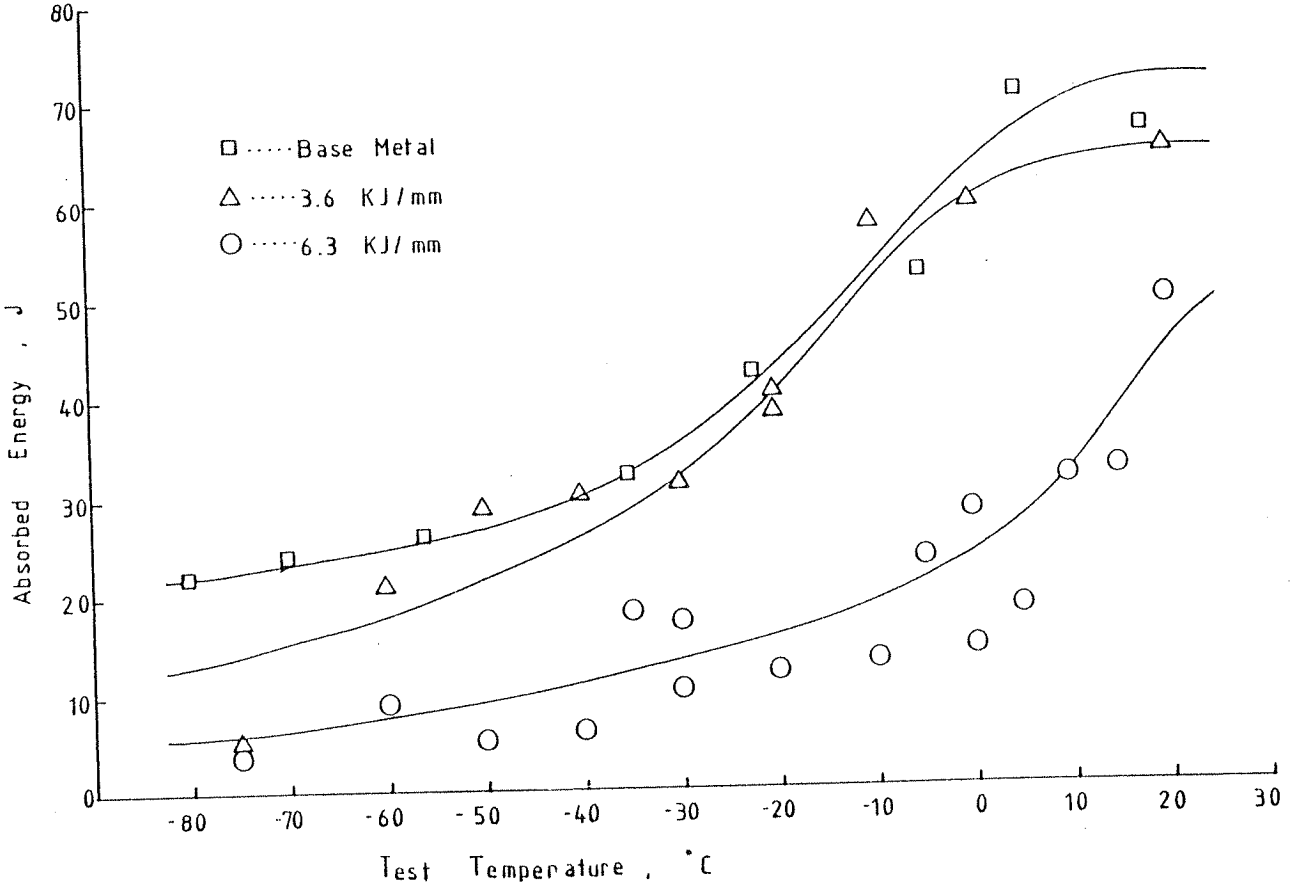

Figure 41 - Charpy V absorbed impact energies for the 3.6 and 6.3KJ/mm heat input actual weld conditions and for the base metal. Transverse specimens.

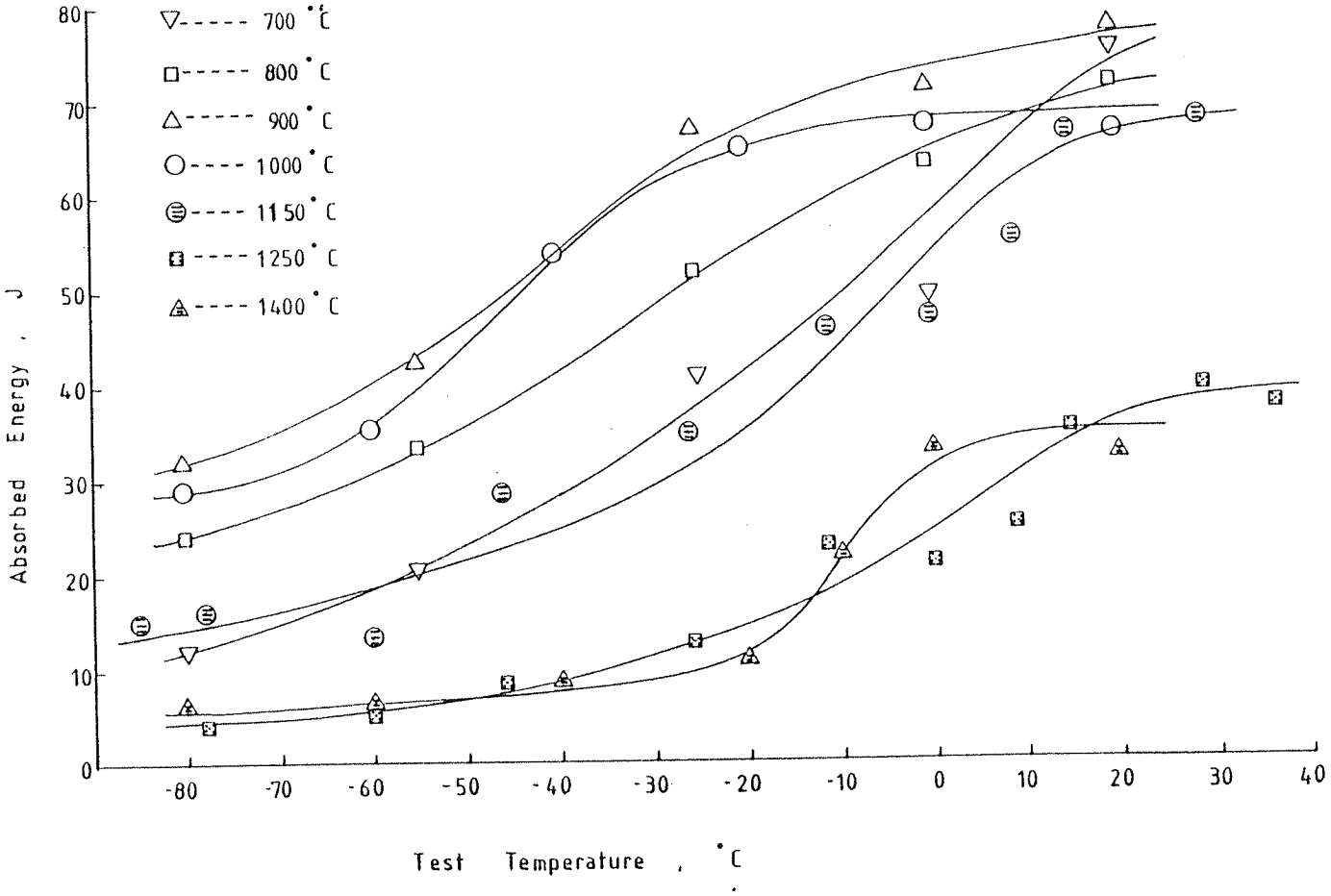

Figure 42 - Charpy V absorbed impact energy for the specimens simulated at 3.6KJ/mm over the peak temperature of 700 to 1400^{o}C.

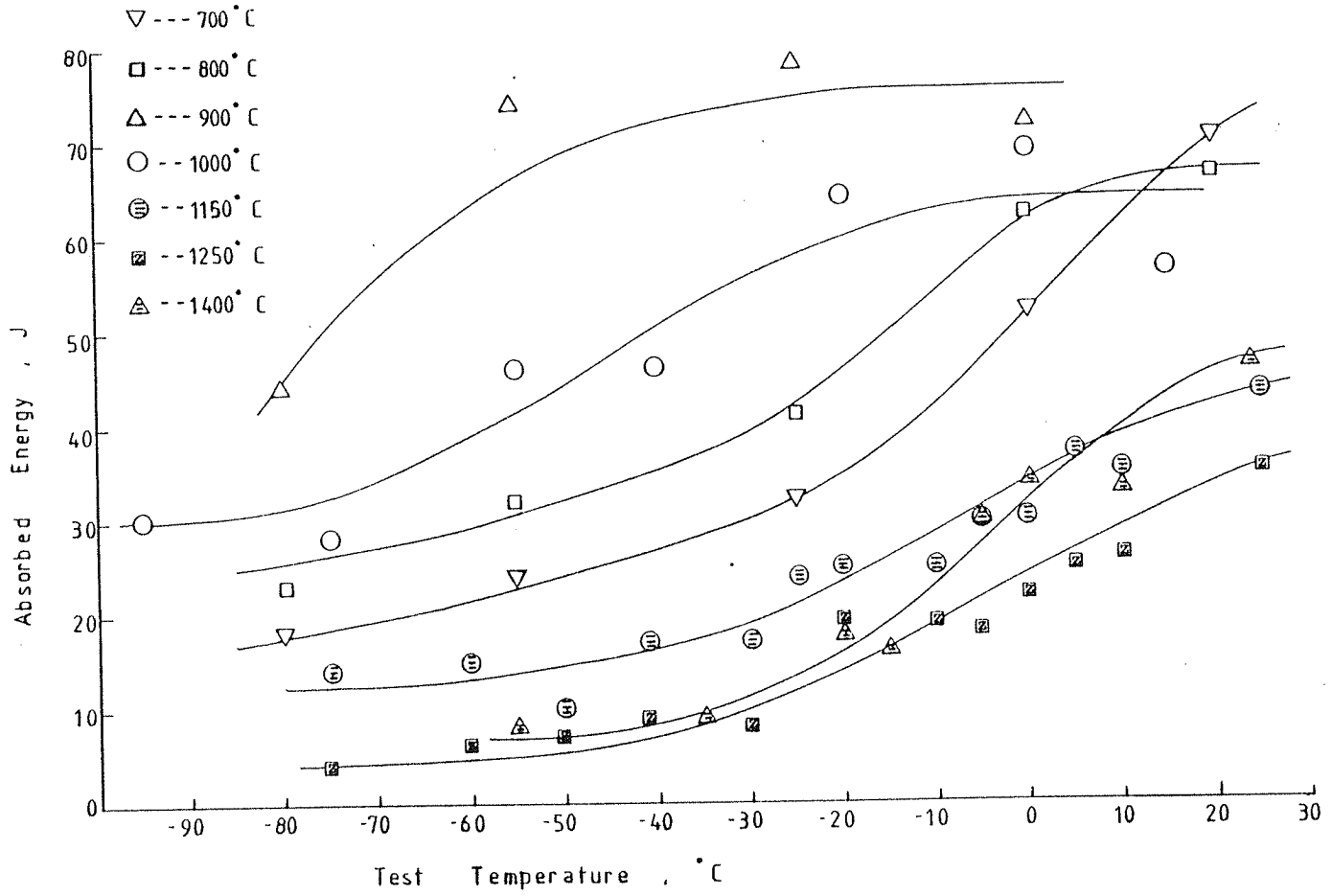

Figure 43 - Charpy V absorbed impact energy for the specimens simulated at 6.3KJ/mm over the peak temperatures of 700 to 1400°C.

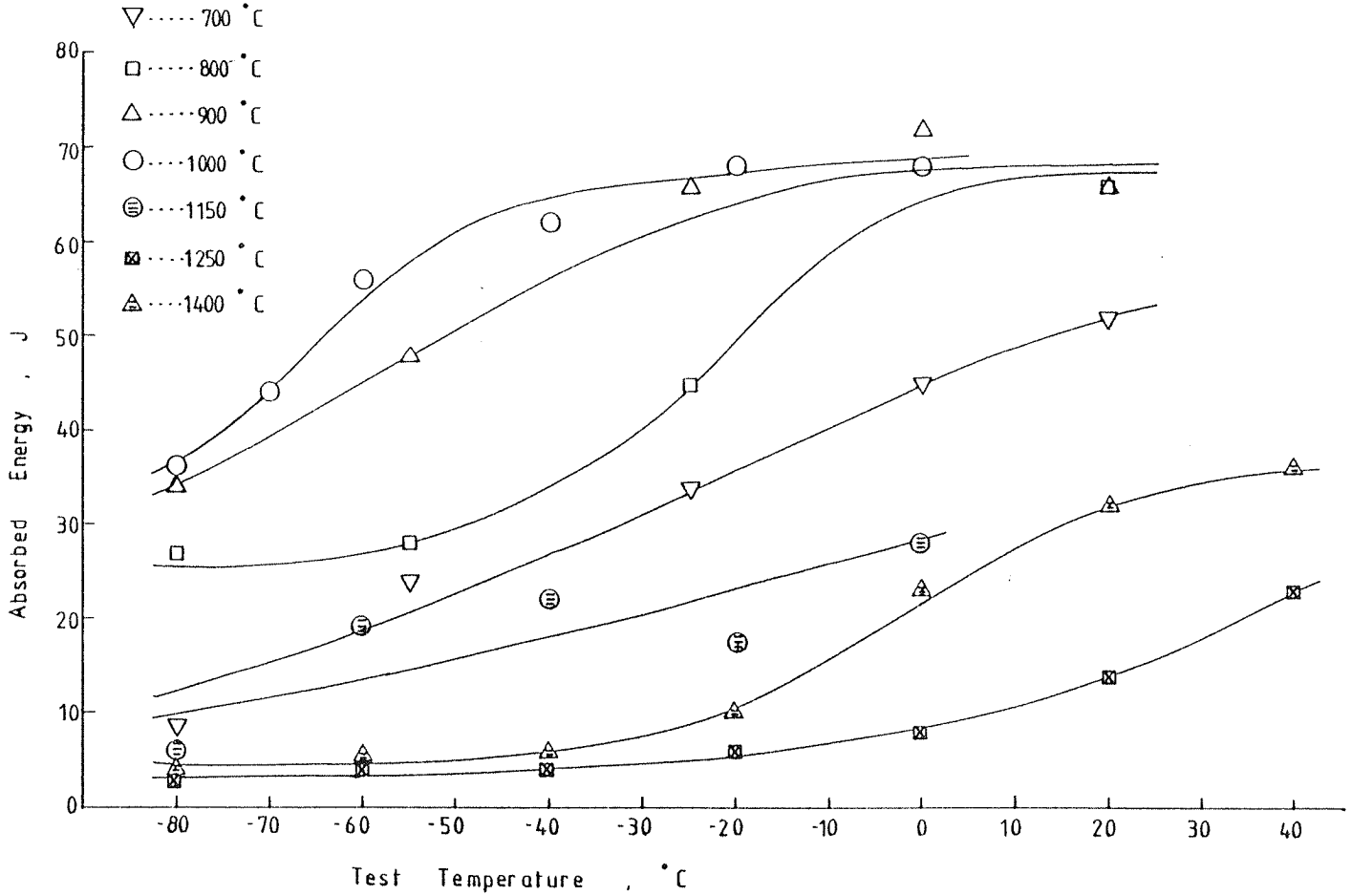

Figure 44 - Charpy V absorbed impact energy for the specimens simulated at 14.4KJ/mm over the peak temperatures of 700 to 1400^{O}C.

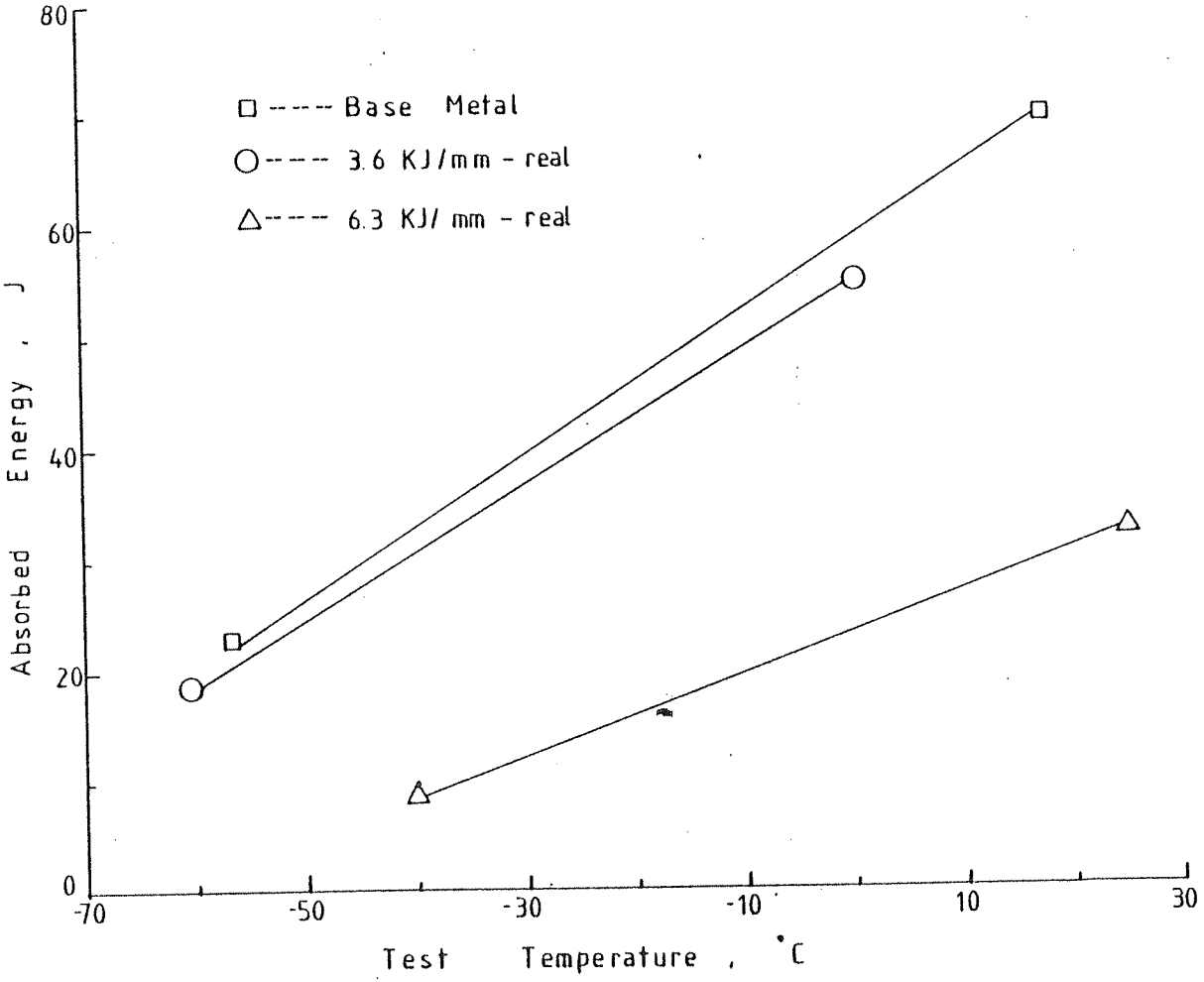

Figure 45 - Charpy V absorbed impact energy for the 3.6 and 6.3KJ/mm heat inputs actual weld conditions and for the base metal. Transitional line representation.

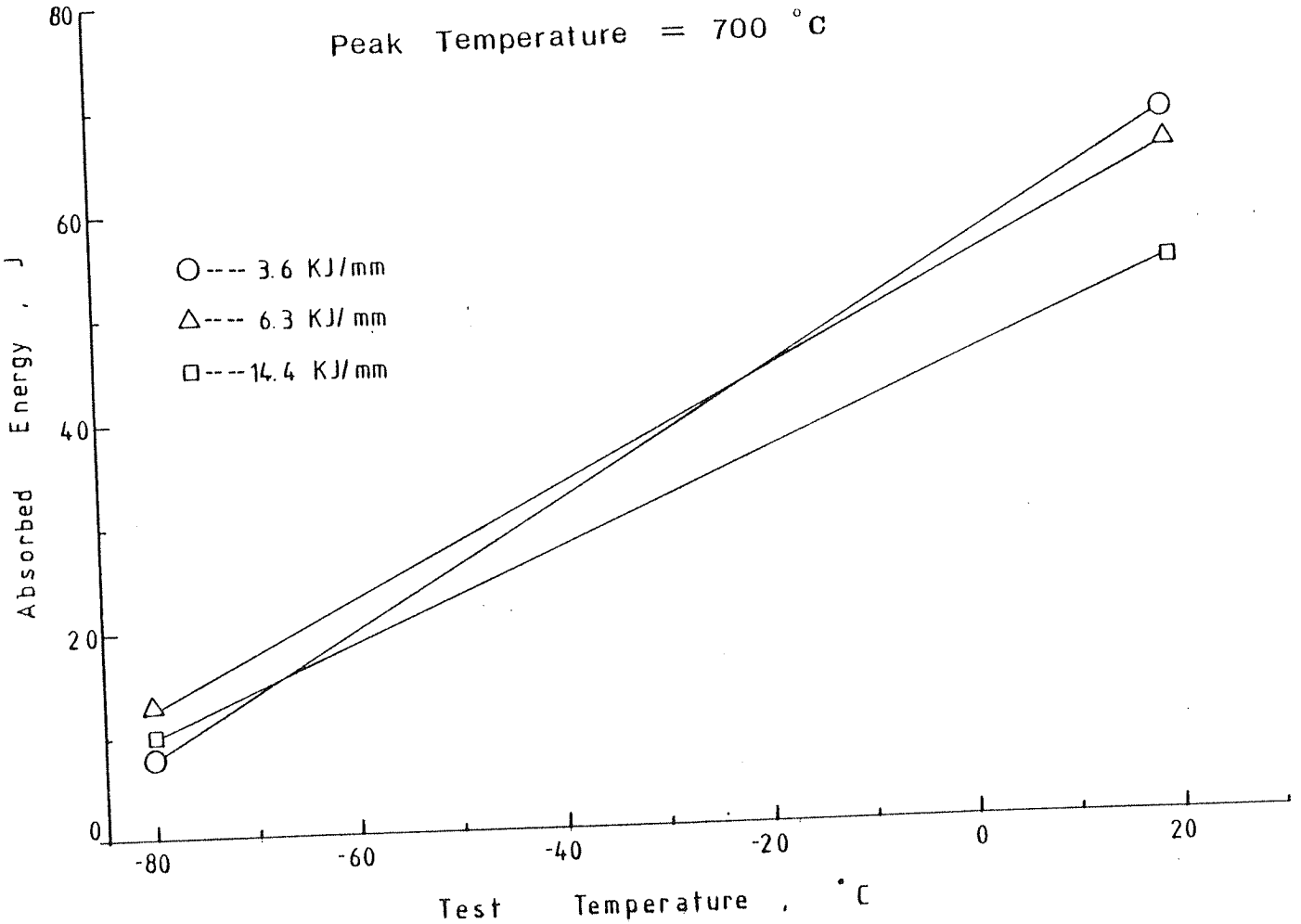

Figure 46 - Effect of the heat input on the transitional line representation for the Charpy V absorbed energy. Peak temperature at 700°C.

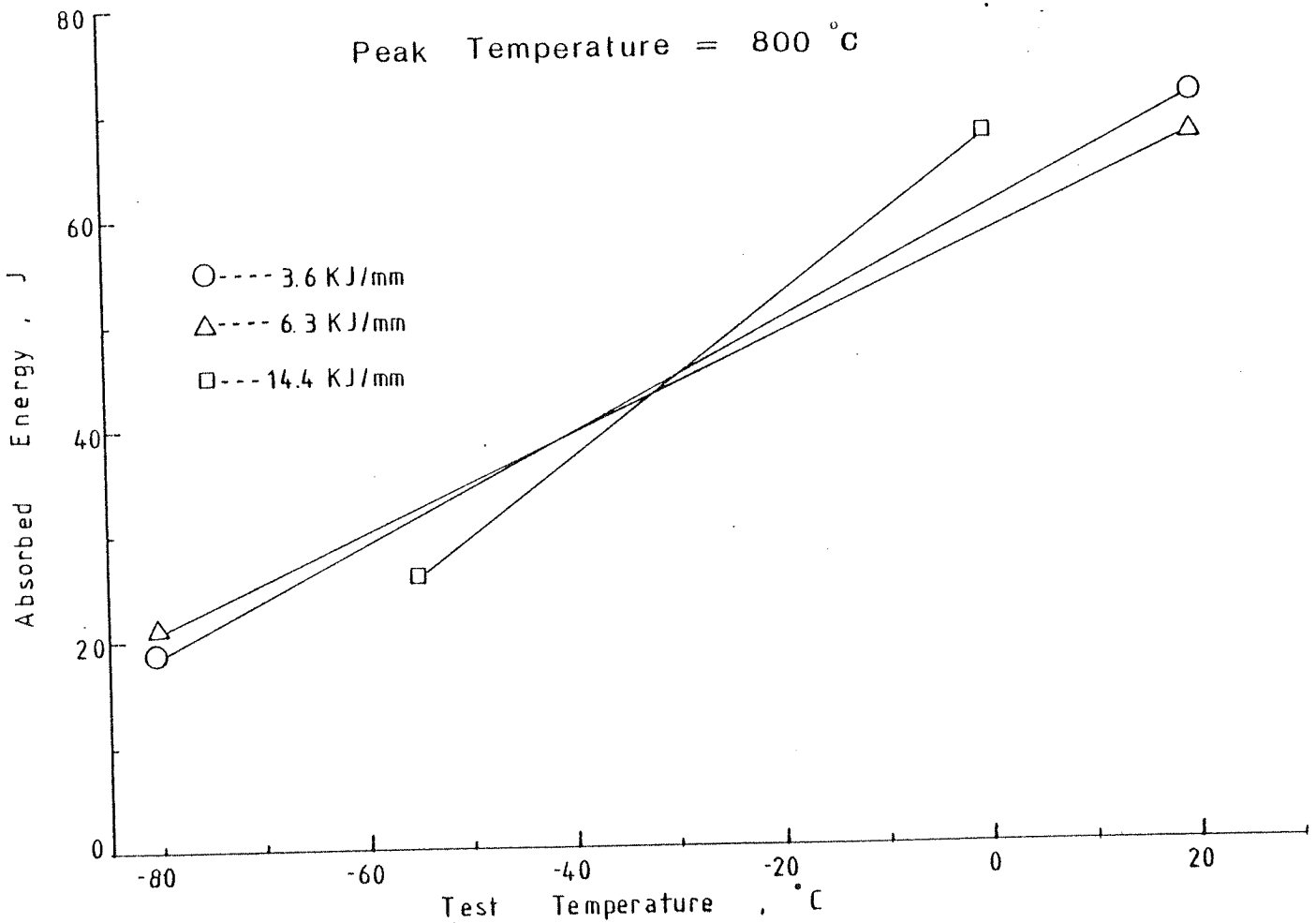

Figure 47 - Effect of the heat input on the transitional line representation for the Charpy V absorbed energy. Peak temperature at 800°C.

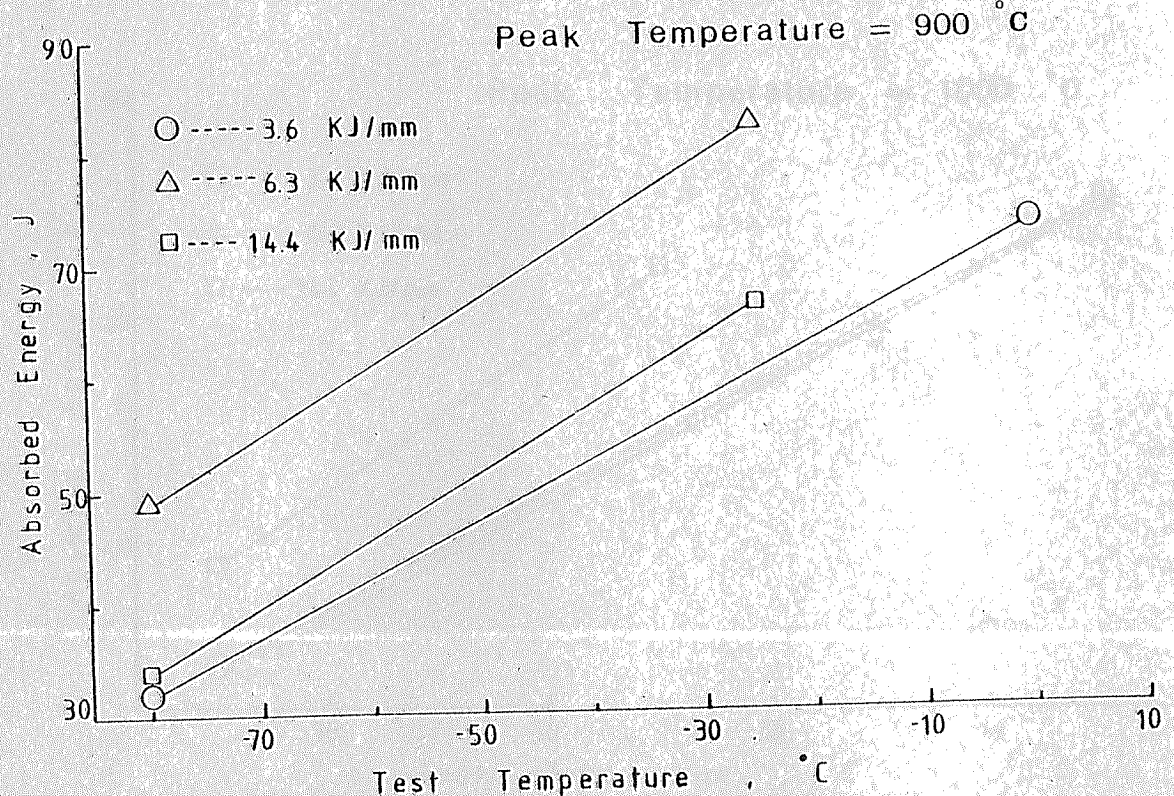

Figure 48 - Effect of the heat input on the transitional line representation for the Charpy V absorbed energy. Peak temperature at 900°C.

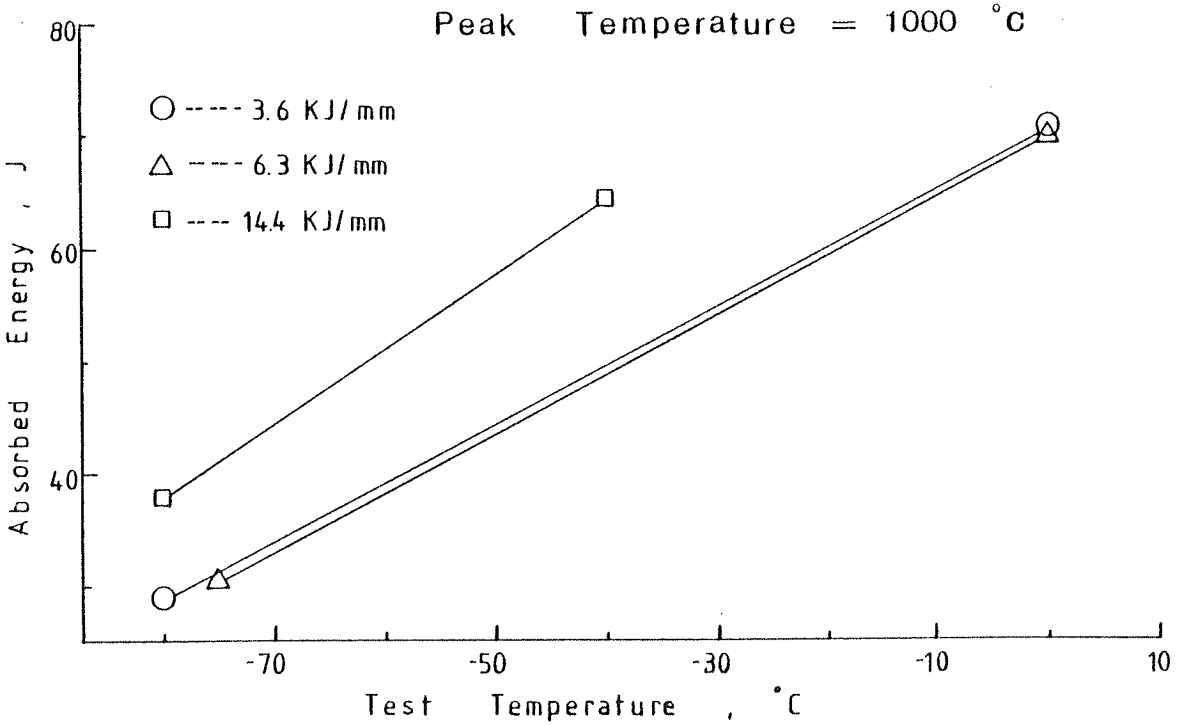

Figure 49 - Effect of the heat input on the transitional line representation for the Charpy V absorbed energy. Peak temperature at 1000°C.

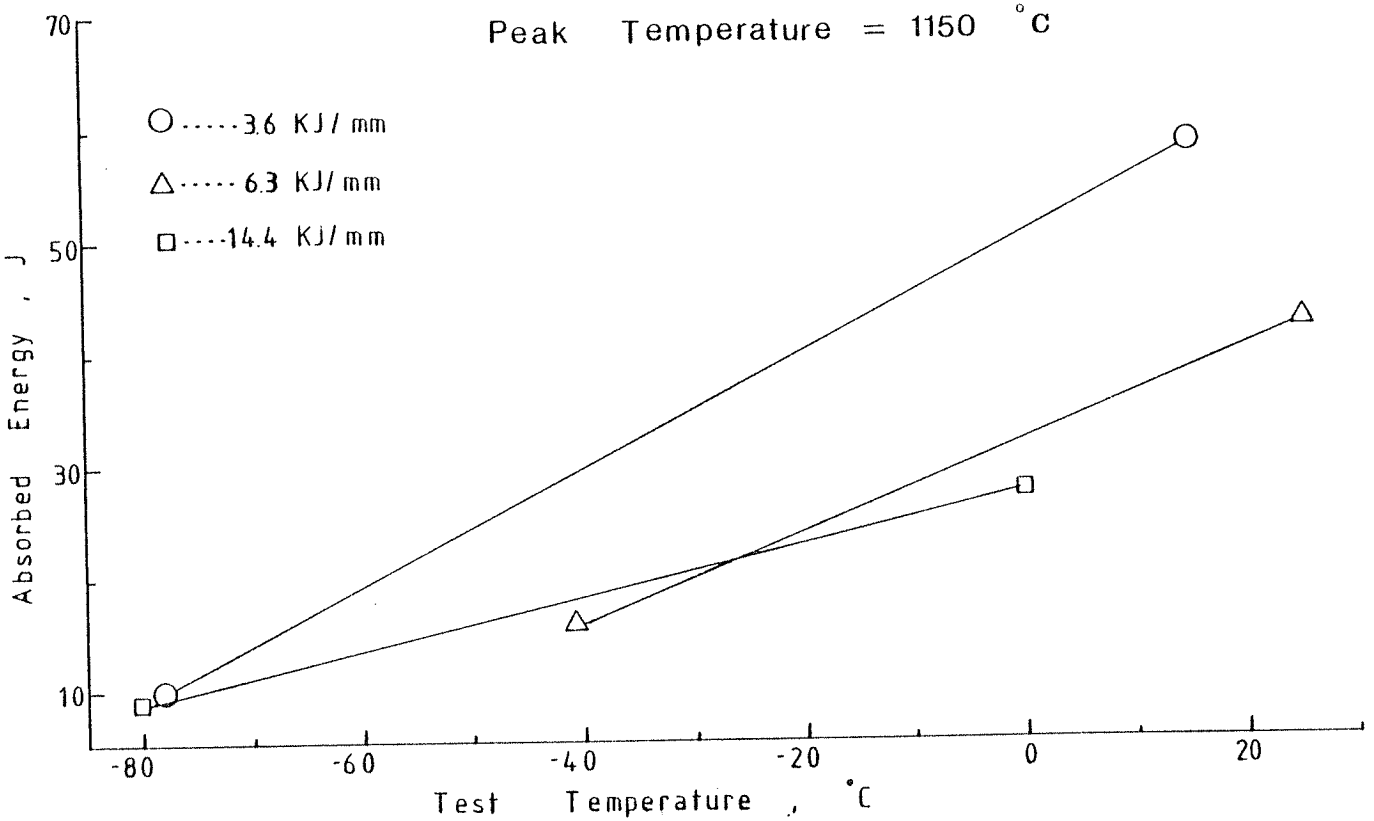

Figure 50 - Effect of the heat input on the transitional line representation for the Charpy V absorbed energy. Peak temperature at 1150°C.

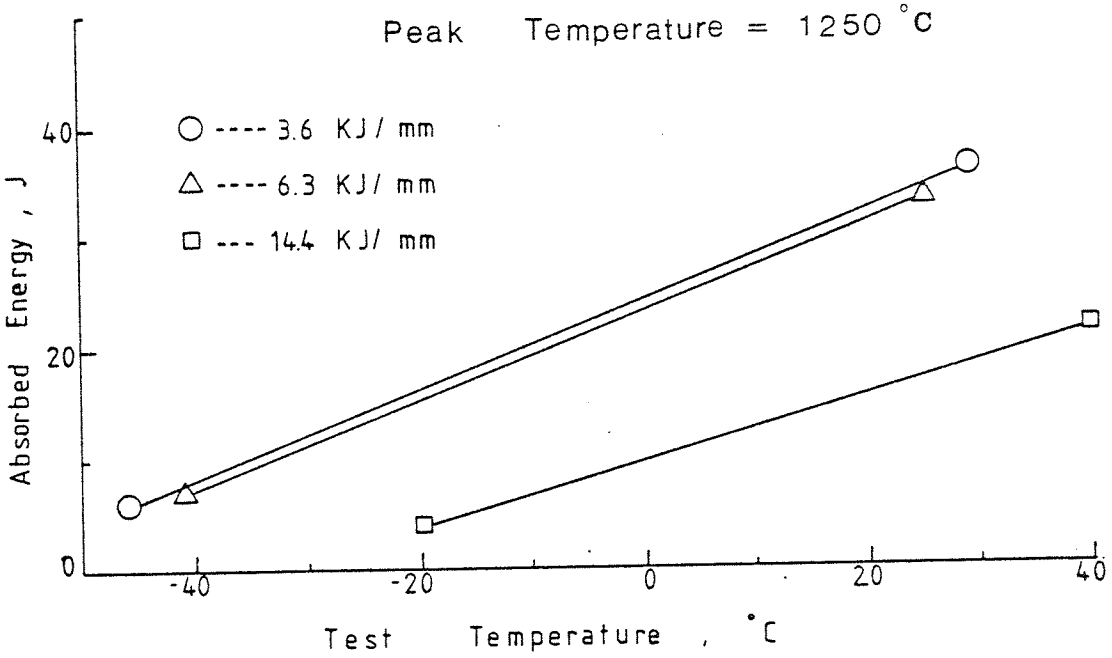

Figure 51 - Effect of the heat input on the transitional line representation for the Charpy V absorbed energy. Peak temperature at 1250°C.

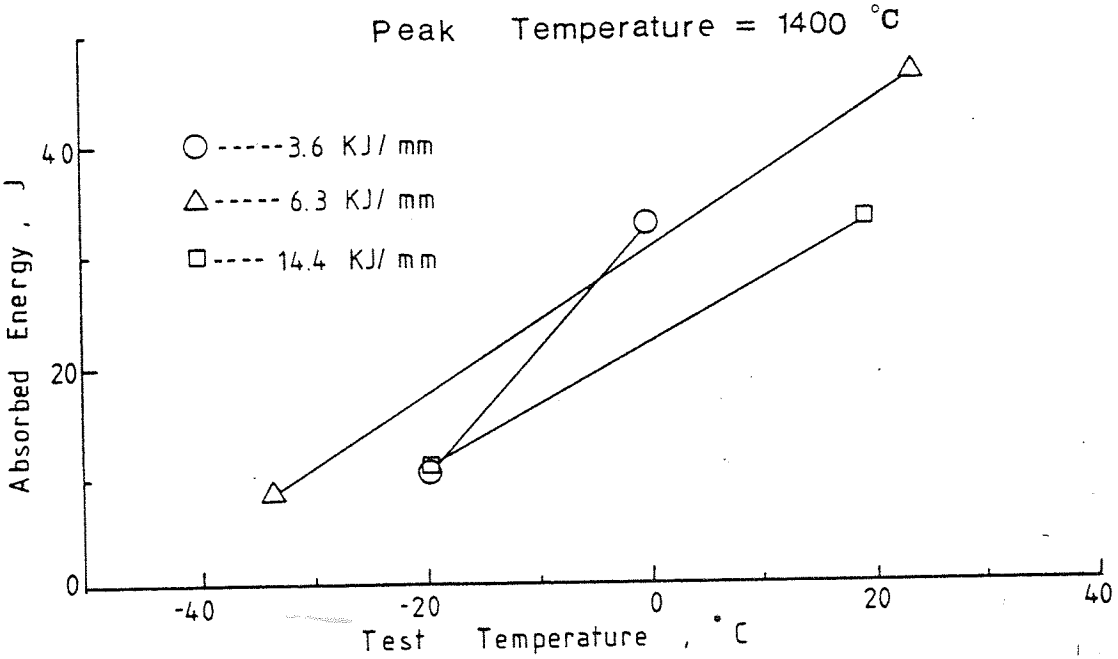

Figure 52 - Effect of the heat input on the transitional line representation for the Charpy V absorbed energy. Peak temperature at 1400°C.

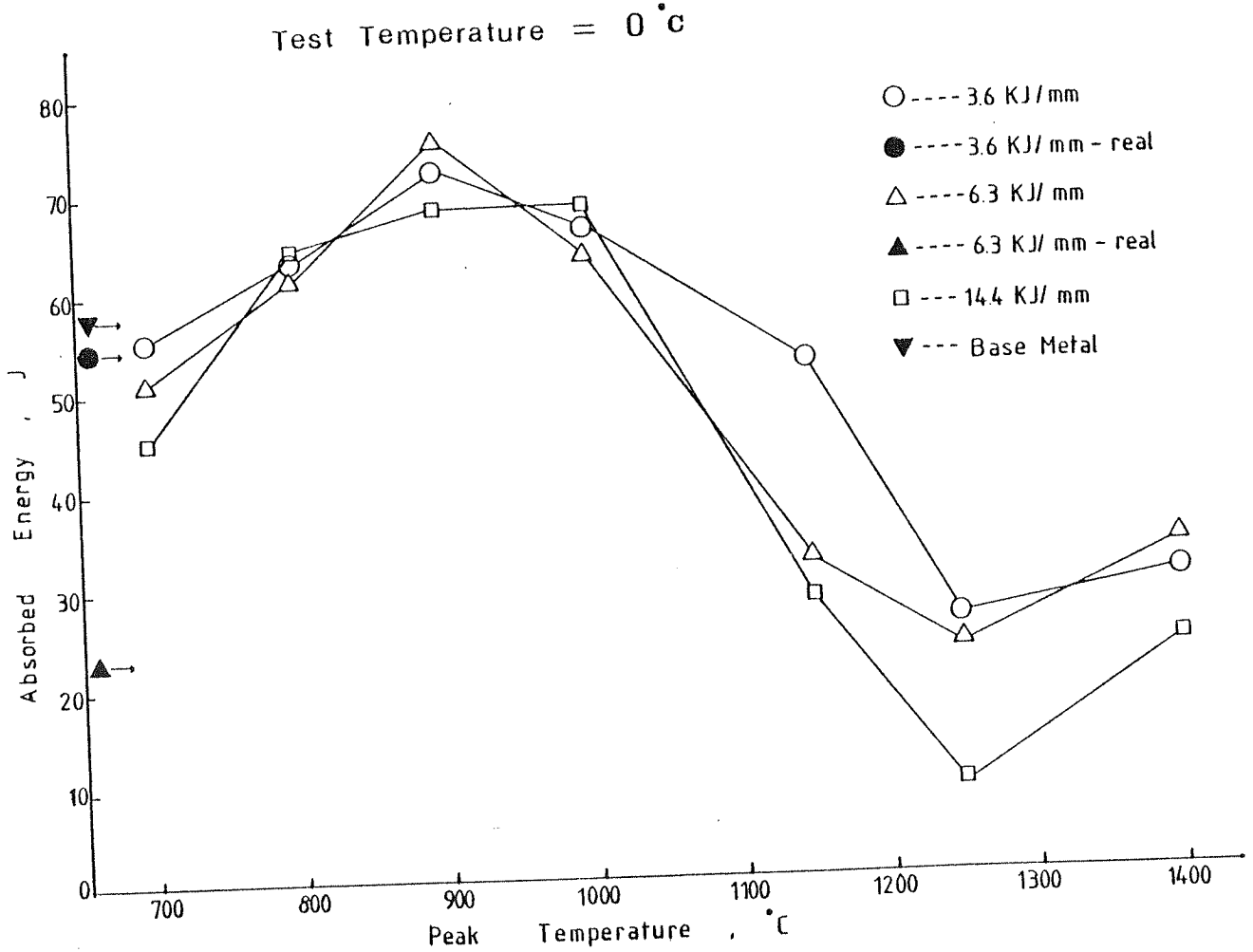

Figure 53 - Effect of the heat input and of the peak temperature in the Charpy V absorbed impact energy of simulated specimens test at 0°C. Base metal and actual welds at the heat inputs of 3.6 and 6.3KJ/mm also included for comparisons.

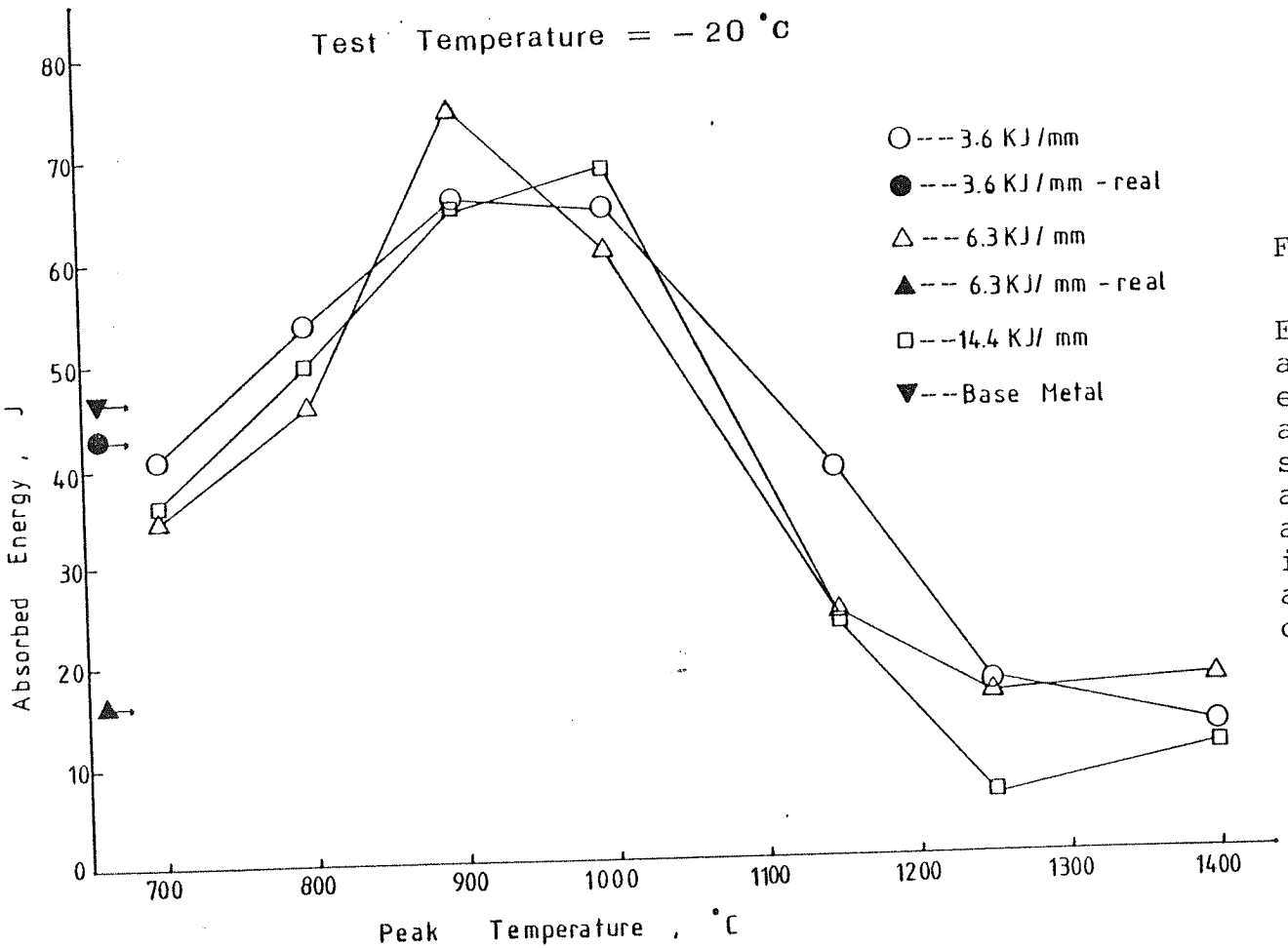

Figure 54

Effect of the heat input and of the peak temperature in the Charpy V absorbed energy of simulated specimens tested at -20°C. Base metal and actual welds at the heat inputs of 3.6 and 6.3KJ/mm also included for comparison.

Figure 55

Macrograph of the fractured surface of a Charpy V test piece showing ductile zones surrounding the inclusions. Specimen simulated at 14.4KJ/mm - 1000^{o}C and tested at -80^{o}C.

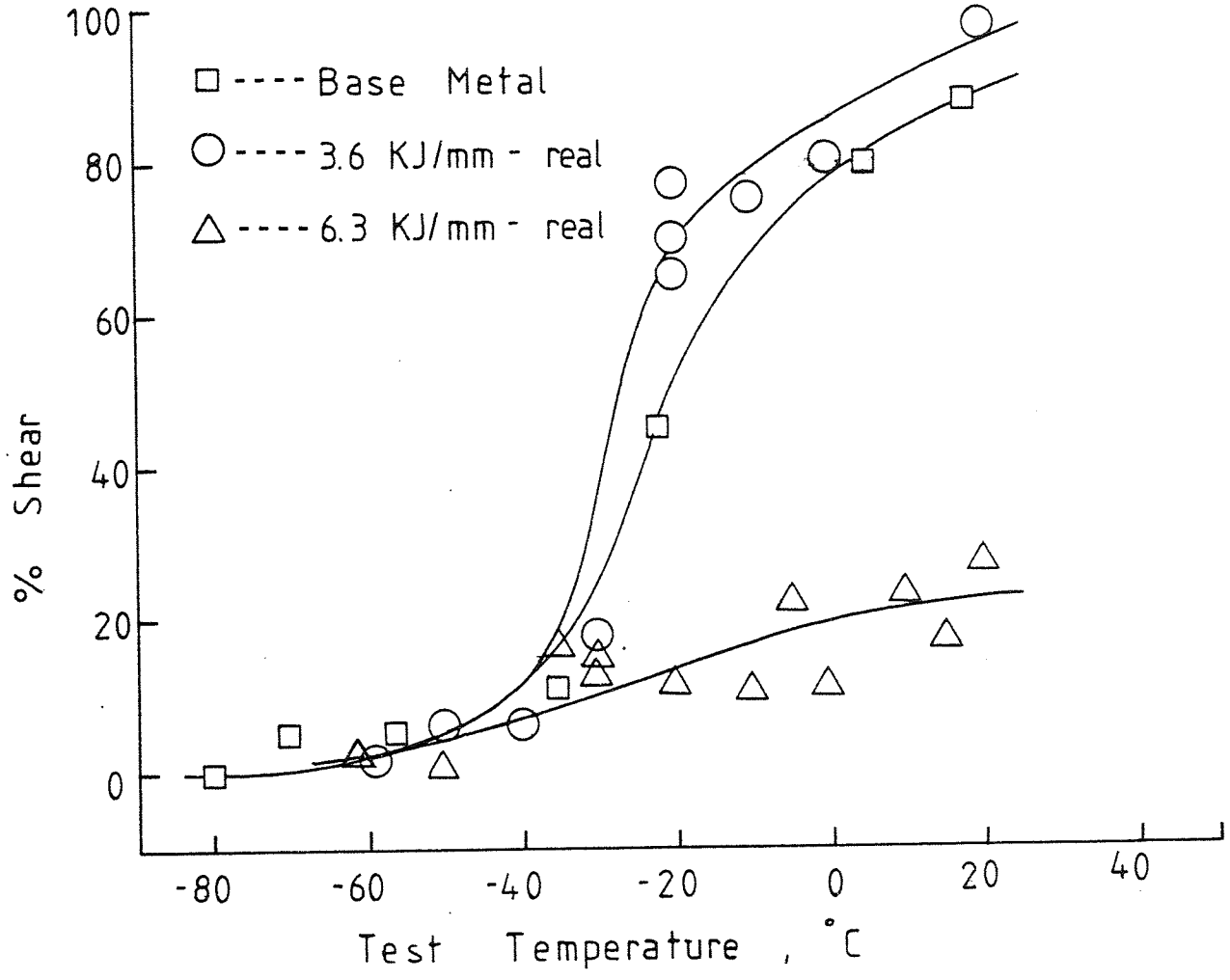

Figure 56

Effect of the test temperature on the fracture appearance of the actual 3.6 and 6.3KJ/mm heat input weld conditions and on the base metal

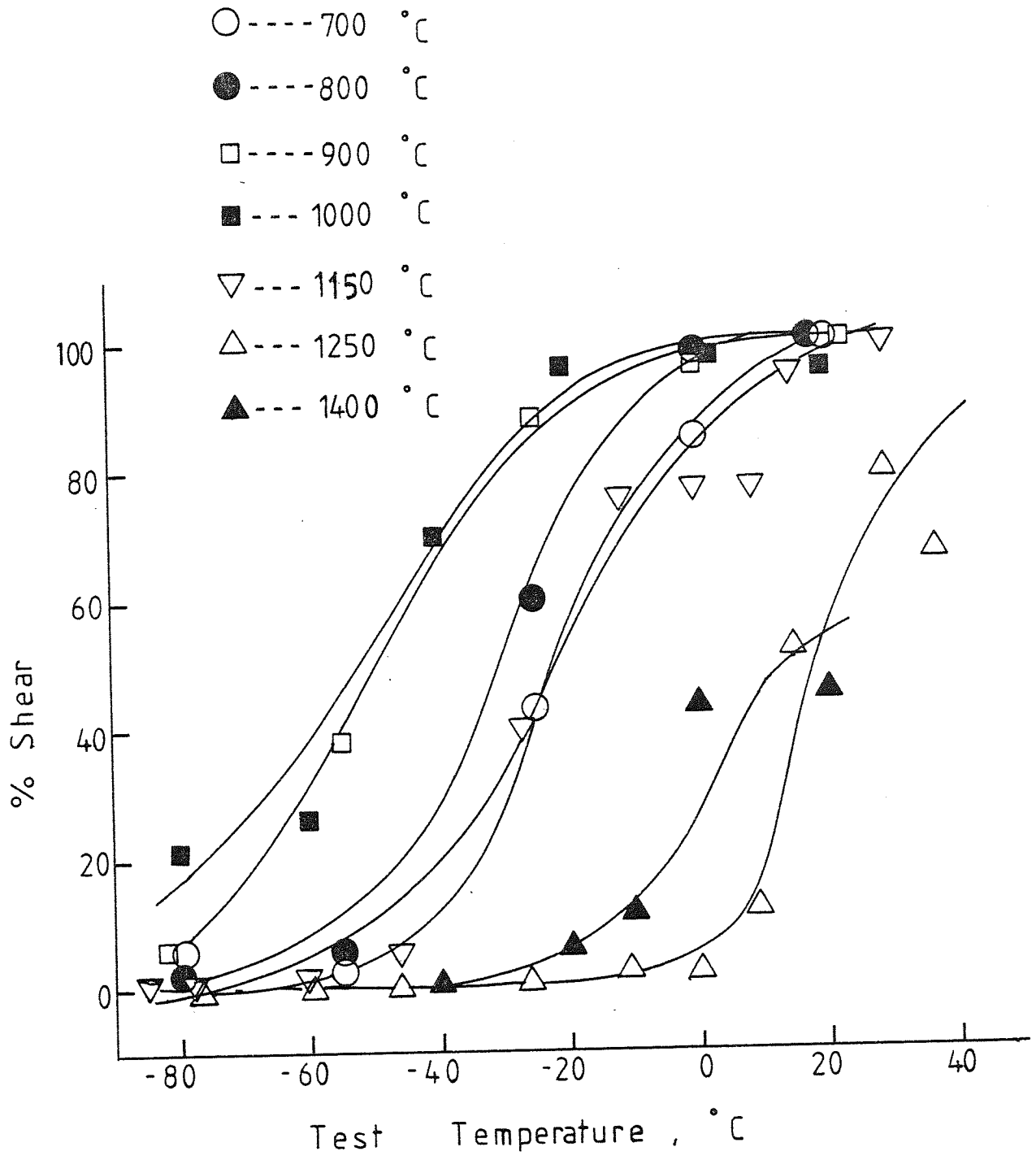

Figure 57

Effect of the test temperature on the fracture appearance of the specimens simulated at 3.6KJ/mm over the peak temperatures of 700 to 1400°C.

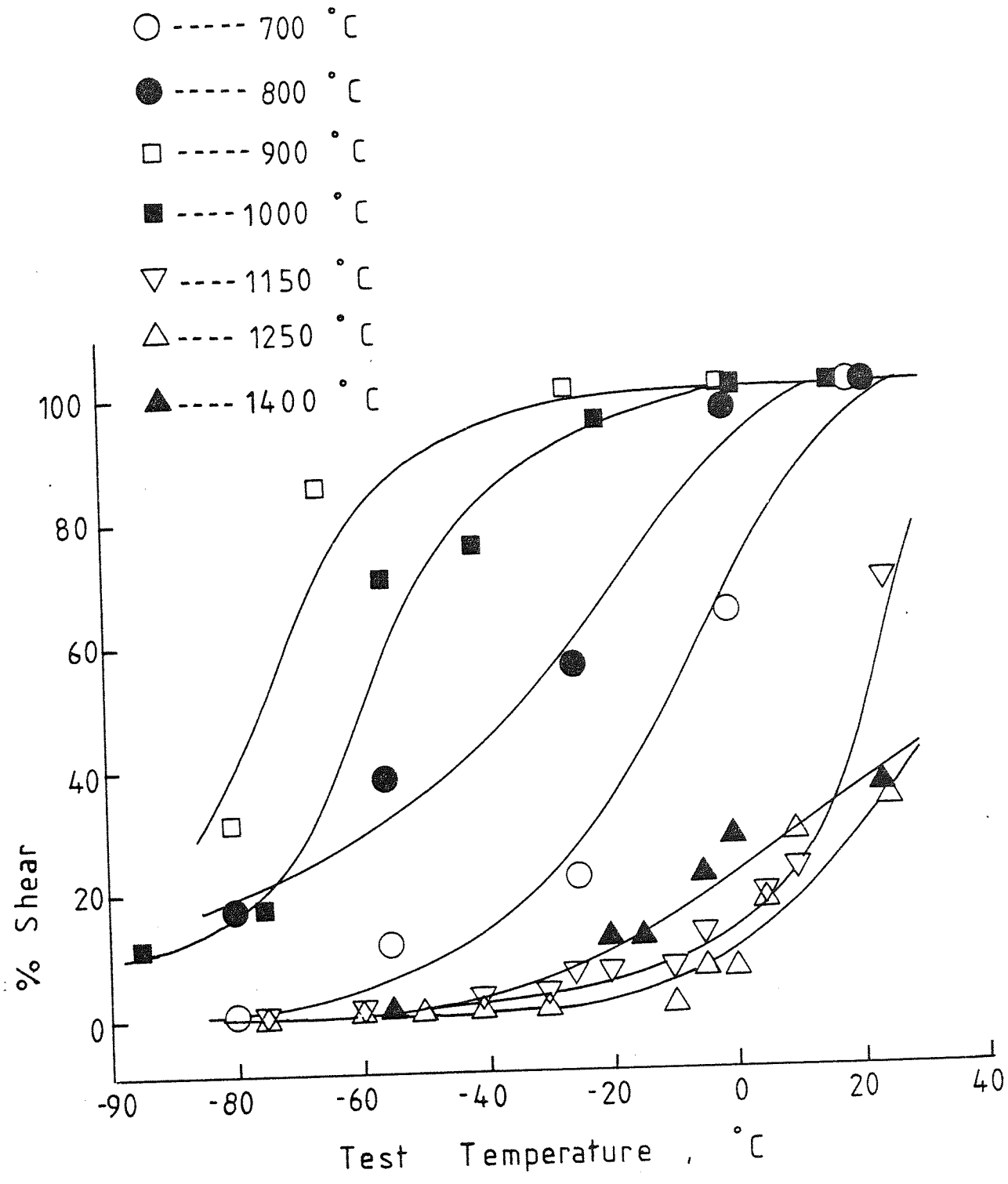

Figure 58

Effect of the test temperature on the fracture appearance of the specimens simulated at 6.3KJ/mm over the peak temperatures of 700 to 1400°C.

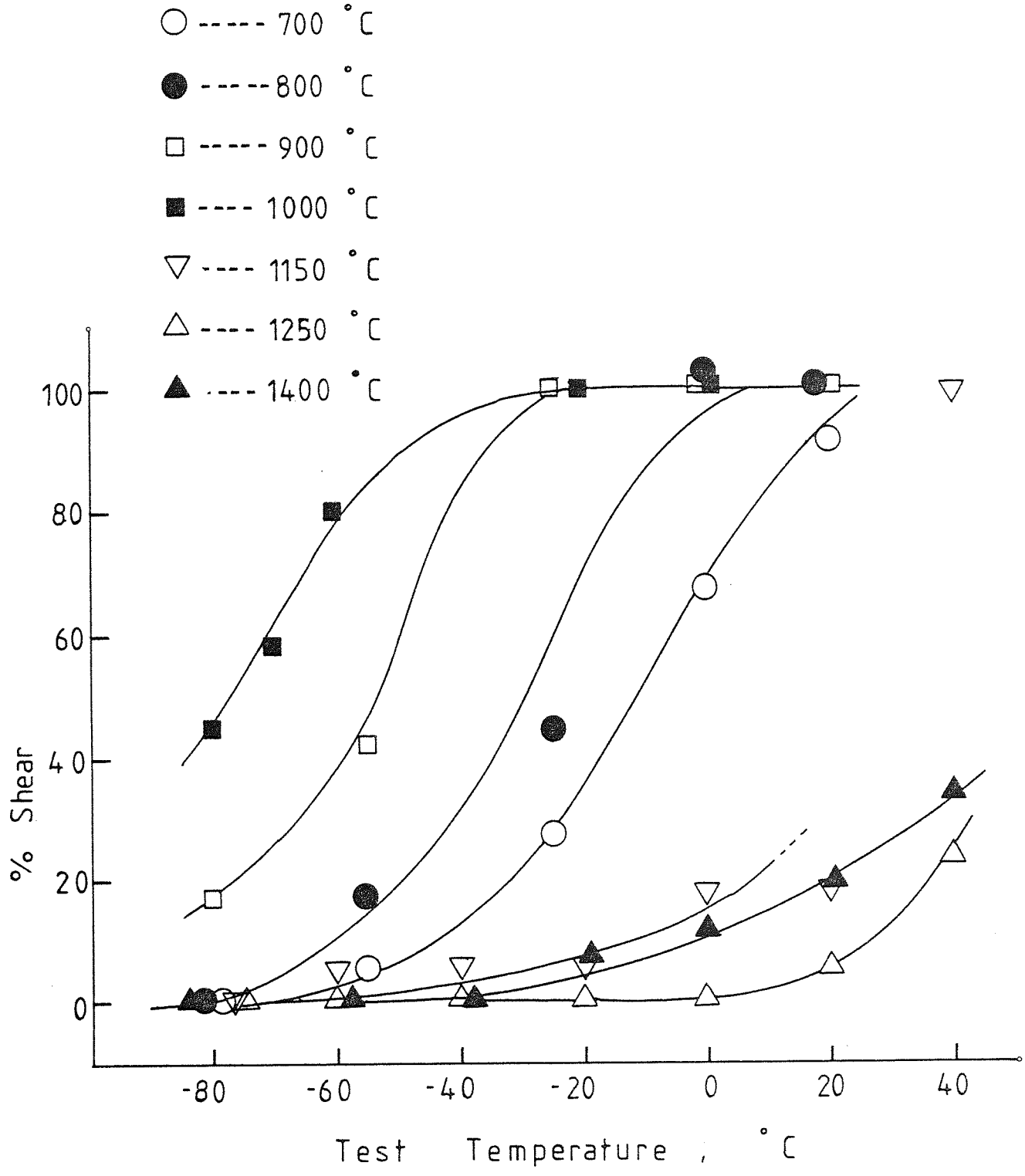

Figure 59

Effect of the test temperature on the fracture appearance of the specimens simulated at 14:4KJ/mm over the peak temperatures of 700 to 1400°C.

Figure 60
Base Metal
Nital II, X1000
Ferrite,
tempered Martensite
needles (a) and intra-
granular carbides.

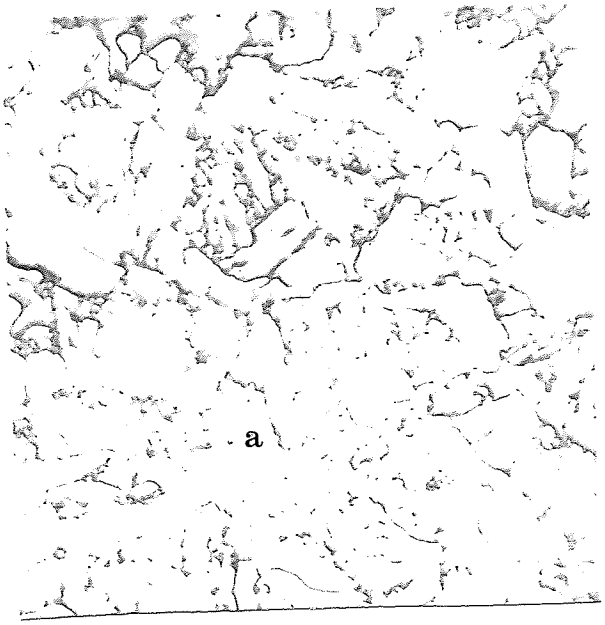

Figure 61
Simulated Sample
Heat Input = 3.6KJ/mm
Peak Temp. = 700°C
Nital II, X1000
Ferrite,
tempered Martensite
needles (a) and intra-
granular carbides.

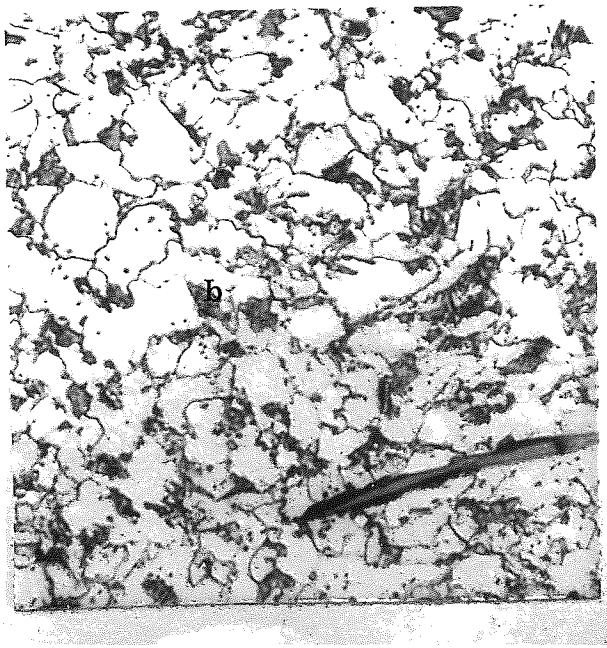

Figure 62
Simulated Sample
Heat Input = 3.6KJ/mm
Peak Temp. = 800°C
Nital II, X1000
Ferrite, ferrite plus
carbide aggregates
(b) and intragranular
carbides.

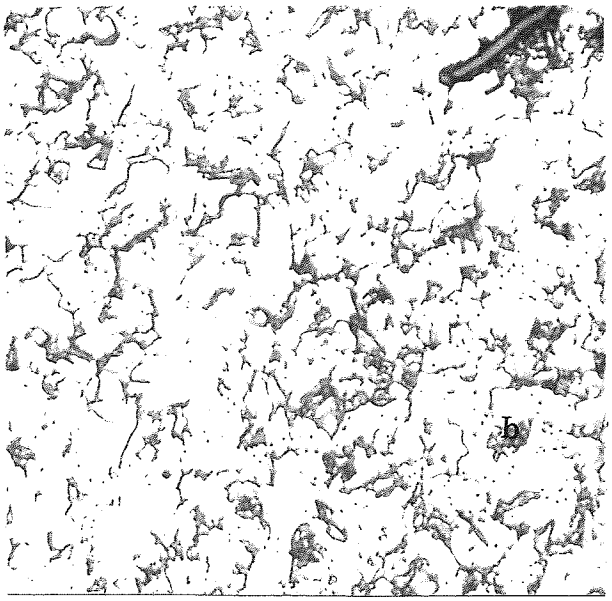

Figure 63
Simulated Sample
Heat Input = 3.6KJ/mm
Peak Temp. = 900°C
Nital II, X1000
Ferrite, ferrite plus carbide aggregates (b) and intragranular carbides.

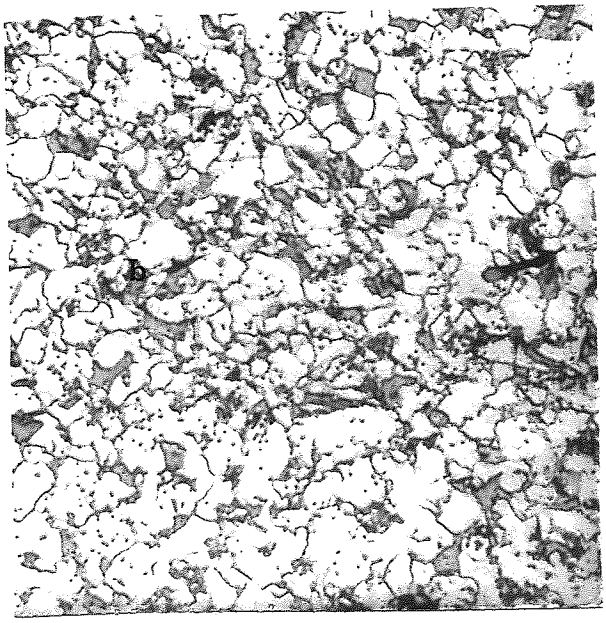

Figure 64
Simulated Sample
Heat Input = 3.6KJ/mm
Peak Temp. = 1000°C
Nital II, X1000, Ferrite, ferrite plus carbide aggregates (b) and intrgranular carbides.

Figure 65
Simulated Sample
Heat Input = 3.6KJ/mm
Peak Temp. = 1150°C
Nital II, X1000, intragranular ferrite (e), interlocking acicular ferrite (f) and upper bainite (g). Note : unetched upper bainite as "white area" (h).

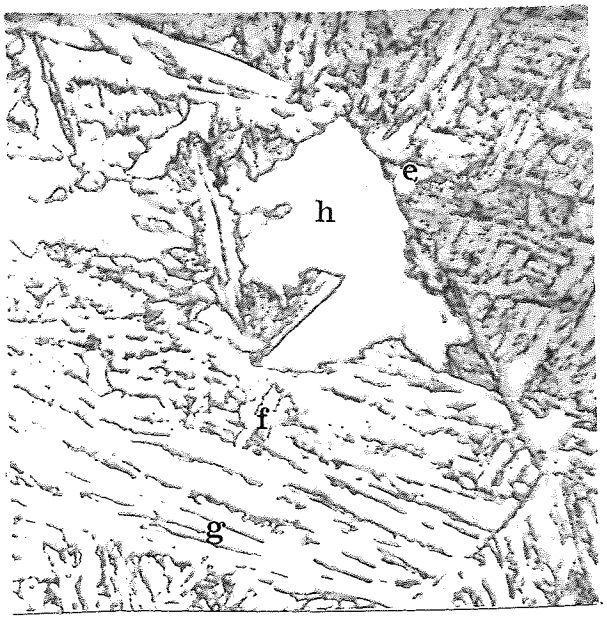

Figure 66
Simulated Sample
Heat Input = 3.6KJ/mm
Peak Temp. = 1250°C
Nital II, X1000, intragranular ferrite (e), interlocking acicular ferrite (f) and upper bainite (g). Note : unetched upper bainite as "white area" (h).

Figure 67
Simulated Sample
Heat Input = 3.6KJ/mm
Peak Temp. = 1400°C
Nital II, X1000, intragranular ferrite (e), interlocking acicular ferrite (f) and upper bainite (g). Structure representative of Curve VI from CCT diagram.

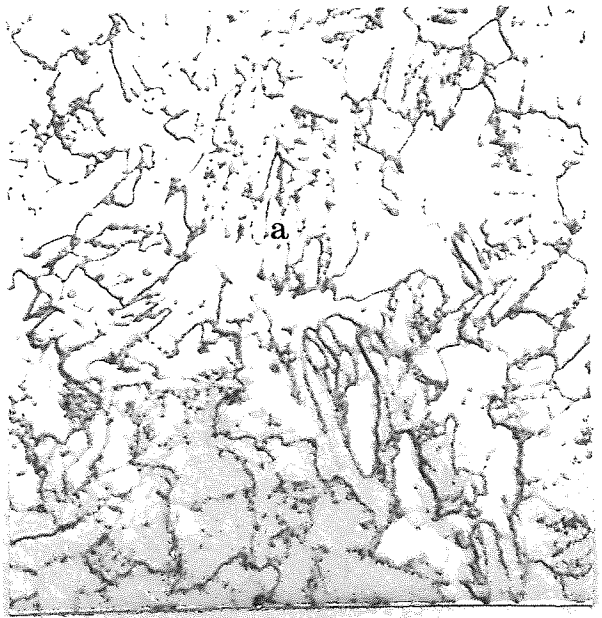

Figure 68
Simulated Sample
Heat Input = 6.3KJ/mm
Peak Temp. = 700°C
Nital II, X1000, Ferrite tempered martensite needles (a) and intragranular carbide.

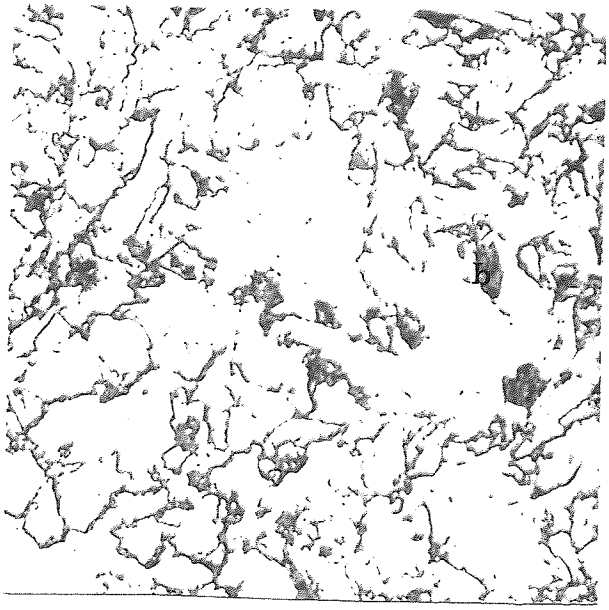

Figure 69
Simulated Sample
Heat Input = 6.3KJ/mm
Peak Temp. = 800°C
Nital II, X1000, Ferrite, ferrite plus carbide aggregates (b) and intragranular carbides.

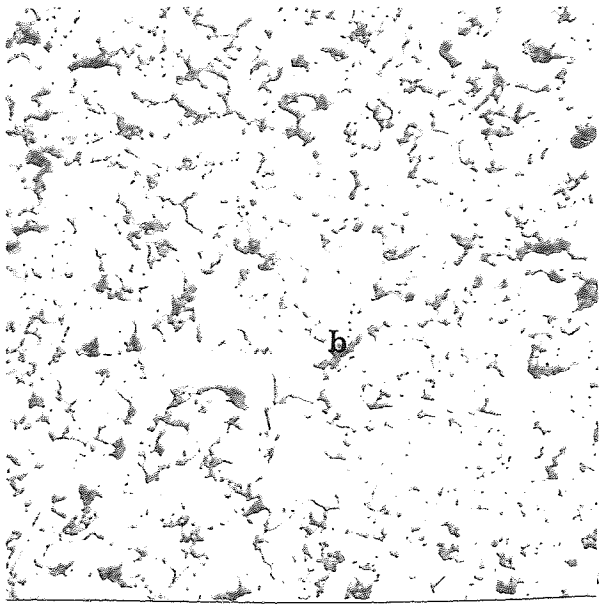

Figure 70
Simulated Sample
Heat Input = 6.3KJ/mm
Peak Temp. = 900°C
Nital II, X1000, Ferrite, ferrite plus carbide aggregates (b) and intragranular carbides.

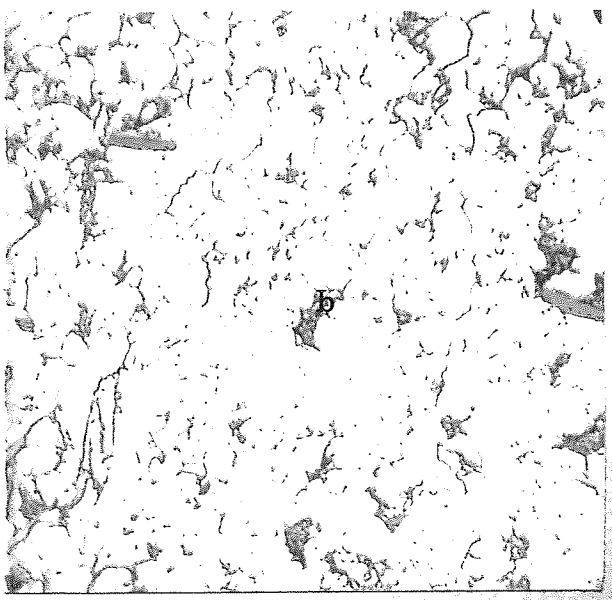

Figure 71
Simulated Sample
Heat Input = 6.3KJ/mm
Peak Temp. = 1000°C
Ferrite, ferrite plus carbide aggregates (b) and intragranular carbides.
Nital II, X1000.

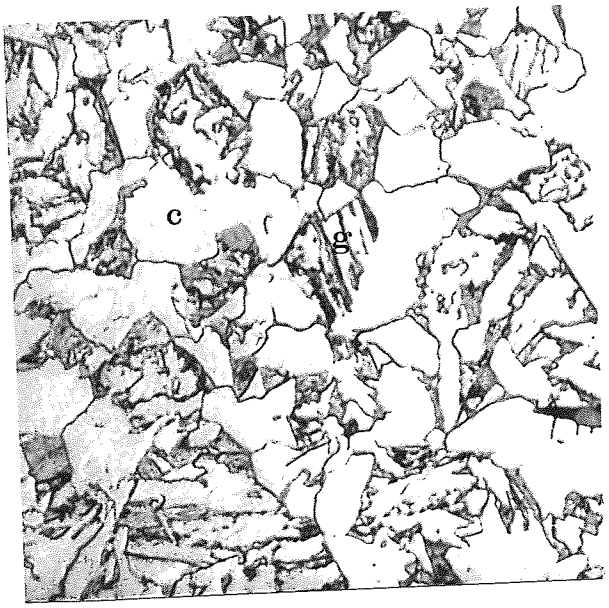

Figure 72
Simulated Sample
Heat Input = 6.3KJ/mm
Peak Temp. = 1150°C
Nital II, X1000
Proeutectoid ferrite (c) and upper bainite (g).

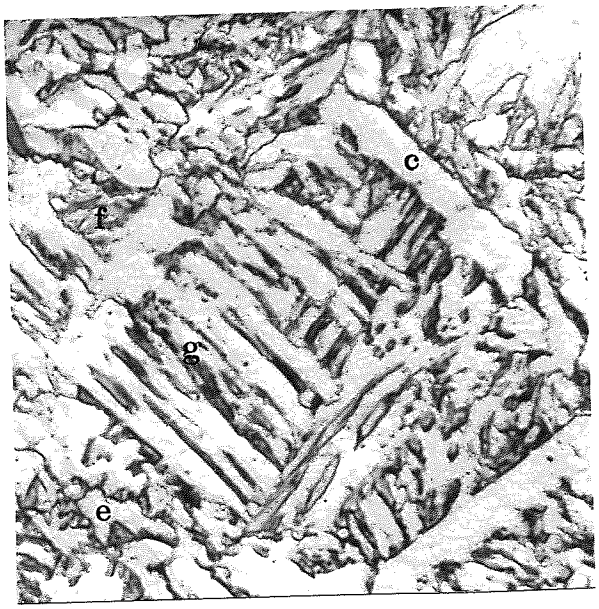

Figure 73
Simulated Sample
Heat Input = 6.3KJ/mm
Peak Temp. = 1250°C
Nital II, X1000
Proeutectoid ferrite (c), intragranular ferrite (e), interlocking acicular ferrite (f) and upper bainite (g).

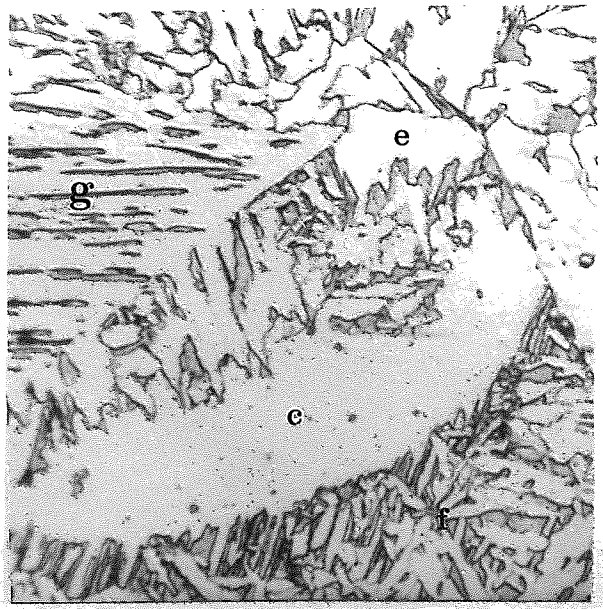

Figure 74
Simulated Sample
Heat Input = 6.3KJ/mm
Peak Temp. = 1400°C
Nital II, X1000
Proeutectoid ferrite (c), intragranular ferrite (e), interlocking acicular ferrite (f) and upper bainite (g).

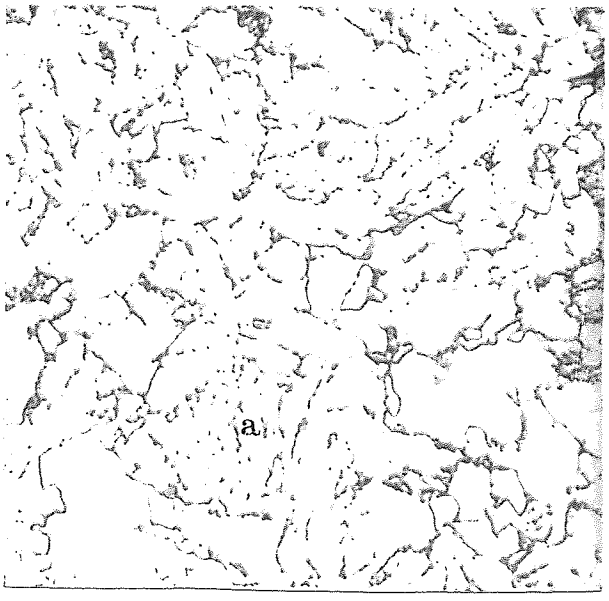

Figure 75
Simulated Sample
Heat Input = 14.4KJ/mm
Peak Temp. = 700°C
Nital II, X1000, Ferrite, tempered martensite needles (a) and intragranular carbides.

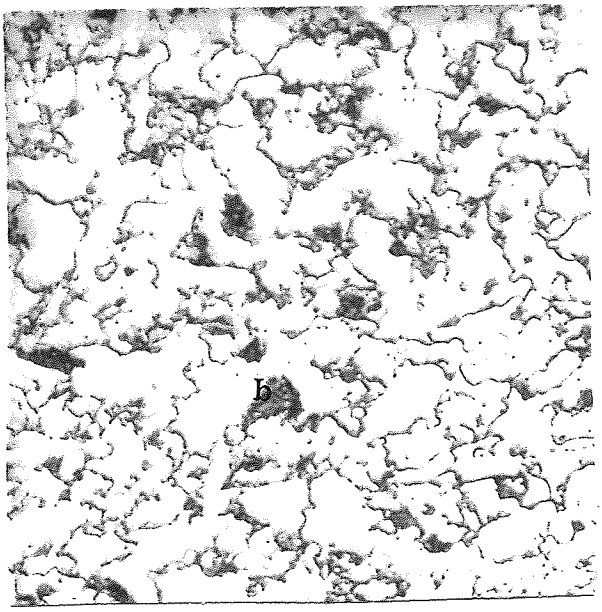

Figure 76
Simulated Sample
Heat Input = 14.4KJ/mm
Peak Temp. = 800°C
Nital II, X1000, Ferrite, ferrite plus carbide aggregates (b) and intragranular carbides.

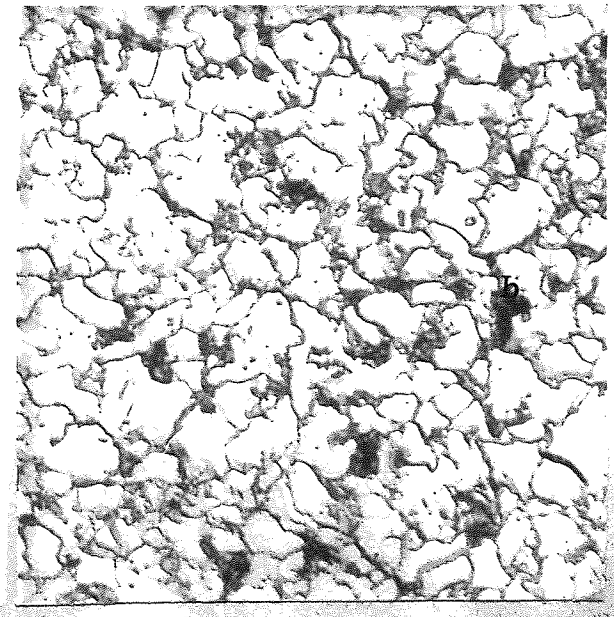

Figure 77
Simulated Sample
Heat Input = 14.4KJ/mm
Peak Temp. = 900°C
Nital II, X1000, Ferrite, ferrite plus carbide aggregates (b) and intragranular carbides.

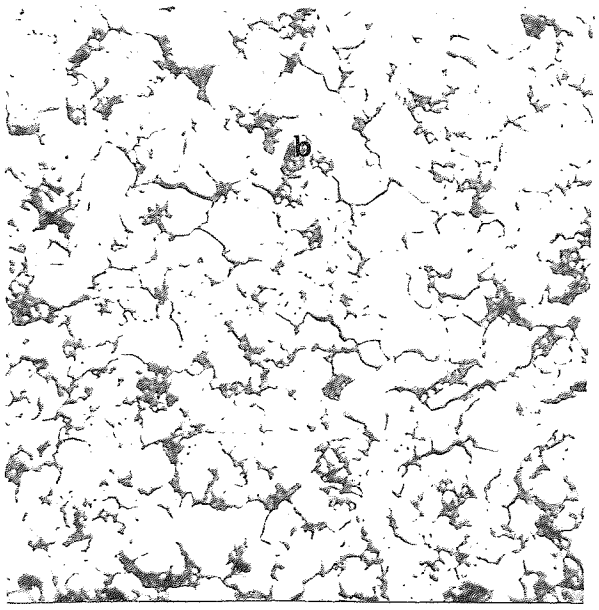

Figure 78
Simulated Sample
Heat Input = 14.4KJ/mm
Peak Temp. = 1000°C
Nital II, X1000, Ferrite, ferrite plus carbide aggregates (b) and intragranular carbides.

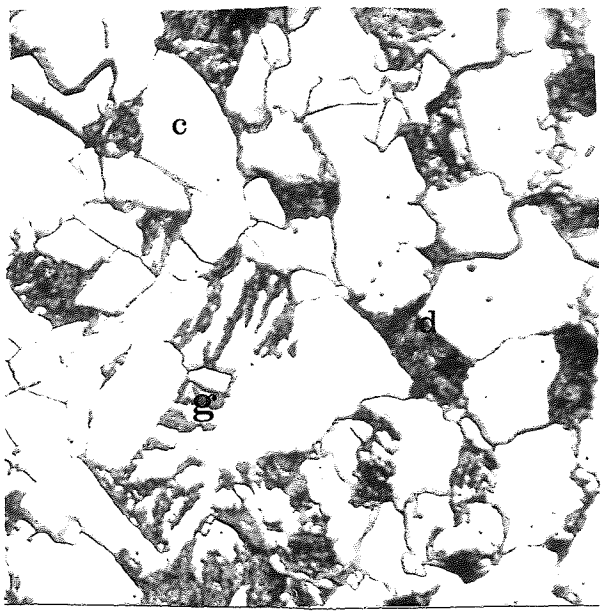

Figure 79
Simulated Sample
Heat Input = 14.4KJ/mm
Peak Temp. = 1150°C
Nital II, X1000
Proeutectoid ferrite (c), pearlite (d) and upper bainite (g).

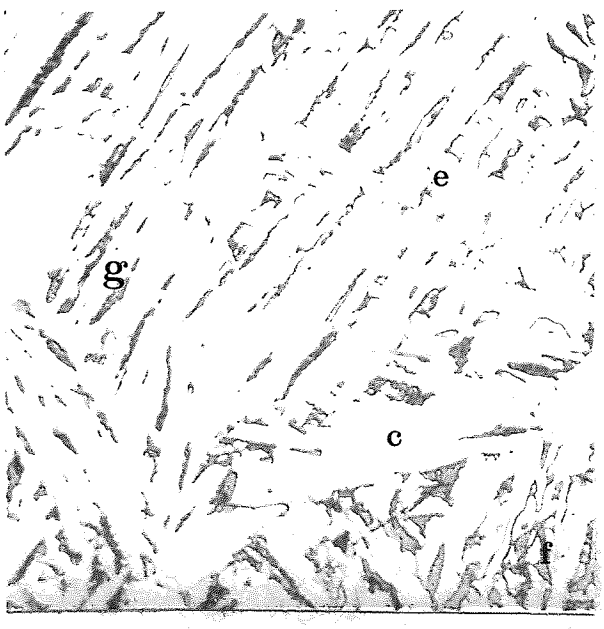

Figure 80
Simulated Sample
Heat Input = 14.4KJ/mm
Peak Temp. = 1250°C
Nital II, X1000
Proeutectoid ferrite (c), intragranular ferrite (e), interlocking acicular ferrite (f) and upper bainite (g).

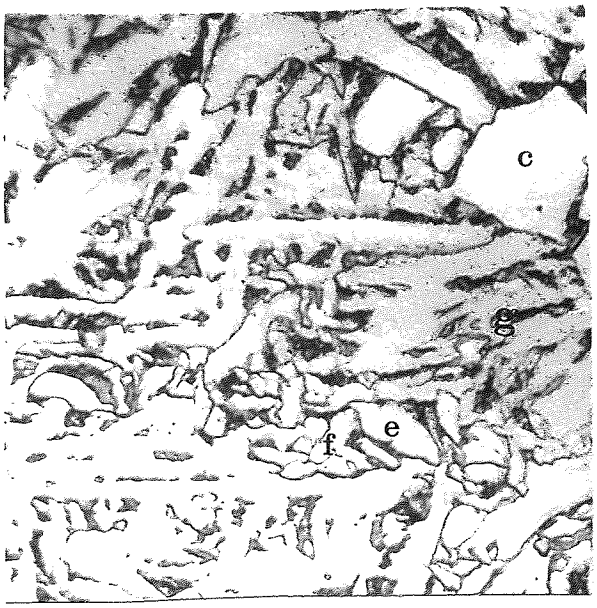

Figure 81
Simulated Sample
Heat Input = 14.4KJ/mm
Peak Temp. = 1400°C
Nital II, X1000
Proeutectoid ferrite (c), intragranular ferrite (e), interlocking acicular ferrite (f) and upper bainite (g).

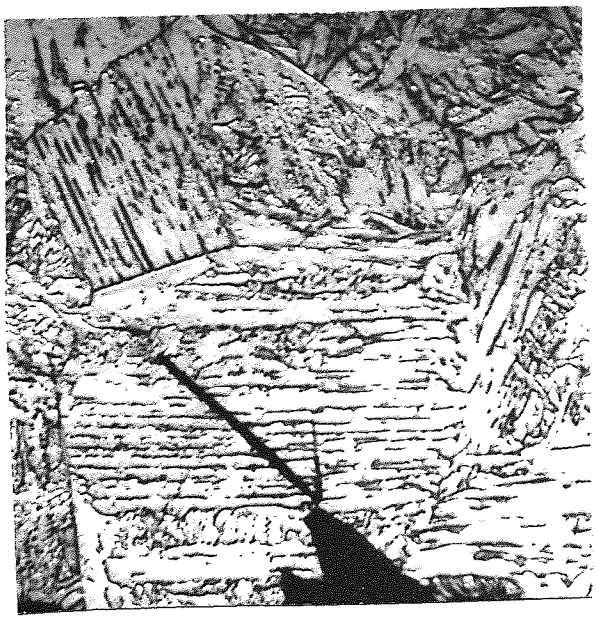

Figure 82
Simulated Sample
Heat Input = 3.6KJ/mm
Peak Temp. = 1250°C
Nital II, X1000, Cleavage cracks cutting across an upper bainite colony.

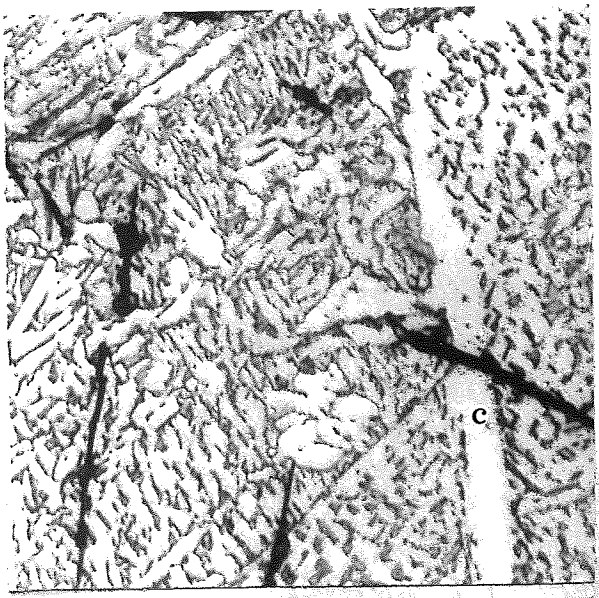

Figure 83
Simulated Sample
Heat Input = 3.6KJ/mm
Peak Temp. = 1400°C
Nital II, X1000, Cleavage cracks cutting across upper bainite colonies. At "C" a proeutectoid ferrite vein is observed. Note : cracks being arrested at "higher angles".

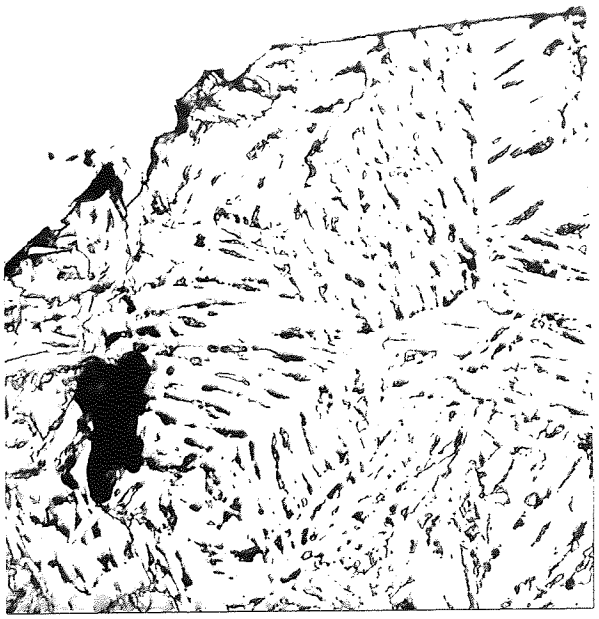

Figure 84
Real Weld HAZ
Nickel plate fracture profile
Heat Input = 6.3KJ/mm
o.3% CTAB, X550
Crack propagation straight through the upper bainite and changing direction in the interlocking acicular ferrite.

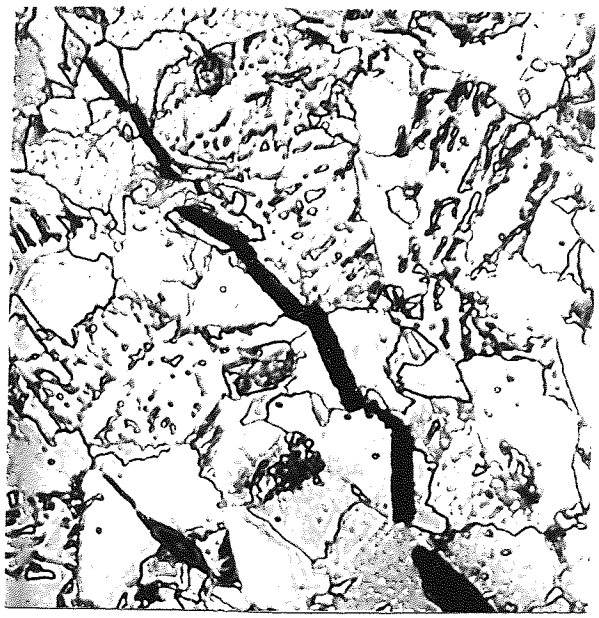

Figure 85
Simulated Sample
Heat Input = 6.3KJ/mm
Peak Temp. = 1150°C
Nital II, X1000,Cleavage cracks across the proeutectoid ferrite and changing direction at the cells boundaries.

Figure 86
Simulated Sample
Heat Input = 14.4KJ/mm
Peak Temp. = 1250°C
Nital II, X1000,Cleavage cracks cutting across the proeutectoid ferrite and changing direction at the cells boundaries.

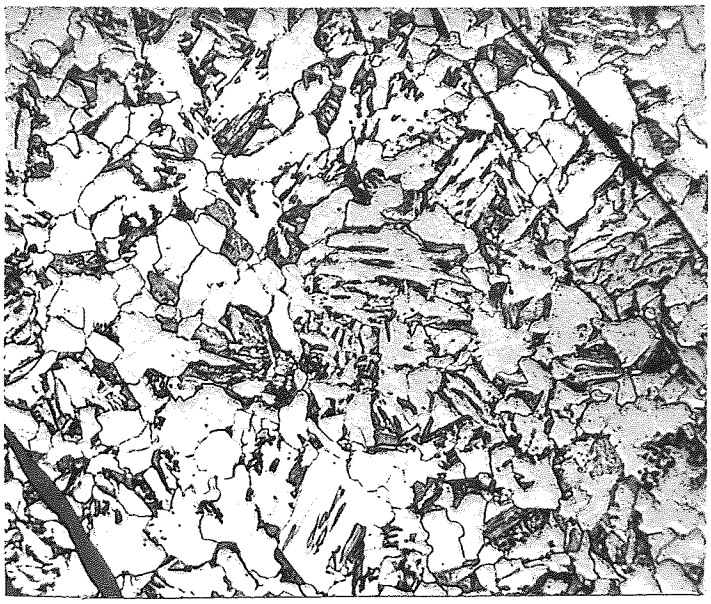

Figure 87
Simulated Sample
Heat Input = 6.3KJ/mm
Peak Temp. = 1150°C
Nital II, 550X
proeutectoid ferrite
tending to form at
inclusion sites.

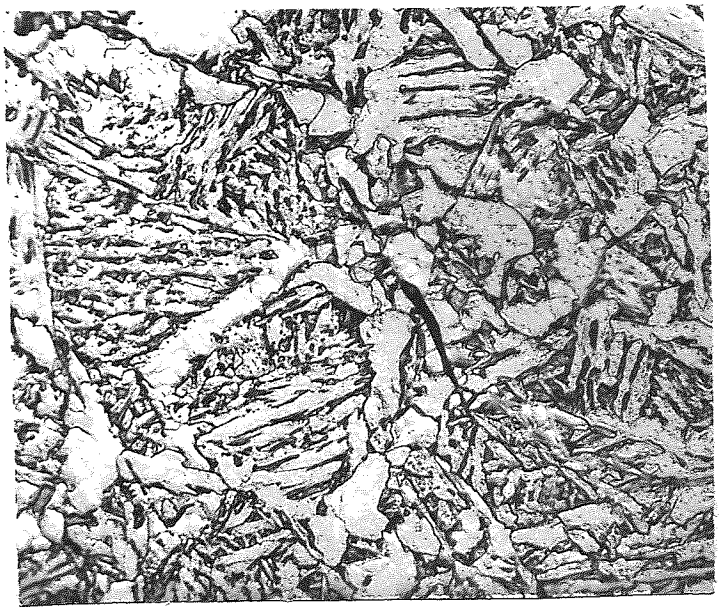

Figure 88
Simulated Sample
Heat Input = 6.3KJ/mm
Peak Temp. = 1250°C
Nital II, 550X
proeutectoid ferrite
tending to form at
inclusion sites.

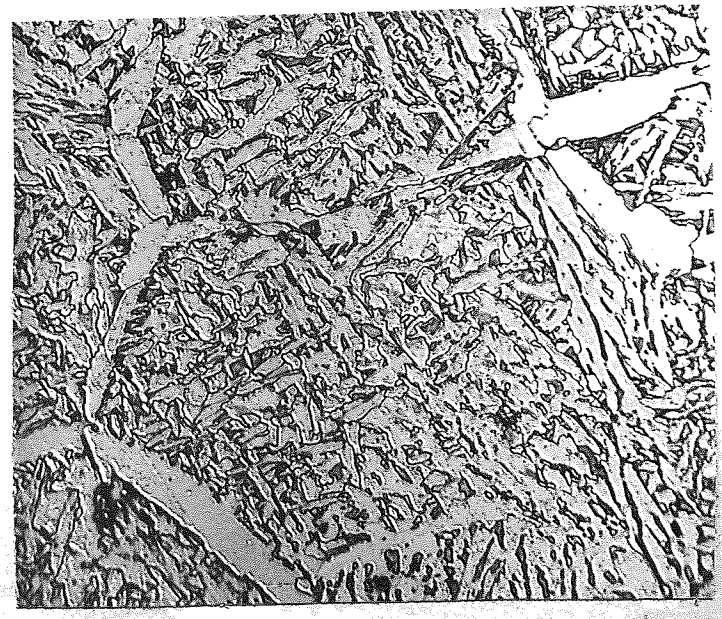

Figure 89
Simulated Sample
Heat Input = 6.3KJ/mm
Peak Temp. = 1400°C
Nital II, 550X
structure represent-
ative of curve VII
for the CCT diagram.

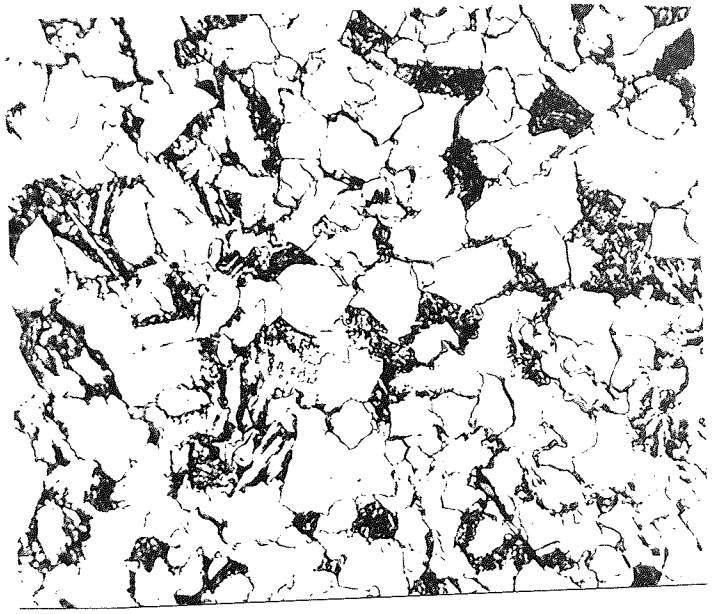

Figure 90
Simulated Sample
Heat Input = 14.4KJ/mm
Peak Temp. = 1150°C
Nital II, 550X

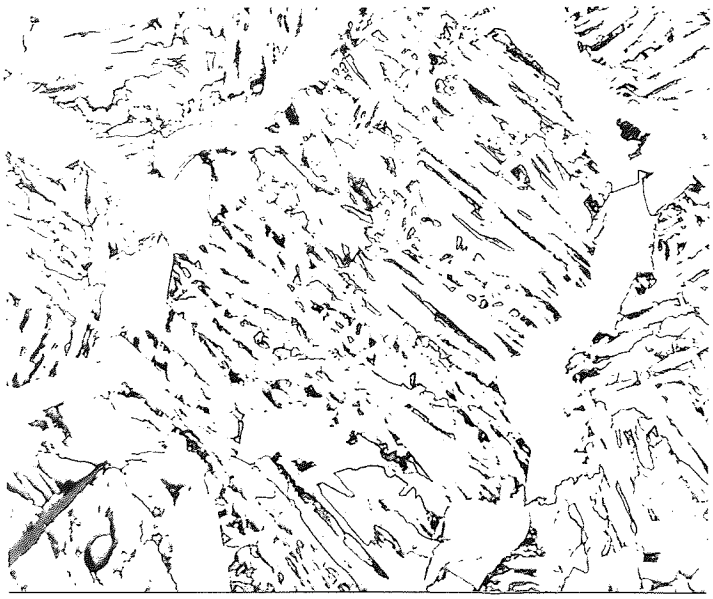

Figure 91
Simulated Sample
Heat Input = 14.4KJ/mm
Peak Temp. = 1250°C
Nital II, 550X

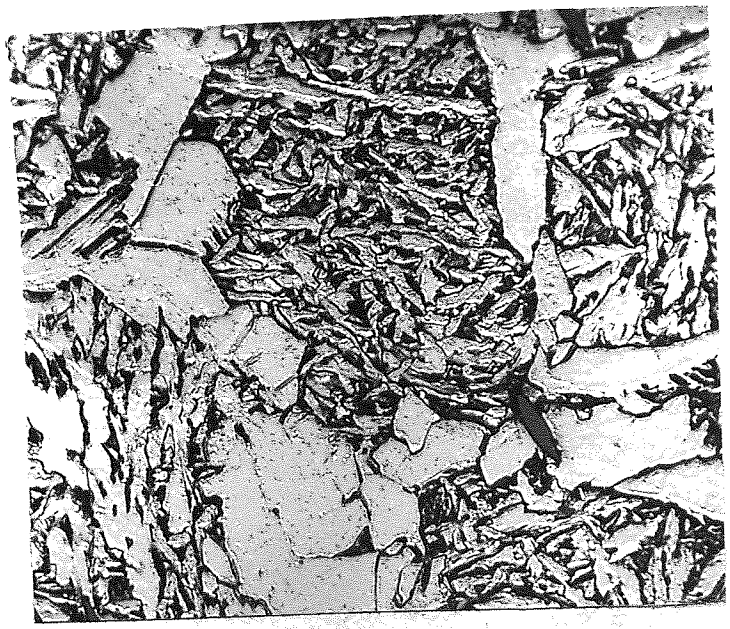

Figure 92
Simulated Sample
Heat Input = 14.4KJ/mm
Peak Temp. = 1400°C
Nital II, 550X
structure representative
of curve VIII for the
CCT diagram.

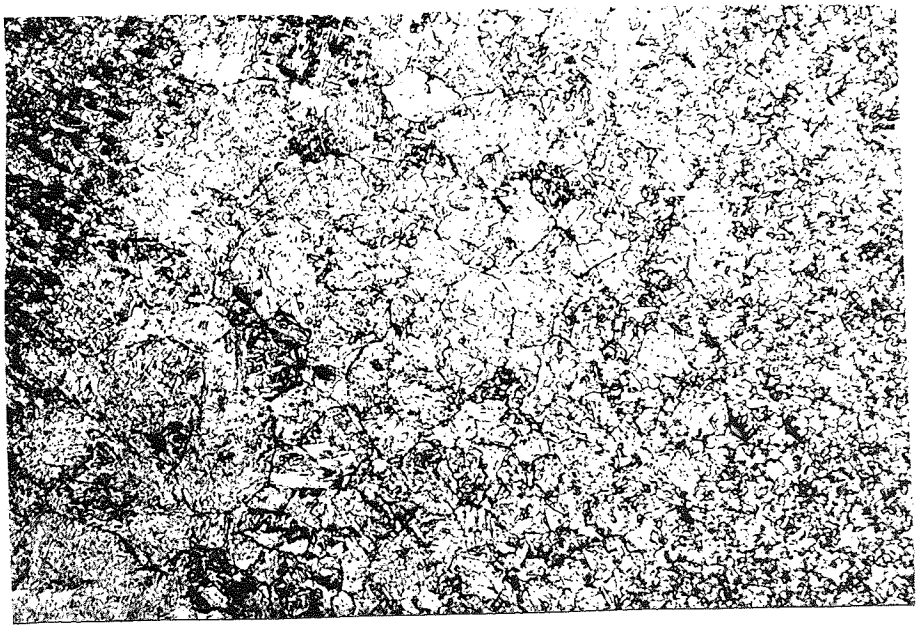

Figure 93
Two different aspects of the real weld HAZ with increasing penetration of the welding bead
Heat Input = 3.6KJ/mm, 0.3% CTAB, X100.

Figure 94
Real Weld HAZ, Heat Input = 3.6KJ/mm, 0.3%CTAB, X200. Coarse grains next to the weld metal, near the plate surface.

Figure 95
Simulated HAZ, Heat Input = 3.6KJ/mm, Peak Temp. = 1400^{o}C, 0.3% CTAB, X200.

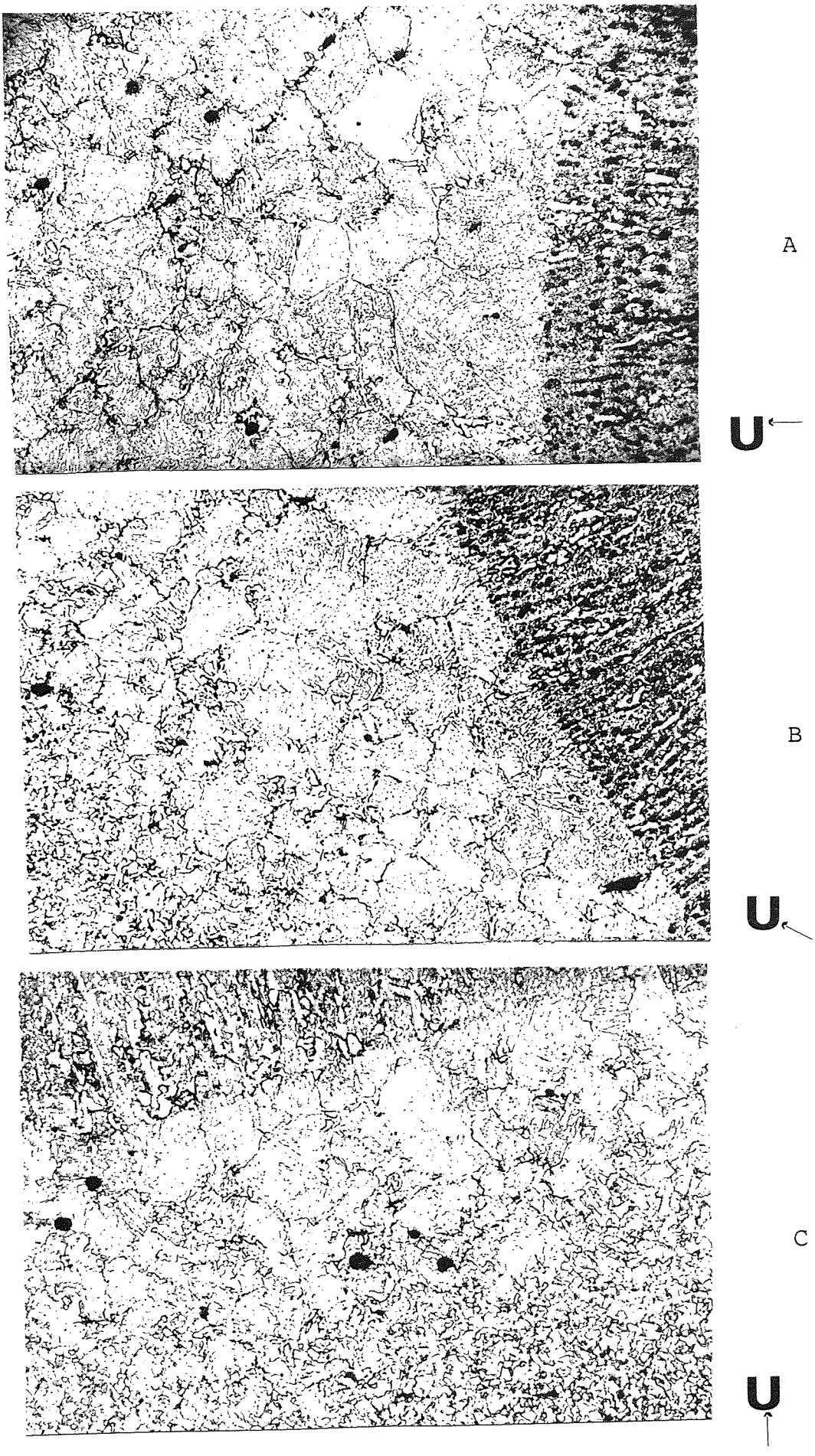

Figure 96
Three different aspects of the real HAZ, with the increasing penetration of the welding bead. Heat Input = 6.3KJ/mm, 0.3% CTAB, X200.

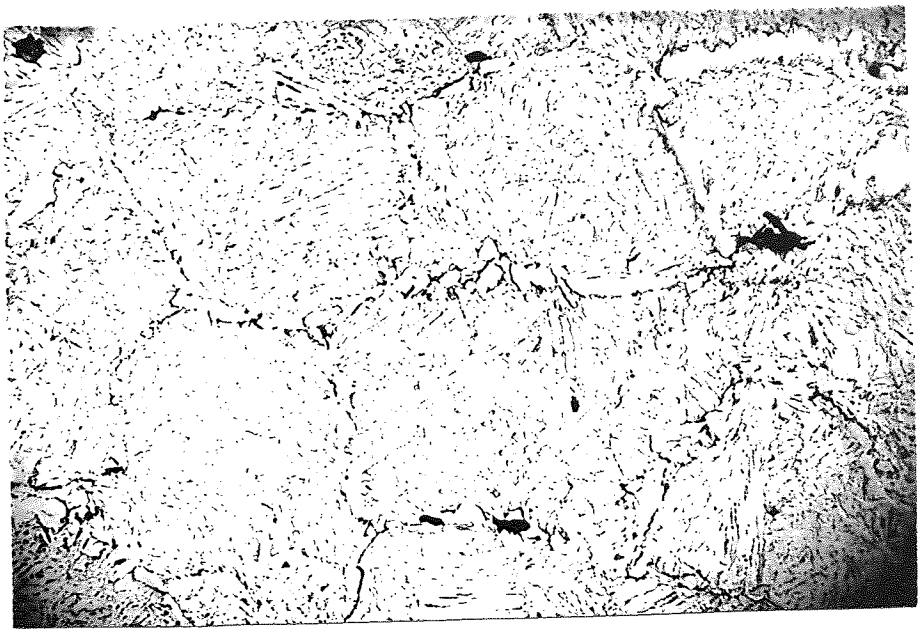

Figure 97
Real Weld HAZ, Heat Input = 6.3KJ/mm, 0.3% CTAB, X200. Picture taken next to the weld metal, near the plate surface.

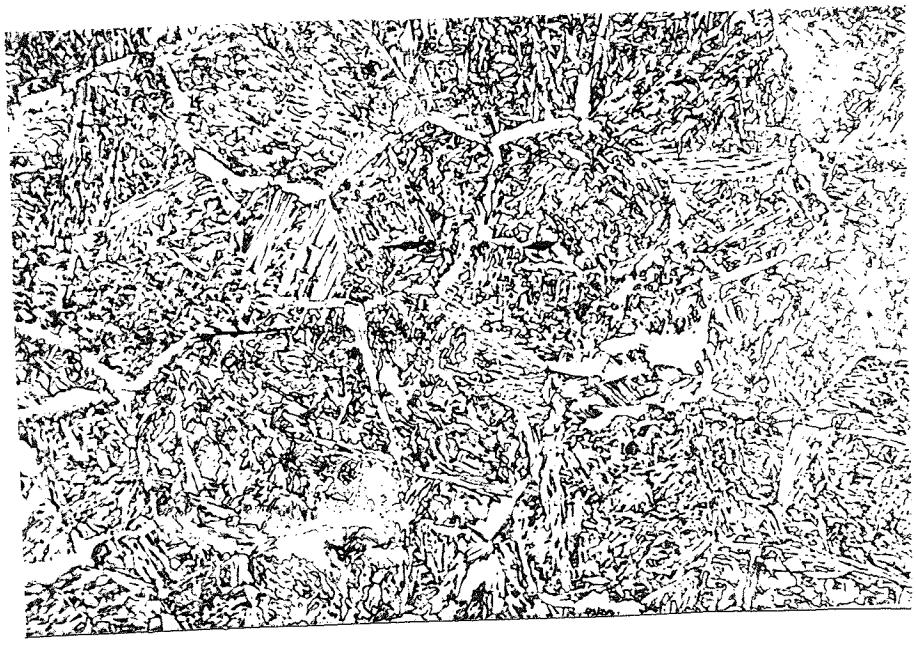

Figure 98
Simulated HAZ, Heat Input = 6.3KJ/mm, Peak Temp. = 1400^{o}C. Nital II, X200.

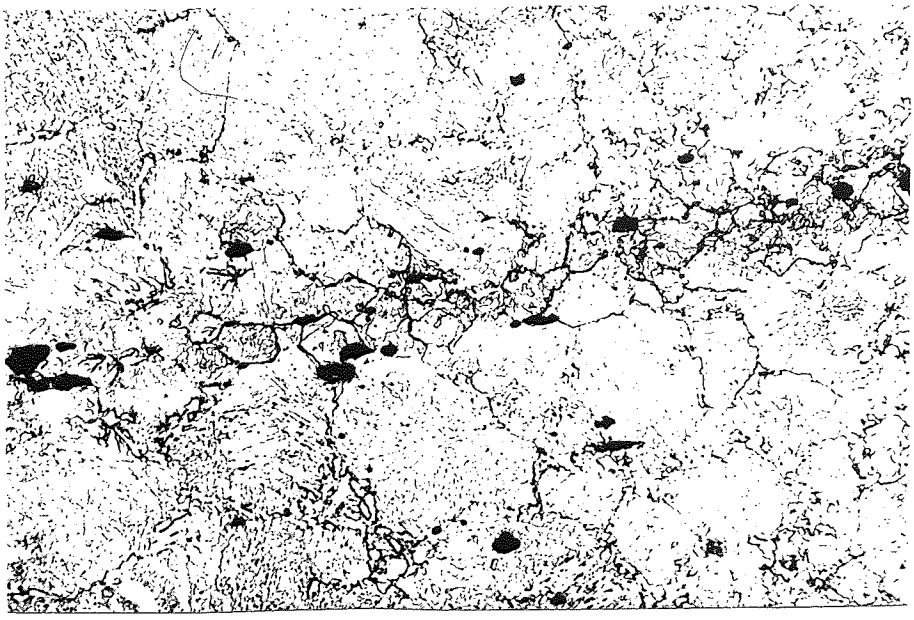

Figure 99
Peak Weld HAZ, Heat Input = 6.3KJ/mm, 0.3% CTAB, X200. Note the influence of the inclusion in line, limiting the prior austenite grain sizes.

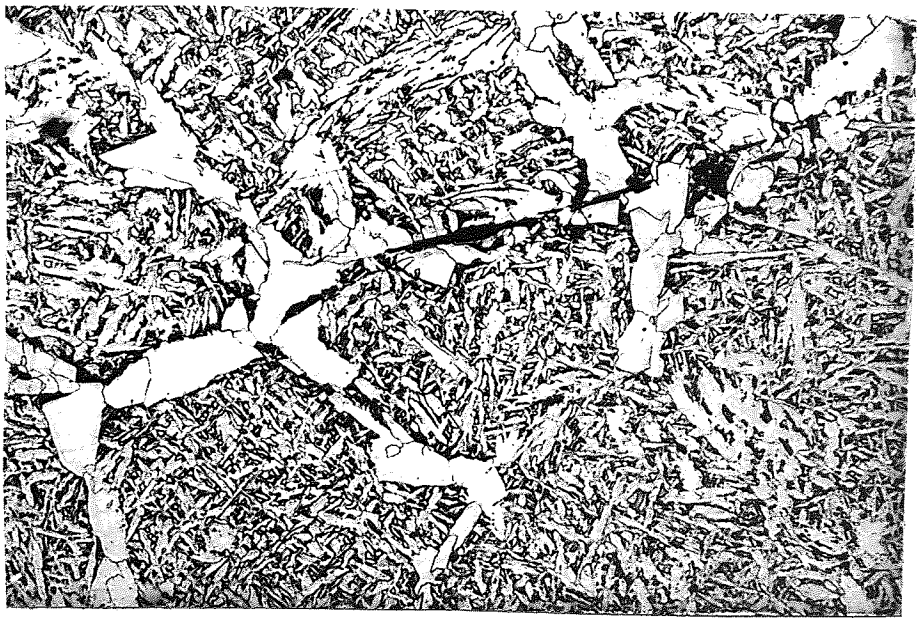

Figure 100
Simulated HAZ, Cooling Time $\Delta t_{800-500}$ = 526 s. Nital II, X200. Note the proeutectoid ferrite forming at the inclusion sites. Structure representative of curve IX for the CCT diagram.

Figure 101
Simulated Sample
$\Delta t_{800-500} = 4$ s
Nital II, X1000
Martensitic structure
Curve I from CCT
diagram.

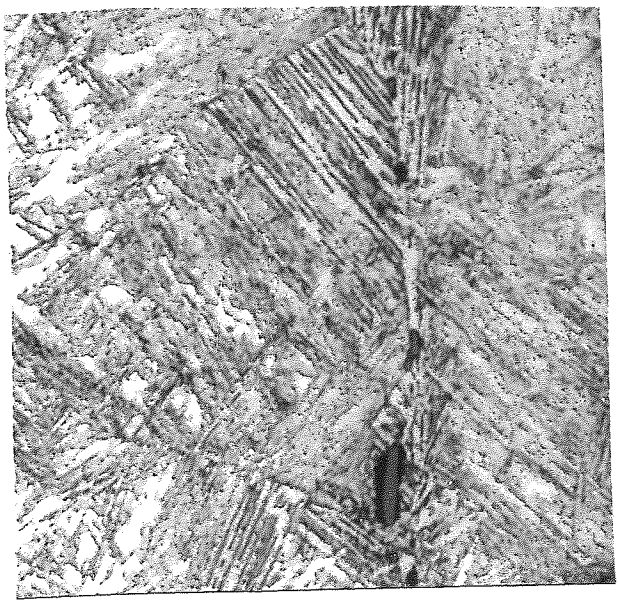

Figure 102
Simulated Sample
$\Delta t_{800-500} = 6$ s
Nital II, X1000
Martensitic structure
containing occasionally
fine upper bainite
Curve II from CCT
diagram.

Figure 103
Simulated Sample
$\Delta t_{800-500} = 8$ s
Nital II, X1000
Martensitic and upper
bainitic structures
Curve III from CCT
diagram.

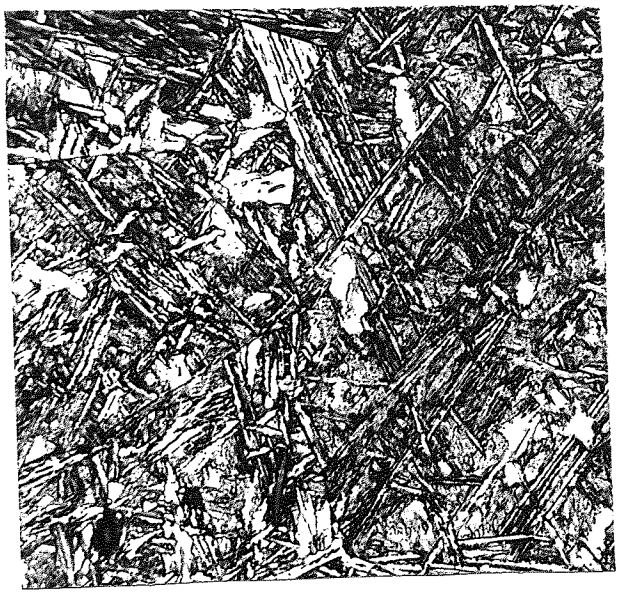

Figure 104
Simulated Sample
$\Delta t_{800-500}$ = 10 s
Nital II, X1000
Martensitic and upper bainitic structures
Curve IV from CCT diagram.

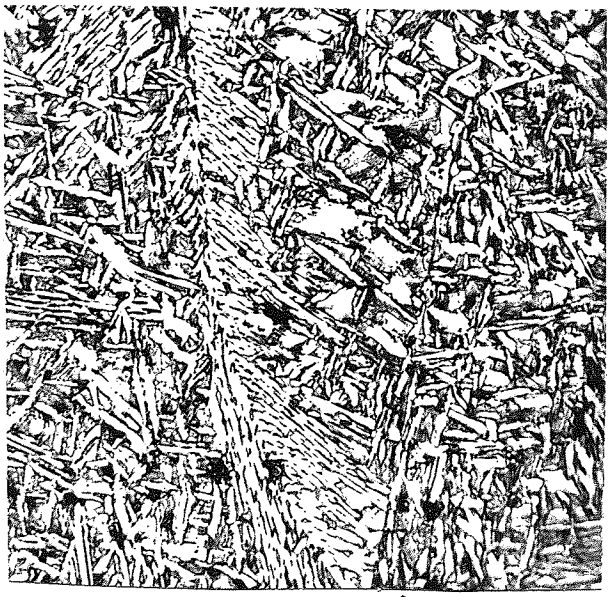

Figure 105
Simulated Sample
$\Delta t_{800-500}$ = 14 s
Nital II, X1000
Martensitic and upper bainitic structures
Curve V from CCT diagram.

Figure 106
Simulated Sample
$\Delta t_{800-500}$ = 954 s
Nital II, X200 structures representative of Curve XI from CCT diagram.

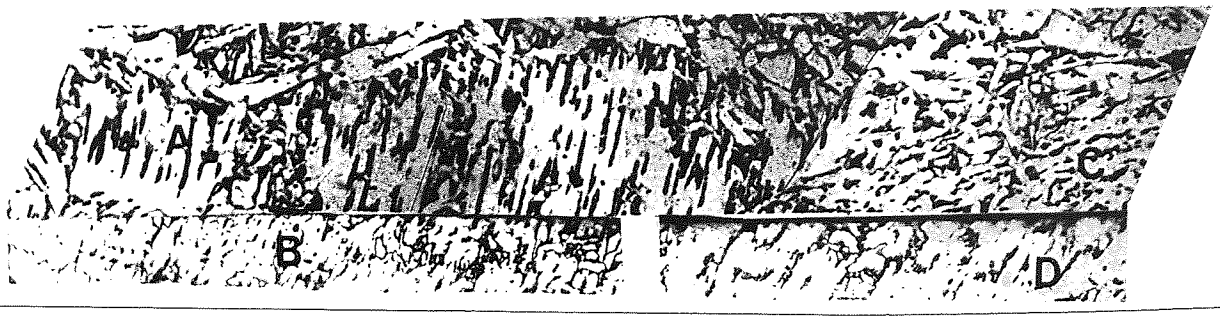

Figure 107
Lath Microstructure (upper bainite) - 90" views.
X600, after Levine and Hill (72).

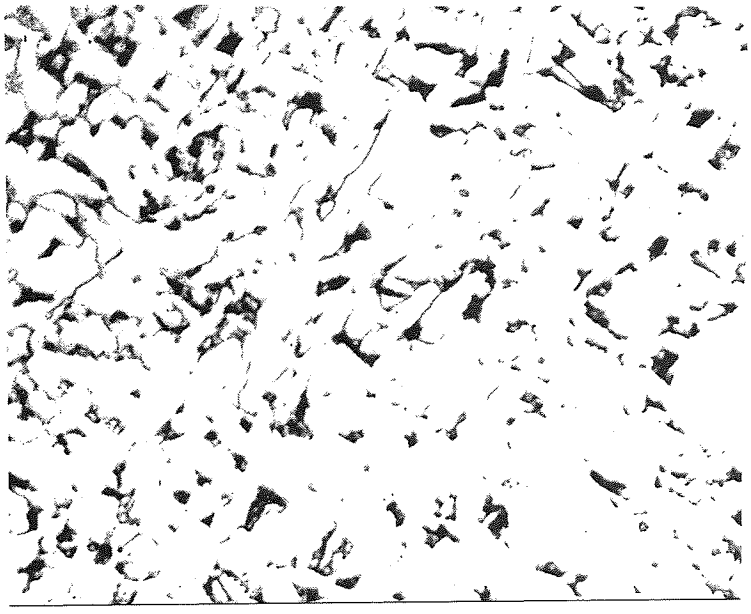

Figure 108
Interlocking acicular ferrite, X1700, after
Levine and Hill (72).

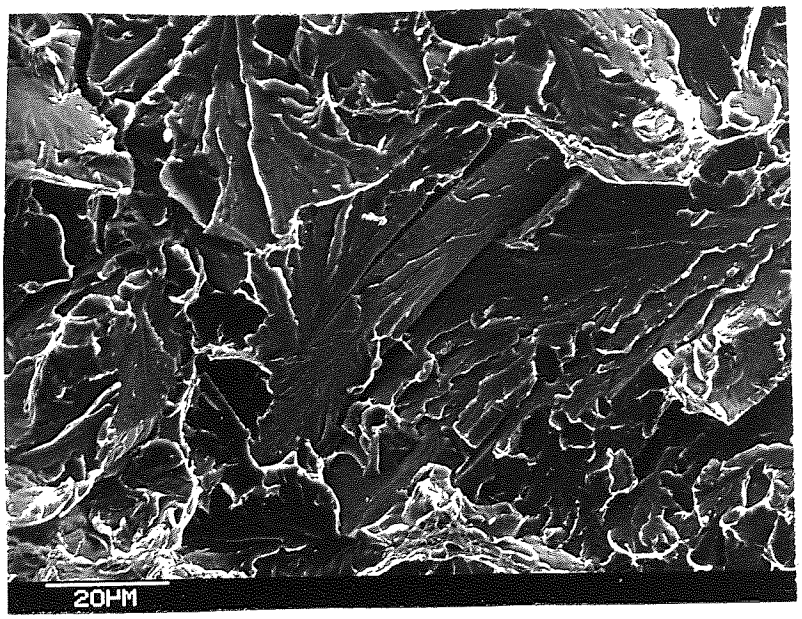

Figure 109
Simulated Sample
Heat Input = 14.4KJ/mm
Peak Temp. = 1400°C
Fractured at - 60°C

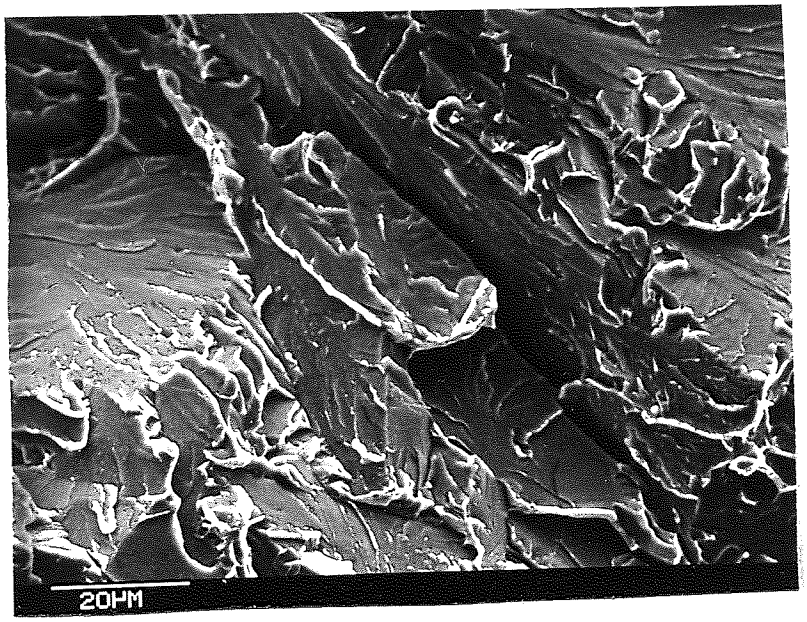

Figure 110
Simulated Sample
Heat Input = 14.4KJ/mm
Peak Temp. = 1250°C
Fractured at - 60°C

Figure 111
Simulated Sample
Heat Input = 14.4KJ/mm
Peak Temp. = 1150°C
Fractured at - 60°C

Figure 112
Simulated Sample
Heat Input = 14.4KJ/mm
Peak Temp. = 1000°C
Fractured at - 60°C

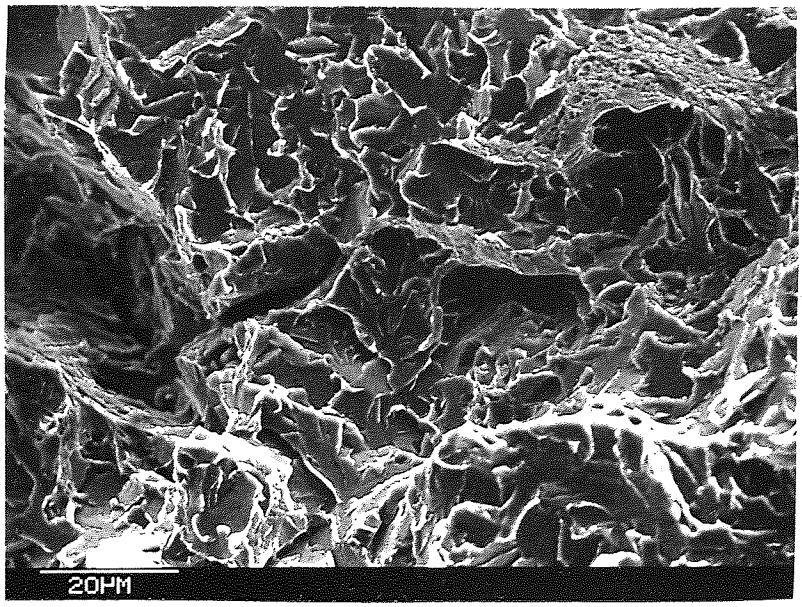

Figure 113
Simulated Sample
Heat Input = 14.4KJ/mm
Peak Temp. = 900°C
Fractured at - 55°C

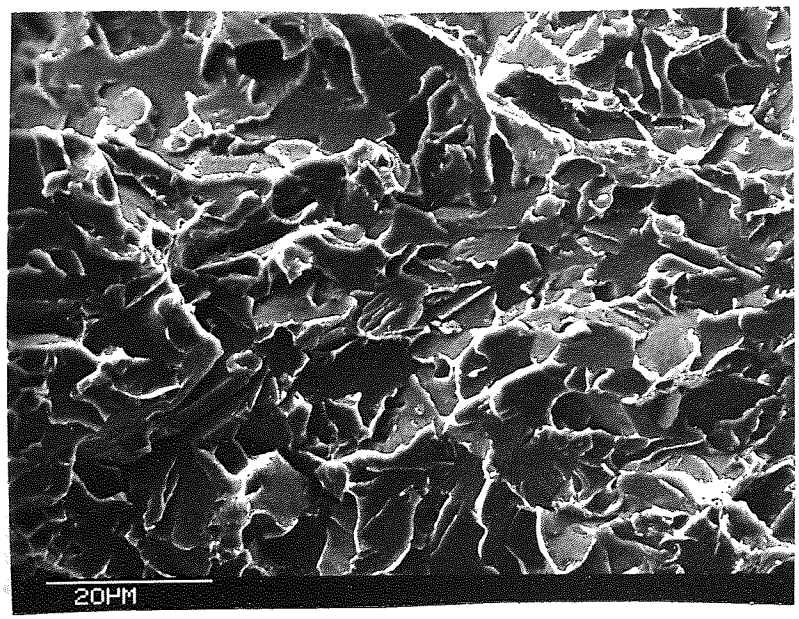

Figure 114
Simulated Sample
Heat Input = 14.4KJ/mm
Peak Temp. = 800°C
Fractured at - 55°C

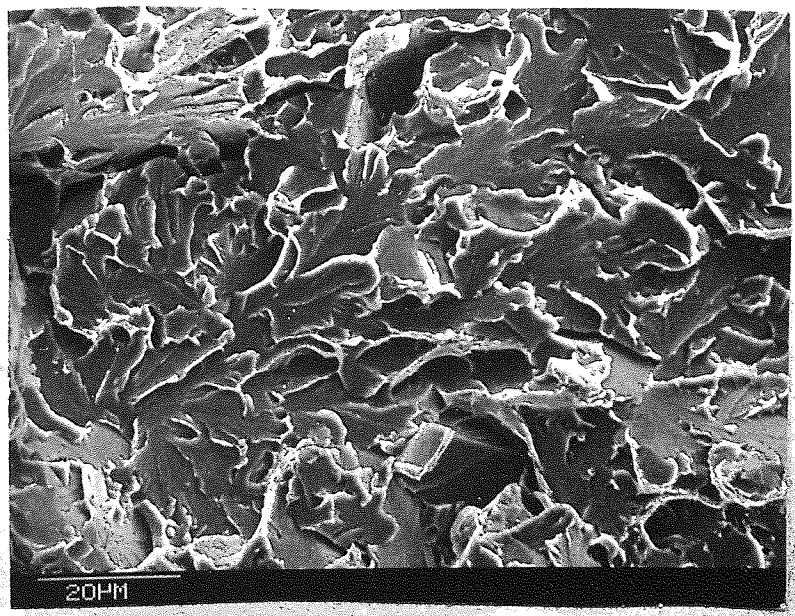

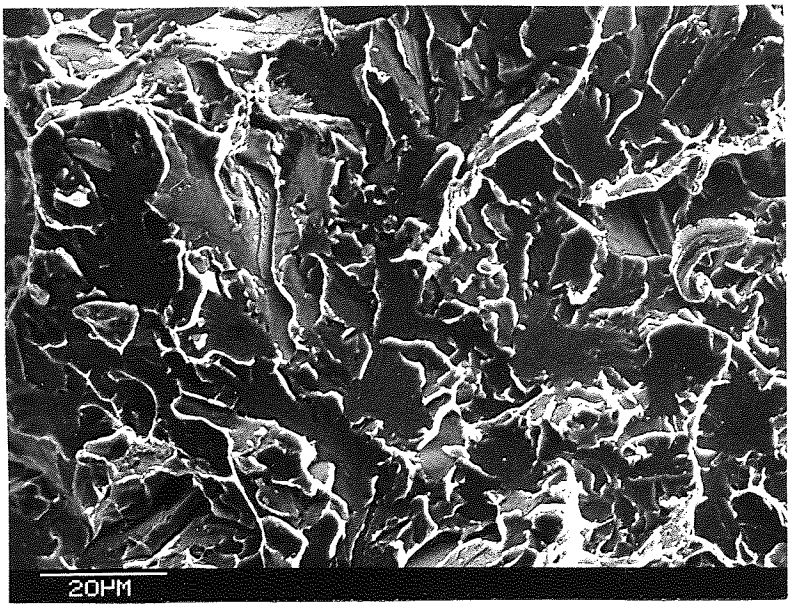

Figure 115
Simulated Sample
Heat Input = 14.4KJ/mm
Peak Temp. = 700°C
Fractured at - 55°C

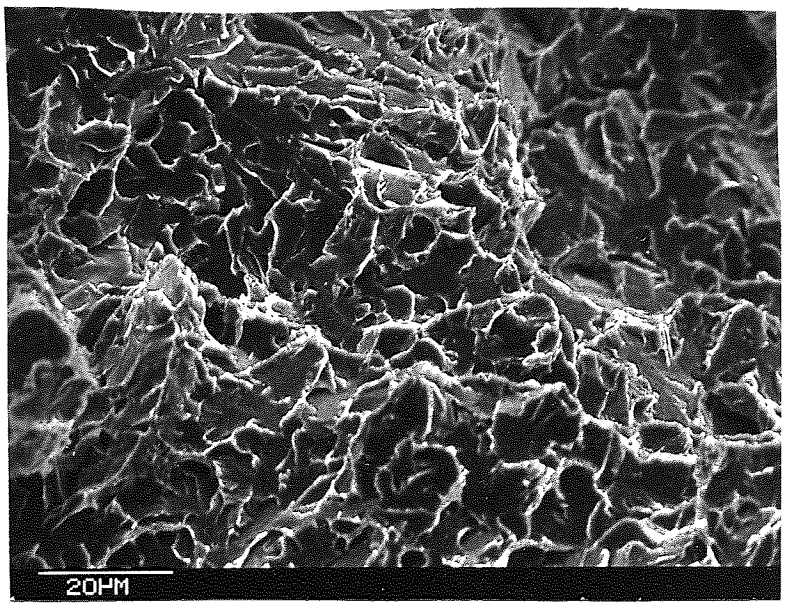

Figure 116
Simulated Sample
Heat Input = 6.3KJ/mm
Peak Temp. = 900°C
Fractured at - 55°C

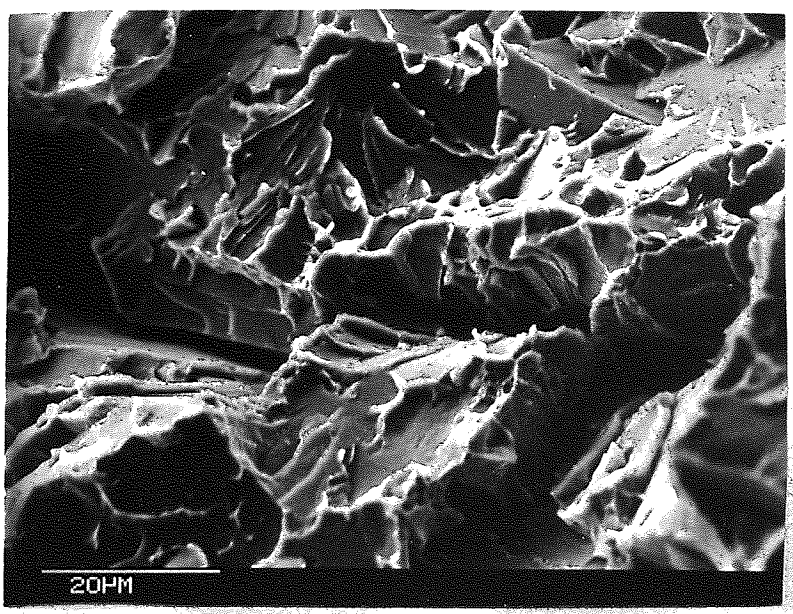

Figure 117
Base Metal
Fractured at - 56°C

Figure 118
Simulated Sample
Heat Input = 6.3KJ/mm
Peak Temp. = 1400°C
Fractured at - 35°C

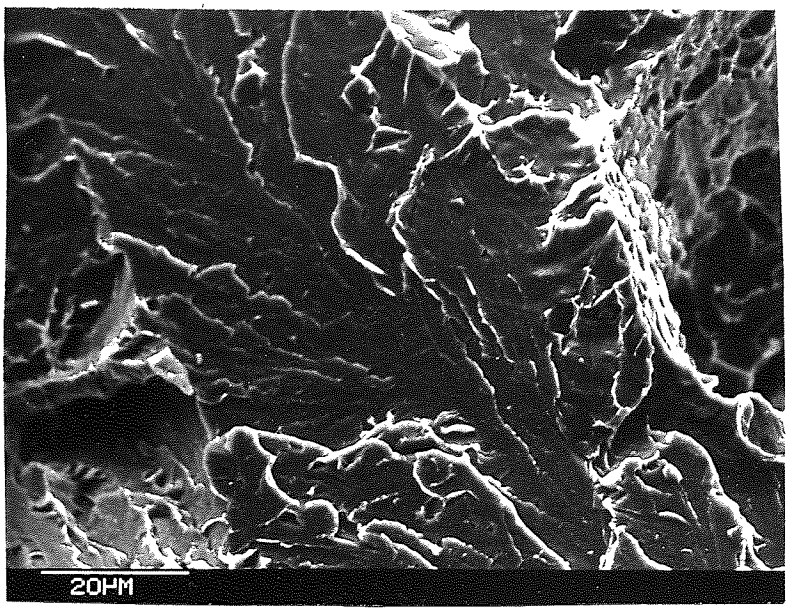

Figure 119
Simulated Sample
Heat Input = 6.3KJ/mm
Peak Temp. = 1250°C
Fractured at - 50°C

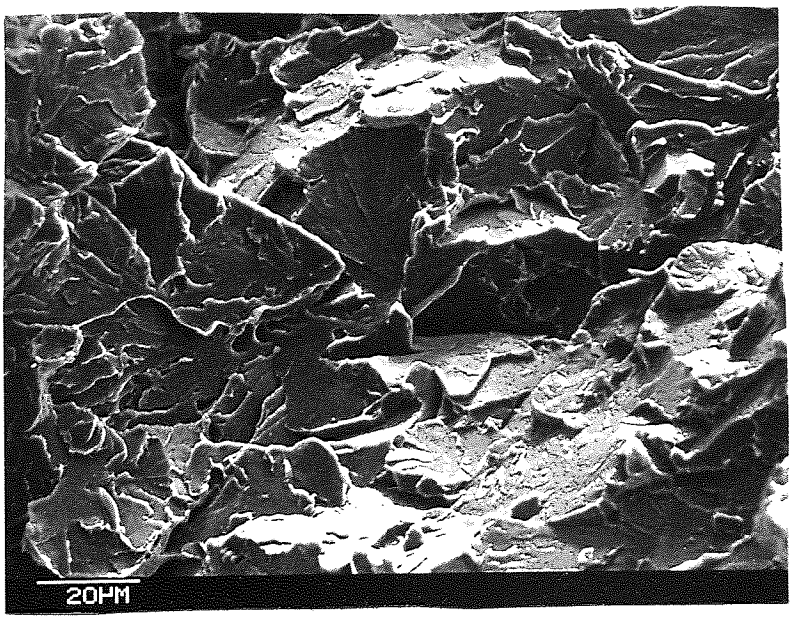

Figure 120
Simulated Sample
Heat Input = 6.3KJ/mm
Peak Temp. = 1150°C
Fractured at - 41°C

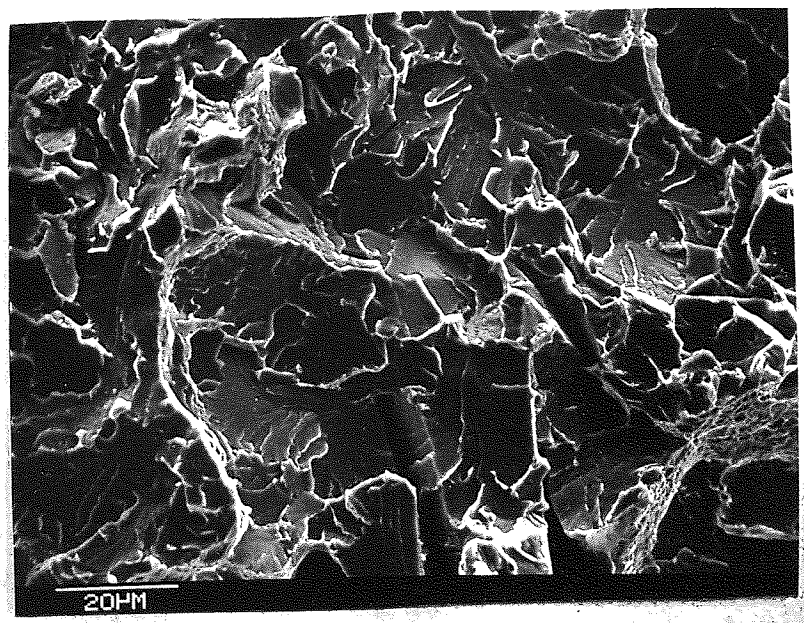

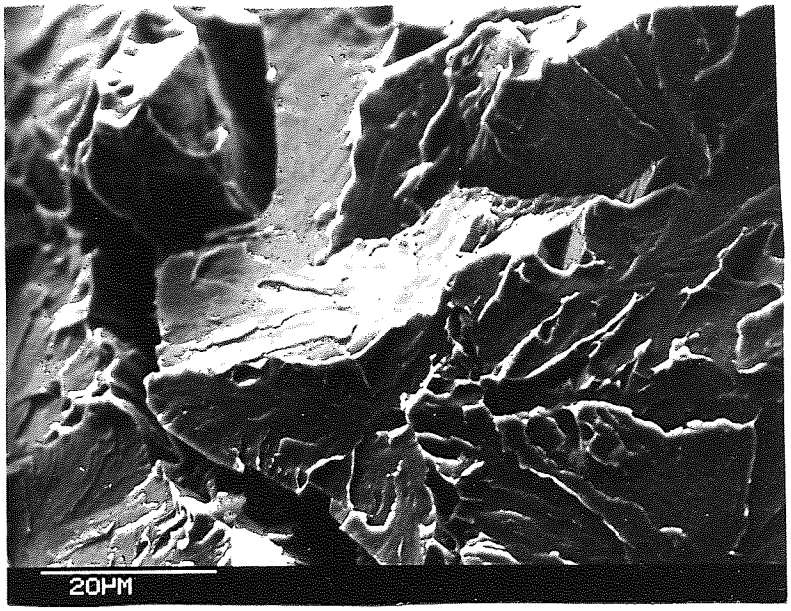

Figure 121
Simulated Sample
Heat Input = 3.6KJ/mm
Peak Temp. = 1400°C
Fractured at - 40°C

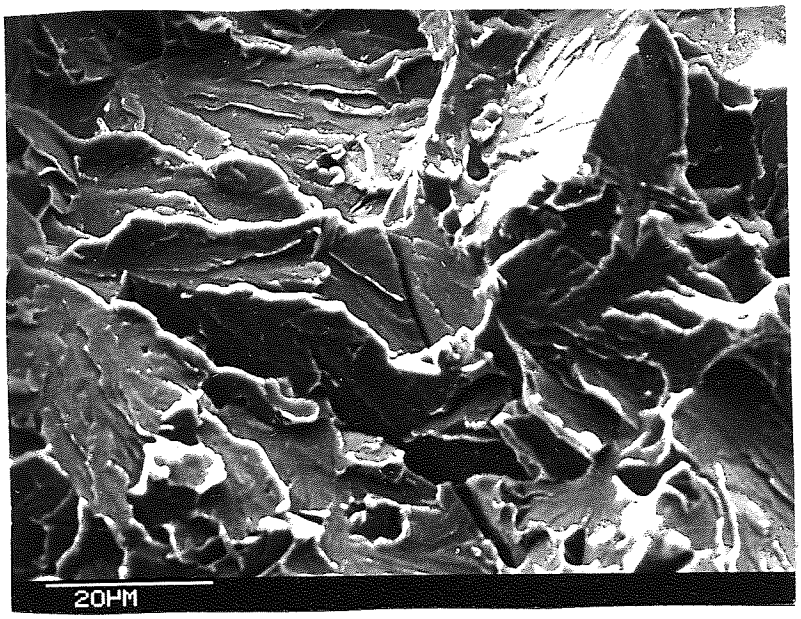

Figure 122
Simulated Sample
Heat Input = 3.6KJ/mm
Peak Temp. = 1250°C
Fractured at - 46°C

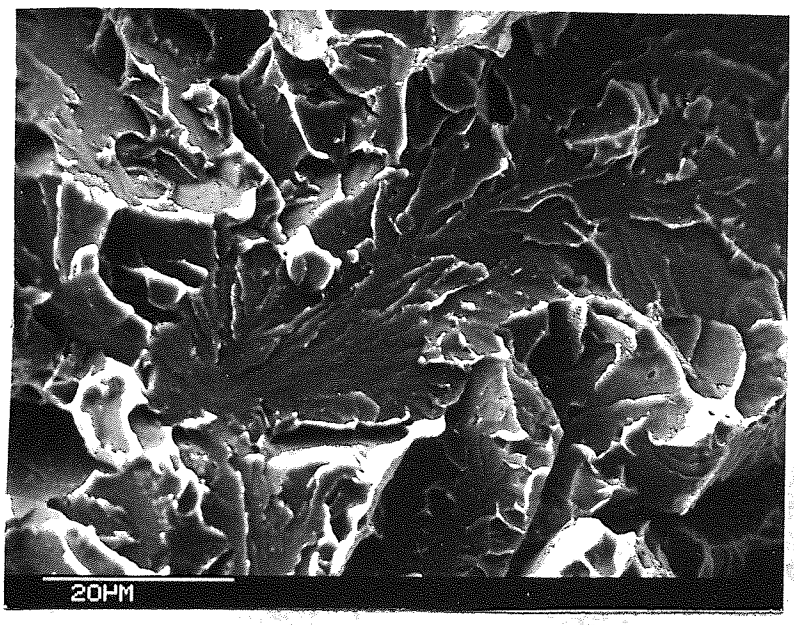

Figure 123
Simulated Sample
Heat Input = 3.6KJ/mm
Peak Temp. = 1150°C
Fractured at - 46°C

Figure 124
Base Metal
Heat treated at
600°C for one hour
Fractured at - 20°C

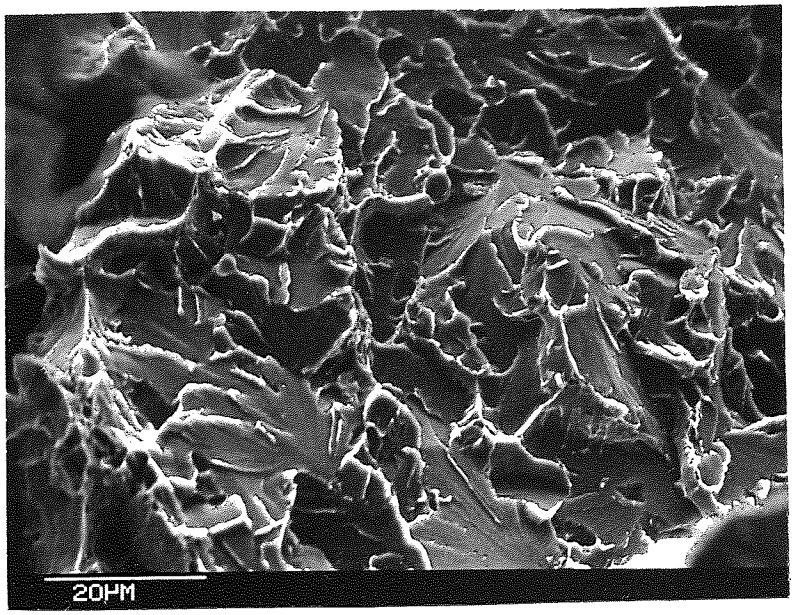

Figure 125
Simulated Sample
Heat Input = 14.4KJ/mm
Peak Temp. = 1250°C
Tempered for one hour
at 600°C. Fractured
at - 20°C. Note
possible temper
embrittlement at triple
point fracture facet.

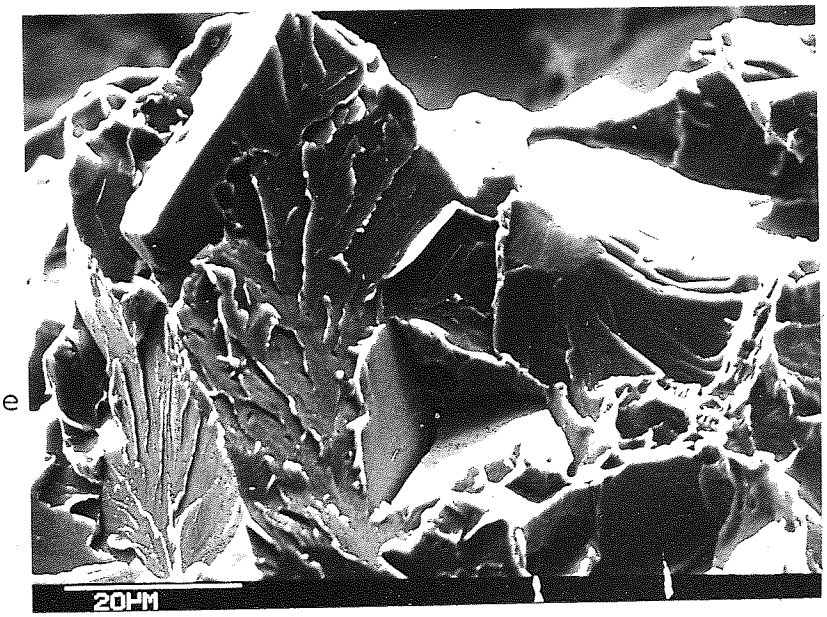

Figure 126
Real Weld HAZ
Coarse grained HAZ
Heat Input = 6.3KJ/mm
Fractured at - 40°C
Fracture crack inter-
rupted and changing
path at different
structures.

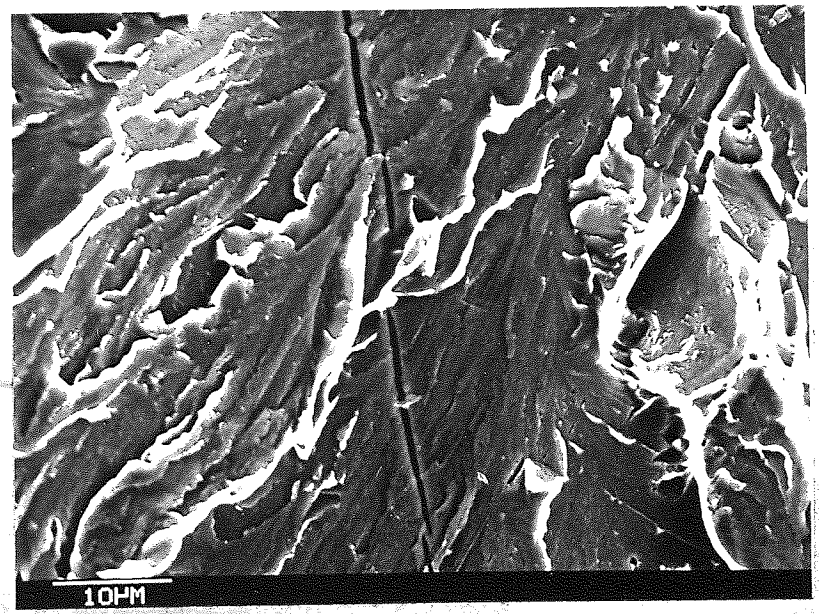

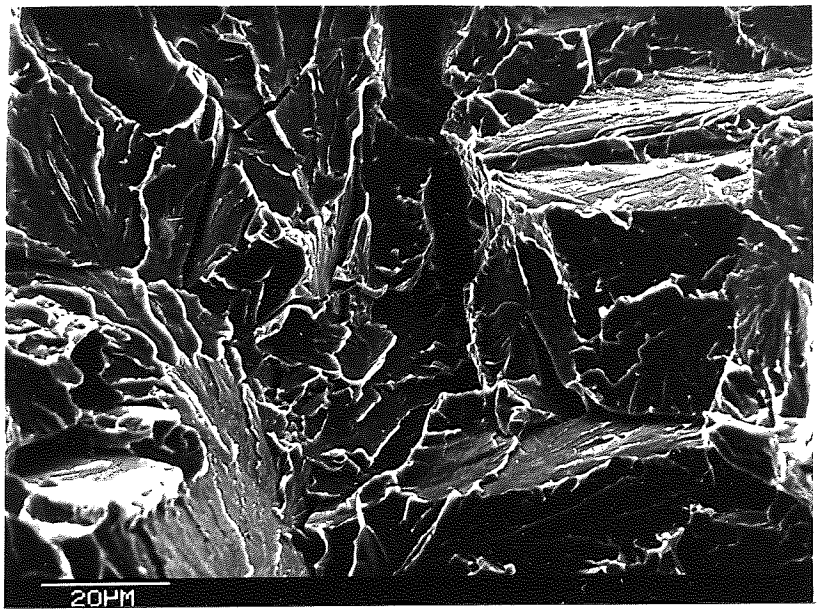

Figure 127
Real Weld HAZ
Coarse grained region
Heat Input = 6.3KJ/mm
Fractured at - 40°C

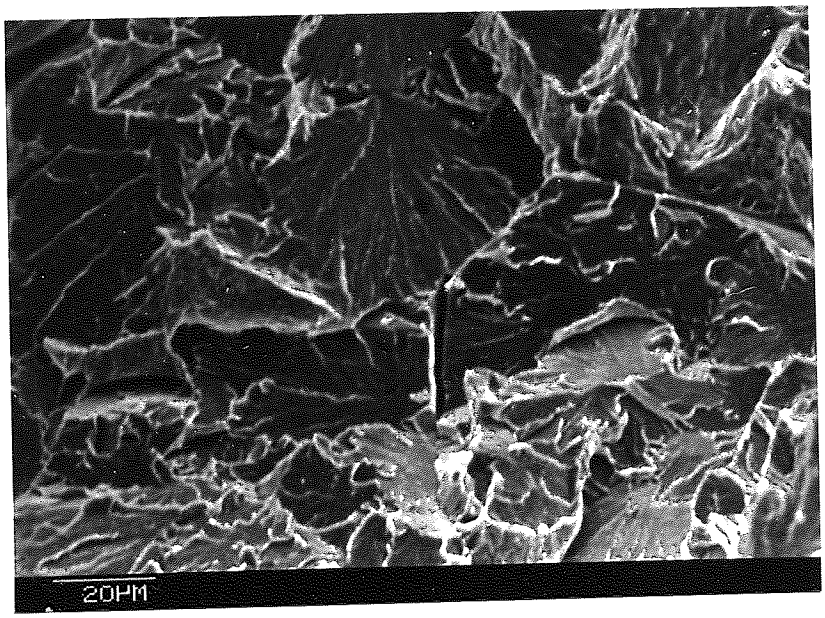

Figure 128
Real Weld HAZ
Coarse grained region
Heat Input = 3.6KJ/mm
Fractured at - 30°C

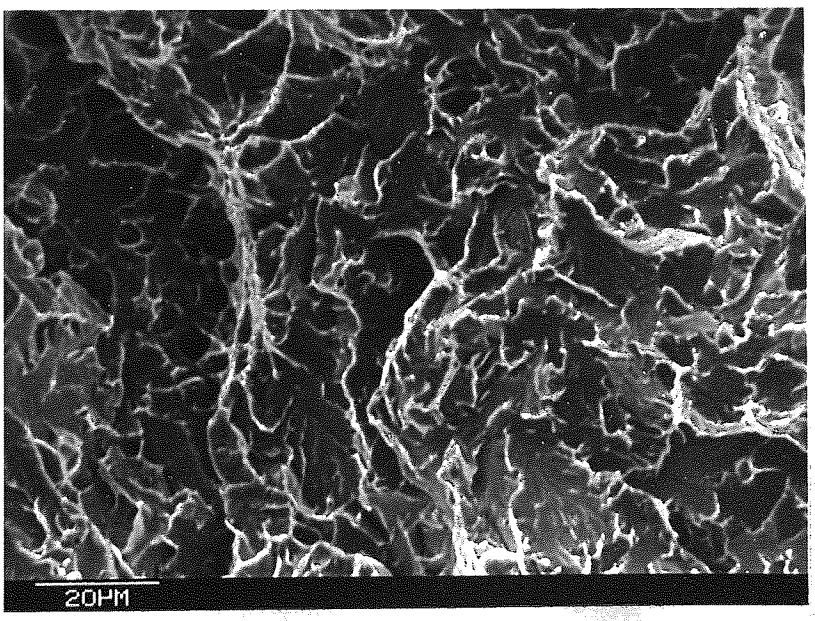

Figure 129
Real Weld HAZ
Fine grained region
Heat Input = 3.6KJ/mm
Fractured at - 30°C

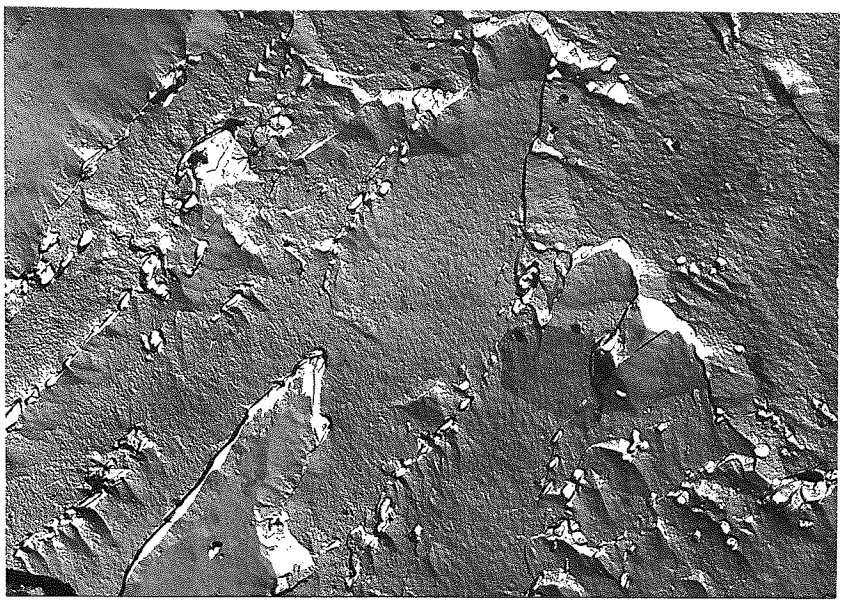

Figure 130
Simulated Sample
Double stage
shadowed replica
Heat Input = 3.6KJ/mm
Peak Temp. = 700°C
X5000
Carbide precipitation
at martensite tempered
needles.

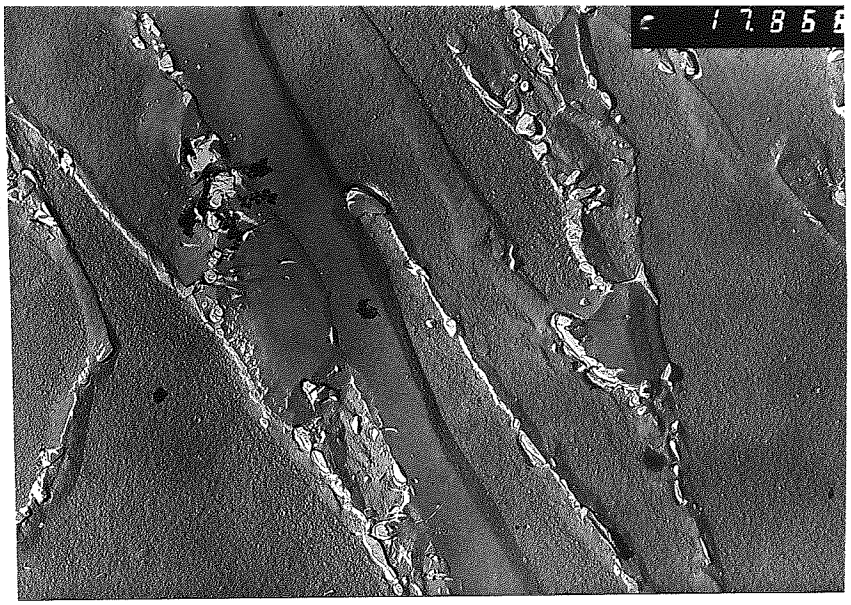

Figure 131
Base Metal
Double stage shadowed
replica
X5500
Carbide precipitation
at martensite tempered
needles.

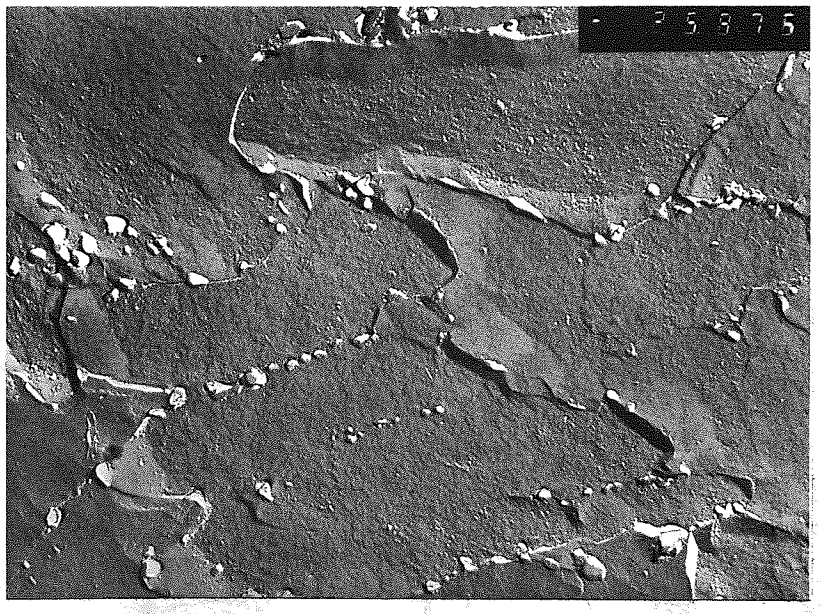

Figure 132
Base Metal
Tempered at 600°C for
one hour
Double stage shadowed
replica
X8300
Carbide precipitation
at martensite tempered
needles.

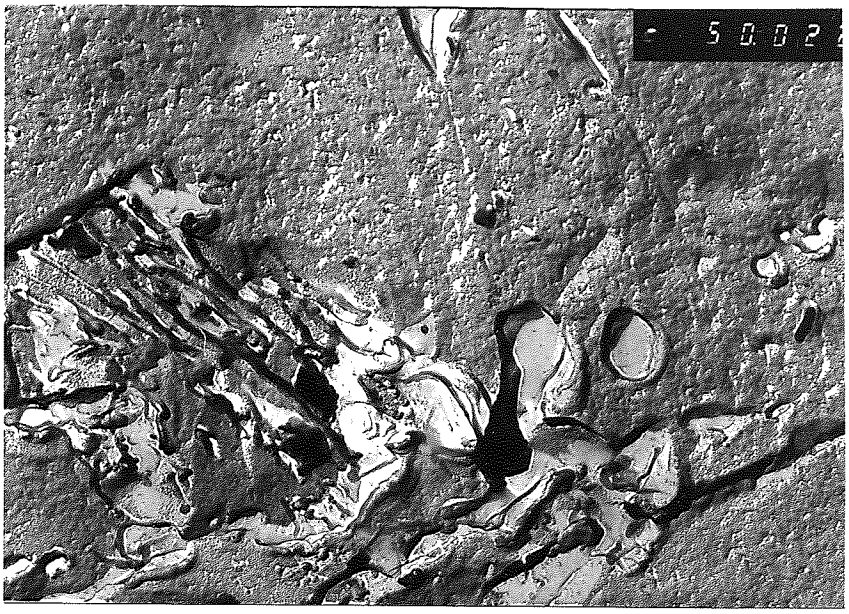

Figure 133
Simulated Sample
Double stage
shadowed replica
Heat Input = 6.3KJ/mm
Peak Temp. = 800°C
X16 600
Ferrite plus carbide
aggregates.

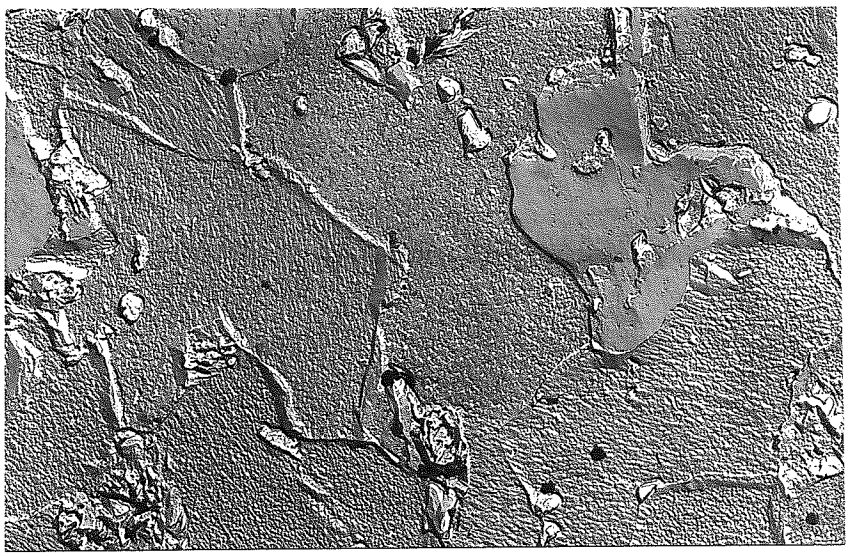

Figure 134
Simulated Sample
Double stage
shadowed replica
Heat Input = 6.3KJ/mm
Peak Temp. = 900°C
X5500
Intragranular carbides
and ferrite plus
carbide aggregates.

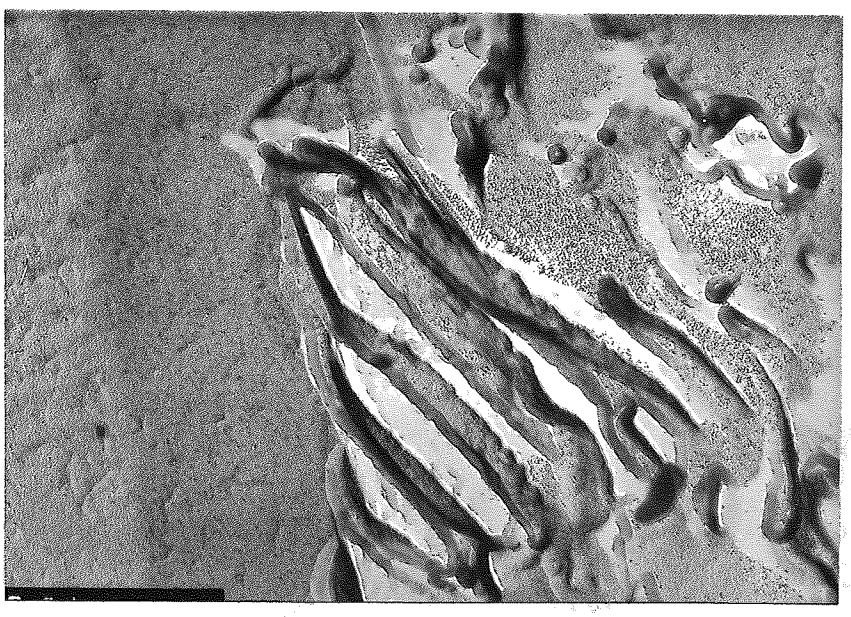

Figure 135
Simulated Sample
Double stage
shadowed replica
Heat Input = 14.4KJ/mm
Peak Temp. = 1000°C
X40 000
Ferrite plus carbide
aggregates tending
to pearlite
configuration.

Figure 136
Simulated Sample
Double stage shadowed replica
Heat Input = 3.6KJ/mm
Peak Temp. = 1150°C
X5500
Upper bainite and interlocking acicular ferrite.

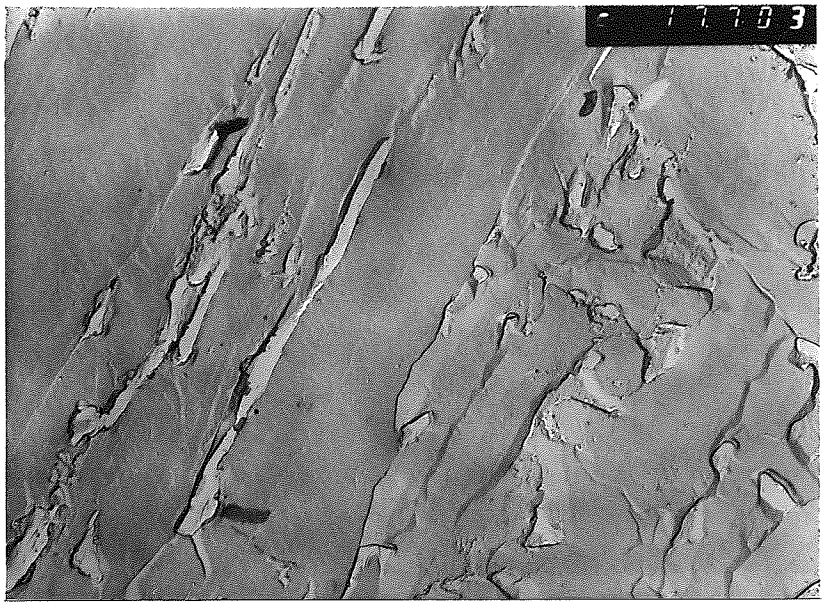

Figure 137
Simulated Sample
Double stage shadowed replica
Heat Input = 3.6KJ/mm
Peak Temp. = 1250°C
X5500
Upper bainite

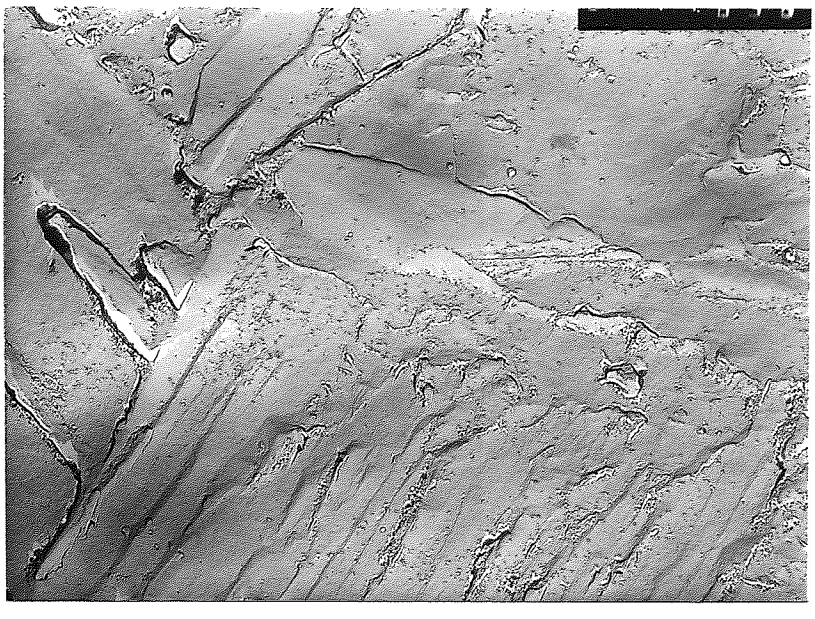

Figure 138
Simulated Sample
Double stage shadowed replica
Heat Input = 3.6KJ/mm
Peak Temp. = 1400°C
X6600
Interlocking acicular ferrite.

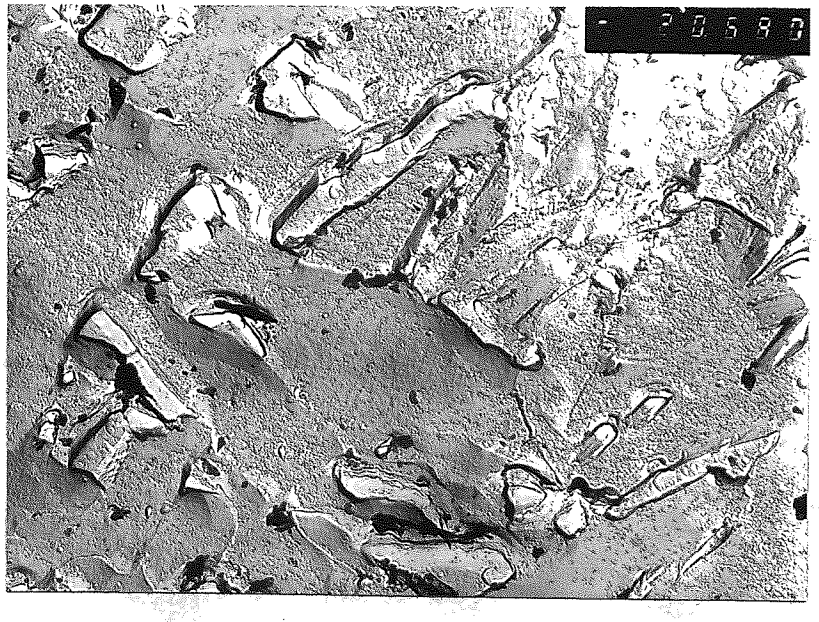

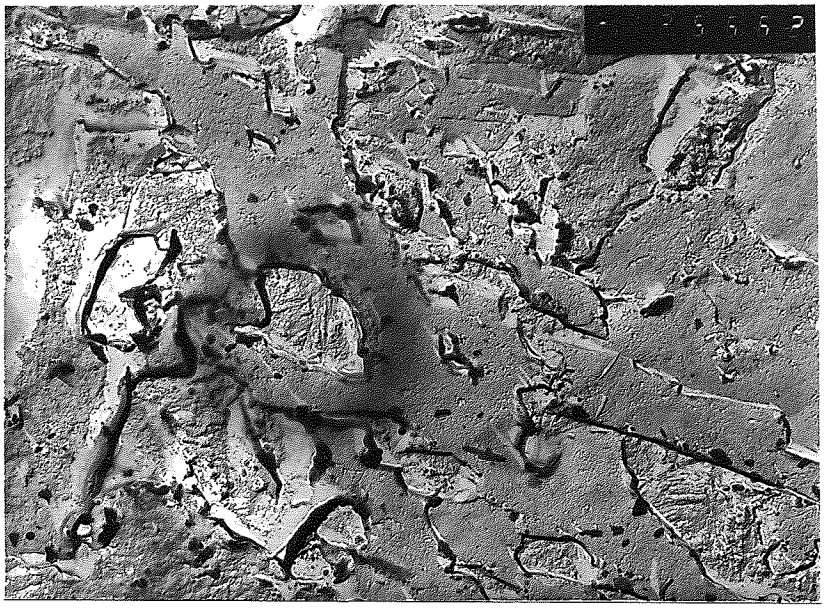

Figure 139
Simulated Sample
Double stage
shadowed replica
Heat Input = 6.3KJ/mm
Peak Temp. = 1150°C
X8300
Proeutectoid ferrite
and upper bainite.

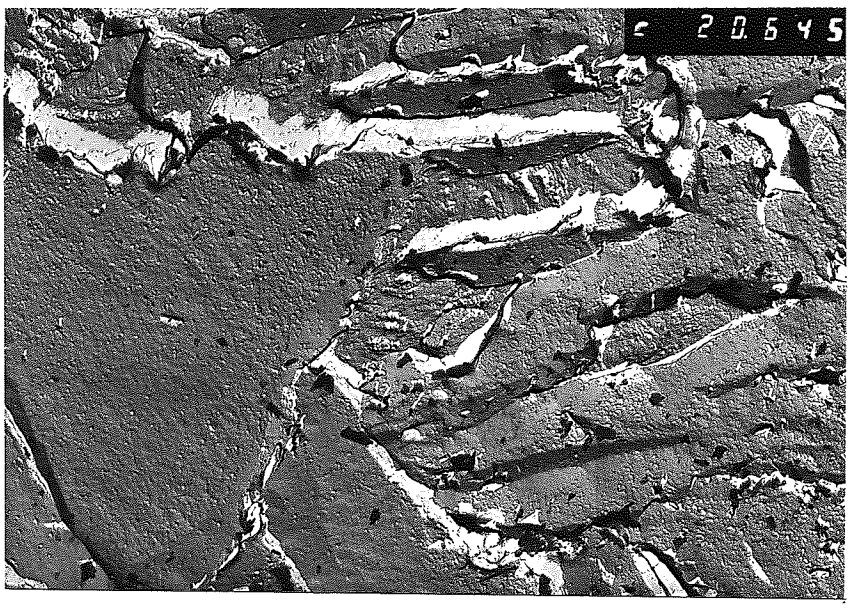

Figure 140
Simulated Sample
Double stage
shadowed replica
Heat Input = 6.3KJ/mm
Peak Temp. = 1250°C
X6600
Proeutectoid ferrite
and upper bainite.

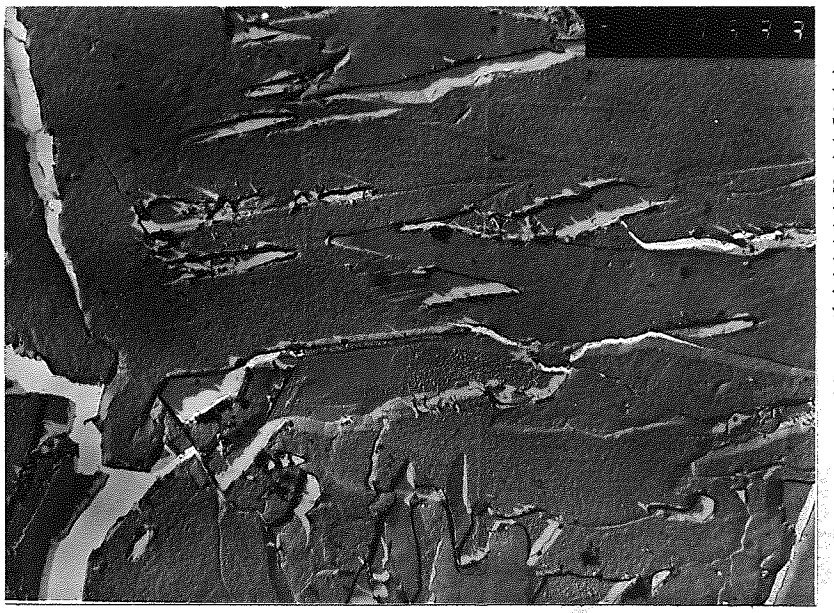

Figure 141
Simulated Sample
Double stage
shadowed replica
Heat Input = 6.3KJ/mm
Peak Temp. = 1400°C
X3300
Upper bainite and
interlocking acicular
ferrite.

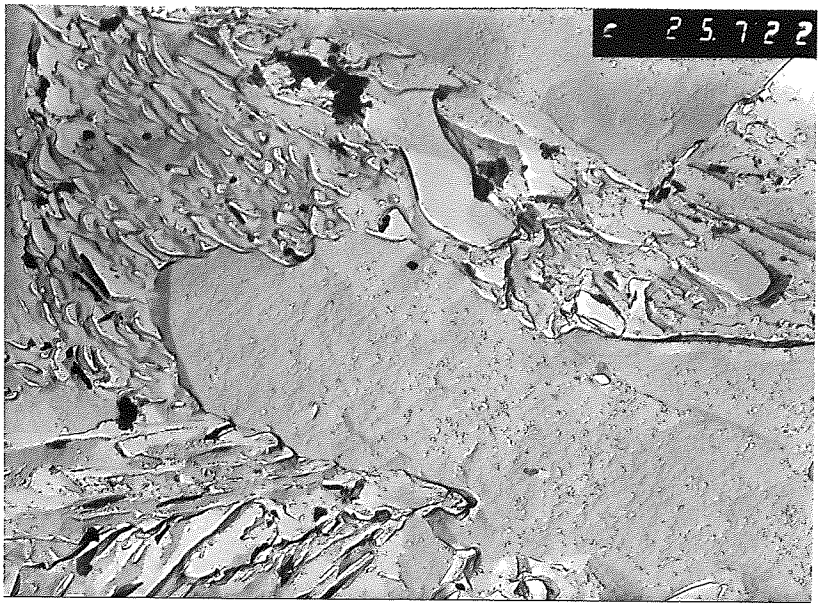

Figure 142
Simulated Sample
Double stage
shadowed replica
Heat Input = 14.4KJ/mm
Peak Temp. = 1150°C
X8300
Proeutectoid ferrite
and pearlite.

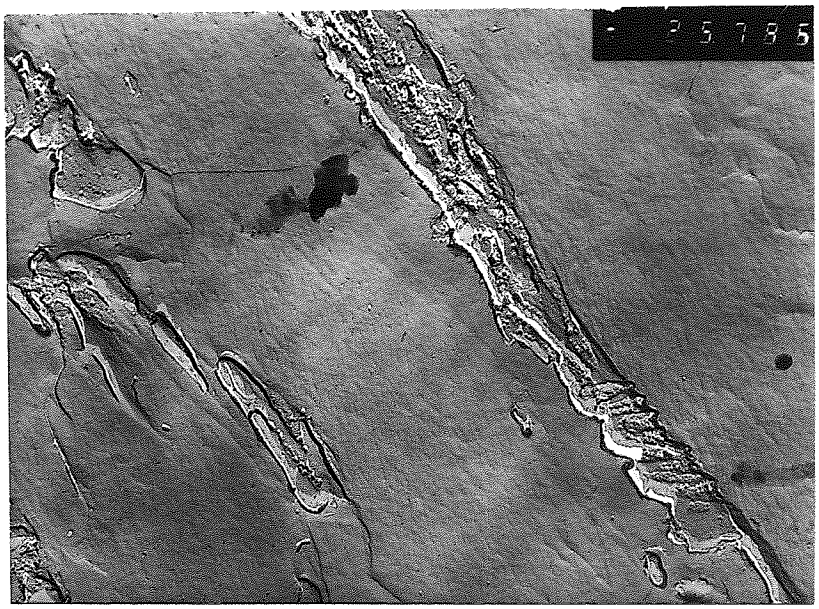

Figure 143
Simulated Sample
Double stage
shadowed replica
Heat Input = 14.4KJ/mm
Peak Temp. = 1250°C
X8300
Upper bainite.

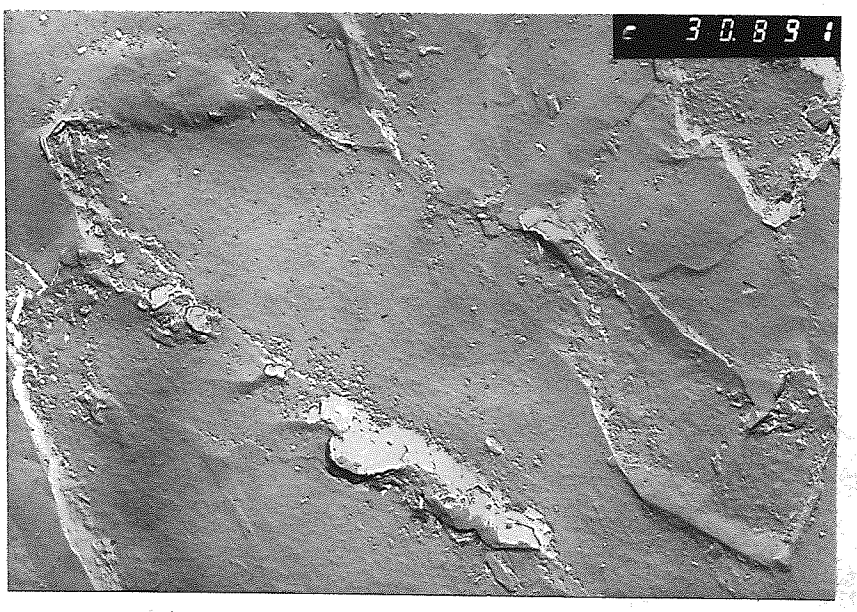

Figure 144
Simulated Sample
Double stage
shadowed replica
Heat Input = 14.4KJ/mm
Peak Temp. = 1250°C
Tempered at 600°C for
one hour
X 10 000
Bainitic ferrite laths.

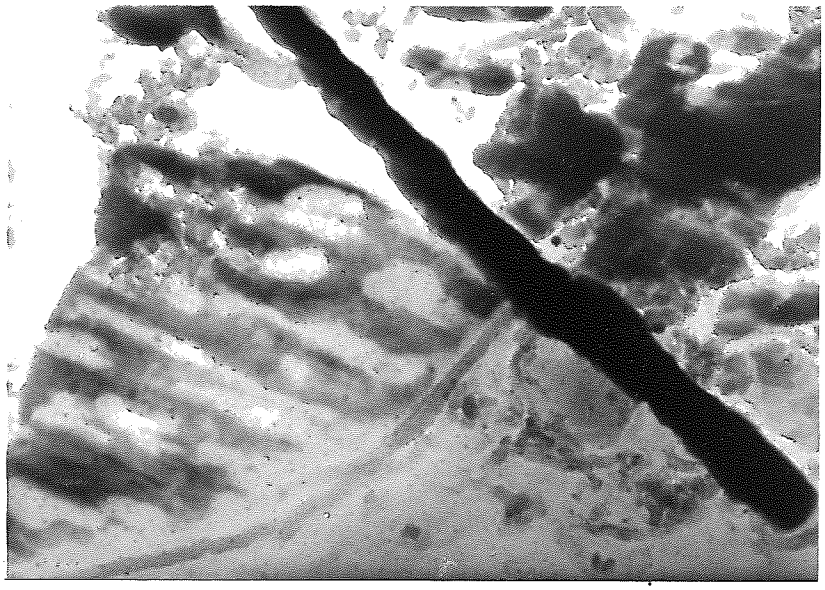

Figure 145

Carbide extracted from the 14.4KJ/mm - 1250°C HAZ heat treated for one hour at 600°C. Bright field, 70K.

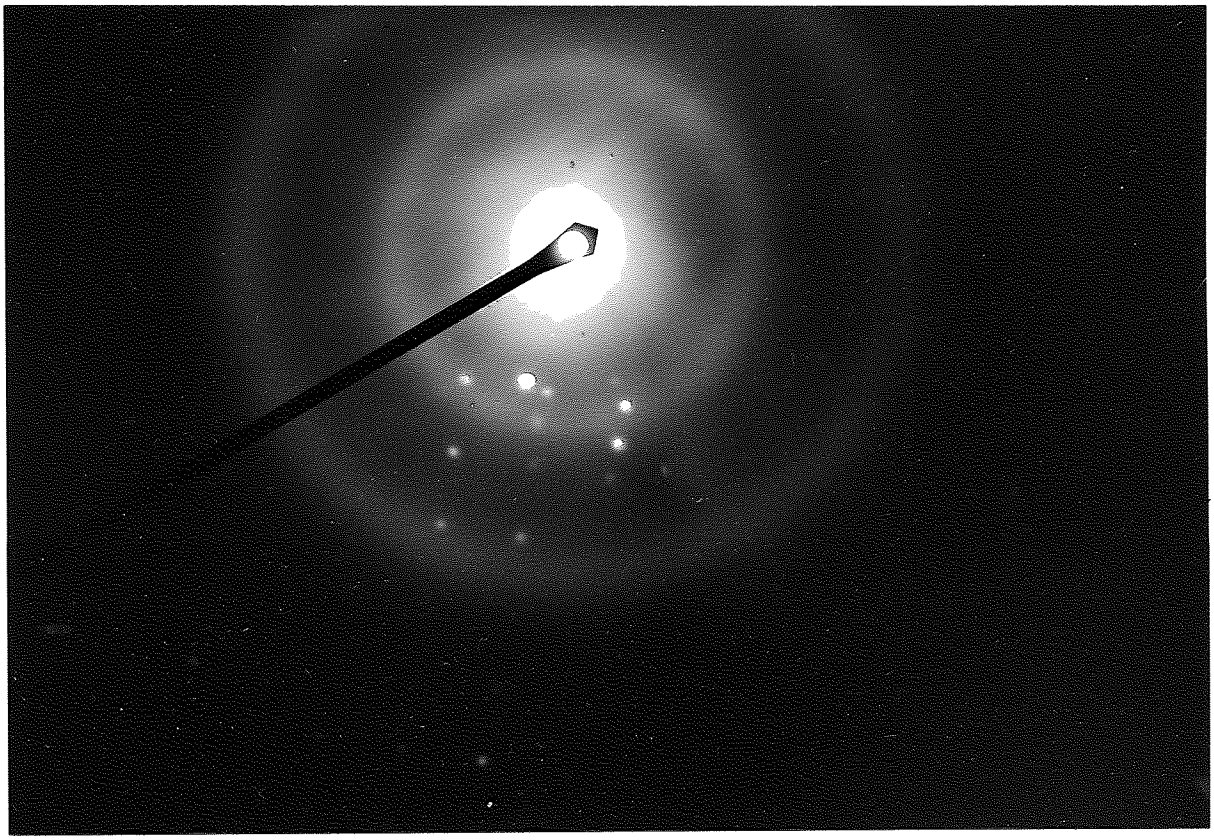

Figure 146

80KV, selected area diffraction pattern obtained from the carbide seen in figure 145.

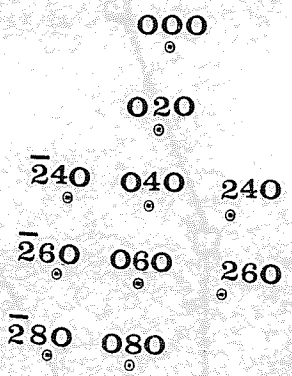

d spacings A^{o}

Plane	Measured	Fe_3C (Ref. 126)
260	0.780	0.794
240	1.108	1.109
280	0.604	0.612

Figure 147

Interpretation of the diffraction pattern of the figure 146, from the cementite particles of the figure 145.

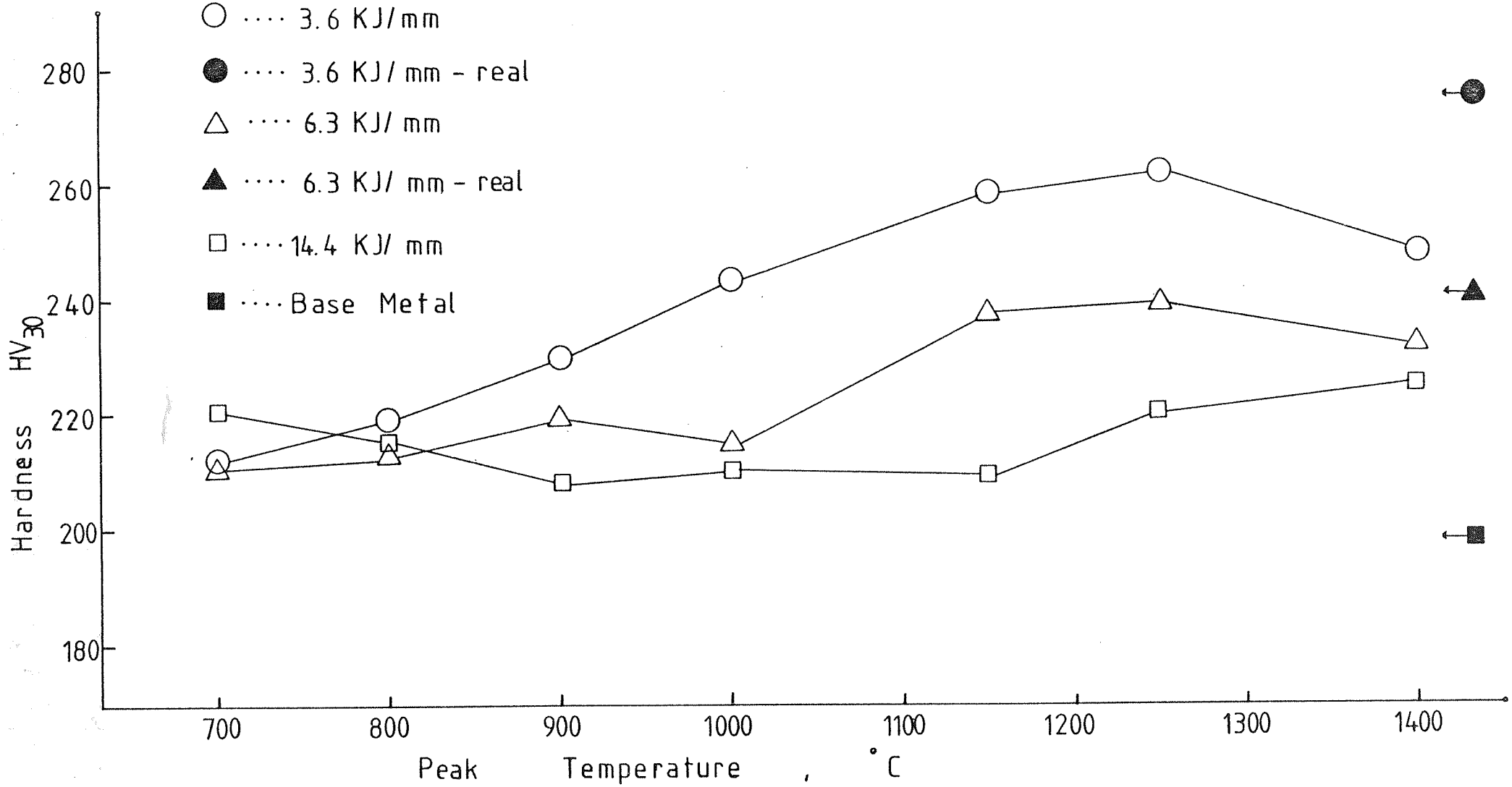

Figure 148 - Effect of the heat input and of the peak temperature on the hardness HV_{30} of the simulated specimens. The results for the actual welds and for the base metal are also represented for comparison.

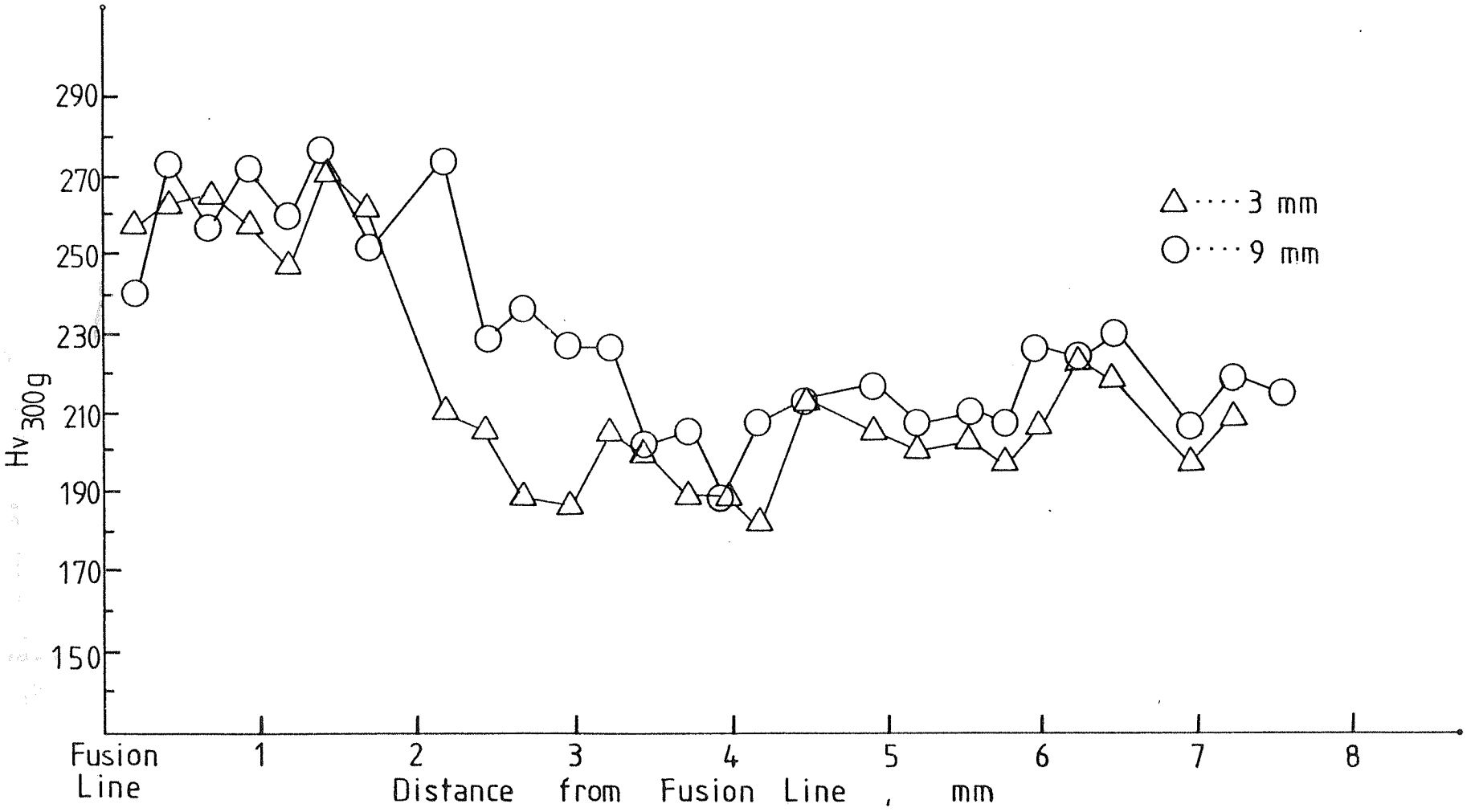

Figure 149 - Effect of the depth of the weld bead (3 and 9mm) and of the distance from the fusion line on the behaviour of the microhardness. HV_{300g} for the actual 3.6KJ/mm heat input weld condition.

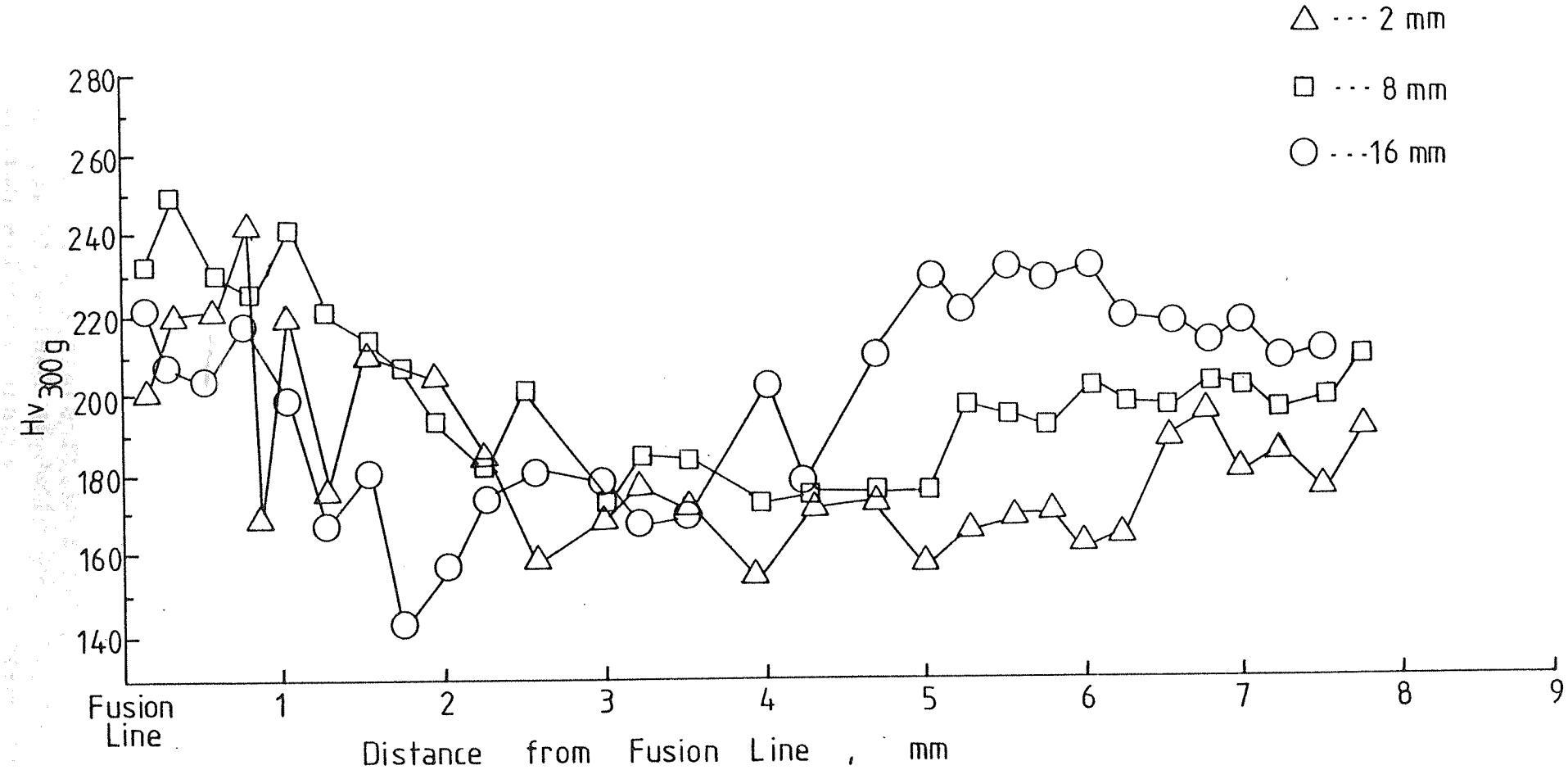

Figure 150 - Effect of the depth of the weld bead (2, 8 and 16mm) and of the distance from the fusion line on the behaviour of the microhardness HV_{300g} for the actual 6.3KJ/mm heat input weld condition.

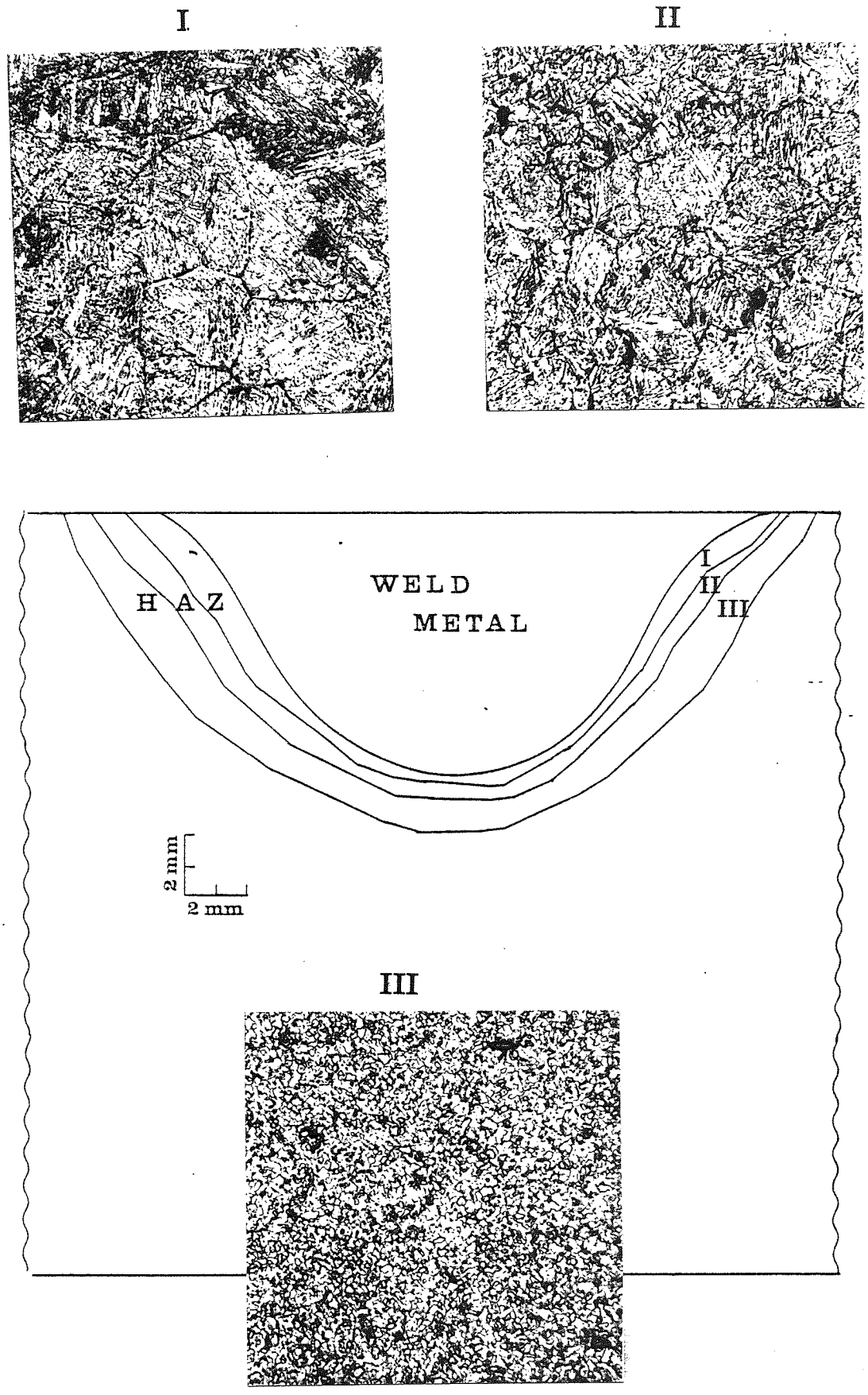

Figure 151

Qualitative differentiation of the regions of the actual HAZ welded at 3.6KJ/mm. (I) Coarse grained region - larger grains. (II) Coarse grained region - smaller grains. (III) Fine grained region.

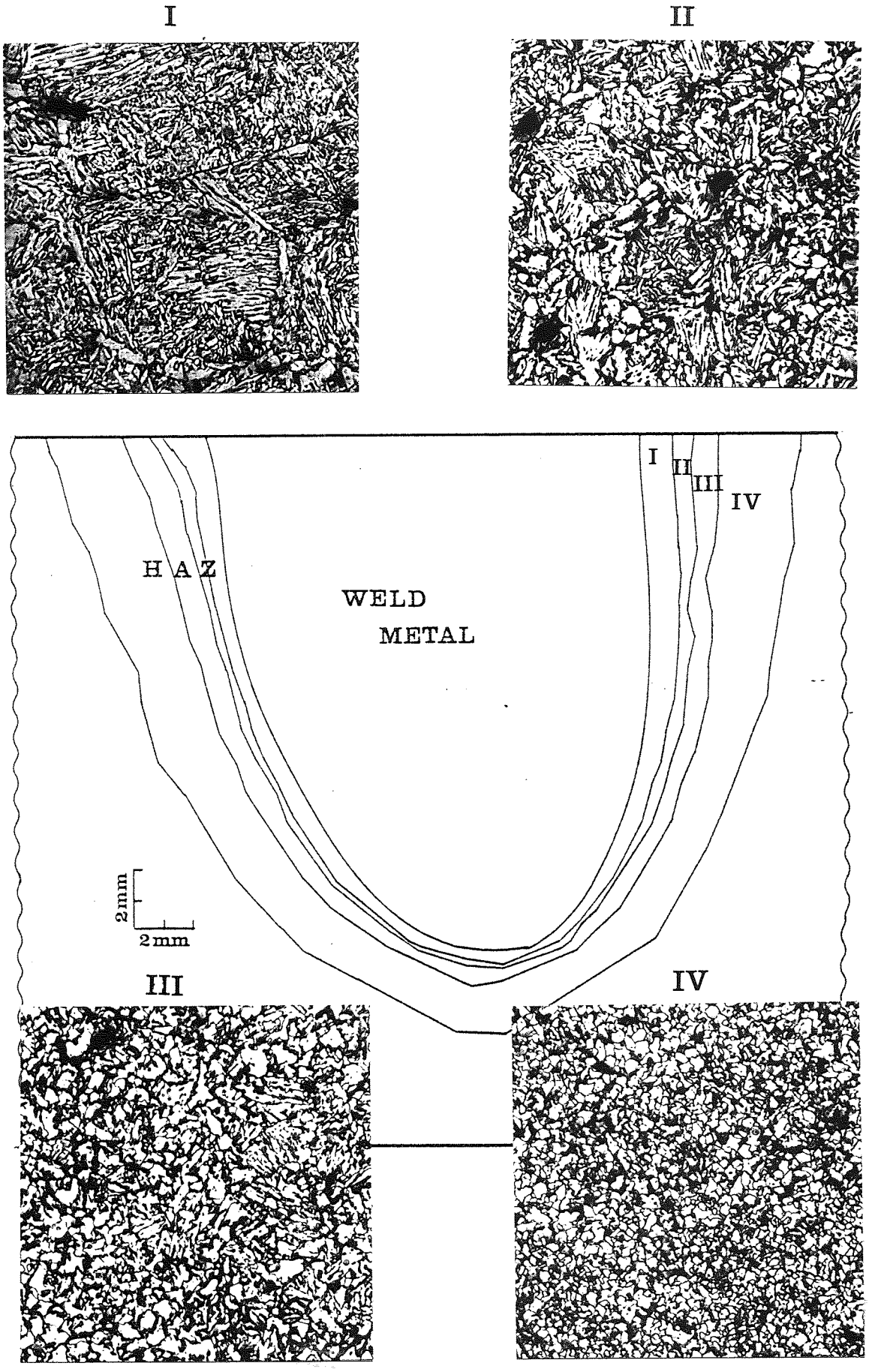

Figure 152

Qualitative differentiation of the regions of the actual HAZ welded at 6.3KJ/mm. (I) Coarse grained region - larger grains. (II) Coarse grained region - smaller grains. (III) Region of coarse platelets of proeutectoid ferrite. (IV) Fine grained region.

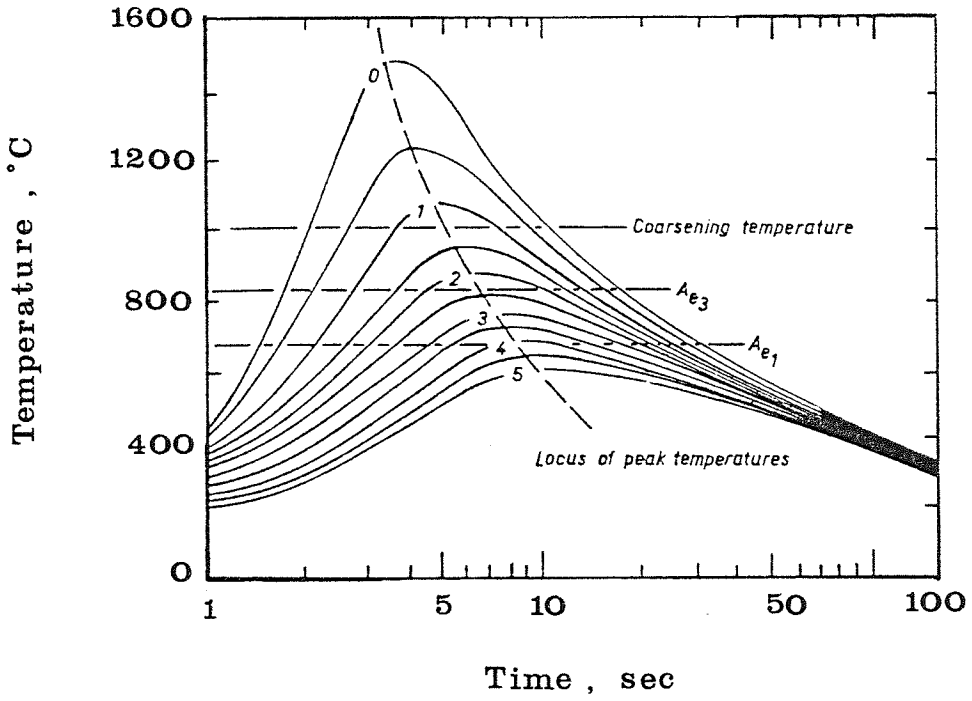

Figure 153 - Typical thermal cyles near an arc weld made with 2.75KJ/mm in 12mm steel plate (after Savage [117]).

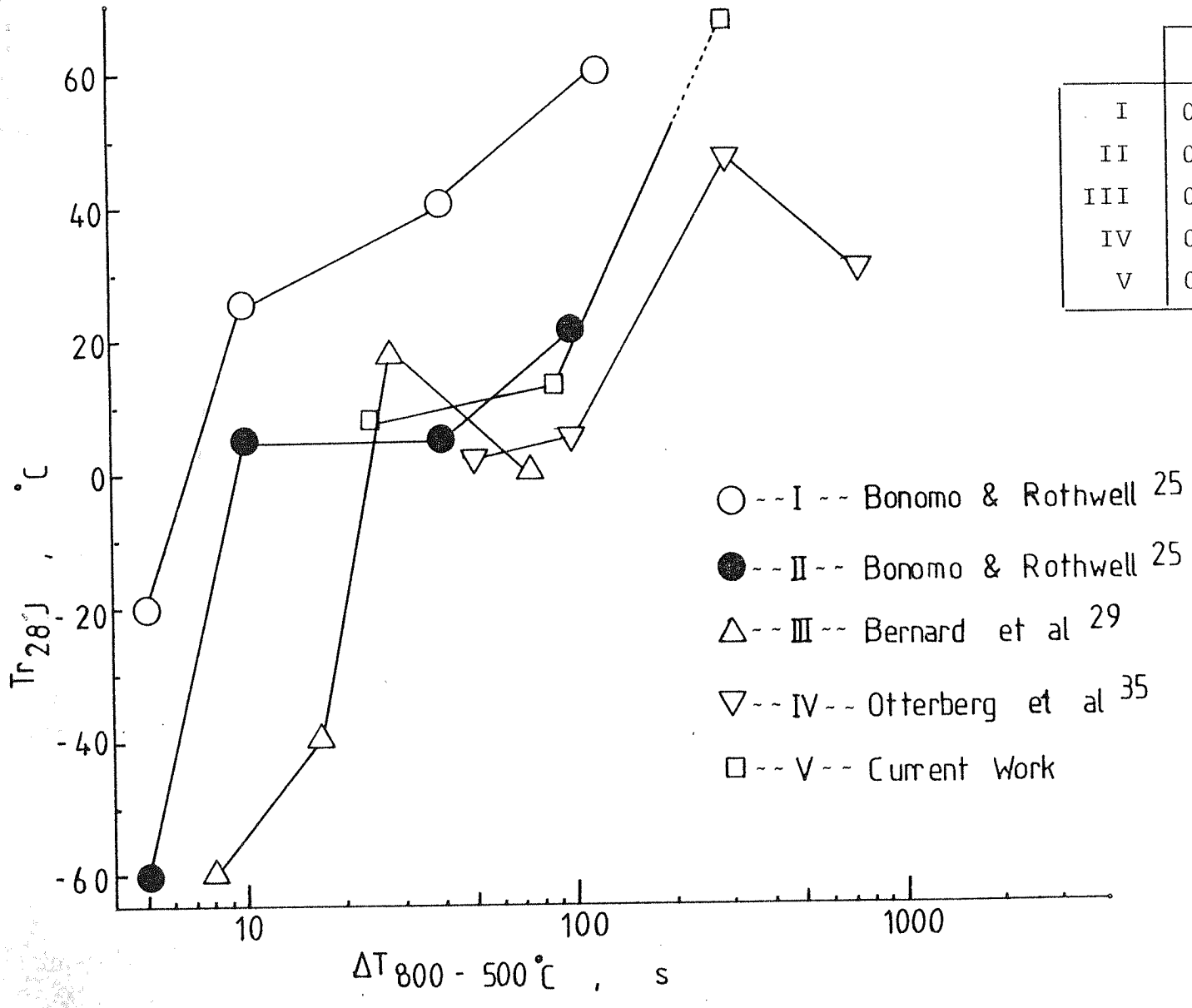

	C	Mn	Nb	V
I	0.16	1.32	0.047	0.1
II	0.16	1.26	0.05	0.006
III	0.12	1.53	0.031	-
IV	0.14	1.33	0.03	-
V	0.15	1.44	0.06	0.003

Figure 154 - Behaviour of the transition temperature associated with 28J of absorbed impact energy with the variation of the heat input. Results from several authors.

APPENDIX I - COMPUTING

APPENDIX I-1 - THEORETICAL CALCULATION OF THE COOLING TIME $\Delta t_{800-500}$

I-1.1 Introduction

It is the scope of the present appendix to relieve the body of the thesis from a considerable amount of information concerning the theoretical calculation of the distribution of temperatures on a plate caused by a welding source of energy. Had this part been included in the results, it might have proved to be a distraction. Here there will be an explanation why a mild steel computer program (1) was applied to the steel RQT-500 with no modifications. There will also be considerations on the choices made, and the approximations involved in the trial runs, A broad explanation on how to interpret the results output is given, and finally, a slight but time-saving improvement devised with the application of the graph plotter will be commented on.

I-1.2 Geometry Of The Model

The program VARIAB (1) is built up for temperature calculation by means of the finite difference technique, and the model used simulates a plate as work piece. Since the temperature distribution is symmetrical with respect to the vertical plane passing through the centreline of the weld, it is sufficient to calculate the temperature distribution for half of the model.

The volume elements of the model are small in the neighbourhood of the heat source, and larger at some distance from the

heat source. The total volume of small elements represents the so called inner zone, whereas the volume consisting of the large elements is referred to as the outer zone. At the boundary of the two zones, there is some overlapping of their elements.

The temperature points are always located in the middle of the volume elements. For the inner zone, they are three-dimensional, named $T_{i,j,k}$ and are distant from each other by Δh, Δb, and Δl, whereas for the outer zone they are two-dimensional, denominated $F_{j,k}$ and separated from each other by 3 Δb and 3 Δl. Figure 1' helps the explanation.

I-1.3 Numerical Temperature Calculations With Temperature Dependent Material Properties

The general three-dimensional differential equation for heat conduction in a solid body is :

$$c\,\gamma\,\frac{\partial T}{\partial t} = \frac{\partial}{\partial x}\left(k\,\frac{\partial T}{\partial x}\right) + \frac{\partial}{\partial y}\left(k\,\frac{\partial T}{\partial y}\right) + \frac{\partial}{\partial z}\left(k\,\frac{\partial T}{\partial z}\right) + \dot{W}\ (\mathrm{cal/cm^3 s}) \qquad [1]$$

but the use of eq. [1] for numerical calculations is inadequate and to avoid difficulties, two variables ϕ and H, which equations are seen below :

$$\phi = \int_0^T \frac{k}{ko}\,dT \qquad [2] \qquad \text{and} \qquad H = \int_0^T c\,dT \qquad [3]$$

are introduced into that equation under the following form (2) :

$$k = ko \frac{d\phi}{dT} \quad [4] \qquad \text{and} \quad c = \frac{dH}{dT} \quad [5]$$

and after the substitution eq. [1] becomes

$$\frac{dH}{dT} = \frac{ko}{\gamma} \left(\frac{\partial^2 \phi}{\partial x^2} + \frac{\partial^2 \phi}{\partial y^2} + \frac{\partial^2 \phi}{\partial z^2} \right) + \frac{\dot{W}}{\gamma} \qquad [6]$$

With the finite differences eq. [6] can be expressed in the following way :

$$H_1 = H_{i,j,k} + \frac{\Delta W}{\gamma} + \frac{k_o \cdot \Delta t}{\gamma} \left(\frac{\phi_{i+1,j,k} + \phi_{i-1,j,k} - 2\phi_{i,j,k}}{\Delta h^2} + \frac{\phi_{i,j+1,k} + \phi_{i,j-1,k} - 2\phi_{i,j,k}}{\Delta b^2} + \frac{\phi_{i,j,k+1} + \phi_{i,j,k-1} - 2\phi_{i,j,k}}{\Delta l^2} \right) \qquad [7]$$

To perform the substitutions of the variables ϕ and H, the equations [2] and [3] must be known, consequently the mode of variable of k and c with the temperature, for a specific material, must be obtained from practical measurements. Now appears the first problem, these parameters are not of simple determination and usually are not available for temperatures as high as the ones attained in a welding process.

The RQT-500 data for k and c was obtained for temperatures up to 900°C (3) and can be seen from tables I and II, whereas their graphical representation is observed from the points in figures 2' and 3'. With the help of a Hewlett Packard 9810 Desk Calculator, regression analysis was applied to this data and the results will be presented as follows :

I-1.3.1 Modified Temperature ø

The curve for the modified temperature can be obtained from eq. [2] and the curves of the function k = f (T) were obtained by regression analysis applied on the data of table I, whose curve plotting can also be seen from figure 2', and are mathematically expressed in the following way :

$k = 0.11$ for $T \leqslant 150^{\circ}C$

$k = 0.1193761905 - 0.6142857143 \times 10^{-4} \times T$ for $150 < T \leqslant 820^{\circ}C$

$k = 0.199 - 0.16 \times 10^{-3} \times T$ for $820 < T \leqslant 850^{\circ}C$

$k = 0.46 \times 10^{-1} + 0.2 \times 10^{-4} \times T$ for $850 < T \leqslant 900^{\circ}C$

Substituting these curves in the integral of eq. [2], with the omission of the first curve to simplify the calculations only introducing an insignificant error, we will have :

$$\phi = \frac{1}{0.11}\left\{\left[0.1193761905 \times T - \frac{1}{2}\ 0.6142857143 \times 10^{-4} \times T^2\right]_0^{820} + \left[0.199 \times T - \frac{1}{2}\ 0.16 \times 10^{-3} \times T^2\right]_{820}^{850} + \left[0.46 \times 10^{-1} \times T + \frac{1}{2}\ 0.2 \times 10^{-4} \times T^2\right]_{850}^{900}\right\}$$

and the results of the calculation can be seen in table III and the graphical representation from figure 4'.

I-1.3.2 Heat Content H (Cal/g)

The curve for the heat content H can be obtained from eq. [3]

and the curves of the function c = f' (T) were obtained by regression analysis applied on the data of table II, whose curve plotting can also be seen from figure 3', and are mathematically expresses in the following way :

$$c = 0.1146143856 + 0.337662377 \times 10^{-5} \times T + 0.1798201798 \times 10^{-6} \times T^2 \quad \text{for } T \leqslant 675^{\circ}C$$

$$c = 0.17855 \times 10 + 0.294 \times 10^{-2} \times T \quad \text{for } 675 < T \leqslant 725^{\circ}C$$

$$c = 0.105826375 \times 10^{2} - 0.24634 \times 10^{-1} \times T + 0.145 \times 10^{-4} \times T^2 \quad \text{for } 725 < T \leqslant 875^{\circ}C$$

Substituting these curves in the integral of eq. [3], we will have :

$$H = \left[0.1146143856 \times T + \frac{1}{2} 0.337662377 \times 10^{-5} \times T^2 + \frac{1}{3} 0.1798201798 \times 10^{-6} \times T^3 \right]_{0}^{675} + \left[0.17855 \times 10 \times T + \frac{1}{2} 0.294 \times 10^{-2} \times T^2 \right]_{675}^{725} + \left[0.105826375 \times 10^{2} \times T - \frac{1}{2} 0.24634 \times 10^{-1} \times T^2 + \frac{1}{3} 0.145 \times 10^{-4} \times T^3 \right]_{725}^{875}$$

and the results of that calculation can be seen in table IV and the graphical representation from figure 5'.

I-1.3.3 The Heat Content As A Function Of The Modified Temperature

The interpolation of the values of $\phi = \varphi(T)$ and $H = \varphi'(T)$ for discrete temperature values can be seen from table V, and the equivalent figure 6'. Also in table V are included the correspondent values derived by Westby (1) for mild steel, as well as the difference between his results and those of the present work.

One will notice that the mismatch, small at the beginning, is amplified up to 20% for the higher temperature data. However, it must be remembered that the availability of data extends only to 900°C for the material of the current work. Furthermore, consideration must be given to the many approximations involved in Westby's calculations for mild steel, as listed below :

i) The extrapolation of the k values at temperatures in excess of 1200°C.

ii) The "chosen as compromise" conductivity value in the molten pool.

iii) The range for estimation of the coefficient of heat transfer from the arc to the weldment.

In the light of this, it was decided not to perform modifications in the equations of the original program before attempting a comparison of trial run results with those already available from the actual measurements.

For the reasons given above, and due to the success of the

trial run results, the mathematical expressions for the curves representative of the function $H = \psi(\phi)$ were not derived.

I-1.4 Trial Runs And Choice Of Data

To run the program one needs a set of data consisting of two lines: one concerning the operating welding parameters, and the other related to the dimensions of the inner and outer zone for the numerical calculations, as well as the thermo-physical properties of the material at the start of the calculations. The listing and ordering of these data are found in table VI.

The arcing time, as well as the dimensions for the inner and outer zone, are obtained by trial and error to suit the area of temperatures of interest, and may vary for different heat inputs.

The former estimated efficiency factor has been $\eta = 0.90$ (4) and supplied values for the cooling time t in excess of those observed from practice, but when the calculations were performed for $\eta = 0.85$ (5) the values obtained proved to be in good agreement with the actual figures, so 0.85 was the value chosen as the coefficient of efficiency for the present work.

To complete the set of data to be fed to the program, the welding parameters for the specific heat inputs must be known. These parameters were not only recorded from the practical welding experiments involving heat inputs of 3.6, 5.6 and

6.3KJ/mm respectively, which have already been mentioned as the content of table 4 of the main body of this work, but also they were hypothetically derived to provide figures for the regression analysis calculation of the equation shown in item 3.4.2 - also from the main body of the thesis, and their values can be seen from table VII. Table VIII gives us the listing of all data used in this work.

I-1.5 Interpretation Of The Numerical Output

The computer program's original output consists of groups of numbers, as it can be seen from a copy of the printout in figure 7. Each group represents a set of temperatures for the combinations of elements Δh and Δb of the plate, in a cross section, at a certain distance $K\Delta l$ behind the arc.

For any chosen combination of a distance $K\Delta l$ behind the arc and a height $I\Delta h$, one can trace the cooling cycle curve for the points $J\Delta b$, i.e. the points lying in a straight line perpendicular to the welding direction. The many values of K would allow the plotting of a family of these curves, always bearing in mind the height $I\Delta h$ was kept constant.

The outer intercept of the fusion temperature of the steel with a curve of the mentioned family is the representation of the boundary point between the weld metal and the HAZ for the height $I\Delta h$ considered, and for the welding heat input used. Thus, if a straight line parallel to the y-axis is traced from that point towards the x-axis, its interception with the other curves of the graph plotting will represent the

temperatures experienced by that boundary point before, during and after the passage of the welding arc. The same reasoning will be valid for temperatures other than the fusion temperature and what they really are is the Peak Temperature experienced by that "outer intercept" point.

If one remembers that each distance K$\triangle$l is associated with a time after which the arc was struck, and makes the conversion from distance to time, the final result can be represented by a curve of the temperatures of this outer point as a function of time, i.e. the welding thermal cycle for that specific point. This observation is valid when the process is in steady state. The three-dimensional representation of the above explanation is seen from figure 8'.

I-1.6 Development Of A Graphical Output

The first step in the interpretation of the numerical printout of the computer program, i.e. the determination of a family of cross sectional cooling cycle curves, would be inaccurate, and time consuming if hand plotted and the use of a computer graph plotting also involved a great deal of time in transforming the output figures into data for a graph plotting program. Therefore, an improvement was attempted in order to have the program output already on a graphical form.

This was accomplished by means of a Macro which runs the program in the usual way, but saving the numerical results in a storage file. Obyeing an extra set of data, specific rows and columns are read and chosen temperatures are selected from

the lot and stored in another file which will supply the data for a plotting program with consequent graphical output of the desired cooling curves. In the present work, VDU input was used instead of punched cards and the information on the use of the macro, as well as on the new set of data, can be seen from Appendix I-2.

I-1.7 Results And Discussion

A typical graph plotting for the cross sectional cooling curves representing the calculation for the heat input of 6.3 and an η factor equal to 0.85, can be seen from figure 9'. Every alternate curve is represented by a dotted line to facilitate the visualisation and also the calculation of the interception distances. The thermal cycle associated with these curves and calculated from the peak temperature of 1500°C, is seen from figure 10', and provided a cooling time $\Delta t = 90s$.

The results for the cooling times of the thermal cycles associated with the heat inputs of 5.6 and 3.6KJ/mm, calculated employing the efficiency factors of 0.90 and 0.85, respectively, are seen from the figures 11' and 12'. Table IX lists the values of the Δt cooling times for the latter and also for the cooling time Δt for the heat input of 3.6KJ/mm calculated at an efficiency factor of 0.90. It can be seen that the calculated Δt values are independent of the peak temperature considered, for a given efficiency factor and for a given heat input. Other thermal cycles representative of heat inputs used for calculations in the

current work will not be included for simplicity of presentation. The Appendices I-3, I-4 and I-5 are representative of the listing of the macro RAJ-PLOTPACK, of the listing of the adapted VARIAB program named RAJ-PROG and of the listing of the graph plotting program named RAJ-PLOT, respectively. Finally, the Appendix I-6 lists the symbols used in the computer calculations.

APPENDIX I-2 - THE USE OF THE MACRO RAJ-PLOTPACK TO OBTAIN A GRAPHICAL OUTPUT

A) Instruction to run the job :

RJ JOB NAME, RAJ-PLOTPACK, PARAM (NUMBER M N), JD

(JT _____ MZ , 32K)

B) The first set of data is identical to the ones seen from table VI.

C) The introduced set of data is responsible for the selection of the temperature points, and must be named RAJ- PLDM N. It consists of five lines and an explanatory example is given as follows :

500.0 650.0	x and y axis length in mm
TEMPERATURE VS DISTANCE	heading of the graph
DISTANCE (mm)	x axis title
TEMPERATURE (DEG. CENT.)	y axis title
2 4 45	see Note 1

Note 1 : The first figure represents the chosen height, e.g. second height in the group of numbers, whereas the other two figures are representative of the first and last distances behind the arc to be considered, i.e. there will be plotting of curves corresponding to group of numbers No. 4 to group of numbers No. 45.

D) The characters M N must be substituted by any integer, and must be kept the same for running the job and for the two sets of data.

E) An approximated job time for the arcing time of 200s is in the region of 2000 (s).

F) If sets of graphs other than the first one calculated are wanted for the same material and welding conditions, one only has to add PARAM (NUMBER M N, OLD) when running the job, and change the value of the fifth line of the second set of data. Note that M N must not be changed and the new job time is in the region of 50s.

G) The results of data are stored as follows :

Numerical Groups - RAJ - PLRM N

Graph Plotting Data - RAJ - PRROM N

h) Example given :

M = 1, N = 8, than :

1st set of data : RAJ-PRD18
2nd set of data : RAJ-PLD18

PARAM (Number 18) or (Number 18, OLD)

Restuls : Numerical Groups - RAJ-PLR18
Graph Data - RAJ-PRRO18

APPENDIX I-3 : LISTING OF THE MACRO RAJ-PLOTPACK

```
        IF PRE ( OLD ) , GO 2RJ20
        UAFORTRAN LOAD RAJ-PROGBIN,DATA RAJ-PRD%(NUMBER),*LP0 RAJ-PRR0%(NUMBER),-
        *LP1 RAJ-PRR1%(NUMBER),EXIT
2RJ20   CY RAJ-PRR1%(NUMBER),RAJ-PLD%(NUMBER)(APPE)
        DF "****"
        CY !,RAJ-PLD%(NUMBER)(APPE)
        ER !
        UAFORTRAN LOAD RAJ-PLOTBIN,DATA RAJ-PLD%(NUMBER),*LP2 RAJ-PLR%(NUMBER),EXIT
        DF "T5,FE,E"
        ED RAJ-PLD%(NUMBER),,!
        ER RAJ-PLD%(NUMBER)(-1)
        EX
****
```

APPENDIX I-4 : LISTING OF THE ADAPTED VARIAB PROGRAM NAMED RAJ-PROG

```
      NOLIST
      PROGRAM (VARI)
      INPUT 5 = CRD
      OUTPUT 6 = LP0
      TRACE 0
      OUTPUT 7 = LP1
      COMPRESS INTEGER AND LOGICAL
      COMPACT
      END
      MASTER VARIAB
      DIMENSION T(12,14,32),VJ(12),VK(12,32),B(90)
      DIMENSION F(56,32),V4(14),FI(14,32),FY(90)
      REAL H(13)
      COMMON T,B,IMAX2,JMAX2,KM,DL,IMAX1,H
    1 FORMAT(21H REAL ARCING TIME(S)=,F6.1)
    3 FORMAT(/14F8.2)
    5 FORMAT(6F6.1,2F5.2)
    6 FORMAT(23H WANTED ARCING TIME(S)=,F6.1)
    7 FORMAT(21H PLATE THICKNESS(CM)=,F6.1)
    8 FORMAT(22H WELDING CURRENT(AMP)=,F6.1)
    9 FORMAT(19H ARC VOLTAGE(VOLT)=,F6.1)
   10 FORMAT(52H SPEED OF ELECTRODE ALONG THE LINE OF WELDING(CM/S)=,
     1F6.2)
   11 FORMAT(19H EFFICIENCY FACTOR=,F6.2)
   12 FORMAT(35H HEAT SUPPLIED TO THE PLATE(CAL/S)=,F8.1)
   13 FORMAT(14H TIME STEP(S)=  ,F7.2)
   14 FORMAT (F6.2,F5.2,2I2,2I3,3F6.3)
      READ(5,5)TSTART,TYKK,AMP,VOLT,FART,ETA
      WRITE (6,5) TSTART,TYKK,AMP,VOLT,FART,ETA
      READ(5, 14) DB,DL,IMAX,JMAX,KM,KMAX,          GAMMA,AMBDA,ALFAMX
      WRITE (6, 14) DB,DL,IMAX,JMAX,KM,KMAX,          GAMMA,AMBDA,ALFAMX



      WRITE(7,88888)IMAX,JMAX
88888 FORMAT(T1,I5,5X,I5)



      WRITE(6,6)TSTART
      WRITE(6,7)TYKK
      WRITE(6,8)AMP
      WRITE(6,9)VOLT
      WRITE(6,10)FART
      WRITE(6,11)ETA
      A=AMBDA/GAMMA
      DI=FLOAT(IMAX)
      DH=TYKK/DI
      QPRIKK=0.24*ETA*AMP*VOLT
      DH2=DH**2
      DB2=DB**2
      DL2=DL**2
      DD=3.0*DB
```

```
      DV=3.0*DL
      DU2=DU**2
      DV2=DV**2
      M=(JMAX+1)/3+1
      KMAX2=KMAX+0
      N=2*KMAX2/3
      V=DH*DB*DL
      VINV=1.0/DH**2+1.0/DB**2+1.0/DL**2
      DTGO=DL/FART
      IMAX1=IMAX+1
      IMAX2=IMAX+2
      JMAX1=JMAX+1
      JMAX2=JMAX+2
      KMAX1=KMAX2-1
      WRITE(6,12)QPRIKK
   25 BMAX=(FLOAT(JMAX2)-1.5)*DB
      DO 26 J=1,13
   26 B(J)=(FLOAT(J)-1.5)*DH
      DO 27 I=1,IMAX2
   27 H(I)=(FLOAT(I)-1.5)*DH
      TIDINT=0.0
      SUMTID=0.0
   28 VI=0.0
      DO 29 J=1,JMAX2
      V4(J)=0.0
      DO 29 K=1,KMAX2
   29 F(J,K)=2.625
      DO 30 I=1,IMAX2
      VJ(I)=0.0
      DO 30 J=1,JMAX2
      VK(I,J)=0.0
      DO 30 K=1,KMAX2
   30 T(I,J,K)=2.625
   70       DTID = 0.4/ALFAMX/VINV
      IF(DTID .LT. DTGO) GO TO 80
      DTID = DTGO + 1.0E-7
      GO TO 90
   80 DTID = DTGO/FLOAT(IFIX(DTGO/DTID) + 1) + 1.0E-7
   90 WRITE(6,13)DTID
  100 IF (DTGO.GT.(TIDINT+DTID)) GOTO 120
  102 IF(TIDINT.GT.DTGO)GOTO 104
      GOTO 120
  104 SUMTID=SUMTID+TIDINT
      TIDINT=0.0
      DO 110 J=2,M
  110 F(J,N)=T(3,3*J-3,2)
      DO 112 K=2,KMAX2
      DO 112 J=1,JMAX2
      F(J,K-1)=(2.*F(J,K-1)+F(J,K))/3.
      DO112 I=1,IMAX2
  112 T(I,J,K-1)=T(I,J,K)
  120 TIDINT=TIDINT+DTID
      DTP=QPRIKK*DTID/GAMMA/V/2.0
```

```
      T(2,2,KM)=T(2,2,KM)+DTP
      KS=KMAX2-N
      DO 140 K=1,KS,1
      DO 140 KK=1,3
      KE=KK+3*(K-1)
      DO 140 I=1,IMAX2
  140 T(I,JMAX2,KE)=(2.0*T(I,JMAX1,KE)+F(M+1,N+K-1))/3.0
      DO 141 I=1,IMAX2
      DO 141 J=1,JMAX2
  141 T(I,J,KMAX2)=2.625
      DO 142 I=1,IMAX2
      DO 142 K=1,KMAX2
  142 T(I,1,K)=T(I,2,K)
      DO 402 J=2,M
      JJ=-3
  401 JJ=JJ+1
      JE=3*J+JJ
      DO 143 I=1,IMAX2
  143 T(I,JE,1)=(2.0*T(I,JE,2)+F(J,N-1))/3.0
      IF (JJ.NE.-2) GOTO 401
  402 CONTINUE
      DO 145 J=1,JMAX2
      DO 145 K=1,KMAX2
      T(1,J,K)=T(2,J,K)
  145 T(IMAX2,J,K)=T(IMAX1,J,K)
  147 IF(SUMTID.LT.TSTART)GOTO 150
      I = 48
      WRITE(6,1)SUMTID


      WRITE(7,77777) (B(JJ),JJ=2,9)
77777 FORMAT(T2,8(F5.2,2X))


  148 CALL SKRFIR (I)
      IF (I.EQ.2) STOP
      I = I-1
      GOTO 148
  150 DO 160 K=1,KMAX2
      DO 160 J=1,JMAX2
      DO 160 I=1,IMAX2
      TH=T(I,J,K)
      IF(TH.GT.122.0)GOTO 151
      FIK=(8.62-0.032*TH)*TH
      GOTO 159
  151 IF(TH.GT.154.4)GOTO 152
      FIK=249.812+2.67*TH
      GOTO 159
  152 IF(TH.GT.242.0)GOTO 153
      FIK=139.936+5.38*TH
      GOTO 159
```

```
153 IF(TH.GT.277.0)GOTO 154
    FIK=957.948
    GOTO 159
154 IF(TH.GT.313.0)GOTO 155
    FIK=708.648+0.9*TH
    GOTO 159
155 FIK=-1716.852+8.60*TH
159 CONTINUE
    IF(I.EQ.IMAX2.OR.J.EQ.JMAX2.OR.K.EQ.1)GOTO 160
    FIN=FI(I,J)
    VIU=A*(FIN-FI(I+1,J))/DH2
    VJU=A*(FIN-FI(I,J+1))/DH2
    VKU=A*(FIN-FIK)/DL2
    T(I,J,K-1) = T(I,J,K-1)+DTID*(VI+VJ(I)+VK(I,J)-VIU-VJU-VKU)
    VI=VIU
    VJ(I)=VJU
    VK(I,J)=VKU
160 FI(I,J)=FIK
    DO 176 J=2,M
176 F(J,N)=T(3,3*J-3,2)
    I=KMAX2-N-1
    DO 178 K=1,I
178 F(M,N+K)=T(3,JMAX1,2+3*K)
    DO 180 K=1,N
180 F(1,K)=F(2,K)
    DO 195 K=1,KMAX1
    DO 195 J=1,JMAX2
    TH=F(J,K)
    IF(TH.GT.122.0)GOTO 181
    FYK=(8.62-0.032*TH)*TH
    GOTO 189
181 IF(TH.GT.154.4)GOTO 182
    FYK=249.612+2.67*TH
    GOTO 189
182 IF(TH.GT.242.0)GOTO 183
    FYK=139.982+3.33*TH
    GOTO 189
183 IF(TH.GT.277.0)GOTO 184
    FYK=957.948
    GOTO 189
184 IF(TH.GT.313.0)GOTO 185
    FYK=708.648+0.9*TH
    GOTO 189
185 FYK=-1716.852+8.60*TH
189 CONTINUE
    IF(K.EQ.1.OR.J.EQ.JMAX2)GOTO 195
192 FYN=FY(J)
    V1=A*(FYN-FY(J+1))/DU2
    V2=A*(FYN-FYK)/DV2
    F(J,K-1) = F(J,K-1)+DTID*(V3+V4(J)-V1-V2)
    V3=V1
    V4(J)=V2
    FY(J)=FYK
```

```
 195 CONTINUE
     DO 196 J=1,JMAX2
     F(J,KMAX2)=2.525
 196 F(J,1)=F(J,2)
     DO 198 K=1,KMAX2
 198 F(JMAX2,K)=F(JMAX1,K)
     GOTO 100
     END
     SUBROUTINE SKRFIR(L  )
     DIMENSION T(12,14,52),B(90)
     REAL H(13)
     COMMON T,B,IMAX2,JMAX2,KM,DL,IMAX1,H
   1 FORMAT(//41H TEMPERATURES(DEGR.C) IN A CROSS SECTION ,F6.1,
    1 11H CM BEHIND THE ARC)
   2 FORMAT(10H     B(CM)=,14F8.2)
   3 FORMAT(3H H=,F6.2,2HCM,14F8.1)
     K=L
     DO 20 I=1,IMAX2
     DO 20 J=1,JMAX2
     TH=T(I,J,K)
     IF(TH.GT.92.5)GOTO 11
     TT=7.619*TH
     GOTO 19
  11 IF(TH.GT.85.0)GOTO 12
     TT=6.154*TH+77.0
     GOTO 19
  12 IF(TH.GT.130.0)GOTO 13
     TT=4.444*TH+222.0
     GOTO 19
  13 IF(TH.GT.150.0)GOTO 14
     TT=5.0*TH+150.0
     GOTO 19
  14 IF(TH.GT.240.0)GOTO 15
     TT=6.389*TH-58.0
     GOTO 19
  15 IF(TH.GT.275.0)GOTO 16
     TT=1475.0
     GOTO 19
  16 IF(TH.GT.315.0)GOTO 17
     TT=1.375*TH+1097.0
     GOTO 19
  17 TT=4.857*TH
  19 CONTINUE
  20 T(I,J,K)=TT
     RK=FLOAT(KM-L)
     AK=RK*DL
     WRITE(6,1)AK
     WRITE(6,2)(B(J),J=2,9)
     DO 99999 I=2,IMAX1
  10 WRITE(6,3)H(I),(T(I,J,L),J=2,9)

99999 WRITE(7,99998)(T(I,J,L),J=2,9)
99998 FORMAT(T1,8(F7.1,1X))

      RETURN
      END
      FINISH
****
```

APPENDIX I-5 : LISTING OF THE GRAPH PLOTTING PROGRAM NAMED RAJ-PLOT

```
      PROGRAM (RAJS)
      INPUT  1 = CR1
      OUTPUT 2 = LP2
      COMPRESS INTEGER AND LOGICAL
      COMPACT
      TRACE 0
      END


      MASTER  RAJ

      REAL     X POINTS(10) , Y POINTS(10)
      REAL     SIZE / 2.25 / , TICK / 2.0 /
      INTEGER TITLE(16) , PLANE , ROWS , COLUMNS , PLOTS , WIDTH , PLOT
      INTEGER TIMES
      LOGICAL SKIP

      READ(1,34) X MAX , Y MAX , X SCALE , Y SCALE

      CALL OPEN GINO GF

      CALL SCALE2( X SCALE , Y SCALE )
      CALL CHASWI( 1 )
      CALL CHASIZ( SIZE , SIZE )
      CALL SHIFT2( 75.0 , 75.0 )
      CALL MOVTO2( X MAX , 0.0 )
      CALL LINTO2( 0.0   , 0.0 )
      CALL LINTO2( 0.0 , Y MAX )
      CALL MOVTO2( 0.0 , 0.0 )

      TIMES = IFIX( Y MAX / 10.0 ) + 1
      DO 30 I = 1 , TIMES
      CALL MOVBY2( 0.0 , 10.0 )
      CALL LINBY2(-TICK , 0.0 )
      CALL MOVBY2(-SIZE * 7.0 , SIZE * 0.5 )
      CALL CHAINT( I * 50 , 4 )
   30 CALL MOVBY2( TICK + SIZE * 3.0 , -SIZE * 0.5 )
      CALL MOVTO2( 0.0 , 0.0 )

      TIMES = IFIX( X MAX / 20.0 ) + 1
      DO 31 I = 1 , TIMES
      CALL MOVBY2( 20.0 , 0.0 )
      CALL LINBY2( 0.0 , -TICK)
      CALL MOVBY2(-SIZE , -SIZE * 3.0 )
      CALL CHAINT( I , 2 )
   31 CALL MOVBY2(-SIZE , TICK + SIZE * 3.0 )

      CALL MOVTO2( (X MAX / 2.0) - 25.0 , Y MAX + 25.0 )
      READ(1,37) ( TITLE(I) , I = 1 , 16 )
      CALL CHAARR( TITLE , 16 , 4 )
      CALL MOVTO2( (X MAX / 2.0) - 25.0 ,        - 25.0 )
      READ(1,37) ( TITLE(I) , I = 1 , 16 )
      CALL CHAARR( TITLE , 16 , 4 )
```

```
      CALL MOVTO2(                    - 25.0 , (Y MAX / 2.0) - 25.0 )
      CALL ROTAT2( 90.0 )
      READ(1,27) ( TITLE(I) , I = 1 , 16 )
      CALL CHARR( TITLE , 16 , 4 )
      CALL ROTAT2(-90.0 )
      CALL MOVTO2( 0.0 , 0.0 )

      READ(1,36) PLANE , MINI DEPTH , MAXI DEPTH
      READ(1,36) ROWS , COLUMNS
      READ(1,36) ( X POINTS(WIDTH) , WIDTH = 1 , COLUMNS )
      WRITE(2,36) ( X POINTS(WIDTH) , WIDTH = 1 , COLUMNS )
      DO 99 WIDTH = 1 , COLUMNS
99    X POINTS(WIDTH) = X POINTS(WIDTH) * 200.0

      DO 34 PLOTS = 1 , 50
      SKIP = .TRUE.
      IF ( PLOTS .LT. MINI DEPTH ) SKIP = .FALSE.
      IF ( PLOTS .GT. MAXI DEPTH ) GO TO 35
      DO 32 I = 1 , PLANE
      READ(1,36 ,END=35) ( Y POINTS(WIDTH) , WIDTH = 1 , COLUMNS )
32    CONTINUE
      PLANE = ROWS
      IF ( .NOT. SKIP ) GO TO 34
      WRITE(2,39) ( Y POINTS(PLOT) , PLOT = 1 , COLUMNS )
      DO 33 PLOT = 1 , COLUMNS
      Y POINTS(PLOT) = Y POINTS(PLOT) * 0.2
      IF ( Y POINTS(PLOT) .GT. 400.0 ) Y POINTS(PLOT) = 400.0
33    CONTINUE
      CALL CURTO2( X POINTS , Y POINTS , COLUMNS , 0 , 0 )
34    CONTINUE

35    CALL DEVEND

      STOP 'ALL CURVES PLOTTED RAJ'

36    FORMAT(10G0.0)
37    FORMAT(16A4)
38    FORMAT(T5,' X-COORDINATES ARE',/,T5,1X,10(F7.2,2X)//)
39    FORMAT(T5,1X,10(F7.2,2X))

      END


      FINISH
```

APPENDIX I-6 - SYMBOLS USED IN THE COMPUTER CALCULATIONS

a	Heat Diffusion Coefficient , $a = k/c$	cm^2/s
a_o	Heat Diffusion Coefficient at Room Temperature	cm^2/s
c	Specific Heat	$cal/g\ ^oC$
k	Thermal Conductivity Factor	$cal/cm\ s\ ^oC$
k_o	Thermal Conductivity Factor at Room Temperature	$cal/cm\ s\ ^oC$
γ	Density	g/cm^3
W	Intensity Of Specific Heat Exchange With The Surroundings	$cal/cm^3\ s$
ϕ	Modified Temperature Scale	
H	Heat Content	cal/g
η	Efficiency Factor For Heat Transfer From Arc To Weldment	
x,y,z	Cartesian Co-ordinates	

BIBLIOGRAPHY FOR THE APPENDIX I

1. WESTBY, O., Inst. for Mekanisk Teknologies Norges Tekniske Høgskole, Trondheim 1968.

2. SARJANT, R.J. and SLACK, M.R., "Internal Temperature Distribution in the Cooling and Reheating of Steel Ingots", J. Iron and Steel Inst. vol. 177, no. 8, 1954, p. 428, as quoted in ref. 1.

3. BILTON, D., Private Communication, British Steel Corporation, Ladgate Lane Laboratory, Middlesbrough, March 1977.

4. CHRISTENSEN, N. and GJERMUNDSEN, K., "Measurements of Temperatures Outside and in the Weld Pool in Submerged Arc Welding", Contract DA-91-591-EVC-1530, U.S. Dept. of Army, European Research Office, Jan. 1962, as quoted in ref. 1.

5. IVENS, P.F. and VAN DEN BERGH, A.A., "Impact Testing of the HAZ", Metal Construction and British Welding Journal, vol. 6, no. 7, 1974, p. 234.

TABLE I - VARIATION OF THE THERMAL CONDUCTIVITY K, OF THE STEEL RQT-500 WITH THE TEMPERATURE

Temp. °C	k cal/cm s °C
0	0.110
50	0.110
100	0.111
150	0.109
200	0.107
250	0.105
300	0.103
350	0.099
400	0.096
450	0.092
500	0.089
550	0.086
600	0.082
650	0.078
700	0.075
750	0.073
800	0.071
850	0.063
900	0.064

TABLE II - VARIATION OF THE SPECIFIC HEAT C, OF THE STEEL RQT-500 WITH THE TEMPERATURE

Temp. °C	C cal/g °C
50 - 100	0.114
100 - 150	0.118
150 - 200	0.122
200 - 250	0.126
250 - 300	0.130
300 - 350	0.135
350 - 400	0.141
400 - 450	0.147
450 - 500	0.155
500 - 550	0.166
550 - 600	0.177
600 - 650	0.186
650 - 700	0.200
700 - 750	0.346
750 - 800	0.196
800 - 850	0.133
850 - 900	0.128

TABLE III - VARIATION OF THE MODIFIED TEMPERATURE Ø CALCULATED VALUES WITH THE TEMPERATURE

Temp. °C	Ø
0	0
50	53.56
100	105.72
150	156.50
200	205.87
250	253.85
300	300.44
350	345.63
400	389.42
450	431.81
500	472.81
550	512.42
600	550.62
650	587.43
700	622.85
750	656.86
800	689.48
820	702.15
850	719.98
900	748.84

TABLE IV - VARIATION OF THE HEAT CONTENT H, CALCULATED VALUES WITH THE TEMPERATURE

Temp. °C	H cal/g
25	2.86
75	8.63
125	14.47
175	20.43
225	26.55
275	32.89
325	39.48
375	46.37
425	53.61
475	61.24
525	69.31
575	77.85
625	86.92
675	96.56
725	110.19
775	123.48
825	131.37
875	137.48

TABLE V - VARIATION OF THE MODIFIED TEMPERATURE Ø WITH THE HEAT CONTENT H, FOR REFERENCE TEMPERATURES

$Ø_1$ = Values for the steel RQT-500

$Ø_2$ = Values for the mild steel[1]

$Ø = Ø_1 - Ø_2$

Temp. °C	H cal/g	$Ø_1$	$Ø_2$	Ø
0	0	0	0	0
50	5.74	53.56	48.42	5.14
100	11.52	105.72	95.05	10.67
150	17.39	156.50	140.22	16.28
200	23.40	205.87	184.18	21.69
250	29.59	253.85	227.04	26.81
300	36.00	300.44	268.84	31.60
350	42.69	345.63	309.66	35.97
400	49.68	389.42	349.26	40.16
450	57.04	431.81	387.57	44.24
500	64.80	472.81	424.20	48.61
550	73.02	512.42	458.81	53.61
600	81.72	550.62	490.72	59.90
650	90.97	587.43	519.34	68.09
(675)	96.57	605.32	534.00	71.32
700	102.46	622.85	547.26	75.59
(725)	110.76	640.03	562.18	77.85
750	118.31	656.86	571.92	84.94
800	128.45	689.48	592.57	96.91
/820/	130.46	702.15	597.74	104.41
/850/	135.00	719.94	610.06	109.88
(875)	137.48	733.80	616.68	117.12
/900/	141.58	748.80	627.63	121.17

Temperatures inside brackets indicate points of change of curve for H values, whereas temperatures inside slashes indicate points of change of curve for Ø values.

TABLE VI - LISTING AND ORDERING OF THE COMPUTER PROGRAM DATA

FIRST LINE		
	Decimal dot in column number	Number of Decimals
Arcing time (S)	5	1
Plate thickness (Cm)	11	1
Welding Current (A)	17	1
Arc Voltage (V)	23	1
Welding Speed (Cm/s)	27	2
Efficiency factor	32	2

SECOND LINE		
	Decimal dot in column number	Number of Decimals
B	4	2
L	9	2
IMAX	Col. No. 13	Integer
JMAX	" " 15	"
KM	" " 17 & " " 18	"
KMAX	" " 20 & " " 21	"
	24	3
ko	30	3
ao	36	3

TABLE VII - HYPOTHETICAL VALUES FOR WELDING PARAMETERS

Heat Input KJ/mm	Current A	Voltage V	Weld Speed cm/s
2.7	600	30	0.66
4.5	940	32	0.66
7.0	1340	35	0.66

TABLE VIII - COMPUTER PROGRAM COMPLETE DATA SET

Heat Input (KJ/mm)	Arcing Time(s)	Plate Thickness (cm)	Weld Current (A)	Arc Voltage (V)	Weld Speed (cm/s)	Efficiency Factor η		
	B (cm)	L (cm)	IMAX (cm)	JMAX (cm)	KM (cm)	KMAX (cm)	ko (cal/cm s ^{o}C	ao (cm^2/s)
2.7	200 0.30	2.5 1.00	600 6	8	30 45	0.66 48	0.85 0.110	0.110
3.6*	200 0.30	2.5 1.00	753 6	8	32 45	0.66 48	0.90 0.110	0.110
3.6	200 0.30	2.5 1.00	753 6	8	32 45	0.66 48	0.85 0.110	0.110
4.5	200 0.30	2.5 2.0	940 6	8	32 45	0.66 48	0.85 0.110	0.110
5.6*	200 0.30	2.5 2.5	1073 6	8	35 45	0.66 48	0.90 0.110	0.110
5.6	200 0.30	2.5 2.5	1073 6	8	35 45	0.66 48	0.85 0.110	0.110
6.3	200 0.30	2.5 2.5	1200 6	8	35 45	0.66 48	0.85 0.110	0.110
7.0	200 0.30	2.5 4.0	1340 6	8	35 45	0.66 48	0.85 0.110	0.110

* - $\eta = 0.90$

Note : $h = \frac{\text{Plate Thickness}}{\text{IMAX}}$

TABLE IX - CALCULATED $\Delta t_{800-500}$ COOLING TIME VALUES

EFFICIENCY FACTOR		HEAT INPUT - KJ/mm		Peak Temp. °C	$\Delta t_{800-500}$ S
0.90			5.6	1500	82
				1240	82
				1000	83
				970	83
				930	83
				880	85
				800	92
			3.6	1500	39
				1200	40
0.85		H/INPUT KJ/mm	3.6	1500	24
				1300	24
				1000	26

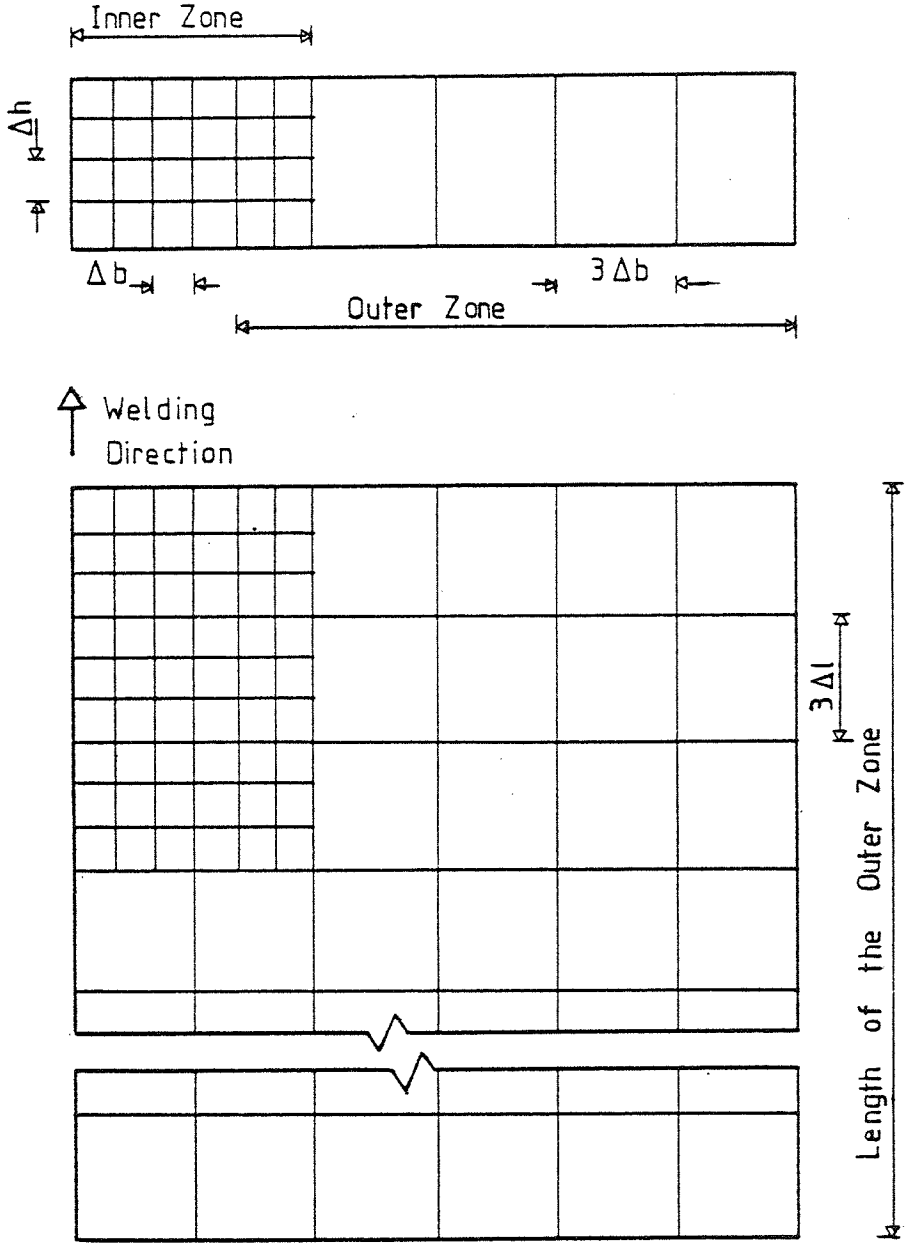

Figure 1'

Model of a half plate divided into volume elements

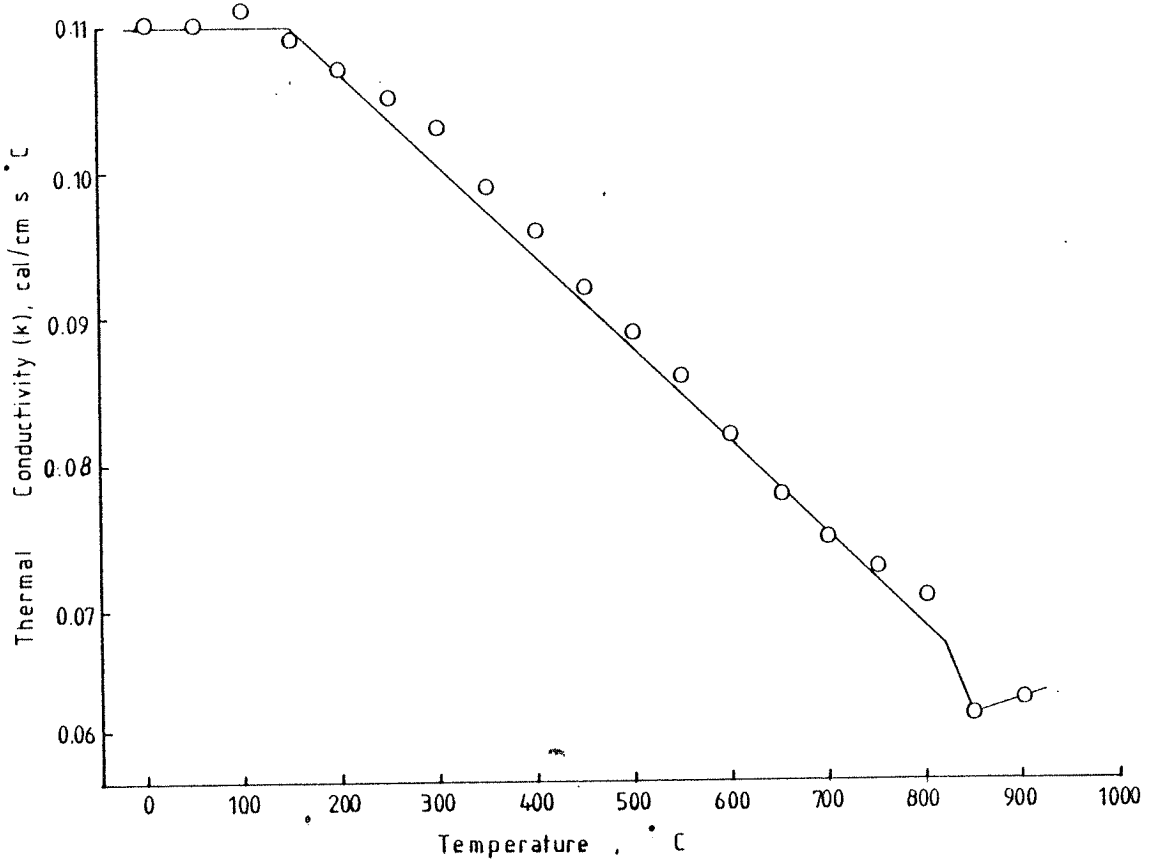

Figure 2'

Variation of the thermal conductivity factor k with the temperature, for the steel RQT-500

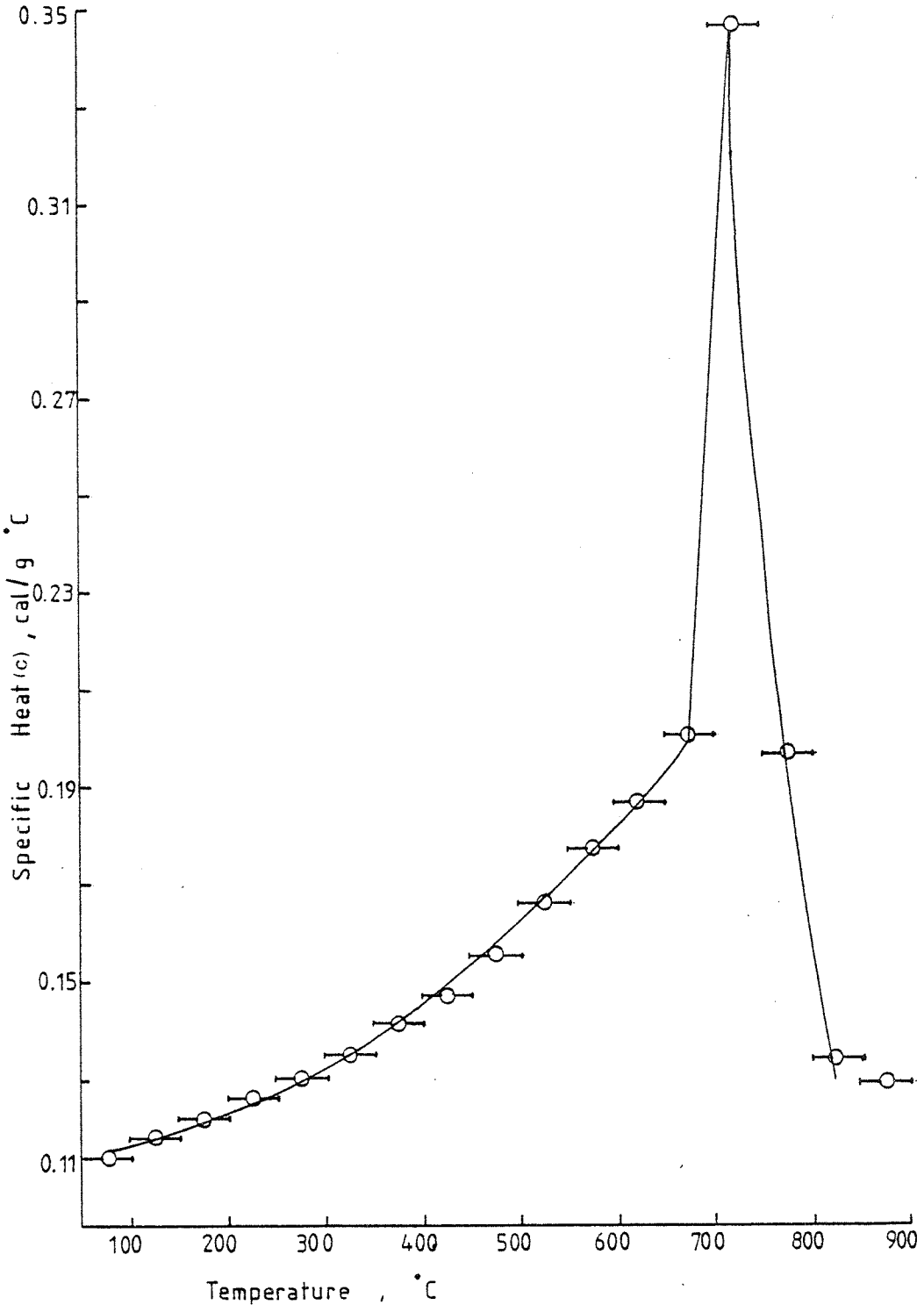

Figure 3'

Variation of the specific heat c with the temperature, for the steel RQT-500.

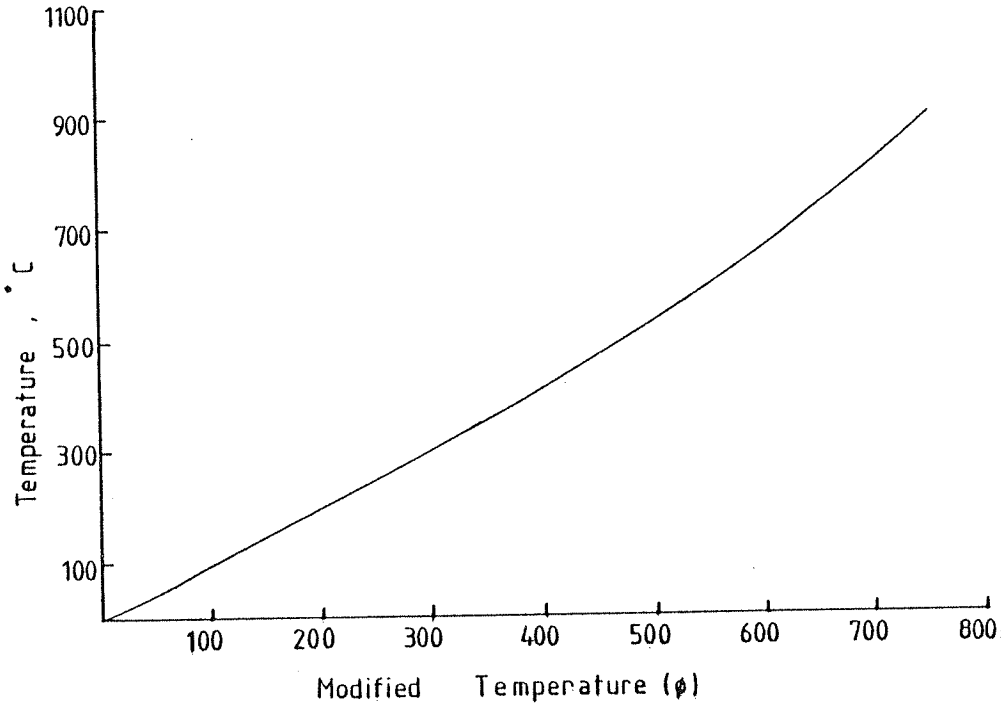

Figure 4'

Modified temperature Ø for the steel RQT-500

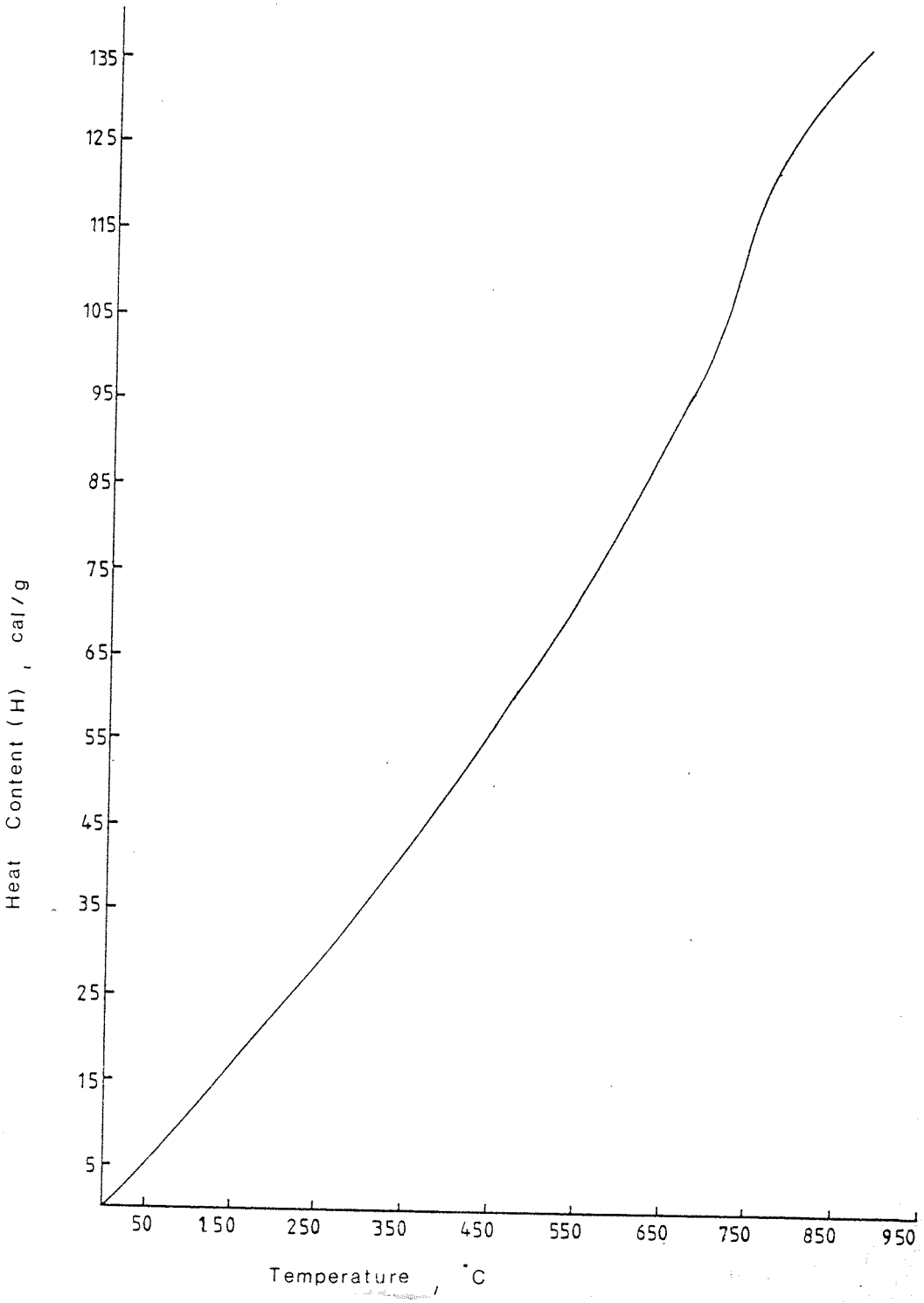

Figure 5'

Heat content H, in the steel RQT-500

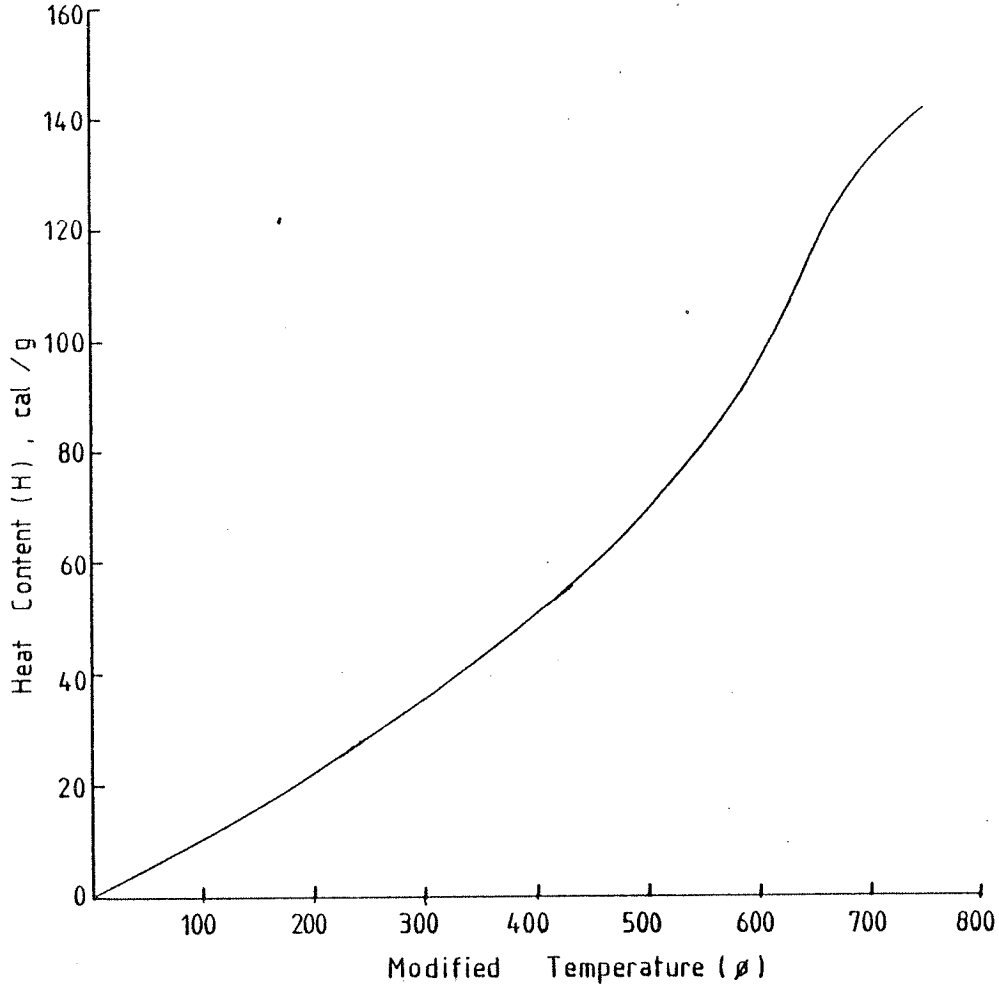

Figure 6' - Relation between the heat content H and the modified temperature Ø, for the steel RQT-500.

TEMPERATURES(DEGR.C) IN A CROSS SECTION 1.0 CM BEHIND THE ARC

R(CM) =	0.15	0.45	0.75	1.05	1.35	1.65	1.95	2.25
H= 0.21CM	3a94.2	3a53.9	1959.8	465.9	170.3	75.0	42.7	32.0
H= 0.63CM	2482.7	1787.4	597.7	230.6	106.8	56.4	36.6	29.6
H= 1.04CM	784.3	402.6	206.2	107.6	61.4	39.7	30.1	26.7
H= 1.46CM	163.3	120.0	79.4	53.6	37.8	29.5	25.6	24.6
H= 1.87CM	58.9	49.0	39.9	32.4	27.4	24.6	23.2	23.4
H= 2.29CM	33.0	31.0	25.2	25.6	23.7	22.5	22.3	22.9

TEMPERATURES(DEGR.C) IN A CROSS SECTION 2.0 CM BEHIND THE ARC

R(CM) =	0.15	0.45	0.75	1.05	1.35	1.65	1.95	2.25
H= 0.21CM	2759.2	2532.1	1a12.9	12a4.8	471.6	209.9	1a6.0	64.3
H= 0.63CM	2077.2	1535.7	1a73.4	651.9	308.1	153.9	84.6	54.9
H= 1.04CM	1376.3	1092.4	556.6	308.1	170.4	97.2	60.2	43.4
H= 1.46CM	394.3	316.6	213.3	142.6	90.9	59.5	42.4	34.4
H= 1.87CM	140.5	124.1	97.0	71.5	52.1	39.4	32.3	29.0
H= 2.29CM	73.3	66.5	56.1	45.6	37.1	31.2	27.9	26.6

TEMPERATURES(DEGR.C) IN A CROSS SECTION 3.0 CM BEHIND THE ARC

R(CM) =	0.15	0.45	0.75	1.05	1.35	1.65	1.95	2.25
H= 0.21CM	1967.9	1661.0	1659.8	1270.3	515.6	324.3	182.7	114.8
H= 0.63CM	1753.3	1651.2	1469.8	852.8	440.5	231.3	150.3	98.3
H= 1.04CM	1344.0	1106.7	707.5	489.9	273.4	170.2	109.4	78.9
H= 1.46CM	511.8	440.3	383.0	233.9	159.6	108.1	75.2	56.3
H= 1.87CM	230.2	205.9	157.6	128.5	93.0	69.9	53.0	43.1
H= 2.29CM	134.1	123.1	104.9	84.8	66.6	52.3	42.5	36.8

TEMPERATURES(DEGR.C) IN A CROSS SECTION 4.0 CM BEHIND THE ARC

R(CM) =	0.15	0.45	0.75	1.05	1.35	1.65	1.95	2.25
H= 0.21CM	1687.0	1652.7	1526.1	1153.0	659.6	396.5	246.5	170.3
H= 0.63CM	1504.2	1342.5	1372.4	925.9	519.3	325.6	211.1	150.3
H= 1.04CM	1195.6	1048.2	830.5	516.9	350.5	233.2	161.3	121.1
H= 1.46CM	566.3	499.2	407.7	334.0	219.7	157.8	116.7	93.7
H= 1.87CM	296.6	272.5	230.1	183.6	141.5	108.3	85.6	74.1
H= 2.29CM	195.6	181.8	158.4	131.3	105.4	84.3	70.1	64.1

TEMPERATURES(DEGR.C) IN A CROSS SECTION 5.0 CM BEHIND THE ARC

R(CM) =	0.15	0.45	0.75	1.05	1.35	1.65	1.95	2.25
H= 0.21CM	1561.1	1542.2	1475.0	1077.9	672.2	433.7	291.8	208.0
H= 0.63CM	1318.7	1475.8	1206.5	860.3	553.7	375.3	256.6	187.0
H= 1.04CM	1077.8	956.8	797.2	556.5	403.0	282.7	203.9	154.7
H= 1.46CM	566.1	530.1	447.5	356.3	269.3	202.1	154.1	123.0
H= 1.87CM	349.7	324.3	281.7	232.6	186.0	147.1	118.0	99.4
H= 2.29CM	249.9	234.9	208.8	177.4	146.4	119.7	99.6	87.0

TEMPERATURES(DEGR.C) IN A CROSS SECTION 6.0 CM BEHIND THE ARC

R(CM) =	0.15	0.45	0.75	1.05	1.35	1.65	1.95	2.25
H= 0.21CM	1529.4	1515.5	1362.9	1033.9	678.8	457.4	323.4	235.3

Figure 7'

Example of the original printout supplied by the VARIAB program

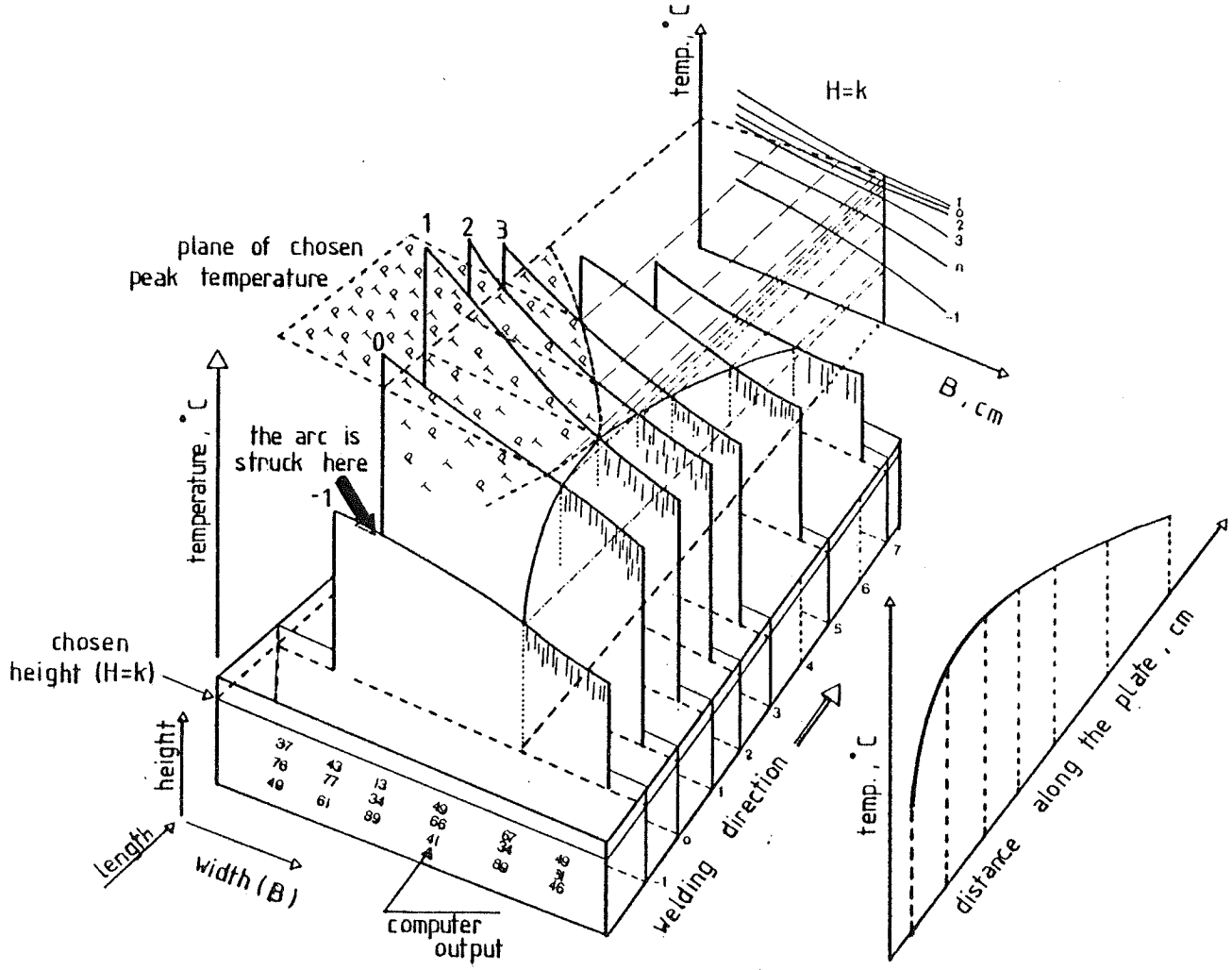

Table 8'

Three dimensional interpretation of the thermal cycle calculated by the VARIAB program.

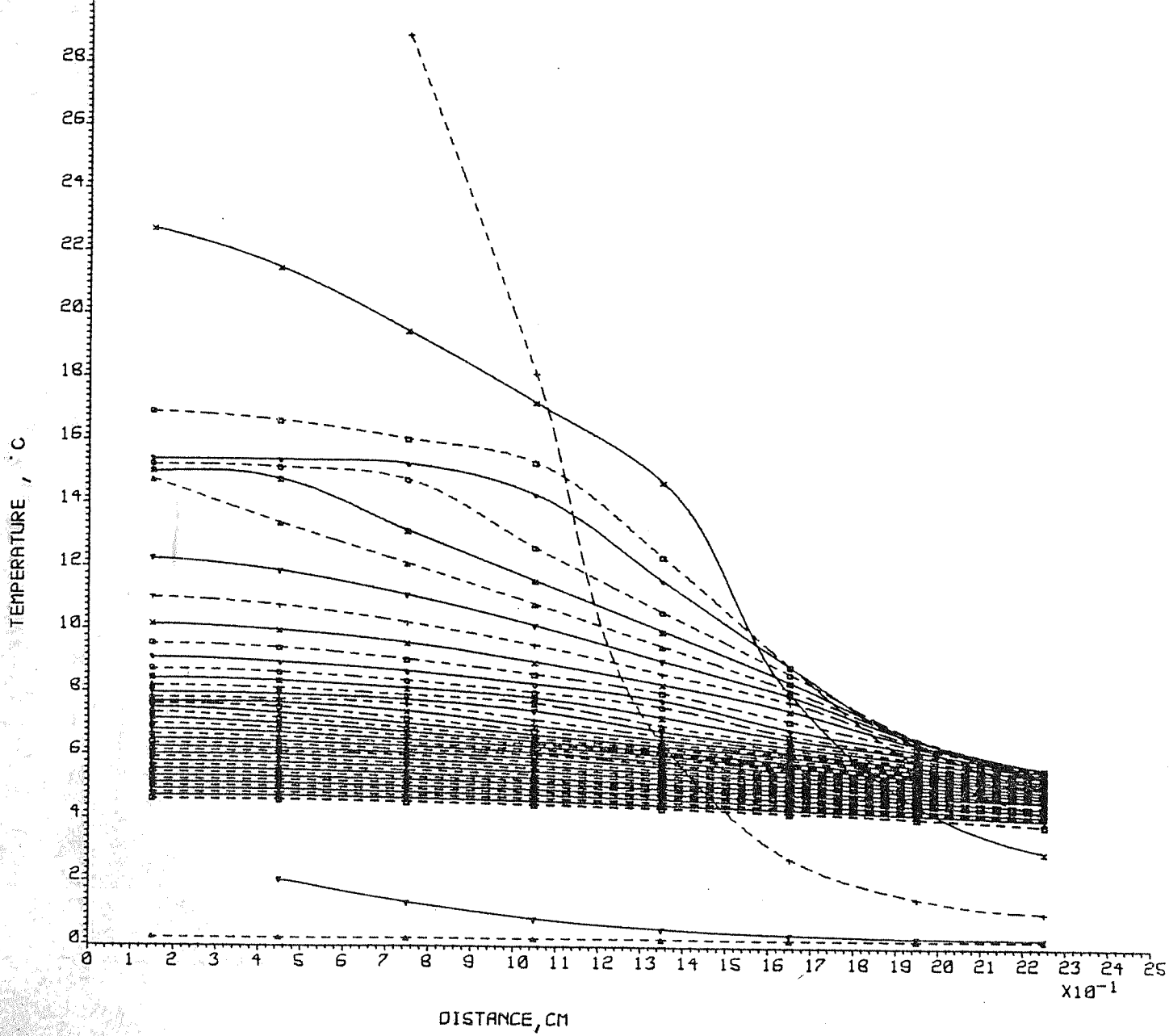

Figure 9'

Typical calculated cross sectional cooling cycles, along the weld direction. Example given for the 6.3KJ/mm heat input condition, efficiency factor of 85%.

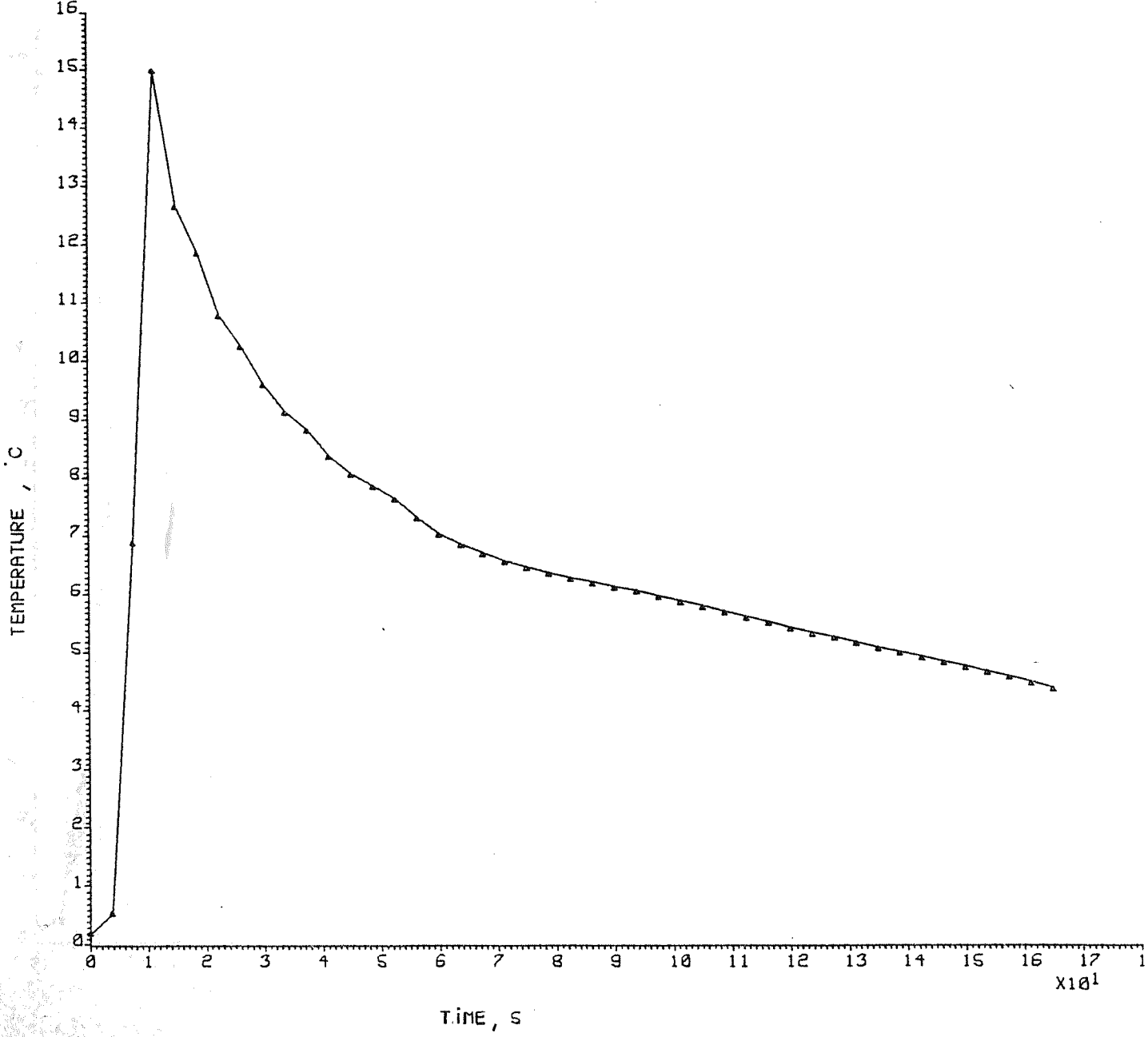

Figure 10'

Thermal cycle calculated for the 6.3KJ/mm heat input condition from a peak temperature of 1500°C. Effiency factor of 85%, cooling time t = 90s.

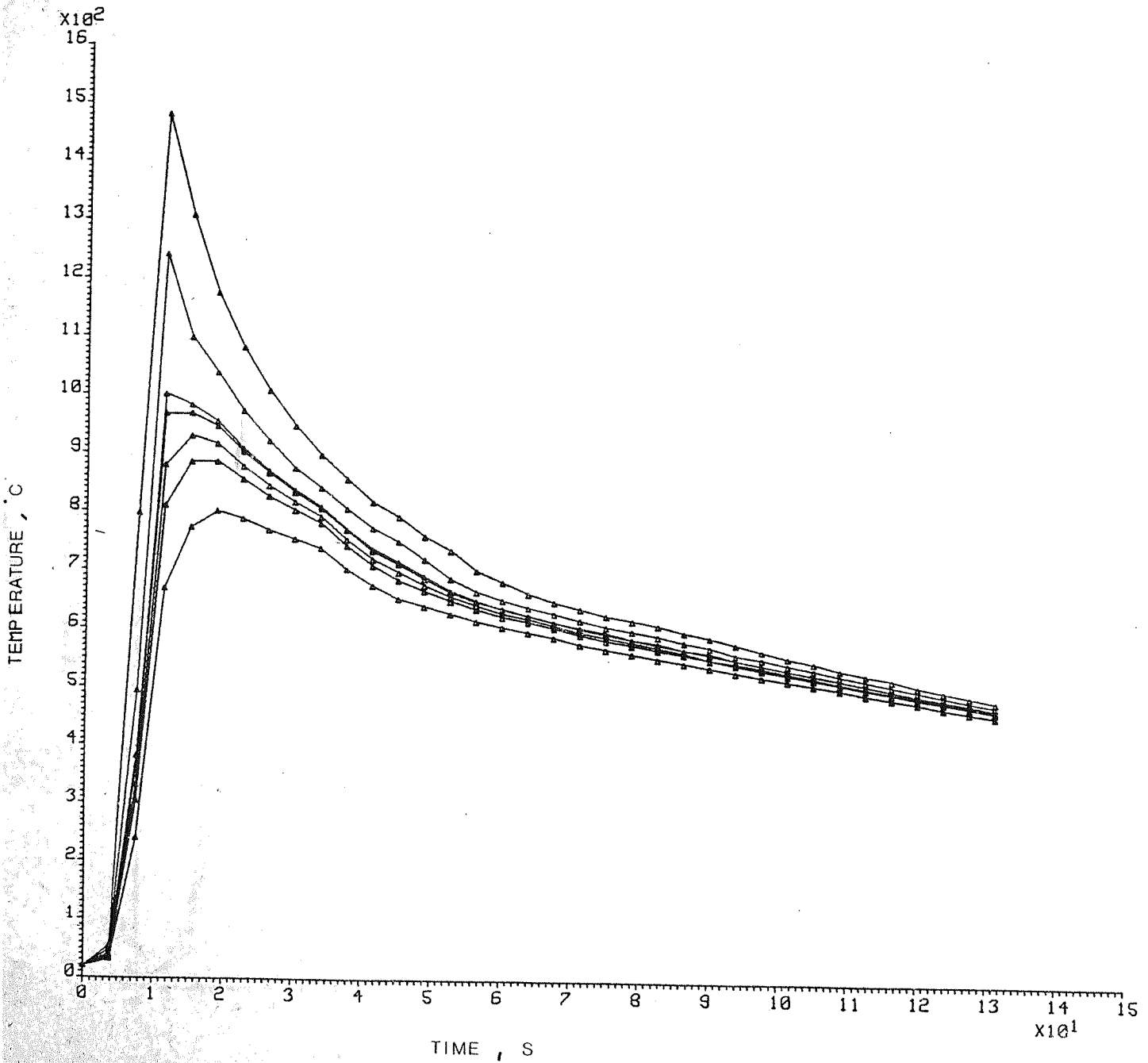

Figure 11'

Thermal cycles calculated for the 5.6KJ/mm heat input condition, from several peak temperatures. Efficiency factor of 90%.

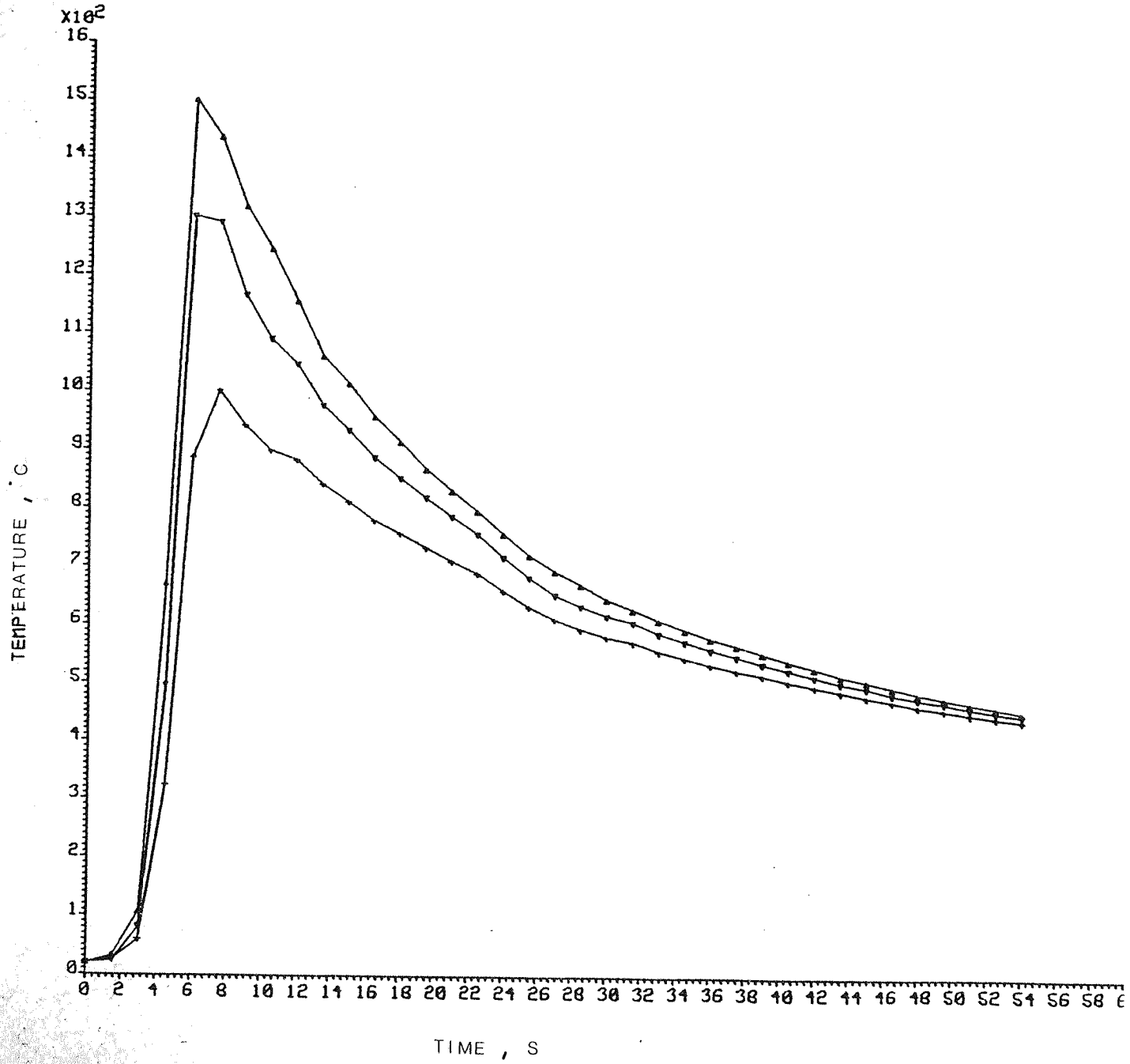

Figure 12'

Thermal cycle calculated for the heat input of 3.6KJ/mm, from several peak temperatures. Efficiency factor of 85%.

APPENDICES - II, III, IV AND V

APPENDIX II - AUXILIARY EQUIPMENT INVOLVED AND CONDITIONS USED IN THE WELDING SIMULATION EXPERIMENTS

A. Equipment involved in the Welding Simulation Experiments.

Hydraulic Power Supply = Dowty Gear Pump
Serial No. 2P3105CTDFB
Capacity : 3000 lb/in^2
10 gallons per minute

Vacuum Pump : Rotary Piston Vacuum Pump Single Stage
GENEVAC - Type GH6 - 6
Displacement : 168 liters per minute

Electrical Supply : MTC - Midland Transformer Co.
Serial No. T2/615

Temperature Control :

i) Eurotherm series 070

ii) Data Track Programmer (RI controls), Model FGE 5110

XY recorder : Bryan XY recorder 29000A3

Xt recorder : RE recorder 520.20

Creep Monitor : RDP Electronics, Type D8

Microspot Welder : Hirst make

B. Conditions used in the Welding Simulation Experiments :

i) Start in position control to mount the specimen, range of the lower jaw at $\pm$ 5mm.

ii) Thermal cycle simulation performed under load control. The operational values used were :

- Load Cell Amplifier at 5KN
- Load Applied : 0.05KN

iii) Dilation set up :

a) XY Scales : Temperature at 1mv/cm
Dilation at 25mv/cm

b) Creep Monitor Conditions :

Signal A + B - Scale at 10 and occasionally at 3

APPENDIX III - REGRESSION EQUATION VALUES FOR THE POINTS IN THE TRANSITION RANGE OF THE CHARPY TESTS RESULTS

1. Base Metal

   $Y = 57.965 + 0.62937\ x$

   Sum of squared deviations = 128.53

2. Real Weld, 3.6KJ/mm

   $Y = 54.47 + 0.6006\ x$

   Sum of squared deviations = 182.63

3. Real Weld, 6.3KJ/mm

   $Y = 22.99661 + 0.36483\ x$

   Sum of squared deviations = 154.71

4. Simulated Samples at 3.6KJ/mm

   a) Peak Temperature = 700°C

      $Y = 55.317 + 0.58989\ x$

      Sum of squared deviations = 124.53

   b) Peak Temperature = 800°C

      $Y = 60.493 + 0.51761\ x$

      Sum of squared deviations = 120.47

   c) Peak Temperature = 900°C

      $Y = 73.103 + 0.51507\ x$

      Sum of squared deviations = 50.67

   d) Peak Temperature = 1000°C

      $Y = 70 + 0.515\ x$

      Sum of squared deviations = 64.30

   e) Peak Temperature = 1150°C

      $Y = 50.403 + 0.5189\ x$

      Sum of squared deviations = 153.84

   f) Peak Temperature = 1250°C

      $Y = 24.297 + 0.40269\ x$

      Sum of squared deviations = 64.20

   g) Peak Temperature = 1400°C

      $Y = 32 + 1.1\ x$

      Sum of squared deviations = 0

5. Simulated Samples at 6.3KJ/mm

a) Peak Temperature = 700°C
Y = 53.47 + 0.50965 x
Sum of squared deviations = 148.69

b) Peak Temperature = 800°C
Y = 57.522 + 0.45436 x
Sum of squared deviations = 50.70

c) Peak Temperature = 900°C
Y = 97.451 + 0.6022 x
Sum of squared deviations = 140.65

d) Peak Temperature = 1000°C
Y = 70.63 + 0.53236 x
Sum of squared deviations = 63.10

e) Peak Temperature = 1150°C
Y = 31.983 + 0.40469 x
Sum of squared deviations = 39.84

f) Peak Temperature = 1250°C
Y = 22.97819 + 0.39096 x
Sum of squared deviations = 67.87

g) Peak Temperature = 1400°C
Y = 30.268 + 0.63112 x
Sum of squared deviations = 59.27

6. Simulated Samples at 14.4KJ/mm

a) Peak Temperature = 700°C
Y = 44.58 + 0.42787 x
Sum of squared deviations = 15.72

b) Peak Temperature = 800°C
Y = 67.055 + 0.73956 x
Sum of squared deviations = 19.12

c) Peak Temperature = 900°C
Y = 80.36 + 0.5824 x
Sum of squared deviations = 0.19

d) Peak Temperature = 1000°C
Y = 90.571 + 0.65714 x
Sum of squared deviations = 33.14

e) Peak Temperature = 1150^{o}C

Y = 27.6 + 0.21 x

Sum of squared deviations = 126

f) Peak Temperature = 1250^{o}C

Y = 9.9 + 0.285 x

Sum of squared deviations = 12.30

g) Peak Temperature = 1400^{o}C

Y = 21.667 + 0.55 x

Sum of squared deviations = 2.66

APPENDIX IV - SYMBOLS AND ABBREVIATIONS

HSLA	High Strength Low Alloy (Steels)
HAZ	Heat Affected Zone
SAW	Submerged Arc Welding
PWHT	Post Weld Heat Treatment
DCEP	Direct Current Electrode Positive
COD	Crack Opening Displacement (Test)
TEM	Transmission Electron Microscope
SEM	Scanning Electron Microscope
C.E., C.Eq.,	Carbon Equivalent
P.cm	Ito-Bession Factor
ITT	Impact Transition Temperature
$\Delta t_{800-500}$, Δt,	Cooling Time From 800 to 500 °C
η	Arc Efficiency Factor
A_1, A_s (tables)	Austenite Transformation Start Temperature On Heating
A_3, A_f (tables)	Austenite Transformation Finish Temperature On Heating
T_s (tables)	Transformation Start Temperature On Cooling
T_f (tables)	Transformation Finish Temperature On Cooling
B_s (tables)	Bainite Transformation Start Temperature On Cooling
M_s (tables)	Martensite Transformation Start Temperature On Cooling
M_f (tables)	Martensite Transformation Finish Temperature On Cooling
M-A	Martensite-Austenite Microstructure
UB	Upper Bainite Microstructure
PEF	Proeutectoid Ferrite Structure
Nital II	2% Nitric Acid In Alcoholic Solution
ASM	American Society For Metals
BOC	British Oxygen Co. Limited
BSC	British Steel Corporation
BWI, WI	British Welding Institute
CANMET	Canada Centre For Mineral And Energy Technology
IIW	International Institute Of Welding

APPENDIX V - ACKNOWLEDGEMENTS

The author acknowledges the CNPq and GTSid for the support to the present work, and PEMM/COPPE/UFRJ for leave granted.

Thanks are also due to Professor R.H. Thornley, Head of the Department of Production Engineering, for providing laboratory facilities, and also to Professor I. Dillamore, Head of the Metallurgy Department, for the use of the metallographic facilities.

The author would like to extend his gratitude to Raj, Dr. J.L. Aston and Dr. P.M. Appoo for their advice on the computer calculations, to Dr. S. Murphy for many helpful discussions, and to Dr. M.F. Jordan for supervising the project.

In conclusion, the author would like to thank Dr. L. Cotterill and Dr. R. Fenn for their continuous moral support, Mrs. Foster-Partridge for proof reading the script, and Miss J. Cope for the typing of this thesis.